PHYSICS REPORTS (Review Section of Physics Letters) 69, No. 3 (1981) 195–333. North-Holland Publishing Company

PERTURBATIVE QUANTUM CHROMODYNAMICS

E. REYA

Institut für Physik, Universität Dortmund, 4600 Dortmund, Germany

and

Deutsches Elektronen-Synchrotron DESY, Hamburg, Germany

Received 8 September 1980

Contents:

Single orders for this issue

PHYSICS REPORTS (Review Section of Physics Letters) 69, No. 3 (1981) 195–333.

Copies of this issue may be obtained at the price given below. All orders should be sent directly to the Publisher. Orders must be accompanied by check.

Single issue price Dfl. 64.00 postage included.

PERTURBATIVE QUANTUM CHROMODYNAMICS

E. REYA

Institut für Physik, Universität Dortmund, 4600 Dortmund, Germany

and

Deutsches Elektronen-Synchrotron DESY, Hamburg, Germany

NORTH-HOLLAND PUBLISHING COMPANY - AMSTERDAM

Abstract:

A large variety of modern perturbative aspects of QCD is critically reviewed from a theoretical as well as phenomenological point of view. The first part of this review is devoted to the classical more formal approach of summing leading logs: After a brief discussion of the basic concepts of renormalization theory, we review the renormalization group and its predictions for the effective (running) coupling constant in any field theory (asymptotic freedom as well as 'fixed point' theories). Using, in addition, the operator product expansion for deep inelastic scattering we calculate scaling violations of structure functions and show how to compare these results with experiment. Furthermore, dynamical calculations of parton distributions are discussed, as well as σ_L/σ_T, jets in leptoproduction and subleading corrections. We then proceed to show how these renormalization group improved results can be also derived using a simple perturbative language (Kogut–Susskind; Altarelli–Parisi) or by summing parton (Bethe–Salpeter) ladders. The universal validity (process independence) of the resulting Q^2 dependencies of parton distributions is emphasized and their factorization from the uncalculable non-perturbative piece (infrared divergences) is discussed. These latter results enable us to make rather unambiguous predictions for processes other than deep inelastic scattering, to which the remainder of this review is devoted. The hard scattering processes discussed in detail include hadronic (Drell–Yan) production of lepton pairs as well as their transverse momenta, the hadronic production of heavy quark flavors, semi-inclusive processes and fragmentation functions, high-p_T reactions and some recent topics and problems of jet production in e^+e^- annihilation.

Introduction

This article originated from a series of lectures given at the Herbstschule für Hochenergiephysik at Maria Laach in 1977. These lectures were intended for young (mostly non-expert) theorists and experimentalists as an introduction to the theoretical basis of Quantum Chromodynamics (QCD) and its application to leptonic and hadronic scattering processes. The aim of this introductory review is to teach – hopefully – even the uninitiated how to calculate "from scratch" scale violating effects and how to apply them to actually measured quantities. In order to make these rather complicated field theoretic techniques comprehensible, as far as possible, also to progressive experimentalists, this article will be oriented rather pragmatically. Special emphasis will be given to show how various quantities of interest can be and are calculated – details which are usually not found in the literature. By doing this I hope to reveal the physics hidden behind the rather awkward formalisms more clearly and to help also experimentalists to understand their (nowadays exciting) measurements in terms of modern field theoretic concepts.

These notes owe obvious important debts to original articles and reviews listed among the references. There exists already a variety of excellent reviews [1–11] regarding the perturbative treatment of QCD at small distances. We refer the German speaking reader also to the Maria Laach lectures [12] of 1977 (where not only strong interaction theories are discussed, but also the unified gauge theories of weak and electromagnetic interactions are treated rather comprehensively) and to ref. [13]. A discussion of the more formal and non-perturbative aspects of QCD, such as the path-integral formulation of quantum field theories, vortex solutions, solitons, instantons and related questions of quark confinement, can be found, for example, in refs. [14, 3 and 12].

In order to guide the theoretically not so well equipped reader through the jungle of presently existing reviews, let me briefly discuss those reviews which appeared in the past few years, mainly in Physics Reports. The article of Marciano and Pagels [14] concerns itself with the formal field theoretic and non-perturbative aspects of QCD, but does not cover the vast area of phenomenological applications of perturbative QCD. Peterman's review [10] deals with all the mathematical subleties underlying the renormalization group and their connection with measured structure functions together with a comparison with deep inelastic scattering data. Similarly, the excellent and very comprehensive review of Buras [11] concentrates on leading order and especially on higher order QCD corrections to structure functions using both the more formal language of the operator product expansion and renormalization group, and the intuitive parton model picture of Altarelli and Parisi; furthermore a systematic comparison of asymptotic freedom predictions with deep inelastic data is presented. The recent article of Dokshitzer, Dyakonov and Troyan [169] is very theoretically oriented in treating, using the parton (Bethe–Salpeter) ladder approach, perturbative QCD corrections for various hard scattering process, with little phenomenological applications. The present review is, as far as possible, theoretically self-contained by discussing and comparing all three calculational approaches (renormalization group and operator product expansion, Altarelli–Parisi equations, and parton ladders); the main emphasis is then put on the phenomenology how to apply these perturbative QCD predictions to all presently known hard scattering processes and to compare them with experiment.

The first part of this review (sections 1–5) is devoted to the classical more formal approach to scaling violations using Wilson's operator product expansion for deep inelastic processes. Here we shall discuss not only how to calculate scale violating effects, i.e. Q^2-dependent parton distributions, from general field theories of strong interactions (QCD as well as "fixed point" theories), but also how to compare these formal results with experiment such as x- and Q^2-dependencies of deep inelastic structure functions as well as their moments. We then discuss in section 6 how these renormalization group improved results can be understood and derived from a simple perturbative language, which will reveal the physics more clearly than the formal approach of the previous sections. Furthermore, perturbation theory is an essential tool for studying whether asymptotic freedom can be used to make predictions for processes about which the operator product expansion yields no information. In section 7 we shall see that the results derived for deep inelastic lepton–nucleon processes have indeed universal validity such that the leading Q^2-dependencies of parton distributions remain the same for all processes studied so far (semi-inclusive reactions, Drell–Yan dimuon production, hadronic high-p_T processes, etc.), regardless of space-like or time-like momenta-transfer-squared; furthermore non-perturbative infrared effects will factorize to all orders. Thus QCD can make unique, in principle parameter-free predictions for a wide class of processes, once scale violating effects have been calculated for, say, deep inelastic scattering. This ambitious, so far not fully solved program will be studied in the remainder of this review (sections 8–12), and in the last section we briefly discuss some recent topics and problems of jet production in e^+e^- annihilation.

1. The concept of color

There are numerous empirical and theoretical arguments [15, 16] which made us believe that the conventional quark model carrying only $SU(N_f = 3, \ldots)$ flavor degrees of freedom, i.e. u, d, s, c, ... quarks, should be extended to include additional "color" degrees of freedom described by the color-group $SU(N_c = 3)_c$. The most convincing arguments in favor of the color quantum number are the following:

(i) *Fermi–Dirac statistics*: It is well-known that in the non-relativistic naive quark model the low-lying baryon states are totally symmetric in the quark- and spin-indices, for example

$$|\Delta^{++}, J_z = +\tfrac{3}{2}\rangle = |u^\uparrow u^\uparrow u^\uparrow\rangle. \tag{1.1}$$

Thus the ground state of the three quark system, composed of three identical u-quarks, corresponds to a totally symmetric wave function. On the other hand, this cannot be the case if quarks, like other known fermions with spin 1/2, obey Fermi–Dirac statistics. The by now most convincing way out of this puzzle is to assume [15] that each quark flavor comes in *three* different "colors", say *red* (R), *green* (G) and *blue* (B). In this case the wave functions of the ground states are still symmetric in space, flavor and spin, but can be simply made antisymmetric in color:

$$|\Delta^{++}, J_z = +\tfrac{3}{2}\rangle = \frac{1}{\sqrt{6}} \sum_{\mathrm{R,G,B}} \varepsilon_{ijk} |\mathrm{u}_i{}^{\uparrow}\ \mathrm{u}_j{}^{\uparrow}\ \mathrm{u}_k{}^{\uparrow}\rangle \tag{1.2}$$

with i, j, k being the color indices. Similarly, the Pauli-principle can be satisfied for any physical baryon state consisting of three identical flavor quarks. In group theoretic terms the form of the wave function (1.2) means nothing else that three quarks can form only a singlet under $SU(3)_c$

$$3 \otimes 3 \otimes 3 = 1 \oplus 8 \oplus 8 \oplus 10 \tag{1.3}$$

where a given flavor q transforms as a (color) triplet (q_R, q_G, q_B) under $SU(3)_c$. The singlet state 1 in (1.3) is just the one which is totally antisymmetric in the color index, given by eq. (1.2). Thus a consistent way to describe the baryon spectrum would be to suppose that all baryons are singlets under $SU(3)_c$, i.e. $|\text{baryon}\rangle \sim \sum \varepsilon_{ijk} |q_i q_j q_k\rangle$. Furthermore, the same principle can be applied to mesons ($\sim |q\bar{q}\rangle$) as well, since we can form $SU(3)_c$ singlets out of quarks and antiquarks,

$$3 \otimes \bar{3} = 1 \oplus 8 \tag{1.4}$$

where the singlet 1 state, to be identified with physical mesons, is given by

$$|\text{meson}\rangle = \frac{1}{\sqrt{3}} \sum_{i=\mathrm{R,G,B}} |q_i \bar{q}_i\rangle. \tag{1.5}$$

Note that two quarks cannot form a color-singlet state since $3 \otimes 3 = 6 \oplus \bar{3} \not\ni 1$, and a similar situation holds for a four quark system. Fortunately, two- and four-quark states have never been observed. Therefore a consistent way to describe the whole spectrum of hadrons is to postulate the

"*confinement dogma*": all physical observables (hadrons, currents, ...) are *color-singlets*, i.e. are "colorless".

It should be emphasized that the arguments presented above lead necessarily to a *three* color structure. Any other number of colors is clearly ruled out since, for example, four colors would imply that the simplest multiquark state is of the form $|qqqq\rangle$.

Thus we imagine that the world of observed hadrons can be described by colored quarks of the, so far, following type

$$\underset{\text{light}}{\begin{pmatrix} u_R & u_G & u_B \\ d_R & d_G & d_B \end{pmatrix}}, \quad \underset{\text{heavy}}{\begin{pmatrix} c_R & c_G & c_B \\ s_R & s_G & s_B \end{pmatrix}}, \quad \underset{\text{superheavy}}{\begin{pmatrix} t_R & t_G & t_B \\ b_R & b_G & b_B \end{pmatrix}}, \ldots \tag{1.6}$$

where the light up (u) and down (d) quarks together with the strange quark (s) build up the "conventional" hadrons (π, K, p, ...), the charmed quark (c) forms the "hidden"-charm ($J/\psi = c\bar{c}, \ldots$)

and "open"-charm ($D, F, \ldots$) states, and the b-quarks are the constituents of the $\Upsilon(=b\bar{b})$ family. The even heavier t-quarks have yet to be discovered.

(ii) *Seeing color "experimentally"*: There are two processes which allow us to infer the number of colors in a rather direct way, one of which is the decay $\pi^0 \to 2\gamma$. Applying PCAC one can describe [17] this decay by relating it to the coupling of the axial-vector current to two photons which, to lowest order, is given by the famous triangle diagram

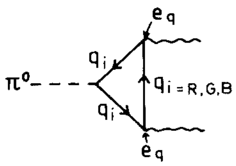

The decay rate is calculated to be [17]

$$\Gamma_{\pi^0 \to 2\gamma} = \frac{m_\pi^3}{64\pi} \left(\frac{2\alpha}{\pi f_\pi} N_c S \right)^2 \tag{1.7}$$

with

$$S = \sum_q (I_3)_q e_q^2 = \tfrac{1}{2}(\tfrac{2}{3})^2 - \tfrac{1}{2}(-\tfrac{1}{3})^2 = \tfrac{1}{6}$$

and where we have summed over color which gives N_c times the amplitude corresponding to the naive (colorless) quark model. For the semileptonic π-decay constant we take $f_\pi \simeq 93\,\text{MeV}$. Using the experimental decay rate $\Gamma_{\pi^0 \to 2\gamma} = (7.95 \pm 0.55)\text{eV}$, eq. (1.7) implies

$$N_c = 3.06 \pm 0.10 \tag{1.8}$$

in perfect agreement with the theoretically anticipated value of $N_c = 3$. Note that for $N_c = 1$ (naive quark model) eq. (1.7) predicts $\Gamma_{\pi^0 \to 2\gamma} = 0.89\,\text{eV}$ in striking disagreement with experiment.

The other experimental evidence for color comes from the cross section ratio for $e^+e^- \to \gamma^* \to$ hadrons relative to $e^+e^- \to \gamma^* \to \mu^+\mu^-$. Since, in the naive parton model the hadronic amplitude in fig. 1.1 (for $q^2 \to \infty$) is, up to the fractional quark charges e_q, the same as for $e^+e^- \to \mu^+\mu^-$, the ratio of cross sections should be

$$R_{e^+e^-} \equiv \frac{\sigma(e^+e^- \to \text{hadrons})}{\sigma(e^+e^- \to \mu^+\mu^-)} = N_c \sum_q e_q^2. \tag{1.9}$$

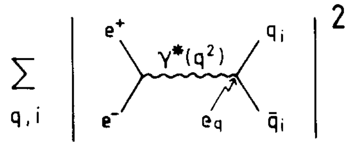

Fig. 1.1. The cross section for $e^+e^- \to \gamma^* \to$ hadrons. The sum runs over the flavors q and colors i.

In the absence of color ($N_c = 1$), this ratio would be 2/3 below charm threshold (q = u, d, s), and 10/9 above charm threshold (q = u, d, s, c). Experimentally [18] this ratio is about 2–2.5 below charm threshold and about 4.5–5 above charm threshold. Allowing for one charge unit of $R^{\exp}_{e^+e^-}$ due to heavy lepton (τ^-) production above charm threshold, these values are not inconsistent with $R_{e^+e^-} = 2$ and 10/3 expected for $N_c = 3$.

(iii) *Renormalizability of unified gauge theories*: A related reason for color is the cancellation of the Adler–Bell–Jackiw [19] anomalous triangle diagrams (i.e. triangle graphs with one axial-vector and two vector couplings) which is required to ensure [20, 21] the renormalizability of a gauge theory of weak and electromagnetic interactions. In all models based on SU(2) × U(1) which have been proposed so far, the condition for having an axial vector anomaly-free theory reads [20]

$$\mathrm{Tr}\, Q_{\mathrm{tot}} \equiv \mathrm{Tr}(Q_{\mathrm{lept}} + Q_{\mathrm{hadr}}) = 0 \tag{1.10}$$

with Q_{tot} being the total fermionic charge matrix of the theory. So, if the sum of the charges of all (leptonic and hadronic) elementary spinor fields vanishes, the anomaly cancels. This condition can be satisfied by arranging the quark charges in a suitable way. (Note, however, that it is not possible to cancel the electron against the muon anomaly since they have the same charge.) Let us consider for example a conventional theory with four leptons and quark-flavors, where the charge matrices are given by

$$\mathrm{Tr}\, Q_{\mathrm{lept}} = \mathrm{Tr}\begin{pmatrix} 0 & & & 0 \\ & -1 & & \\ & & 0 & \\ 0 & & & -1 \end{pmatrix}\begin{matrix} \nu_e \\ e \\ \nu_\mu \\ \mu \end{matrix} = -2$$

$$\mathrm{Tr}\, Q_{\mathrm{hadr}} = \mathrm{Tr}\begin{pmatrix} 2/3 & & & 0 \\ & -1/3 & & \\ & & -1/3 & \\ 0 & & & 2/3 \end{pmatrix}\begin{matrix} u \\ d \\ s \\ c \end{matrix} = +\tfrac{2}{3}$$

which cannot satisfy condition (1.10). However, in a theory with 3 colors the sum over hadronic charges will be three times as large, i.e. $\mathrm{Tr}\, Q_{\mathrm{hadr}} = +2$, and eq. (1.10) is satisfied. Thus, our renormalizability condition (1.10) directly implies the existence of three additional degrees of freedom (call them color) in the quark sector. The requirement for having a strictly renormalizable theory, i.e. eq. (1.10), implies an additional remarkable and far reaching consequence: It gives a close connection between the leptons and elementary hadrons (quarks)! To see how this comes about, let us include the heavy lepton τ^-: in a SU(2) × U(1) gauge theory this amounts to adding a third left-handed doublet (ν_τ, τ) to the "standard" doublets (ν_e, e) and (ν_μ, μ). Thus, $\mathrm{Tr}\, Q_{\mathrm{lept}} = -3$. In a 3-color quark model this immediately implies, via eq. (1.10), the existence of *new* quark-flavor degrees of freedom in the hadronic sector: The most natural and so far the only extension, which is consistent with all present experiments (such as deep inelastic neutrino scattering), is to add in analogy to the leptonic sector a new quark doublet (t, b) to the "standard" ones (u, d) and (c, s). Thus

$$\mathrm{Tr}\, Q_{\mathrm{hadr}} = 3(\underset{u}{2/3} - \underset{d}{1/3} + \underset{c}{2/3} - \underset{s}{1/3} + \underset{t}{2/3} - \underset{b}{1/3}) = +3,$$

and again the renormalizability condition (1.10) can now be satisfied. Needless to say that one of these anticipated new quark flavors b have been found already experimentally ($\Upsilon = b\bar{b}$), whereas the predicted t-quark states will be hopefully found at PETRA and PEP in the near future. This very close and symmetric interrelation between leptons and hadrons, resulting solely from the renormalizability constraint (1.10), is usually referred to as Glashow's *lepton–hadron universality.*

Without going into details, we just mention that there are further more technical reasons for a color field theory of strong interactions such as for example to account for the observed $\Delta I = 1/2$ rule in non-leptonic weak decays [22], or to resolve the U(1)-η problem (in order to avoid a pseudoscalar meson with mass no larger than $\sqrt{3}m_\pi$; see for example refs. [14] and [9]).

2. The Lagrangian of QCD

QCD is a renormalizable Lagrangian quantum field theory of the strong interactions. The formulation of it is based on (i) the numerous successful predictions of the conventional (flavor) quark-parton model as well as on the results of including color as discussed in the previous section, and (ii) the successful description of dynamical effects in QED – a minimal *locally* gauge invariant field theory. The fundamental spin 1/2 constituents in (1.6) are thus supposed to form color triplets of $SU(3)_c$ and the strong interactions between these *colored* quarks are mediated by an octet of colored vector fields $A^\mu_{a=1,\dots,8}$, called *gluons* (not carrying flavor), which transform according to the adjoint representation of $SU(3)_c$. More explicitly,

$$\psi_j:\ \underbrace{\begin{pmatrix} u_R \\ u_G \\ u_B \end{pmatrix},\ \begin{pmatrix} d_R \\ d_G \\ d_B \end{pmatrix},\ \begin{pmatrix} s_R \\ s_G \\ s_B \end{pmatrix},\ \begin{pmatrix} c_R \\ c_G \\ c_B \end{pmatrix},\ \dots}_{\text{weak, elm. (flavor) interactions}}\ \updownarrow \text{strong(color) interactions} \tag{2.1}$$

Since by construction the strong interactions take place only in the color sector, being thus independent of all other non-strong interactions, the strong gauge group will always be orthogonal to the weak gauge group, say, i.e. $G_s \times G_w$ where $G_s = SU(3)_c$ and, for example, $G_w = SU(2) \times U(1)$ according to the standard Weinberg–Salam model of weak and electromagnetic interactions. Thus, the fields in (2.1) can have for instance the following interactions

strong: 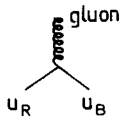

; but 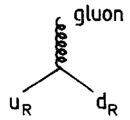

forbidden!

weak, elm.: 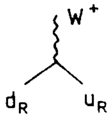

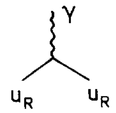

; but 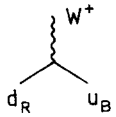

forbidden!

The static baryon and meson wave functions discussed in the previous section, e.g. eq. (1.5), have now a simple dynamical interpretation: The strongly interacting colored quarks, being in a color-singlet state, are bound together by colored gluon fields (gluons are the "glue of matter"). For example

$p \sim \sum_{\text{color}} \varepsilon_{ijk} u_i u_j d_k =$ 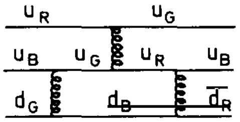

$\pi^+ \sim \sum_{\text{color}} u_i \bar{d}_i =$ 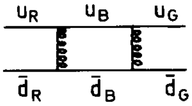

and, in addition, hadrons might also consist of two and more gluon bound states [23], the so-called "glue balls".

The main idea of QCD is to make the $SU(3)_c$ color symmetry a *local*, rather than just a global symmetry. QCD is thus a *non-abelian* gauge theory (gauge group $SU(3)_c$), in contrast to QED which is an abelian gauge theory (gauge group U(1)). The formal Lagrangian of QCD is then given by

$$\mathscr{L} = -\tfrac{1}{4} F_a^{\mu\nu} F_{a\mu\nu} + \mathrm{i}\bar{\psi}_j \gamma_\mu \mathrm{D}_{jk}^\mu \psi_k - \bar{\psi}_j M_{jk} \psi_k \tag{2.2}$$

where the first term is the pure Yang–Mills Lagrangian for self-interacting $SU(3)_c$ gauge fields with

$$F_a^{\mu\nu} = \partial^\mu A_a^\nu - \partial^\nu A_a^\mu + g f_{abc} A_b^\mu A_c^\nu \tag{2.3}$$

and f_{abc} being the structure constants of $SU(3)_c$, i.e., $[T_a, T_b] = \mathrm{i} f_{abc} T_c$ with the $SU(3)_c$ matrices $T_a = \frac{1}{2}\lambda_a$. The interactions of the quarks with gluons are described by the second term in (2.2) where the covariant derivative acting on a quark field is defined by

$$\mathrm{D}_{jk}^\mu = \delta_{jk}\, \partial^\mu - \mathrm{i} g (T_a)_{jk} A_a^\mu . \tag{2.4}$$

As far as light quarks (u, d, s) are concerned, we shall neglect the mass term in eq. (2.2), since we always will consider energies or more specifically momentum-transfers-squared $Q^2 \equiv |q^2|$ such that $m^2_{q=u,d,s}/Q^2 \simeq 0$. A few comments are in order regarding the structure of interactions implied by eq. (2.2):

(i) the strength of *all* interactions between quarks and gluons is specified by just *one* universal coupling g;

(ii) the Feynman rules corresponding to $\mathscr{L}$ are well known [1], but we would like to stress again the most essential qualitative new features of interaction vertices of QCD. Only a non-abelian local vector gauge theory implies, as we can read off eqs. (2.2) and (2.3), besides quartic self-couplings of the vectors fields also triple gluon couplings, namely

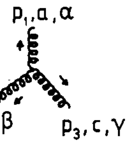

$$= -g f_{abc} [g_{\alpha\beta}(p_1 - p_2)_\gamma + g_{\beta\gamma}(p_2 - p_3)_\alpha + g_{\gamma\alpha}(p_3 - p_1)_\beta] . \tag{2.5}$$

This gluon self-coupling is mainly responsible for "asymptotic freedom", a unique feature of non-abelian local gauge theories, which means that the interaction strength g becomes smaller the smaller the distance R between two particles becomes (or the larger Q^2, since $R \sim 1/\sqrt{Q^2}$); asymptotically, for $R \sim 1/\sqrt{Q^2} = 0$ the theory becomes a free field theory, i.e. $g = 0$ (see section 4). Furthermore, the quark–gluon vertex is similar to the electron–photon vertex of QED, but with the additional non-abelian structure according to eq. (2.4)

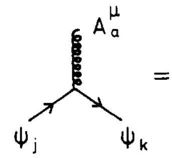

$$= ig\gamma^\mu (T_a)_{jk}\,; \qquad (2.6)$$

(iii) one can easily verify that (2.2) is invariant under local gauge transformations of the form

$$\begin{aligned} &\psi_j(x) \to U(x)\,\psi_j(x) \\ &T_a A^\mu_a(x) \to U(x)\, T_a A^\mu_a(x)\, U^{-1}(x) - \frac{i}{g}(\partial^\mu U(x))U^{-1}(x) \end{aligned} \qquad (2.7)$$

where $U(x) = \exp(-iT_a\alpha_a(x))$ with $\alpha_a(x)$ being the space-time dependent parameters of the local $SU(3)_c$ gauge transformation $U(x)$. Or, the infinitesimal form of (2.7) simply reads ($\alpha_a(x)$ infinitesimal)

$$\begin{aligned} &\delta\psi_j(x) = -iT_a\psi_j(x)\,\alpha_a(x) \\ &\delta A^\mu_a(x) = -\frac{1}{g}\,\partial^\mu\alpha_a(x) + f_{abc}\alpha_b(x)A^\mu_c(x). \end{aligned} \qquad (2.8)$$

For comparison recall that for an abelian local gauge theory such as QED, the Lagrangian is formally the same as in eq. (2.2) but with all group indices dropped and instead of eqs. (2.3) and (2.4) we have

$$F^{\mu\nu} = \partial^\mu A^\nu - \partial^\nu A^\mu, \qquad D^\mu = \partial^\mu - igA^\mu \qquad (2.9)$$

i.e. there exists now no self-coupling of the vector gauge field (photon) and we have only one interaction vertex

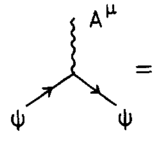

$$= ig\gamma^\mu.$$

The well-known abelian version of the local gauge transformation (2.7) or (2.8) now reads

$$\psi \to e^{-i\alpha(x)}\psi, \qquad \delta A^\mu = -\frac{1}{g}\,\partial^\mu\alpha(x). \qquad (2.10)$$

Before going into the details of how to extract the numerous phenomenological consequences of the

QCD Lagrangian (2.2), we will first turn to a discussion of the renormalization group – the "classical" field theoretic approach for calculating scaling violations in deep inelastic processes.

3. The renormalization group

In general renormalizable field theories the basic interaction vertex g depends on the momenta q which are fed into it, i.e. graphs like

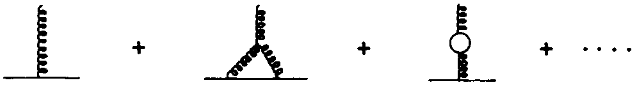

give rise to logarithms

$$g \to g + \mathcal{O}(g^3 \ln q^2) + \mathcal{O}(g^5 \ln^2 q^2) + \cdots . \tag{3.1}$$

Fortunately, in a locally gauge invariant QCD (*triple* gluon vertex!), where this expansion turns out to be an alternating series, the leading logarithms can be summed exactly [24] and give an effective coupling which *decreases* as $|q^2| \to \infty$

$$g^2(q^2) = \frac{g^2}{1 + bg^2 \ln |q^2|}. \tag{3.2}$$

This is in contrast to all other field theories known, e.g. no Yang–Mills vector gluons (where the last term in eq. (2.3) is absent) or scalar gluons, where the interactions in finite order of perturbation theory *grow* [25] as $|q^2| \to \infty$. We will now see how these leading logarithms of perturbation theory can be summed to all orders using the renormalization group [26, 27]. For an excellent general introduction we refer the reader to Coleman's Erice lectures [28], and a clear and thorough discussion for the case of asymptotically free gauge theories (QCD) can also be found in refs. [1], [5] and [10].

To avoid any double counting, let us consider a one-particle-irreducible (1PI) Green's function (which is the sum of all connected Feynman diagrams that cannot be cut in two by breaking a single internal line) with n external lines denoted by

$$\Gamma^{(n)}(p_1, \dots, p_n) \equiv$$

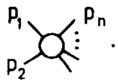

A renormalizable Lagrangian contains in general, besides dimensionless coupling constants, a number of terms with dimensions of masses, such as $m\bar{\psi}\psi$, $m^2\phi^2$, $\lambda\phi^3$, etc. An intuitive statement is that at high values of all external momenta the Green's functions should be independent of the mass. To be more precise, consider some Feynman diagram with all four-momenta being (nonexceptional) deep Euclidean; that is to say, $p_i^2 = (\mathrm{i}p_i^0)^2 - \boldsymbol{p}_i^2 \to -\infty$ with $p_i \cdot p_j/\Sigma_{k=1}^n p_k^2$ finite for all i and j. In this case the above statement can be proven order by order in perturbation theory (Weinberg theorem [29]). This restriction to the deep Euclidean region at nonexceptional values of momenta (i.e. the sum of any subset of momenta does not vanish) is necessary in order to stay away from thresholds and to make sure that the momenta flowing in the internal lines are all large. As a consequence, the asymptotic behavior of Green's functions in the deep Euclidean region should naively be independent of any mass in the theory and consequently amplitudes would scale in terms of ratios of kinematic invariants in a way determined by dimensional analysis, as in a massless theory. This naive expectation is, however, *not* the case. The reason is that in order to give sense to the theory through a renormalization procedure a subtraction point

$$p_i^2 = -\mu^2 \tag{3.3}$$

must be selected, where for example ultraviolet divergences in Feynman integrals are regulated in some way ($p_i^2 = 0$ is excluded because of infrared divergences), which necessarily introduces a parameter with dimensions. This *arbitrary* mass parameter μ is introduced solely to define the theory, but is without any physical significance. Thus, any measurable physical quantity must not depend on different choices of μ. The renormalization group expresses the fact that any physical amplitude is invariant under changes of μ, i.e. $\delta\Gamma^{(n)} = 0$ for $\mu \to \mu + \delta\mu$, or formally

$$\Gamma^{(n)}(p_i, \mu, g; Z) = \Gamma^{(n)}(p_i, \mu + \delta\mu, g + \delta g; Z + \delta Z) \tag{3.4}$$

where the variation $\delta g = \beta(g)\, \delta\mu/\mu$ of the renormalized coupling $g(\mu)$ is described by the Callan–Symanzik function $\beta(g) \equiv \mu\, \partial g/\partial\mu$. In addition, any Green's function depends also on the normalization of the fields, generically denoted by $Z(\mu)$, the change $\delta Z = \gamma(g) Z\, \delta\mu/\mu$ of which is fixed by the so called "anomalous dimension" γ. To formulate these intuitively qualitative remarks in a mathematically more precise language, let us briefly recall the main ideas of renormalization theory.

In a theory with n_A external bosons and n_ψ fermions, our 1PI truncated Green's function Γ is defined by removing from the Green's function G all external propagators, i.e.

$$\Gamma^{(n_A, n_\psi)}(p_i) \equiv [G^{(2,0)}(p_A)]^{-n_A} [G^{(0,2)}(p_\psi)]^{-n_\psi} G^{(n_A, n_\psi)}(p_i). \tag{3.5}$$

Suppose there is a bare $\bar\psi\psi A$ coupling g_0 so that (in 0th order)

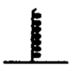 $:\quad \Gamma_0^{(1,2)} = g_0$ (3.6)

(we suppress obvious factors such as Dirac matrices and/or Gell-Mann matrices which depend on the specific theory under consideration). Higher order graphs in perturbation theory like

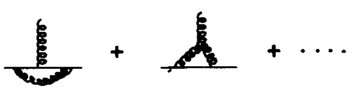

will modify the simple vertex in (3.6). We denote the result of adding them to (3.6) by $\Gamma_u^{(1,2)}$ – the so called unrenormalized Green's function. This quantity is in general infinite because of divergent loop integrals. There is a variety of ways to make Γ_u finite, one of which would be to introduce a cut-off Λ into the divergent loop momentum integral:

$$\Gamma_u^{(n_A, n_\psi)} = \Gamma_u^{(n_A, n_\psi)}(p_i, g_0, \Lambda). \tag{3.7}$$

There is then a theorem [30] that in any gauge theory one can introduce multiplicative factors $Z_A(\Lambda)$ and $Z_\psi(\Lambda)$ with the property that

$$\lim_{\Lambda\to\infty} Z_A(\Lambda)^{n_A} Z_\psi(\Lambda)^{n_\psi} \Gamma_u^{(n_A,n_\psi)}(p_i, g_0, \Lambda) \tag{3.8}$$

exists and is finite. (More generally, we call any quantum field theory with this property "renormalizable".) This implies that we can define renormalized Green's functions by

$$\Gamma^{(n_A,n_\psi)} \equiv \lim_{\Lambda\to\infty} Z_A^{n_A} Z_\psi^{n_\psi} \Gamma_u^{(n_A,n_\psi)} \tag{3.9}$$

which are *finite* and cut-off independent. As we have already emphasized, one can perform these subtractions of infinities in divergent loop integrals (which amounts to introducing a cut-off Λ) at any convenient spacelike (Euclidean) subtraction point $p_i^2 = -\mu^2$. Thus the dimensionless numbers Z can only depend on dimensionless ratios Λ/μ and g_0, i.e. $Z = Z(g_0, \Lambda/\mu)$, and our renormalization condition (3.9) can be finally written as

$$\Gamma^{(n_A,n_\psi)}(p_i, g, \mu) = \lim_{\Lambda\to\infty} Z_A(g_0, \Lambda/\mu)^{n_A} Z_\psi(g_0, \Lambda/\mu)^{n_\psi} \Gamma_u^{(n_A,n_\psi)}(p_i, g_0, \Lambda) \tag{3.10}$$

where for convenience we have replaced the g_0 dependence of the physical renormalized Green's function in terms of a dimensionless physical renormalized coupling constant

$$g = g(g_0, \Lambda/\mu). \tag{3.11}$$

These finite renormalized amplitudes Γ, or equivalently the renormalization constants Z are in praxi fixed by the *renormalization condition* at some arbitrary $p_i^2 = -\mu^2$:

$$\begin{aligned}
Z_A:&\quad \Gamma^{(2,0)}|_{p^2=-\mu^2} = Z_A^2 \Gamma_u^{(2,0)}|_{p^2=-\mu^2} \equiv -g_{\mu\nu}p^2 + p_\mu p_\nu \\
Z_\psi:&\quad \Gamma^{(0,2)}|_{p^2=-\mu^2} = Z_\psi^2 \Gamma_u^{(0,2)}|_{p^2=-\mu^2} \equiv \not p \\
g:&\quad \Gamma^{(1,2)}(0, p, -p)|_{p^2=-\mu^2} = Z_A Z_\psi^2 \Gamma_u^{(1,2)}(0, p, -p)|_{p^2=-\mu^2} \equiv g
\end{aligned} \tag{3.12}$$

where the Λ-dependent Γ_u's are calculated from the well known diagrams

$\Gamma_u^{(2,0)}$:

$\Gamma_u^{(0,2)}$:

$\Gamma_u^{(1,2)}$:

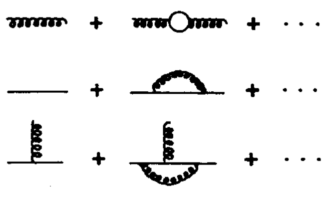

It should be noted that $\Gamma^{(2,0)}$ refers to the transverse (conserved) part of the boson propagator and that, for simplicity we use always the Landau gauge ($\alpha = 0$) in the boson (gluon) propagator $-(i/k^2)\times [g_{\mu\nu} - (1-\alpha)k_\mu k_\nu/k^2]$; this will make the renormalization group equations independent of the gauge parameter α.

We are now in the position to derive the renormalization group equations which follow from the requirement that any physically observable (renormalized) quantity must be invariant under changes of μ. Referring back to eq. (3.10) we recall that $\Gamma^{(n_A,n_\psi)}$ and $Z_{A,\psi}$ depend on the renormalization scale μ, whereas $\Gamma_u^{(n_A,n_\psi)}$ is independent of μ. We now calculate $\mu\,(d/d\mu)\,\Gamma^{(n_A,n_\psi)}$ by using eq. (3.10):

$$\left(\mu\frac{\partial}{\partial\mu}+\mu\frac{\partial g}{\partial\mu}\frac{\partial}{\partial g}\right)\Gamma^{(n_A,n_\psi)}(p_i,g,\mu)=\mu\lim_{\Lambda\to\infty}\left[n_A\frac{1}{Z_A}\frac{\partial Z_A}{\partial\mu}+n_\psi\frac{1}{Z_\psi}\frac{\partial Z_\psi}{\partial\mu}\right]Z_A^{n_A}Z_\psi^{n_\psi}\Gamma_u^{(n_A,n_\psi)} \tag{3.13}$$

and define

$$\begin{aligned}\beta(g)&\equiv\lim_{\Lambda\to\infty}\mu\frac{\partial}{\partial\mu}g(g_0,\Lambda/\mu)\\ \gamma_j(g)&\equiv-\lim_{\Lambda\to\infty}\mu\frac{1}{Z_j}\frac{\partial}{\partial\mu}Z_j(g_0,\Lambda/\mu).\end{aligned} \tag{3.14}$$

The Callan–Symanzik function β and the anomalous dimensions γ_A and γ_ψ, referring to the A- and ψ-fields of the theory respectively, are dimensionless and depend therefore only on g. It should be emphasized that, according to eq. (3.14), these functions β and γ_j are intrinsic quantities of a theory and are independent of the specific Green's function (scattering amplitude) chosen. Equation (3.13) can now be rewritten in a more convenient form [26, 28]

$$\left[\mu\frac{\partial}{\partial\mu}+\beta(g)\frac{\partial}{\partial g}+n_A\gamma_A(g)+n_\psi\gamma_\psi(g)\right]\Gamma^{(n_A,n_\psi)}(p_i,g,\mu)=0 \tag{3.15}$$

which is the famous renormalization group (RG) equation of Stueckelberg, Peterman, Gell-Mann and Low, or the homogeneous Callan–Symanzik equation [27]. The physical interpretation of this equation is straightforward: for any small change in μ there exist appropriate changes in g and in the normalization Z_j of the external fields such that *any* physical quantity Γ remains unchanged.

The RG equation tells us about the behavior of a scattering amplitude for varying μ at fixed momenta p_i. The value of μ, however, also fixes the scale of momenta in the theory, and therefore the knowledge of how the Γ's react to a change of μ contains all the information on how they change when the p_i are changed at fixed μ. This translation is easily achieved by using naive dimensional analysis. If Γ has naive mass dimension d, then

$$\Gamma^{(n_A,n_\psi)}(\lambda p_i,g,\mu)=\mu^d f(\lambda^2 p_i\cdot p_j/\mu^2) \tag{3.16}$$

where λ scales the momenta up and f is a dimensionless function of kinematic invariants. Introducing the variable $t=\ln\lambda$ and differentiating Γ with respect to t and μ one obtains

$$\left[\frac{\partial}{\partial t}+\mu\frac{\partial}{\partial\mu}-d\right]\Gamma^{(n_A,n_\psi)}(\lambda p_i,g,\mu)=0 \tag{3.17}$$

which, when subtracted from eq. (3.15), gives

$$\left[-\frac{\partial}{\partial t}+\beta(g)\frac{\partial}{\partial g}+d+n_A\gamma_A(g)+n_\psi\gamma_\psi(g)\right]\Gamma^{(n_A,n_\psi)}(\lambda p_i,g,\mu)=0. \tag{3.18}$$

This equation expresses directly the effect on Green's functions of scaling up the momenta by λ. (In actual calculations this scaling parameter has to be identified with those momenta which become large; for example, for deep inelastic processes we will have $\lambda \equiv \sqrt{|q^2|/\mu^2}$.) The following simple consequences of eq. (3.18) are apparent:

(i) If all interactions are "turned off", $\beta = \gamma = 0$, then scale invariance with naive canonical dimensions holds for the massless theory (and hence asymptotically in the deep Euclidean region) and eq. (3.18) gives

$$\Gamma^{(n_A, n_\psi)}(\lambda p_i) \simeq \lambda^d. \tag{3.19}$$

(ii) If $\beta = 0$ but $\gamma_j \neq 0$, then scale invariance holds but with "anomalous dimensions"

$$\Gamma^{(n_A, n_\psi)}(\lambda p_i) \simeq \lambda^{d + n_A\gamma_A + n_\psi\gamma_\psi} \tag{3.20}$$

and therefore the $\gamma_j(g)$ are called "anomalous dimensions".

(iii) If $\beta(g) \neq 0$ and $\gamma_j(g) \neq 0$, scale invariance for the massless theory is lost completely. In this case the general solution of eq. (3.18) can be obtained in the following way. For brevity, let us first write eq. (3.18) in the form

$$[-\partial/\partial t + \beta(g)\, \partial/\partial g + \gamma(g)]\Gamma(\lambda p, g) = 0 \tag{3.21}$$

which is conveniently solved in two steps. First we solve the equation

$$(-\partial/\partial t + \beta\, \partial/\partial g)\phi = 0.$$

The solution is

$$\phi = \phi(\bar{g}(g, t)) \tag{3.22}$$

where $\bar{g}$ satisfies the ordinary differential equation

$$\mathrm{d}\bar{g}(g, t)/\mathrm{d}t = \beta(\bar{g}) \tag{3.23}$$

subject to the boundary condition $\bar{g}(g, t = 0) = g$. This equation describes the change of the "effective coupling" $\bar{g}$ when changing the distance $R \sim 1/p$ between two particles. The fact that (3.22) is a solution of the homogeneous equation can be checked by noting that solutions with different g's are related by a translation of the origin in t

$$\bar{g}(g + \delta g, t) = \bar{g}(g, t + \delta t):$$

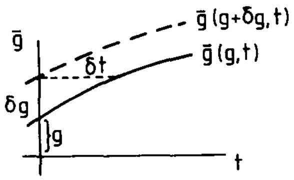

where $\delta g = \beta(g)\,\delta t$, so that

$$\mathrm{d}\bar{g}/\mathrm{d}t = \beta(g)\, \mathrm{d}\bar{g}/\mathrm{d}g$$

which implies

$$\left[-\frac{\partial}{\partial t}+\beta(g)\frac{\partial}{\partial g}\right]\phi(\bar{g})=\left[-\frac{\partial \bar{g}}{\partial t}+\beta(g)\frac{\partial \bar{g}}{\partial g}\right]\frac{\partial\phi(\bar{g})}{\partial \bar{g}}=0.$$

The general solution of the complete RG equation (3.21) is then obviously given by

$$\Gamma(\lambda p, g)=\Gamma(p,\bar{g})\exp\left[\int_0^t \gamma(\bar{g}(g,t'))\,\mathrm{d}t'\right]=\Gamma(p,\bar{g})\exp\left[\int_g^{\bar{g}}\frac{\gamma(g')}{\beta(g')}\mathrm{d}g'\right] \tag{3.24}$$

which is the famous prediction of the RG for the ultraviolet (large λ) momentum dependence of Green's functions, and will be the basic starting point, together with eq. (3.23), for our studies of scaling violations in deep inelastic reactions. Thus the large-λ behavior of a scattering amplitude is controlled by the effective coupling constant $\bar{g}(g,t)$ and the anomalous dimension $\gamma(\bar{g})$ in the renormalization group exponent of eq. (3.24). This exponent, being an asymptotic series [28] in all leading logarithms and in all orders of g (see for example eq. (3.1)), is uniquely determined by calculating β and γ in lowest order (1-loop) of perturbation theory, provided of course $\bar{g}$ is small. Therefore, the only requirement for our RG improved perturbation theory to be useful for practical calculation is, that the effective coupling $\bar{g}$ satisfies

$$\bar{g}^2 \ll 1$$

(or more precisely the effective expansion parameter $\bar{g}^2/4\pi^2$ must be small), whereas all large logarithms, such as in eq. (3.1), are automatically taken care of by the RG exponent in eq. (3.24). This is in contrast to conventional order-by-order perturbation theory where a perturbation expansion makes sense only if

$$g^2 \ll 1, \qquad g^2 \ln q^2/\mu^2 \ll 1, \ldots.$$

because of the appearance of large logarithms in each order of the perturbation series in (3.1).

To summarize, the renormalization group enables us to compute *all* the leading logarithms to *all* orders of g in any Green's function [28], just from the *first* non-trivial (1-loop) order in perturbation theory in g. Likewise, by going to the next order in g, we can get *all* the next-to-leading logarithms, etc.

4. The effective coupling constant $\bar{g}$

In order to calculate the large (ultraviolet) momentum dependence of scattering amplitudes as given by the RG solution in eq. (3.24), we first need to know the effective coupling $\bar{g}$. This can be obtained by calculating $\beta(g)$ in lowest 1-loop order, $\beta(g)\sim g^3+\mathcal{O}(g^5)$, and then solving the RG equation (3.23) $\mathrm{d}\bar{g}/\mathrm{d}t=\beta(\bar{g})$. This we will do first for the case of QCD and then, for comparison, we will briefly discuss other possible field theories of strong interactions and QED.

4.1. $\bar{g}$ in QCD: asymptotic freedom

Provided there is a value of the normalization point μ for which the effective expansion parameter $g^2/4\pi^2 \ll 1$, the β function, defined in eq. (3.14) as the variation of the renormalized coupling g with μ, may be evaluated perturbatively from the corresponding diagrams contributing in lowest non-trivial order to $\Gamma^{(n_A, n_\psi)}$. This well known result [24] can be derived most easily in the Landau gauge ($\alpha = 0$) where one obtains [1]

$\Gamma^{(2,0)} =$ 

$$= (-g_{\mu\nu}p^2 + p_\mu p_\nu)\left[1 + \left(\frac{13}{6}C_2(G) - \frac{4}{3}T(R)\right)\frac{g^2}{16\pi^2}\ln\frac{-p^2}{\mu^2}\right]$$

$\Gamma^{(0,2)} =$ 

$$= \not p + \mathcal{O}(g^4) \tag{4.1}$$

$\Gamma^{(1,2)} =$ 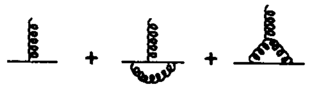

$$= gT_a\gamma_\mu\left[1 - \frac{3}{4}C_2(G)\frac{g^2}{16\pi^2}\ln\frac{-p^2}{\mu^2}\right]$$

where we have kept only the physical transverse polarization part of $\Gamma^{(2,0)}$, and the inverse propagators have been calculated for momentum configurations $(p_1, p_2) = (-p, p)$ and the three-point function for $(p_1, p_2, p_3) = (0, -p, p)$. The dashed line in $\Gamma^{(2,0)}$ refers to the gauge-fixing Feynman–Faddeev–Popov ghosts [1, 24], whereas the lowest-order self-energy diagram in $\Gamma^{(0,2)}$ does not contribute in the Landau gauge $\alpha = 0$. Inserting the various Green's functions of eq. (4.1) into the renormalization group equation (3.15) and then evaluating at $p^2 = -\mu^2$ yields

$$\gamma_A = \left[\frac{13}{6}C_2(G) - \frac{4}{3}T(R)\right]\frac{g^2}{16\pi^2} + \mathcal{O}(g^4)$$

$$\gamma_\psi = 0 + \mathcal{O}(g^4)$$

$$\beta = -\left[\gamma_A + 2\gamma_\psi + 2\frac{3}{4}C_2(G)\frac{g^2}{16\pi^2}\right]g = -\left[\frac{11}{3}C_2(G) - \frac{4}{3}T(R)\right]\frac{g^3}{16\pi^2}. \tag{4.2}$$

The group theoretic color factors derive from the basic building blocks $(T_a)_{jk}$ and f_{abc} of the non-abelian Yang–Mills interaction in eqs. (2.2)–(2.4) and are related to the following vertices:

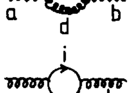

$$= \sum_{c,d=1}^{8} f_{acd}f_{bcd} \equiv C_2(G)\delta_{ab}$$

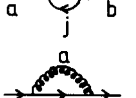

$$= \sum_{i,j=1}^{3}(T_a)_{ji}(T_b)_{ij} = \mathrm{Tr}(T_aT_b) \equiv T(R)\delta_{ab} \tag{4.3}$$

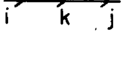

$$= \sum_{a=1}^{8}\sum_{k=1}^{3}(T_a)_{ik}(T_a)_{kj} = \sum_{a=1}^{8}(T_aT_a)_{ij} \equiv C_2(R)\delta_{ij}$$

where we have written only the color content of each diagram. For $G = \mathrm{SU}(3)_c$ and R denoting the fundamental (color) triplet representation, and for a flavor $\mathrm{SU}(N_f)$ group these color factors are given by

$$C_2(G) = 3, \qquad C_2(R) = \tfrac{4}{3}, \qquad T(R) = \tfrac{1}{2}N_f = \begin{cases} \tfrac{3}{2} & \text{for u, d, s} \\ 2 & \text{for u, d, s, c.} \end{cases} \tag{4.4}$$

This allows us to calculate the final leading order result for the β-function in eq. (4.2)

$$\beta(g) = -\frac{1}{16\pi^2}\left[\frac{33}{3} - \frac{2}{3}N_f\right]g^3 \equiv -bg^3. \tag{4.5}$$

The important result is that $\beta(g)$ is *negative* for sufficiently small g as long as $N_f \leq 16$ (for the time being we have experimental evidence for five quark flavors $N_f = 5$: u, d, s, c, b, . . . ?). This unique feature of a locally gauge invariant non-abelian vector gluon theory is entirely due to the *triple*-gluon-vertex contributions in (4.1), i.e., the term proportional to $C_2(G)$ in $\beta(g)$, which does not exist in any other known field theory [25]. Inserting eq. (4.5) into the renormalization group equation (3.23), $\mathrm{d}\bar{g}/\mathrm{d}t = \beta(\bar{g})$, and solving for the effective "running coupling" $\bar{g}$ yields

$$\bar{g}^2(t) = \frac{g^2}{1 + 2bg^2 t}. \tag{4.6}$$

Because of the *positive* sign in the denominator, a direct consequence of β being *negative*, we can take the ultraviolet (UV) limit $t = \ln\lambda \to +\infty$ which implies

$$\bar{g}^2(t) \to 0 \quad \text{for} \quad t \to +\infty, \tag{4.7}$$

i.e. "*asymptotic freedom*": the larger the scale parameter λ, i.e. the larger the momenta, or the smaller the distance between two particles, the smaller becomes $\bar{g}$ and thus the more reliable perturbation theory becomes for strong interactions! This is the enormous advantage and beauty of the locally gauge invariant field theory QCD. Asymptotically the theory becomes a free field theory and therefore the origin $\bar{g} = 0$ is called "UV fixed point".

Let us rewrite eq. (4.6) in a more convenient form. Since λ is an arbitrary parameter to be identified with the large momentum scale of a given process, we choose $\lambda = \sqrt{Q^2/\mu^2}$ appropriate for deep inelastic processes where the momentum transfer squared from the leptonic to the hadronic system $Q^2 \equiv -q^2 > 0$ constitutes the only large momentum scale of the problem. Therefore, eq. (4.6) gives, for $t = \ln\lambda \equiv \frac{1}{2}\ln(Q^2/\mu^2)$,

$$\bar{g}^2(Q^2) = \frac{g^2}{1 + bg^2\ln(Q^2/\mu^2)} \equiv \frac{1}{b\ln(Q^2/\Lambda^2)} \tag{4.8}$$

with $\Lambda^2 = \mu^2\exp(-1/bg^2)$ and $g = \bar{g}(Q^2 = \mu^2)$. Using eq. (4.5) gives us the final result for the "strong fine structure constant"

$$\alpha_s(Q^2) \equiv \frac{\bar{g}^2(Q^2)}{4\pi} = \frac{12\pi}{(33-2N_f)\ln(Q^2/\Lambda^2)} = \begin{cases} \dfrac{12\pi}{27\ln(Q^2/\Lambda^2)} & \text{flavor SU(3)} \\[2ex] \dfrac{12\pi}{25\ln(Q^2/\Lambda^2)} & \text{flavor SU(4)} \end{cases} \tag{4.9}$$

with Λ being the *only free* parameter of QCD which has to be fixed by experiment. However, it is possible to set some a priori limits [31]. From eq. (4.9) it is clear that Λ is the value at which α_s becomes large and perturbation theory breaks down. We know that for $Q^2 \simeq \langle r_p^2\rangle^{-1} \simeq (0.8\,\text{fermi})^{-2} \lesssim (0.3\,\text{GeV})^2$, the typical scale of the intrinsic transverse momentum in the parton wave function, the strong interactions must indeed be strong, for they must provide for quark binding not amenable to a perturbative analysis. On the other hand, approximate (precocious) scaling is observed in deep inelastic lepton–nucleon scattering processes at $Q^2 \simeq 2\,\text{GeV}^2$, implying that the effective coupling

$$\alpha_s(2\,\text{GeV}^2)/\pi \ll 1 .$$

Since we know the behavior of $\alpha_s(Q^2)$ for small α_s, these two requirements limit Λ to the range

$$0.2\,\text{GeV} \lesssim \Lambda \lesssim 0.7\,\text{GeV} \tag{4.10}$$

as can be seen by inspection of fig. 4.1 which shows $\alpha_s(Q^2)$ as a function of Q^2 for different values of Λ.

It is now straightforward to calculate the momentum dependence of scattering amplitudes as predicted by the RG in eq. (3.24) when the momenta are changed by $p \to \lambda p$. Using eq. (4.6), the RG

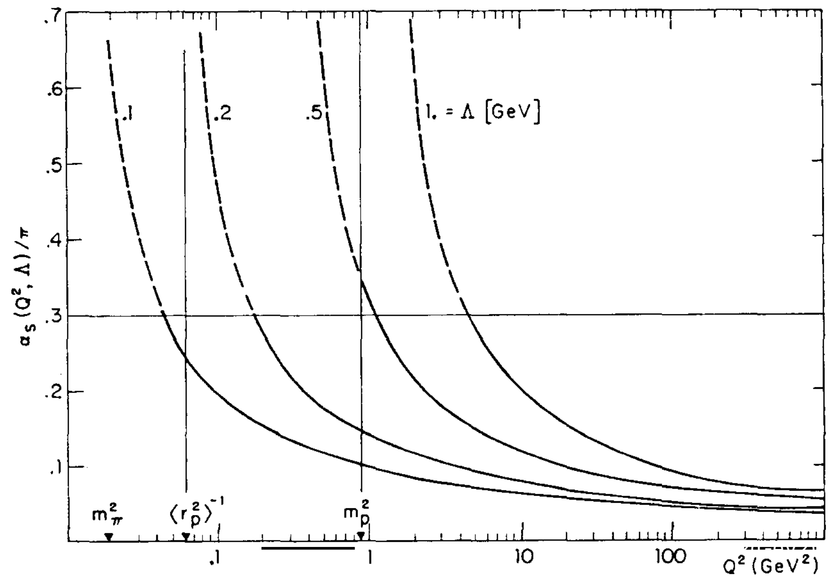

Fig. 4.1. α_s/π as a function of Q^2 for various values [31] of Λ.

exponent in (3.24) becomes

$$\exp\left[\int_0^t \gamma(\bar{g}(t'))\,\mathrm{d}t'\right] = \exp\left[cg^2 \int_0^t \frac{\mathrm{d}t'}{1+2bg^2t'}\right] = \left(\frac{g^2}{\bar{g}^2}\right)^{c/2b} \tag{4.11}$$

where we have set $\gamma(g) = cg^2$ with c calculable perturbatively as we shall see later. Thus, eq. (3.24) yields

$$\Gamma(\lambda p, g) = \Gamma(p, \bar{g})\,[g^2/\bar{g}^2]^a \qquad \text{with} \quad a = c/2b. \tag{4.12}$$

Since $[g^2/\bar{g}^2]^a \sim [\ln \lambda]^a$, the Green's functions depend *logarithmically* on the momentum scale, which is so very typical for an asymptotically free theory (QCD)!

To summarize, we have found that for sufficiently small g the Callan–Symanzik β-function is *negative* for a non-abelian gauge theory (QCD)

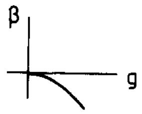

and therefore $g = 0$ is a UV stable fixed point since the "running coupling" $\bar{g}(t)$ decreases ($\mathrm{d}\bar{g}/\mathrm{d}t < 0$) for increasing momenta or the smaller the distance $R \sim 1/\sqrt{Q^2}$ between two particles becomes:

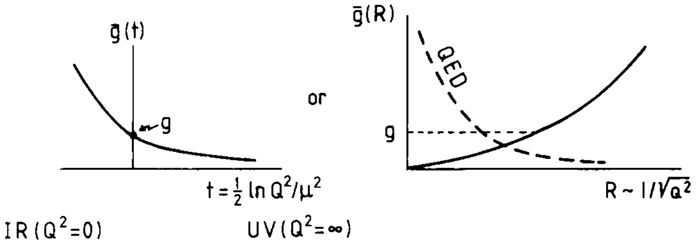

where for comparison we also show the opposite behavior of $\bar{g}$ as expected in conventional field theories such as QED. The infrared (IR) long-distance region, where $\bar{g}$ increases, is obviously not accessible to perturbation theory and is usually referred to as the "confinement region" ($\alpha_s \gtrsim 1$). On the other hand, the small distance region (Q^2 large) will prove to be a unique perturbative test-ground for QCD – a region where deep inelastic or "hard" processes are operative, such as lepton–nucleon scattering, Drell–Yan processes, high-p_T reactions etc.

Qualitatively, the asymptotic freedom behavior of QCD can be understood in a simple intuitive way [32]. QCD can be viewed as an extension of QED in which the vector field carries (color) charge and, in contrast to *all* other conventional field theories, due to the local gauge invariance there exist self-interactions of these vector fields as in eq. (2.5) which allow for a charge transfer from the field ψ to the field A_a^μ and vice versa. Thus we find two opposite effects which contribute to g. On the one hand the bare (color) charge g_0(>0) will produce a vacuum polarization of the same type as in QED: this will induce a "*negative*" (color) charge density in the neighborhood ($R < m^{-1}$) of g_0 as shown in fig. 4.2(a).

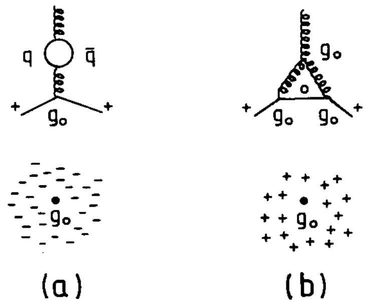

Fig. 4.2. Quantum corrections contributing to g: (a) vacuum polarization; (b) charge exchange with field (exists only in non-abelian Yang–Mills theories).

On the other hand, the gluon self-couplings also produce a charge exchange between the source g_0 and the field surrounding it, as shown in fig. 4.2(b). This effect produces a "*positive*" (color) charge density in the neighborhood of g_0. This virtual charge creation is of the *same* sign as g_0 and is therefore called "anti-shielding". There is no simple way to show which of the two effects is the stronger one. As discussed above, only a detailed calculation reveals that the positive charge density wins, except in cases where there are a large number of different flavor ψ fields ($N_f > 16$ in lowest order perturbation theory) which can be virtually created via the vacuum polarization in fig. 4.2(a) – an understandable effect. Since the total charge is fixed, the bare charge must vanish at the centre in fig. 4.2(b); the theory is asymptotically free.

4.2. *The effective coupling in QED and the "rest of the world" (fixed point field theories)*

Usually the complication of a Q^2 dependent coupling does not concern us in QED because the rate of change ($\sim \alpha \ln Q^2$) is very small. Since all other possible known field theories of strong interactions have, except QCD, the same basic structure with respect to the virtual quantum corrections as QED, it is instructive to study the well known case of QED first. In electrodynamics the physical coupling e, or $\alpha \equiv e^2/4\pi$, is defined by the large distance behavior of the electric potential (Thomson limit) $V = -\alpha/R$ for $R \gg m_e^{-1} \simeq 10^{-11}$ cm with R being the distance between the two charges $+e$ and $-e$. This charge e is smaller than the effective coupling constant $\bar{e}$ one would measure at small distances $R \ll m_e^{-1}$, due to the presence of vacuum polarization effects as shown in fig. 4.2(a) and since no anti-shielding effects (triple gluon vertex) as shown in fig. 4.2(b) exist. The vacuum polarization gives the famous Uehling-correction to Coulomb's law for $R \ll m_e^{-1}$:

$$V(R) = -\frac{\alpha}{R}\left[1 + \frac{2\alpha}{3\pi}\ln\frac{1}{m_e R} + \mathcal{O}(\alpha^2)\right] \equiv -\frac{\bar{\alpha}(R)}{R} \tag{4.13}$$

which, in lowest non-trivial order, describes the potential of two interacting charges whose virtual vacuum polarization clouds overlap. The leading logarithmic term obtained in lowest order perturbation theory in the effective coupling

$$\bar{\alpha}(R) = \alpha\left[1 + \frac{2\alpha}{3\pi}\ln\frac{1}{m_e R} + \cdots\right] > \alpha \tag{4.14}$$

can be summed to all orders by simply using our renormalization group equation (3.23): From eq. (4.2) we can read off the β function for QED where $C_2(G) \equiv 0$ and $T(R) = 1$ (since we have only one fermion field):

$$\beta_{\mathrm{QED}} = +\frac{4}{3}\frac{e^3}{16\pi^2} \tag{4.15}$$

which upon inserting into $\mathrm{d}\bar{e}/\mathrm{d}t = \beta(\bar{e})$ yields

$$\bar{\alpha}(t) = \frac{\alpha^2}{1 - 2(\alpha/3\pi)t} \tag{4.16}$$

with $t = \ln(1/m_e R) \equiv \ln\sqrt{Q^2/m_e^2}$. Thus, in contrast to the effective QCD coupling in eq. (4.6), we have a *negative* sign in the denominator of eq. (4.16) because of β_{QED} being *positive* for sufficiently small e in eq. (4.15), and therefore $e = 0$ is *not* UV stable (for $t \to \infty$ or $R \to 0$) but instead IR stable since $\mathrm{d}\bar{e}/\mathrm{d}t > 0$ as illustrated in fig. 4.3. Nonetheless, in the case of QED perturbation theory is applicable and meaningful even in the UV region (large momentum transfers Q^2 or small distances R) because of the smallness of α: The first few terms in the perturbation expansion (4.13) should suffice unless R is as small as $m_e^{-1}\exp(-3\pi/2\alpha) \simeq 10^{-291}$ cm [or $\sqrt{Q^2}$ less than 10^{277} GeV], a ridiculously small distance. In fact, we have no reason to believe that at such distances quantum electrodynamics has any validity whatsoever, particularly when interactions of the electromagnetic field with particles other than the electron are ignored.

The positivity of the β-function near the origin as well as the asymptotically non-free behavior of the effective coupling constant as illustrated in fig. 4.3 is basically the same for all conventional field theories [25] which might be alternatives for describing fundamental strong interactions [33–35]. Although theoretically far less appealing and elegant, examples for conventional (asymptotically non-free) strong interaction field theories are as follows (for reasons discussed in section 1 we always stick to *three* colors of a given quark flavor):

(i) An abelian vector-gluon theory (non-colored gluons) with an interaction similar to QED, i.e., $g\bar{\psi}\gamma_\mu\psi A^\mu$. In this case we have:

$$C_2(G) \equiv 0, \qquad C_2(R) = 1, \qquad T(R) = 3N_f. \tag{4.17}$$

The β-function, as given in eq. (4.2), is then positive.

(ii) Non-abelian scalar-gluon theories with an interaction term proportional to $g\bar{\psi}\lambda_a\psi\phi_a$ and where the group invariants are given by

$$C_2(G) \equiv 0, \qquad C_2(R) = \tfrac{4}{3}, \qquad T(R) = \tfrac{1}{2}N_f. \tag{4.18}$$

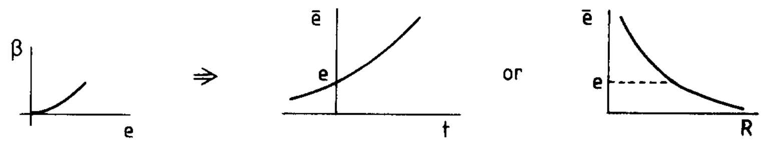

Fig. 4.3. The β-function and the effective coupling in QED. The same qualitative feature holds for all other conventional field theories.

(iii) Abelian (Yukawa) scalar-gluon theories with an interaction $g\bar{\psi}\gamma\psi\phi$ have "group invariants" as given in eq. (4.17). The Callan–Symanzik function for scalar-gluon theories is then given by [36]

$$\beta_{\text{scalar}} = +5T(R)\, g^3/16\pi^2. \tag{4.19}$$

Thus, to lowest order, the effective coupling of conventional field theories behaves as in eq. (4.16), i.e. $\bar{g}^2(t) = g^2/(1-2bg^2t)$, since $\beta = +bg^2 > 0$, which should be compared with the QCD coupling in eq. (4.6). Clearly, $\bar{g}$ is IR stable since only the limit $t \to -\infty$ ($Q^2 \to 0$) exists. Nevertheless, these theories could in principle be also applied to deep inelastic processes in the presently measured range of Q^2 without any additional assumptions as those made in QCD, provided one chooses μ and g such that $\bar{g}^2/16\pi^2$ is small (in this case $\bar{g}$ is only slightly increasing for $Q^2 \lesssim 200\,\text{GeV}^2$). In order to study the true asymptotic behavior of these theories one has of course to assume that the UV limit $t \to +\infty$ ($Q^2 \sim 1/R^2 \to \infty$) exists, which means that there exists a finite UV stable fixed point g^*, i.e. $\beta(g^*) = 0$, such that the effective perturbation expansion parameter $g^{*2}/16\pi^2 \ll 1$, in order to account for the approximate scaling observed in deep inelastic reactions. Since $\mathrm{d}\bar{g}/\mathrm{d}t = \beta(\bar{g})$, any value of g in the vicinity of g^* will approach g^* asymptotically, $\lim_{t\to+\infty} \bar{g}(t) = g^*$, as shown in fig. 4.4. We have therefore a similar situation as in QCD, namely that perturbation theory becomes better the larger Q^2, provided $g^{*2}/16\pi^2$ is small. Of course, these conventional field theories are asymptotically *non*-free because $g^* \neq 0$, and therefore the name "fixed point theories".

Apart from the ϕ^4 theory [37], the fixed point structure of quantum field theories is an entirely unsolved and unclear matter [3, 37]. For phenomenological purposes we will therefore simply assume the existence of a finite ultraviolet fixed point g^*, and look how conventional field theories compare with experiment. However, it should be noted that any quantitative calculation requires the approximation $\gamma(g^*) = \sum_{n=1}^{\infty} c_n g^{*2n} \simeq c_1 g^{*2}$, although higher-order terms are certainly important in the perturbative expansion of $\beta(g) = \sum_{n=1}^{\infty} b_n g^{2n+1}$ at $g = g^*$ since cancellations between different orders are needed to get $\beta(g^*) = 0$. It should be emphasized that only $g^{*2}/16\pi^2 \ll 1$ will be used throughout our analysis to be discussed later.

Again, as in the case of QCD, it is now simple to calculate the momentum dependence of scattering amplitudes according to eq. (3.24) for conventional field theories at fixed $g = g^*$. Defining $\gamma(g) = cg^{*2}$, the RG exponent in (3.24) is simply

$$\exp\left[\int_0^t \gamma(\bar{g}(t'))\,\mathrm{d}t'\right] = \exp[cg^{*2}t]$$

and thus

$$\Gamma(\lambda p, g) = \Gamma(p, g^*)[\lambda^2]^a \qquad \text{with} \quad a = \tfrac{1}{2}cg^{*2} \tag{4.20}$$

which, contrary to the QCD result in eq. (4.12), gives a *power-like* dependence on $\lambda^2 \sim Q^2/\mu^2$.

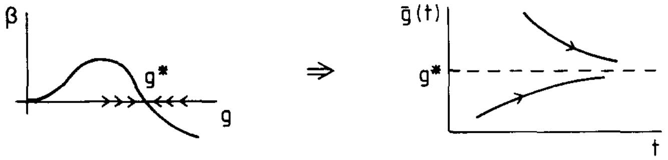

Fig. 4.4. The UV behavior of the effective coupling of conventional field theories, provided there exists a fixed point g^* in β.

We are now equipped with most of the theoretical artillery in order to confront renormalization group improved quantum field theories with experiment. The ideal reactions for applying this formalism are deep inelastic lepton–nucleon scattering processes where Q^2 is large, i.e. $\alpha_s(Q^2)$ small, and therefore calculations based on RG improved perturbation theory should become reliable. As we shall see in the next section all conventional fixed point theories are strongly disfavored by experiment. However, it should be emphasized that all present measurements of scaling violations in structure functions are rather insensitive to the gluon content of the nucleon and therefore also to the gluon self-couplings (triple gluon vertex) which are so very essential for asymptotic freedom.

5. Deep inelastic lepton–nucleon scattering

When a very low mass virtual photon ($Q^2 \equiv -q^2 \ll 1\,\mathrm{GeV}^2$) scatters off a proton, the photon "sees" only the total charge and magnetic moment of the proton and the scattering appears point-like (fig. 5.1(a)). A higher-mass photon of (a few hundred MeV)^2 is able to resolve the individual constituents of the proton's virtual pion cloud, as shown in fig. 5.1(b), and the proton appears as a composite extended object. At high momentum transfers the photon probes the fine structure of the proton charge distribution and sees its elementary constituents (fig. 5.1(c)); if quarks were non-interacting, no further structure would appear for increasing Q^2 and exact scaling would set in. However, in any renormalizable quantum field theory, we have to introduce a Bose-field (gluon) which mediates the interaction in order to form for example bound states of quarks, i.e. the observed hadrons. In such a picture, the quark is then always accompanied by a gluon cloud which will be probed as the momentum transfer is increased. The effect of gluons is then two-fold as illustrated in fig. 5.1(d): A quark carrying a fraction x of the longitudinal momentum of the proton will be seen by the high-Q^2 virtual photon with a momentum fraction *smaller* than x, just because the radiated gluon carries away some of the quark's original momentum; similarly this photon may resolve the radiated gluon into a quark–antiquark pair – a process to be regarded as quark pair creation in the strong gluon field of the nucleon. Both effects will distort a given nucleon structure function $F(x)$ to lower x, and specifically quark pair

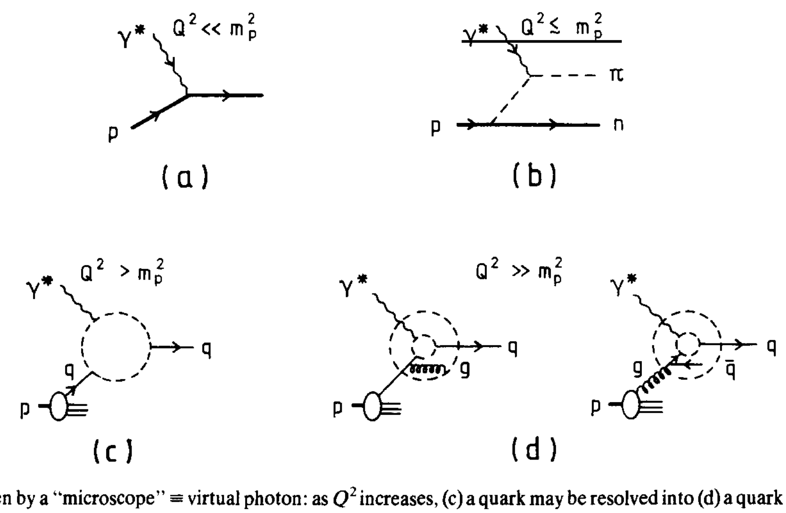

Fig. 5.1. The proton as seen by a "microscope" ≡ virtual photon: as Q^2 increases, (c) a quark may be resolved into (d) a quark and bremsstrahlung gluon g or into a quark–antiquark pair.

creation will enhance the sea contribution at small x. It will be our aim in this section to calculate these effects quantitatively: Thus, for a given wave function $F(x)$ of the nucleon (or pion), we have to calculate its dependence on Q^2, $F(x, Q^2)$, from radiative corrections as depicted in fig. 5.1(d). These effects are usually referred to as "*scaling violations*". (Note that, because of our confinement hypothesis, all fundamental constituent interactions such as in fig. 5.1(d) are supposed to take place in a region $R \lesssim \frac{1}{5} \times 10^{-13}$ cm.)

Before going into the rather involved field theoretic evaluation of scaling violations, we will first briefly recapitulate the basic ideas of the naive parton model.

The cross section for the deep inelastic scattering process $\ell + \mathrm{N} \to \ell' + \mathrm{X}$ can be formally written as

$$d\sigma \sim \sum_X \left| \quad \right|^2 = L^{\mu\nu} W_{\mu\nu} \qquad (5.1)$$

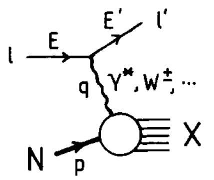

where ℓ and ℓ' are leptons, and the square of the trivial leptonic vertex in (5.1) is given by [38] $L^{\mu\nu}$, whereas the hadronic tensor $W_{\mu\nu}$ describes the strong interaction dynamics explored by this process as shown, for example, in figs. 5.1 (c) and (d). General invariance principles tell us [5, 38] that the dimensionless tensor $W_{\mu\nu}$ can be decomposed into the following structure functions (the covariant normalization of states is $\langle p'|p\rangle = 2p_0\delta^3(\boldsymbol{p}' - \boldsymbol{p})$)

$$\begin{aligned} W_{\mu\nu} &= \frac{1}{4\pi} \sum_X (2\pi)^4 \delta^4(p + q - p_X) \langle p|J^+_\mu(0)|X\rangle \langle X|J_\nu(0)|p\rangle \\ &= \frac{1}{4\pi} \int d^4z \; e^{iq\cdot z} \langle p|J^+_\mu(z) J_\nu(0)|p\rangle \\ &= \frac{1}{4\pi} \int d^4z \; e^{iq\cdot z} \langle p|[J^+_\mu(z), J_\nu(0)]|p\rangle \\ &\equiv \left(-g_{\mu\nu} + \frac{q_\mu q_\nu}{q^2}\right) W_1 + \frac{1}{m_N^2}\left(p_\mu - \frac{p\cdot q}{q^2} q_\mu\right)\left(p_\nu - \frac{p\cdot q}{q^2} q_\nu\right) W_2 - i\frac{\varepsilon_{\mu\nu\alpha\beta} p^\alpha q^\beta}{2m_N^2} W_3 \end{aligned} \qquad (5.2)$$

where the spectral-condition (energy-momentum conservation) allowed us to replace the product $J^+_\mu(z) J_\nu(0)$ by a commutator, and W_3 contributes only to neutrino scattering since it describes parity violating effects which arise from a vector and axial-vector interference. In general we have $W_i = W_i(\nu, Q^2)$, with the kinematical variables defined by

$$Q^2 \equiv -q^2 = \boldsymbol{q}^2 - q_0^2 \geq 0, \qquad \nu = p \cdot q/m_N = E - E'. \qquad (5.3)$$

The inclusive differential cross section for electroproduction (in the one-photon approximation) then reads

$$\frac{d\sigma}{dQ^2 \, d\nu} = \frac{4\pi\alpha^2}{m_N Q^4} \frac{E'}{E} \left[2W_1 \sin^2\frac{\theta}{2} + W_2 \cos^2\frac{\theta}{2}\right] \qquad (5.4)$$

and in the case of neutrino or antineutrino scattering, i.e. $\nu(\bar{\nu})+\mathrm{N}\to\mu^-(\mu^+)+\mathrm{X}$, we have

$$\frac{d\sigma^{\nu(\bar{\nu})}}{dQ^2\,d\nu}=\frac{G_F^2}{2\pi m_N}\frac{E'}{E}\left(\frac{M_w^2}{Q^2+M_w^2}\right)^2\left[2W_1\sin^2\frac{\theta}{2}+W_2\cos^2\frac{\theta}{2}\,(\mp)\,\frac{E+E'}{m_N}W_3\sin^2\frac{\theta}{2}\right] \tag{5.5}$$

where M_w is the intermediate vector boson mass and $Q^2=4EE'\sin^2\theta/2$. For many practical purposes it proves convenient to introduce new dimensionless variables defined by

$$x\equiv\frac{Q^2}{2m_N\nu}\equiv\frac{1}{\omega},\qquad y\equiv\frac{\nu}{E}=\frac{E-E'}{E}=\frac{E_X-m_N}{E} \tag{5.6}$$

where x is the famous Bjorken scaling variable with $0\le x\le 1$, and y is the fractional energy transferred to the hadronic system. Note that $x=1$ corresponds to elastic scattering since in this case the total invariant hadronic energy $W=m_N$, where W is defined by

$$W^2=(p+q)^2=m_N^2+Q^2(1/x-1). \tag{5.7}$$

In the deep inelastic region (Q^2, $m_N\nu$, $W^2\gg m_N^2$ with x fixed) we encounter the naive Bjorken scaling [39] which says that the dimensionless quantities W_1, $\nu W_2/m_N$ and $\nu W_3/m_N$ approach nontrivial functions of only *one* variable x:

$$W_1(\nu,Q^2)\to F_1(x),\qquad \frac{\nu}{m_N}W_{i=2,3}(\nu,Q^2)\to F_i(x) \tag{5.8}$$

for Q^2, $\nu\to\infty$ with x fixed. The naive parton model is defined in this deep inelastic region (based on the impuls approximation idea [40]) with the electromagnetic and weak currents defined in terms of the fundamental quark fields ψ_q by

$$J_\mu^{em}=\tfrac{2}{3}\bar{\psi}_u\gamma_\mu\psi_u-\tfrac{1}{3}\bar{\psi}_d\gamma_\mu\psi_d-\tfrac{1}{3}\bar{\psi}_s\gamma_\mu\psi_s+\cdots \tag{5.9}$$

$$J_\mu^{weak}=\cos\theta_c\,\bar{\psi}_u\gamma_\mu(1-\gamma_5)\psi_d+\sin\theta_c\,\bar{\psi}_u\gamma_\mu(1-\gamma_5)\psi_s+\cdots \tag{5.10}$$

where the dots indicate all possible new heavy quark (c, b, ...) contributions which go beyond the conventional SU(3) quarks, and the Cabibbo angle is $\sin\theta_c\simeq 0.23$. The hadronic part of the process in (5.1) is now viewed as an incoherent scattering of the virtual photon (or $W^\pm$) off the fermionic constituents in the hadron

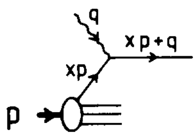

where the fractional momentum x carried by the quarks is defined in eq. (5.6). The total hadronic tensor $W_{\mu\nu}$ in (5.1) is then directly related to the "hand-bag" diagram as shown in fig. 5.2. Cranking through

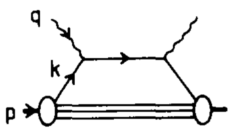

Fig. 5.2. Deep inelastic scattering in the (naive) parton model: The hand-bag diagram.

this hand-bag diagram one finds [5, 38] for electro(muo)production

$$F_2^{eN} = x \sum_q e_q^2 [q(x) + \bar{q}(x)]$$

with an obvious interpretation according to fig. 5.2, and where the quark distribution $q(x)$ in the nucleon is formally defined, apart from the trivial Lorentz structure in eq. (5.2), by (Fourier transformation is always implied)

$$\langle p|\bar{\psi}_q \psi_q|p\rangle = q + \bar{q}. \tag{5.11}$$

Thus $q(x)\,dx$ is the expectation value of the number of quarks of type q having fractional momentum between x and $x + dx$. More specifically we get for the proton (~uud) and neutron (~udd) structure functions

$$\begin{aligned} F_2^{ep} &= \tfrac{4}{9}x(u + \bar{u}) + \tfrac{1}{9}x(d + \bar{d}) + \tfrac{1}{9}x(s + \bar{s}) + \cdots \\ F_2^{en} &= F_2^{ep}(\text{with } u \leftrightarrow d), \end{aligned} \tag{5.12}$$

and the corresponding structure functions for neutrino and antineutrino scattering through the current (5.10) are

$$\begin{aligned} F_2^{\nu p} &= 2x(d + \bar{u}) + \cdots = F_2^{\bar{\nu} n} \\ F_2^{\nu n} &= 2x(u + \bar{d}) + \cdots = F_2^{\bar{\nu} p} \\ F_3^{\nu p} &= 2(\bar{u} - d) + \cdots = F_3^{\bar{\nu} n} \\ F_3^{\nu n} &= 2(\bar{d} - u) + \cdots = F_3^{\bar{\nu} p} \end{aligned} \tag{5.13}$$

and it is a child's play to extend the parton calculations to heavy quarks [41] (indicated by dots).

An immediate consequence of the spin-$\frac{1}{2}$ structure of quarks is [5, 38] the famous Callan–Gross relation [42] (helicity conservation)

$$F_2(x) = 2xF_1(x) \tag{5.14}$$

which is an exact relation only if there are no strong interactions between the quarks in fig. 5.2 (free parton model). (On the contrary, spin-0 partons would imply $F_1(x) = 0$.) Because of charge, isospin, baryon- and strangeness-number conservation the quark distributions must satisfy the following general sum rule constraints

$$\int_0^1 (\mathrm{u}-\bar{\mathrm{u}})\,\mathrm{d}x = 2, \qquad \int_0^1 (\mathrm{d}-\bar{\mathrm{d}})\,\mathrm{d}x = 1, \qquad \int_0^1 (\mathrm{s}-\bar{\mathrm{s}})\,\mathrm{d}x = 0. \tag{5.15}$$

Furthermore, since $\int_0^1 x\,q(x)\,\mathrm{d}x$ is the total fraction of the momentum carried by quarks of type q, momentum conservation tells us that

$$\sum_q \int_0^1 \mathrm{d}x\, x[q(x)+\bar{q}(x)] = 1-\varepsilon \tag{5.16}$$

with $\varepsilon = 0$ if quarks and antiquarks are the only constituents of the nucleon. Experimentally, however, we have [43–45] $\varepsilon \simeq 0.5$ and hence not all the nucleon's momentum is carried by (fermionic) quarks and antiquarks; within QCD it will be natural to expect the gluons to carry these remaining 50% of the momentum. Further very important relations between structure functions are provided by the Adler sum rule [46]

$$\int_0^1 \frac{\mathrm{d}x}{2x}(F_2^{\bar{\nu}\mathrm{p}} - F_2^{\nu\mathrm{p}}) = \int_0^1 \mathrm{d}x\,(\mathrm{u}-\bar{\mathrm{u}}-\mathrm{d}+\bar{\mathrm{d}}) = 2I_3 = 1, \tag{5.17}$$

the Gross–Llewellyn Smith sum rule [47]

$$\begin{aligned}\int_0^1 \mathrm{d}x\,(F_3^{\nu\mathrm{p}} + F_3^{\bar{\nu}\mathrm{p}}) &= -2\int_0^1 \mathrm{d}x\,(\mathrm{u}+\mathrm{d}-\bar{\mathrm{u}}-\bar{\mathrm{d}}) \\ &= -2\int_0^1 \mathrm{d}x\,[(\mathrm{u}+\mathrm{d}+\mathrm{s}-\bar{\mathrm{u}}-\bar{\mathrm{d}}-\bar{\mathrm{s}})-(\mathrm{s}-\bar{\mathrm{s}})] \\ &= -6B+2S = -6\end{aligned} \tag{5.18}$$

and

$$F_3^{\nu\mathrm{p}} - F_3^{\bar{\nu}\mathrm{p}} = 12(F_1^{\mathrm{ep}} - F_1^{\mathrm{en}}) \tag{5.19}$$

$$F_2^{\nu\mathrm{p}} + F_2^{\nu\mathrm{n}} \leq \tfrac{18}{5}(F_2^{\mathrm{ep}} + F_2^{\mathrm{en}}) \tag{5.20}$$

$$\tfrac{1}{4} \leq F_2^{\mathrm{en}}/F_2^{\mathrm{ep}} \leq 4. \tag{5.21}$$

Note that integrally charged Han–Nambu quarks would, instead of eq. (5.21), imply $F_2^{\mathrm{en}}/F_2^{\mathrm{ep}} \geq \frac{1}{2}$. Experimentally [48] the en/ep ratio falls close to 1/4 near $x = 1$ which favors the fractionally charged Gell-Mann–Zweig quarks.

In order to learn more about the qualitative feature of the parton composition of the nucleon, let us consider some measured properties of structure functions. Experimentally it seems likely, as we shall frequently see, that

$$F_1(x) \sim 1/x, \qquad F_2(x) \to \text{const.} \quad \text{as } x \to 0 \tag{5.22}$$

indicating that partons have indeed a bremsstrahlung spectrum $q(x) \sim 1/x$, and that the parton multiplicity in the nucleon grows with increasing energy

$$\langle n_q \rangle = \int q(x)\,dx \sim \int dx/x \sim \ln W^2 \tag{5.23}$$

since the kinematic assumptions we have made so far are only justified for $x|p+q| \gg m_{\text{parton}}$ or $x \gg m^2_{\text{parton}}/W^2$. The behavior (5.22) can be understood in terms of good old Regge phenomenology where, in the limit $\nu \to \infty$ and Q^2 fixed, one expects [49]

$$W_1(\nu, Q^2) \sim \nu^{\alpha} f_1^{(\alpha)}(Q^2), \qquad \nu W_2(\nu, Q^2) \sim \nu^{\alpha-1} f_2^{(\alpha)}(Q^2) \tag{5.24}$$

with α being the appropriate Regge intercept: $\alpha_{\text{P}} \simeq 1$ for the Pomeron, and for the leading Reggeon exchanges $\alpha_{\rho,\omega,\ldots} \simeq \frac{1}{2}$. The Reggeon exchanges contributing to W_1 and W_2 in the Regge limit ($x \simeq 0$) can be illustrated as follows

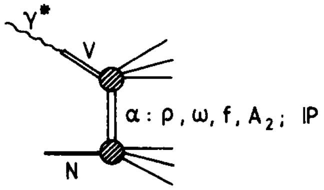

If W_1 and νW_2 scale in the Bjorken limit (5.8), then according to eq. (5.24) we need for the Regge residues f_i

$$f_1^{(\alpha)}(Q^2) \sim (Q^2)^{-\alpha}, \qquad f_2^{(\alpha)}(Q^2) \sim (Q^2)^{1-\alpha} \quad \text{as } Q^2 \to \infty$$

which implies

$$F_1(x) \sim x^{-\alpha}, \qquad F_2(x) \sim x^{1-\alpha} \quad \text{as } x \to 0. \tag{5.25}$$

Thus the observed behavior in eq. (5.22) corresponds to an exchange of the leading trajectory with $\alpha \simeq 1$ – the Pomeron.

The Pomeron carries per definition vacuum quantum numbers ($C = +1$, $I = 0$) and therefore cannot "see" flavor degrees of freedom (e.g. $I \neq 0$, $S \neq 0$) of the nucleon but recognizes only the flavor *singlet* content of hadrons (e.g. $q\bar{q}$ pairs). Therefore, as far as Pomeron exchange is concerned, we expect the scatterings of the leptonic currents J_μ in eqs. (5.9) and (5.10) from p, $\bar{p}$, n or $\bar{n}$ all to be identical as $x \to 0$: from this and eq. (5.25) it follows that

$$\left.\begin{array}{l} u \simeq \bar{u} \simeq d \simeq \bar{d} \sim x^{-\alpha_{\text{P}}} = 1/x \\ s \simeq \bar{s} \sim 1/x \end{array}\right\} \text{as } x \to 0. \tag{5.26}$$

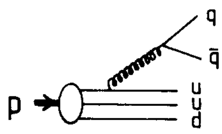

Fig. 5.3. A $q\bar{q}$ pair configuration of "sea" partons.

This part of the parton content of the nucleon is usually referred to as "sea" of quark–antiquark pairs which are important near $x = 0$. In the quark-gluon language of QCD this "sea" of quark–antiquark pairs could arise from the mediation of gluons along the lines suggested in fig. 5.3.

The largest identified fraction of the nucleon momentum is carried by the "valence" quarks which carry the target quantum numbers: this flavor *non-singlet* ($I \neq 0, \ldots$) piece of the parton content in the nucleon corresponds to Regge exchanges with $\alpha < 1$ ($\rho, \omega, \ldots$) and eq. (5.25) implies

$$u_v \sim x^{-\alpha_\rho} = 1/\sqrt{x}, \qquad d_v \sim 1/\sqrt{x} \quad \text{as} \quad x \to 0 \tag{5.27}$$

where the subscript v denotes the valence part of the appropriate parton distribution. In this case, for example, the electromagnetic scattering on p, n, ... is different since the probe (γ^*) can "see" the flavor content (non-singlet) of the hadron.

To summarize, the proton, for example, will in general consist of three different pieces

$$\begin{array}{ccc} p = (u + u + d)_v & + (u\bar{u} + d\bar{d} + s\bar{s} + \cdots) & + \text{gluons} \\ \text{valence} & \text{sea} & \\ (\text{large } \langle x \rangle) & (\text{small } \langle x \rangle) & \end{array}$$

and because of fig. 5.3 we expect the average $\langle x \rangle$ of the gluons to be intermediate between that of valence and sea quarks (momentum conservation!). This decomposition implies the following ansatz for parton distributions

$$\begin{aligned} &u = u_v + \xi, \qquad d = d_v + \xi \\ &\bar{u} \simeq \bar{d} \simeq s \simeq \bar{s} \equiv \xi \end{aligned} \tag{5.28}$$

where, according to eqs. (5.26) and (5.27), $xu_v \sim \sqrt{x}$, $xd_v \sim \sqrt{x}$ and $x\xi \sim$ const. as $x \to 0$. This ansatz (5.28) corresponds to a SU(3)-symmetric sea, although kinematic effects of quark masses ($m_s > m_{u,d}$) may imply that strange and non-strange sea quark distributions are not identical as $x \to 0$. As Q^2 increases the ansatz (5.28) should become more and more appropriate since symmetry breaking effects ($\sim m_q^2/Q^2$) are less important. A possible test of eq. (5.28) is provided by the sum rule

$$\int_0^1 \frac{dx}{x} (F_2^{ep} - F_2^{en}) = \frac{1}{3}.$$

Exact scaling in the form (5.8) as predicted in the naive parton model does not hold in present electron, muon and neutrino scattering data over a wide range of Q^2. In addition, exact scaling seems to be unobtainable in the context of any quantum field theory (except possibly for $Q^2 \to \infty$). Within the framework of field theory one expects, due to the effects of field quanta ("gluons") which mediate the

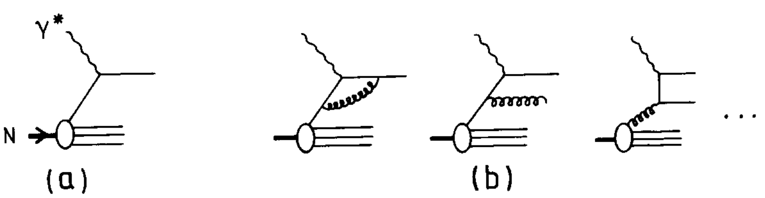

Fig. 5.4. Deep inelastic scattering (a) in the naive parton model and (b) in the field theoretic version of the parton model giving rise to "scaling violations".

strong interactions, that structure functions depend always on *two* variables x and Q^2, say, i.e.

$$F_i = F_i(x, Q^2) \tag{5.29}$$

for any finite values of Q^2. This additional Q^2 dependence is usually referred to as "scaling violation" and typical graphs responsible for it are depicted in fig. 5.4(b), whereas fig. 5.4(a) corresponds to the naive parton model which does not give rise to an additional Q^2 dependence in F_i. We will now calculate this Q^2 dependence of structure functions, i.e. the effects of gluonic corrections as shown in fig. 5.4(b).

5.1. Calculating scaling violations

In order to calculate the Q^2 dependence of deep inelastic structure functions $F_i(x, Q^2)$ we will first use the classical tool of the renormalization group (RG). The momentum dependence of a Green's function Γ is then given by eq. (3.24) or, in leading order, by eq. (4.12). However, these results apply to scattering amplitudes with external momenta p_i in the (unphysical) "deep Euclidean region". It is a unique feature of deep inelastic processes that we can use Wilson's [50] operator product expansion (OPE) on the light cone [51] for the two currents in eq. (5.2), which connects the deep Euclidean RG information to the behavior of deep inelastic structure functions in the physical region. This always leads us to the prediction of the Q^2 evolution of *moments* of structure functions which formally can be written as

$$\int_0^1 dx\, x^{n-2} F_2(x, Q^2) = C^n(Q^2)\langle N|O^n|N\rangle \tag{5.30}$$

where the Q^2 dependence of the light cone expansion coefficients (Wilson coefficients) $C^n(Q^2)$ can be uniquely predicted by QCD (using the RG equations) and the (non-perturbative) bound state of the target is described by the expectation value $\langle N|O^n|N\rangle$ of the Wilson operator O^n. This latter Q^2 independent quantity cannot be calculated perturbatively and has to be taken from experiment at a given $Q^2 = Q_0^2$: we shall relate $\langle N|O^n|N\rangle$ to the parton distributions $q(x)$, $\bar{q}(x)$, ... to be fitted to experiment. Schematically, we shall pursue the following line of arguments:

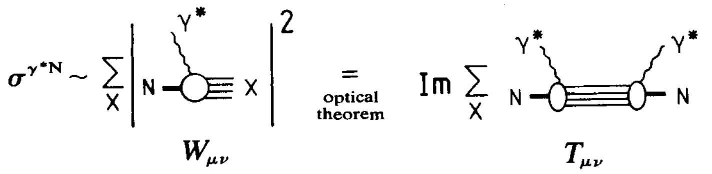

(5.31)

where the virtual Compton amplitude $T_{\mu\nu}$, defined by

$$T_{\mu\nu} \equiv \mathrm{i} \int \mathrm{d}^4 z \, \mathrm{e}^{\mathrm{i}q\cdot z} \, \theta(z_0) \langle \mathrm{p} | [J_\mu^+(z), J_\nu(0)] | \mathrm{p} \rangle \tag{5.32}$$

is related to the deep inelastic scattering amplitude $W_{\mu\nu}$ via the optical theorem

$$W_{\mu\nu} = \frac{1}{2\pi} \operatorname{Im} T_{\mu\nu} \tag{5.33}$$

which can be simply derived from eq. (5.32) by using the well known integral representation for $\exp(\mathrm{i}q_0 z_0)\,\theta(z_0)$. We then write an OPE for $T_{\mu\nu}$ at $-q^2 \to \infty$ (or $z^2 \to 0$)

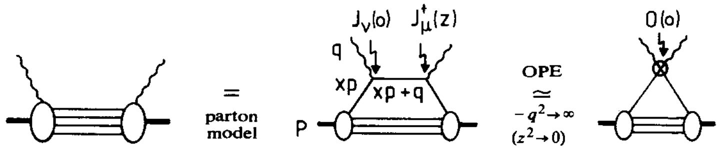

(5.34)

where the matrix elements of the local Wilson operators $O(0)$ between target states will be related to measured parton distributions. Adding the appropriate radiative gluon corrections to the diagrams in (5.34) will allow us to calculate, using the RG equation, all leading ln Q^2 corrections to all orders in α_s.

Simple arguments suggest [51, 5] that at large values of $Q^2 (\gg m_N^2)$ the region $0 \leq z^2 \leq 1/Q^2$ dominates the integral over the one-particle matrix element of a current commutator in eq. (5.2). Matrix elements of current commutators are singular (a typical example would be Gell-Mann's current algebra) on the light-cone and the degree of singularity on the light-cone can be shown [51] to fix the asymptotic behavior of the Fourier integral in eq. (5.2) at high Q^2. To this end we expand the commutator (or in general the product) of two local operators near the light-cone $z^2 \simeq 0$ which is a generalization [51] of the short-distance operator expansion suggested by Wilson [50] that holds near $z_\mu \simeq 0$, i.e. only at the tip of the light-cone. In the simplest case of two scalar operators the light-cone expansion can be written as

$$A(z)\,B(0) \simeq \sum_{i,n} C_i^n(z^2)\, z_{\mu_1} \ldots z_{\mu_n} O_i^{\mu_1 \cdots \mu_n}(0) \tag{5.35}$$

where the sum runs over the spin (n) and over the different possible types (i) of operators O to be specified later. These operators $O_i^{\mu_1 \cdots \mu_n}(0)$ are a string of local, symmetric, and traceless operators which are the same for the product, the commutator, the time-ordered product etc. of the two operators A and B. The expansion parameters C_i^n – the so called Wilson coefficients – are c-number singular functions at $z^2 \simeq 0$ which may be taken to behave as

$$C_i^n(z^2) \underset{z^2 \to 0}{\sim} \left(\frac{1}{z^2}\right)^{[d_A + d_B - (d_{O_i} - n)]/2} \tag{5.36}$$

where d_i denotes the naive mass dimension of the appropriate operators in eq. (5.35). Thus the strongest singularity is obtained for light-cone operators with *minimum twist* τ

$$\tau \equiv (\text{dimension-spin}) = d_{O_i} - n, \tag{5.37}$$

whereas less singular terms do not contribute, as we shall demonstrate below, to the leading power behavior in Q^2 of the Fourier transform. Simple non-trivial examples of local operators $O_i^{\mu_1 \cdots \mu_n}$ of definite twist would be (recall that $d_\phi = 1$ and $d_\psi = \frac{3}{2}$ for scalar and Dirac-fields, respectively)

$$\begin{aligned} \tau = 1: &\quad \phi, \quad \partial_\mu \phi, \quad \partial_\mu \partial_\nu \phi, \ldots . \\ \tau = 2: &\quad \bar{\psi}\gamma_\mu \psi, \quad \bar{\psi}\gamma_\mu \overleftrightarrow{\partial}_\nu \psi, \ldots . \\ &\quad \phi \overleftrightarrow{\partial}_\mu \phi, \ldots . \end{aligned}$$

etc.

where the $\tau = 1$ operators do not contribute in our case, since they yield vanishing diagonal matrix elements. Therefore the leading dominant contributions come from operators with twist $\tau = 2$ which are dominant for deep inelastic scattering processes and, in lowest order, yield [52, 51, 5] the usual scaling laws suggested by Bjorken. For our further discussion it is important to realize that the OPE (5.35) is a genuine operator statement, i.e. taking matrix elements

$$\langle \alpha | AB | \beta \rangle \simeq \sum C_i \langle \alpha | O_i | \beta \rangle \tag{5.38}$$

the C_i's are *independent* of the target states, i.e. of the specific reaction considered.

We will now demonstrate how one can obtain predictions for the (Mellin) moments of measured deep inelastic structure functions from an OPE of the virtual Compton scattering amplitude in the unphysical region along the lines illustrated in (5.34). For the sake of clarity and simplicity we will suppress all obvious Lorentz indices and functional dependencies. For the virtual Compton amplitude we write

$$\begin{aligned} T(\nu, Q^2) &= \int d^4 z \, e^{iq\cdot z} \langle p | i\theta(z_0) [J^+(z), J(0)] | p \rangle \\ &\underset{z^2 \to 0}{=} \sum_{i,n} \int d^4 z \, e^{iq\cdot z} \, C_i^n(z^2) \, z_{\mu_1} \cdots z_{\mu_n} \langle p | O_i^{\mu_1 \cdots \mu_n}(0) | p \rangle \\ &= \sum_{i,n} 2q_{\mu_1} \cdots 2q_{\mu_n} \frac{\partial^n}{\partial (iq^2)^n} \int d^4 z \, e^{iq\cdot z} C_i^n(z^2) \langle p | O_i^{\mu_1 \cdots \mu_n}(0) | p \rangle \\ &\equiv \sum_{i,n} (Q^2/2)^{-n} q_{\mu_1} \cdots q_{\mu_n} C_i^n(Q^2) \langle p | O_i^{\mu_1 \cdots \mu_n}(0) | p \rangle \end{aligned} \tag{5.39}$$

and, according to their most general Lorentz structure, we can express the spin-averaged matrix elements of the O_i as

$$\langle p | O_i^{\mu_1 \cdots \mu_n}(0) | p \rangle = A_i^n (p^{\mu_1} \cdots p^{\mu_n} - m^2 g^{\mu_1 \mu_2} p^{\mu_3} \cdots) \tag{5.40}$$

where the terms proportional to $g^{\mu\nu}$ (the so called "trace terms") ensure the symmetric rank-n tensor which can be formed with the target momentum p to be traceless (operators with definite spin). Equations (5.39) and (5.40) then yield

$$T(\nu, Q^2) = \sum_{i,n} C_i^n(Q^2) x^{-n} A_i^n + O[x^{-n+2} m^2/Q^2]. \tag{5.41}$$

Note that the origin of the neglected terms is twofold: on the one hand they derive from the trace terms in eq. (5.40) and one usually refers to these suppressed contributions as "target mass effects" which we shall discuss later; on the other hand these subleading contributions can also result from higher twist terms with $\tau > 2$ which are suppressed as $(m^2/Q^2)^{\tau/2-1}$ where the mass scale m^2 is not necessarily the target mass since higher twist terms correspond to interactions of the scattered parton with the remaining spectator quarks in the nucleon. These effects are in general not calculable and go beyond the simple hand-bag structure in fig. 5.2 or eq. (5.34). According to the momentum dependence of general Green's functions as given for example in eq. (3.4), the momentum dependence of the above dimensionless Wilson coefficients in any interacting field theory has to be interpreted as $C_i^n(Q^2) \equiv C_i^n(Q^2/\mu^2, g(\mu))$. Since so far we are still in the deep Euclidean limit ($q_0 \to i\infty$), we can write at this stage a RG equation for $C_i^n(Q^2)$ which allows us, as discussed and shown in section 3, to compute the leading Q^2-dependence of eq. (5.41) to all orders in α_s provided we know the first non-trivial (1-loop) order of the anomalous dimensions of $O_i^{\mu_1 \cdots \mu_n}$. This we shall do below. Finally, the connection with the physical deep inelastic region where $0 \le |x| \le 1$ can be obtained by taking Mellin moments of eq. (5.41) and using the optical theorem (5.33): in this region the sum in (5.41) clearly diverges and what is therefore needed is an appropriate analytic continuation in x of eq. (5.41); in this way x-moments of the deep inelastic structure functions naturally arise. Equation (5.41) suffices to define T as a function of complex x which is analytic as $|x| \to \infty$ and has a cut from -1 to $+1$. (T is an analytic function of ν with a cut from $2m_N\nu = Q^2$ to ∞, according to eq. (5.7) with hadron masses neglected, and a cut for the crossed process from $-\infty$ to $2m_N\nu = -Q^2$.) The coefficient of x^{-n} in the expansion (5.41) can now be isolated by taking the x^{n-1} moment and integrating along the contour C indicated in fig. 5.5:

$$\frac{1}{2\pi i} \int_C dx\, x^{n-1}\, T(x, Q^2) = \sum_i C_i^n(Q^2)\, A_i^n. \tag{5.42}$$

Shrinking the contour C to the physical cut, where the discontinuity is W, according to the optical theorem (5.33), we finally get

$$4 \int_0^1 dx\, x^{n-1}\, W(x, Q^2) = \sum_i C_i^n(Q^2)\, A_i^n. \tag{5.43}$$

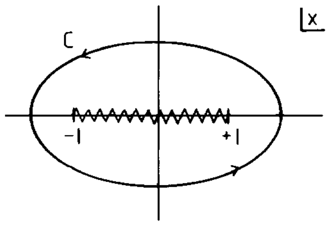

Fig. 5.5. Integration contour C used in evaluating eq. (5.42).

This equation uniquely predicts the Q^2 evolution of the measured deep inelastic structure functions $W(x, Q^2)$, once we know the Q^2-independent (non-perturbative) input wave functions A_i^n which describe the bound state of a hadron and which will be related to the parton distributions to be fixed by experiment. Taking care of the detailed Lorentz structure of the hadronic tensor $W_{\mu\nu}$ the final form of eq. (5.43) reads [1, 34, 53, 54]

$$\int_0^1 \mathrm{d}x\, x^{n-2} F(x, Q^2) = \sum_i C_i^n(Q^2/\mu^2, g(\mu)) A_i^n \tag{5.44}$$

with $F = xF_1$, F_2 or xF_3 and for brevity we define the Mellin moments by

$$\langle F(Q^2)\rangle_n \equiv \int_0^1 \mathrm{d}x\, x^{n-2} F(x, Q^2). \tag{5.45}$$

Before confronting eq. (5.44) with experiment we have first to work out the explicit Q^2 dependence of C_i^n and then we have to relate the so far theoretically unknown matrix elements A_i^n, defined in eq. (5.40), to measured structure functions at a fixed value of $Q^2 = Q_0^2$ or, equivalently, to parton distributions.

In order to obtain the explicit Q^2 dependence of C_i^n we have to derive a renormalization group equation for these Wilson coefficients. Remember, according to our discussion in section 3, that any measurable physical quantity has to satisfy a RG equation (3.15) in order to remain independent of the renormalization convention chosen. The light-cone expansion in eq. (5.39) is given generically by (for a given operator of type i)

$$\mathrm{i}T(JJ) = \sum_n C_i^n O_i^n. \tag{5.46}$$

Since conserved currents J must have anomalous dimensions [5] $\gamma_J = 0$, the RG eq. (3.15) for $\langle\varphi|T(JJ)|\varphi\rangle$, with $\varphi \equiv A_a^\mu$ or ψ_k denoting the fundamental fields of the theory, reads

$$\left(\mu \frac{\partial}{\partial\mu} + \beta \frac{\partial}{\partial g} + 2\gamma_\varphi\right)\langle\varphi|T(JJ)|\varphi\rangle = 0 \tag{5.47}$$

and, because of (5.46) and since different n have different tensor structure,

$$\left(\mu \frac{\partial}{\partial\mu} + \beta \frac{\partial}{\partial g} + 2\gamma_\varphi\right) C_i^n(Q^2/\mu^2, g(\mu))\langle\varphi|O_i^n|\varphi\rangle = 0. \tag{5.48}$$

Furthermore, $\langle\varphi|O_i^n|\varphi\rangle$ must satisfy a RG equation, since it will correspond to measurable parton distributions,

$$\left(\mu \frac{\partial}{\partial\mu} + \beta \frac{\partial}{\partial g} + 2\gamma_\varphi + \gamma_{O_i^n}\right)\langle\varphi|O_i^n|\varphi\rangle = 0 \tag{5.49}$$

where, in order to specify the normalization of O_i^n, their matrix elements should satisfy similar renormalization conditions as the Green's functions in eq. (3.12)

$$\langle\varphi|O_i^n|\varphi\rangle|_{p^2=-\mu^2} = 1. \tag{5.50}$$

Then for a different value of the external quark or gluon momentum p, the normalization of O_i^n will be modified by radiative corrections (fig. 5.6)

$$\langle\varphi|O_i^n|\varphi\rangle = 1 + g^2 b_i^n \ln(-p^2/\mu^2) + \mathrm{O}(g^4) \tag{5.51}$$

where b_i^n is a constant. The anomalous dimension of Wilson operators is then given by

$$\gamma_{O_i^n} = 2g^2 b_i^n - 2\gamma_\varphi \tag{5.52}$$

which follows from eqs. (5.49) and (5.51). Equations (5.48) and (5.49) then yield the RG equation for Wilson coefficients

$$\left(\mu\frac{\partial}{\partial\mu} + \beta\frac{\partial}{\partial g} - \gamma_{O_i^n}\right) C_i^n(Q^2/\mu^2, g(\mu)) = 0 \tag{5.53}$$

which is the basic equation for calculating the Q^2 dependence of eq. (5.44), i.e. the scaling violations in structure functions $F(x, Q^2)$. So far we have assumed that we have only one Wilson operator of type i. If there exist several operators of type i (carrying the same internal quantum numbers and having of course the same Lorentz structure n), then the O_i^n are not separately multiplicatively renormalizable as above but instead they will *mix* under renormalization since $\gamma_{O_i^n}$ will become a matrix of anomalous dimensions for Wilson operators and eq. (5.53) turns therefore into a matrix equation

$$\sum_j \left[\delta_{ij}\left(\mu\frac{\partial}{\partial\mu} + \beta\frac{\partial}{\partial g}\right) - \gamma_{ij}^n\right] C_j^n(Q^2/\mu^2, g(\mu)) = 0 \tag{5.54}$$

with $\gamma_{ij}^n \equiv \gamma_{O_i^n, O_j^n}$. We shall deal with this so called flavor *singlet* mixing problem in the next subsection.

The solution of eq. (5.53) can be read off eq. (3.24) and is given by

$$C_i^n(Q^2/\mu^2, g(\mu^2)) = C_i^n(1, \bar{g}(Q^2)) \exp\left[-\int_0^{(1/2)\ln(Q^2/\mu^2)} \gamma_{O_i^n}(\bar{g}(t'))\,\mathrm{d}t'\right]. \tag{5.55}$$

According to our previous discussion the physical interpretation of this solution is obvious: whereas exp[. . .] includes the leading logarithmic contributions of the fundamental parton scattering cross sections such as shown in fig. 5.4(b) which are summed to all orders in α_s by just knowing the first

Fig. 5.6. Processes contributing to the effective normalization, i.e. to the "anomalous dimensions" of fermionic (O_F^n) and gluonic (O_V^n) Wilson operators.

non-trivial 1-loop order contributions to $\gamma_{O_i^n}$ (fig. 5.6), the Wilson coefficients $C_i^n(1, \bar{g}(Q^2))$ correspond to the remaining "finite" (i.e. non-logarithmic) terms of the cross sections in fig. 5.4. From fig. 5.4 it is clear that the fermionic and gluonic Wilson coefficients C_F and C_G, where a quark and a gluon, respectively, in the initial state scatters off the leptonic current, are of the general form

$$C_F^n(1, \bar{g}) = 1 + O(\alpha_s), \qquad C_G^n(1, \bar{g}) = O(\alpha_s) \tag{5.56}$$

where we have normalized the naive parton model contribution of fig. 5.4(a) to $C_F = 1$. In the leading logarithmic order approximation ($\gamma_{O_i^n} \sim O(\alpha_s)$) we just have to take $C_F = 1$ and $C_G = 0$. For a given i, eqs. (5.44) and (5.55) yield

$$\langle F_i(Q^2)\rangle_n = A_i^n \, C_i^n(1, \bar{g}) \exp[\ldots]. \tag{5.57}$$

It is convenient to express the unknown Q^2-independent matrix element A_i^n by the experimental structure function measured at an arbitrarily chosen momentum transfer Q_0^2:

$$\langle F_i(Q_0^2)\rangle_n = A_i^n C_i^n(1, \bar{g}) \exp[\ldots]_{Q^2=Q_0^2}$$

which, inserted into (5.57), finally gives

$$\langle F_i(Q^2)\rangle_n = \langle F_i(Q_0^2)\rangle_n \left[\frac{\alpha_s(Q_0^2)}{\alpha_s(Q^2)}\right]^{-a_i(n)} \tag{5.58}$$

with $a_i = c_i/2b$ according to eq. (4.11), i.e. $\gamma_{O_i^n} = c_i g^2$ and $\beta = -bg^3$. This is the basic equation for the Q^2 evolution of a given (non-singlet) structure function F_i predicted by the RG improved QCD. So far we have not specified the index i, but this we shall do in the next subsection. Before entering some more technicalities it should be noted that, in our leading logarithmic approximation, all non-perturbative effects which describe the bound state of a nucleon are lumped into $\langle F_i(Q_0^2)\rangle_n$ in eq. (5.58) which factorizes to all orders α_s from the high-Q^2 dependences in (5.58). This so called infrared (IR) factorization property is a typical and very important result of the renormalization group. We shall come back to this crucial point later.

For all remaining conventional (fixed point) field theories, we have instead of eq. (5.58), according to eq. (4.20),

$$\langle F_i(Q^2)\rangle_n = \langle F_i(Q_0^2)\rangle_n [Q^2/Q_0^2]^{-a_i(n)} \tag{5.59}$$

with $a_i = \frac{1}{2}\gamma_{O_i^n} = \frac{1}{2}c_i g^{*2}$, provided of course that a fixed point g^* exists such that perturbative calculations are justified. In contrast to the $\ln Q^2$ behavior predicted by eq. (5.58), we expect from eq. (5.59) structure functions to have a power-like behavior in Q^2 for fixed-point theories with g^* to be determined by experiment.

5.2. Anomalous dimensions of Wilson operators and singlet structure functions

Now we will discuss the various types i of Wilson operators O_i^n and their related anomalous dimensions in order to derive the explicit form of scaling violations in eq. (5.44) for a general measured structure function. There are *three* different types of operators [1, 53, 54] with minimum twist $\tau = 2$. For the flavor *non-singlet* (NS) case we have just *one* operator which carries flavor quantum numbers, such as isospin,

$$O^n_{\rm NS} = \frac{i^{n-1}}{n!}[\bar{\psi}\gamma^{\mu_1}D^{\mu_2}\cdots D^{\mu_n}\lambda_a\psi + \text{perm.}] \tag{5.60}$$

with the covariant derivative defined in eq. (2.4) and where λ_a are the usual flavor Gell-Mann matrices on the space of physical symmetries; the permutations refer to a symmetrization with respect to the vector indices. Note that, for the time being, we neglect trace-terms in (5.60), i.e. the $g^{\mu\nu}$-terms in eq. (5.40) which are suppressed as $m^2_{\rm N}/Q^2$. The 1-loop contributions to the matrix elements of the fermionic NS operator in eq. (5.60) for fermionic ($\mathrm{F} \equiv \psi$) external quark states yield [53–55]

$$\gamma^{\rm F}_{\rm FF} = \frac{\alpha_s}{2\pi} C_2(R)\left[1 - \frac{2}{n(n+1)} + 4\sum_{j=2}^{n}\frac{1}{j}\right] \tag{5.61}$$

with a straightforward notation according to fig. 5.7. It should be noted that the last term in eq. (5.61)

$$\sum_{j=2}^{n}\frac{1}{j} = \psi(n+1) + \gamma_{\rm E} - 1 \tag{5.62}$$

with $\gamma_{\rm E} = 0.5772$, and the digamma function $\psi(z) \equiv \Gamma'(z)/\Gamma(z)$ results from the second and third diagram in fig. 5.7 which, as we shall see, determine the Q^2 dependence of structure functions for large values of x ($x \to 1$). These diagrams are typical for gauge theories and do not exist in scalar-gluon theories, for example, where only the first diagram in fig. 5.7 contributes and thus we expect a totally different threshold ($x \to 1$) behavior of structure functions than for QCD. The scaling violations of a NS structure function are thus simply given by eq. (5.58), i.e.

$$\langle F_{\rm NS}(Q^2)\rangle_n = \langle F_{\rm NS}(Q_0^2)\rangle_n \exp\{-s a_{\rm NS}(n)\} \tag{5.63}$$

with

$$a_{\rm NS} = \frac{\gamma^{\rm F}_{\rm FF}}{8\pi\alpha_s b}, \qquad s = \ln\frac{\ln(Q^2/\Lambda^2)}{\ln(Q_0^2/\Lambda^2)} \tag{5.64}$$

and $b = (11 - \frac{2}{3}N_f)/16\pi^2$. Experimentally measurable non-singlet structure functions which can be directly compared with the predictions of (5.63) are, for example,

$$F_{\rm NS} = F_2^{\rm ep} - F_2^{\rm en}, \qquad F_2^{\nu \rm p} - F_2^{\bar{\nu}\rm p}, \qquad xF_3^{\nu \rm N}, \qquad \text{etc.} \tag{5.65}$$

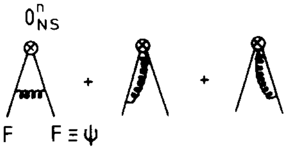

Fig. 5.7. Lowest order contributions to $\gamma^{\rm F}_{\rm FF}(n)$.

In contrast to the NS case, there are *two* types of flavor *singlet* Wilson operators, one fermionic (F) and one gluonic (V) operator which carry no flavor quantum numbers:

$$O_{\mathrm{F}}^{n}=\frac{\mathrm{i}^{n-1}}{n!}[\bar{\psi}\gamma^{\mu_1}\mathrm{D}^{\mu_2}\cdots\mathrm{D}^{\mu_n}\psi+\text{perm.}]$$

$$O_{\mathrm{V}}^{n}=\frac{\mathrm{i}^{n-2}}{2n!}[F^{\alpha\mu_1}\mathrm{D}^{\mu_2}\cdots\mathrm{D}^{\mu_{n-1}}F_{\alpha}^{\mu_n}+\text{perm.}] \tag{5.66}$$

with $\mathrm{D}^{\mu}F_{a}^{\nu\rho}=(\delta_{ac}\partial^{\mu}+gf_{abc}A_{b}^{\mu})F_{c}^{\nu\rho}$. Since O_{F}^{n} and O_{V}^{n} have identical quantum numbers, they will *mix* under renormalization and consequently we get a 2×2 anomalous dimension matrix $\hat{\gamma}(n)$ which forces us to deal with the matrix equation (5.54). According to the two possible external states $F\equiv\psi_{\mathrm{q}}$ and $V\equiv A_{a}^{\mu}$, this matrix has the general form

$\hat{\gamma}(n)=$ 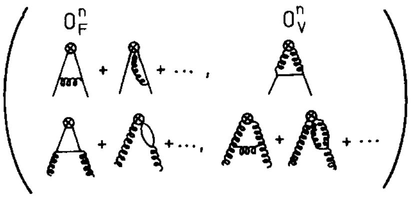 (5.67)

$$\equiv\begin{pmatrix}\gamma_{\mathrm{FF}}^{\mathrm{F}}, & \gamma_{\mathrm{FF}}^{\mathrm{V}}\\ \gamma_{\mathrm{VV}}^{\mathrm{F}}, & \gamma_{\mathrm{VV}}^{\mathrm{V}}\end{pmatrix}$$

with $\gamma_{\mathrm{FF}}^{\mathrm{F}}$ given by eq. (5.61) and [53–55]

$$\gamma_{\mathrm{VV}}^{\mathrm{V}}=\frac{\alpha_{\mathrm{s}}}{2\pi}\left\{C_2(G)\left[\frac{1}{3}-\frac{4}{n(n-1)}-\frac{4}{(n+1)(n+2)}+4\sum_{j=2}^{n}\frac{1}{j}\right]+\frac{4}{3}T(R)\right\}$$

$$\gamma_{\mathrm{VV}}^{\mathrm{F}}=-\frac{\alpha_{\mathrm{s}}}{2\pi}\frac{4(n^2+n+2)}{n(n+1)(n+2)}T(R) \tag{5.68}$$

$$\gamma_{\mathrm{FF}}^{\mathrm{V}}=-\frac{\alpha_{\mathrm{s}}}{2\pi}\frac{2(n^2+n+2)}{n(n^2-1)}C_2(R)$$

where $\alpha_{\mathrm{s}}=g^2/4\pi$ and the color factors are given by eq. (4.4). The calculation of the γ's, using the Feynman rules implied by the above Wilson operators, is rather involved but in section 6 we shall give a simple derivation of these expressions by just using the basic order-α_{s} parton processes of fig. 5.4b. We can solve the RG equation (5.54) by first diagonalizing the singlet anomalous dimension matrix $\hat{\gamma}(n)$ by

$$\hat{\gamma}=\gamma_{-}\hat{P}^{-}+\gamma_{+}\hat{P}^{+} \tag{5.69}$$

where the projection operators are constrained by

$$\hat{P}^{i}\hat{P}^{j}=\delta_{ij}\hat{P}^{i},\qquad \hat{P}^{-}+\hat{P}^{+}=1 \tag{5.70}$$

and with the eigenvalues

$$\gamma_\pm = \tfrac{1}{2}[\gamma^{\mathrm{F}}_{\mathrm{FF}} + \gamma^{\mathrm{V}}_{\mathrm{VV}} \pm \sqrt{(\gamma^{\mathrm{V}}_{\mathrm{VV}} - \gamma^{\mathrm{F}}_{\mathrm{FF}})^2 + 4\gamma^{\mathrm{F}}_{\mathrm{VV}}\gamma^{\mathrm{V}}_{\mathrm{FF}}}] \tag{5.71}$$

i.e. $\gamma_- < \gamma_+$. From eq. (5.69), together with (5.70), we obtain for the projection operator

$$\hat{P}^- = \begin{pmatrix} p^-_{11} & p^-_{12} \\ p^-_{21} & 1 - p^-_{11} \end{pmatrix}$$

with

$$\alpha_n \equiv p^-_{11}(n) = \frac{\gamma^{\mathrm{F}}_{\mathrm{FF}} - \gamma_+}{\gamma_- - \gamma_+}, \qquad \beta_n \equiv p^-_{21}(n) = \frac{\gamma^{\mathrm{F}}_{\mathrm{VV}}}{\gamma_- - \gamma_+}$$
$$p^-_{12}(n) = \frac{\gamma^{\mathrm{V}}_{\mathrm{FF}}}{\gamma_- - \gamma_+} \tag{5.72}$$

where for later convenience we have defined two matrix elements by α_n and β_n; these two quantities will play a crucial role for discriminative tests of QCD.

An important special case is the situation where $n = 2$, since this corresponds to the area under a structure function, $\langle F(Q^2)\rangle_2 = \int_0^1 F(x, Q^2)\,\mathrm{d}x$ which in turn can be related to the total fractional momentum carried by quarks. In this case we have

$$\hat{\gamma}(n=2) = \frac{\alpha_s}{2\pi}\frac{4}{3}\begin{pmatrix} 2C_2(R), & -2C_2(R) \\ -T(R), & T(R) \end{pmatrix}, \qquad \gamma_\pm(2) = \begin{cases} \frac{\alpha_s}{2\pi}\frac{4}{3}[2C_2(R) + T(R)] \\ 0 \end{cases}$$
$$\alpha_2 = \beta_2 = \frac{T(R)}{2C_2(R) + T(R)}, \qquad p^-_{12}(2) = 1 - p^-_{11}(2) = \frac{2C_2(R)}{2C_2(R) + T(R)} \tag{5.73}$$

i.e. for a four-flavor QCD ($N_f = 4$) we would have for example

$$\hat{P}^-(2) = \begin{pmatrix} \frac{3}{7}, & \frac{4}{7} \\ \frac{3}{7}, & \frac{4}{7} \end{pmatrix}. \tag{5.74}$$

We shall come back to these important $n = 2$ results when comparing moments of structure functions with experiment in section 5.5.

Our diagonalized $\hat{\gamma}$-matrix in eq. (5.69) allows us now to define operators $O^n_\pm$ and related Wilson coefficients $C^n_\pm$ which obey simple linear RG equations (5.53), as was the case for non-singlet structure functions, with the anomalous dimensions $\gamma_\pm$ given by eq. (5.71):

$$\begin{aligned} O^n_\pm C^n_\pm(Q^2/\mu^2, g) &\equiv \sum_{i,j=\mathrm{F,V}} O^n_i P^\pm_{ij} C^n_j(Q^2/\mu^2, g) \\ &= (p^\pm_{11}C^n_{\mathrm{F}} + p^\pm_{12}C^n_{\mathrm{V}})O^n_{\mathrm{F}} + (p^\pm_{21}C^n_{\mathrm{F}} + p^\pm_{22}C^n_{\mathrm{V}})O^n_{\mathrm{V}} \\ &\simeq C^n_{\mathrm{F}}(p^\pm_{11}O^n_{\mathrm{F}} + p^\pm_{21}O^n_{\mathrm{V}}) \end{aligned} \tag{5.75}$$

where in the last line we have already made use of eq. (5.56), i.e. $C_F^n(1,\bar{g})=1$ and $C_V^n(1,\bar{g})=0$ to leading order. Note that, although gluons do not directly couple to leptonic currents, they will play a crucial role in calculating the scaling violations for structure functions because of the appearance of the gluonic operator O_V^n in eq. (5.75): This is the so called *singlet-mixing* and eq. (5.75) is the very reason why the gluon distribution in hadrons, to be identified as the target expectation value of O_V, enters the problem. Using

$$C_\pm^n(Q^2/\mu^2, g) = C_\pm^n(1,\bar{g}) \exp\left[-\int_0^{1/2\ln(Q^2/\mu^2)} \gamma_\pm(\bar{g}(t'))\,dt'\right],$$

the Q^2-evolution of a general structure function is predicted to be

$$\langle F(Q^2)\rangle_n = \langle F_{NS}(Q_0^2)\rangle_n \exp\{-sa_{NS}(n)\} + \sum_{i=\pm} \langle F_i(Q_0^2)\rangle_n \exp\{-sa_i(n)\} \tag{5.76}$$

with

$$a_i = \frac{\gamma_i}{8\pi\alpha_s b}, \qquad s = \ln\frac{\ln(Q^2/\Lambda^2)}{\ln(Q_0^2/\Lambda^2)} \tag{5.77}$$

and $b = (11-\frac{2}{3}N_f)/16\pi^2$. The matrix elements of $O_\pm^n$ have been denoted by $\langle F_\pm(Q_0^2)\rangle_n$. It is of course possible to compare eq. (5.76) directly with experiment [56] by fitting the unknown input structure functions $F_i(x, Q_0^2)$ at a fixed value of Q_0^2 to the data. In this way one looses part of the predictive power of eq. (5.76) since it requires to refit the input functions at Q_0^2 for each different structure function $F(x, Q^2)$ considered. One can avoid this by relating the Q^2 dependent structure functions F_{NS} and $F_\pm$ to parton distributions which then in turn can be used to make also predictions for processes other than deep inelastic reactions. This physically most transparent way of treating scaling violations, partly based on eq. (5.75), will be discussed in section 5.4.

The scaling violations predicted by conventional fixed-point field theories are formally the same as in eq. (5.76) but, according to eq. (5.59), we have instead of eq. (5.77)

$$a_i = \tfrac{1}{2}\gamma_i, \qquad s = \ln(Q^2/Q_0^2) \tag{5.78}$$

where now the value of the UV finite fixed point $\alpha_s \equiv \alpha^* = g^{*2}/4\pi$, appearing in γ_i, has to be determined by experiment. The appropriate anomalous dimensions in eq. (5.78) for fixed point theories are summarized in the following subsection.

It should be noted that

$$\gamma_{NS}(n=1) \equiv \gamma_{FF}^F(n=1) = 0 \tag{5.79}$$

$$\gamma_-(n=2) = 0. \tag{5.80}$$

Equation (5.79) implies that the fundamental baryon-number conservation, etc., laws (5.15) hold at all values of Q^2, whereas eq. (5.80) tells us that the operator O_-^2 is conserved, i.e. is not renormalized by the strong interactions. This operator therefore retains its naive mass dimension and is identified with the conserved energy-momentum tensor: $\theta_{\mu\nu} \equiv O_-^2 = O_F^2 + O_V^2$.

5.3. Anomalous dimensions of Wilson operators for fixed point theories

In an abelian vector-gluon theory ($\bar{\psi}\gamma_\mu\psi A^\mu$) the fermionic and gluonic Wilson operators in eq. (5.66) become [34, 35]

$$O_F^n = \frac{i^{n-1}}{n!}[\bar{\psi}\gamma^{\mu_1}D^{\mu_2}\cdots D^{\mu_n}\psi + \text{perm.}]$$
$$O_V^n = \frac{i^{n-2}}{2n!}[F^{\alpha\mu_1}\partial^{\mu_2}\cdots\partial^{\mu_{n-1}}F_\alpha^{\mu_n} + \text{perm.}] \tag{5.81}$$

with $D^\mu = \partial^\mu - igA^\mu$, $F^{\mu\nu}$ being the usual field tensor defined in eq. (2.9), and no covariant derivatives appear in O_V^n because of the absence of gluon self-couplings. The anomalous dimensions are then the same as in eqs. (5.61) and (5.68) with the color factors given by eq. (4.17) and where $\alpha_s \equiv \alpha^*$.

Since scalar-gluon Yukawa-theories ($\bar{\psi}\psi\phi$) are not gauge theories, only simple derivatives occur in the Wilson operators [34, 35]

$$O_F^n = \frac{i^{n-1}}{n!}[\bar{\psi}\gamma^{\mu_1}\partial^{\mu_2}\cdots\partial^{\mu_n}\psi + \text{perm.}]$$
$$O_\phi^n = i^n\phi\partial^{\mu_1}\cdots\partial^{\mu_n}\phi \tag{5.82}$$

which imply the following anomalous dimensions [34]

$$\gamma_{FF}^F = \frac{\alpha^*}{4\pi}C_2(R)\left[1-\frac{2}{n(n+1)}\right], \quad \gamma_{\phi\phi}^F = -\frac{2\alpha^*}{\pi}T(R)\frac{1}{n}$$
$$\gamma_{\phi\phi}^\phi = \frac{\alpha^*}{\pi}T(R), \qquad \gamma_{FF}^\phi = -\frac{\alpha^*}{2\pi}C_2(R)\frac{1}{n+1} \tag{5.83}$$

with $\alpha^* = g^{*2}/4\pi$. For non-abelian scalar-gluon theories ($\bar{\psi}\lambda_a\psi\phi_a$) the color factors are given by eq. (4.18), whereas abelian scalar-gluon theories ($\bar{\psi}\psi\phi$) are characterized by eq. (4.17). It should be noted that now the digamma ψ-function (5.62) does not even occur in γ_{FF}^F, in contrast to eq. (5.61) for vector-gluon theories, because only the first diagram in fig. 5.7 contributes for theories with no gauge-fields.

5.4. The Q^2 dependence of parton distributions

Instead using eq. (5.76) for comparing the predictions of scaling violations with experiment, we shall now relate the quantities $F_{NS}(x, Q^2)$ and $F_\pm(x, Q^2)$ to Q^2-dependent parton distributions for which we then can use the well known naive parton model relations [41] to predict any measured structure functions or even different reactions (such as Drell–Yan dilepton production, high-p_T reactions etc.). To achieve this it is useful to make a change [57] of basis from O_{NS} and $O_\pm$ to operators O_0, O_3, O_8 and O_{15} of definite transformation properties under flavor SU(4), say. Suppressing all obvious factors like Dirac matrices and Lorentz indices, this procedure can be generically illustrated in the following intuitive way. Let us consider the electromagnetic current and a four-flavor (u, d, s, c) theory where

$$J = \tfrac{2}{3}\bar{\psi}_u\psi_u - \tfrac{1}{3}\bar{\psi}_d\psi_d - \tfrac{1}{3}\bar{\psi}_s\psi_s + \tfrac{2}{3}\bar{\psi}_c\psi_c. \tag{5.84}$$

Reducing the time-ordered product in eq. (5.46) by the usual contractions

$$\begin{aligned} T(J(z)\,J(0)) &= \tfrac{4}{9}\bar{\psi}_u(z)\,\underline{\psi_u(z)\,\bar{\psi}_u(0)}\,\psi_u(0) + \tfrac{1}{9}(u\to d) + \tfrac{1}{9}(u\to s) + \tfrac{4}{9}(u\to c) - \cdots \\ &\simeq \tfrac{4}{9}\bar{\psi}_u(z)\,\psi_u(0) + \tfrac{1}{9}\bar{\psi}_d(z)\,\psi_d(0) + \tfrac{1}{9}\bar{\psi}_s(z)\,\psi_s(0) + \tfrac{4}{9}\bar{\psi}_c(z)\,\psi_c(0) \end{aligned} \tag{5.85}$$

where in the last line we have kept only the field operators and have suppressed the c-number contractions (Feynman propagators). In the language of the Wilson expansion, the terms kept in eq. (5.85) correspond to leading twist $\tau = 2$ operators, i.e. where the same quark propagates between the two external current vertices and which does not interact with the remaining spectators in the nucleon as shown for example in fig. 5.8(a). The neglected terms in eq. (5.85) refer to non-leading higher-twist contributions [58, 31] which correspond to configurations where the external currents scatter off different quarks (cat's ear diagrams) or where the struck quark interacts with the spectators in the nucleon as shown in fig. 5.8(b). Taking the expectation value of eq. (5.85) between external proton states, say, immediately gives via eq. (5.11) the parton model relation (5.12). We can now rewrite eq. (5.85) as

$$T(JJ) = \bar{\psi}\hat{Q}^2\psi \quad \text{with} \quad \hat{Q}^2 = \begin{pmatrix} \frac{4}{9} & & & 0 \\ & \frac{1}{9} & & \\ & & \frac{1}{9} & \\ 0 & & & \frac{4}{9} \end{pmatrix}, \quad \psi = \begin{pmatrix} \psi_u \\ \psi_d \\ \psi_s \\ \psi_c \end{pmatrix} \tag{5.86}$$

and expand $\hat{Q}^2$ in a basis with definite SU(4) transformation properties:

$$\hat{Q}^2 = c_0\lambda_0 + c_3\lambda_3 + c_8\lambda_8 + c_{15}\lambda_{15} \tag{5.87}$$

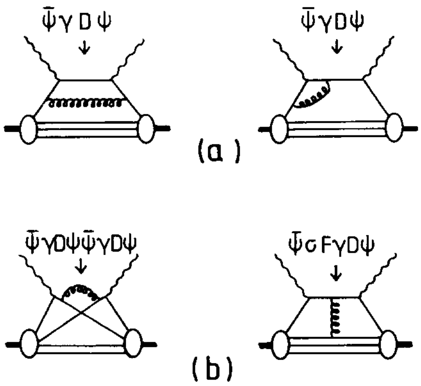

Fig. 5.8. Diagrams illustrating the meaning of twist with the corresponding operator written above each picture: (a) shows typical twist-2 effects (no communication between struck quarks and spectator quarks), and (b) illustrates twist-4 contributions.

where the coefficients c_i can be easily calculated using $\mathrm{Tr}(\lambda_a\lambda_b) = 2\delta_{ab}$. This gives

$$T(JJ) = \tfrac{5}{18}O_0 + \tfrac{1}{6}O_3 + \tfrac{1}{18}O_8 - \tfrac{1}{18}O_{15} \tag{5.88}$$

with

$$\begin{aligned} O_0 &= \bar\psi_u\psi_u + \bar\psi_d\psi_d + \bar\psi_s\psi_s + \bar\psi_c\psi_c \\ O_3 &= \bar\psi_u\psi_u - \bar\psi_d\psi_d \\ O_8 &= \bar\psi_u\psi_u + \bar\psi_d\psi_d - 2\bar\psi_s\psi_s \\ O_{15} &= \bar\psi_u\psi_u + \bar\psi_d\psi_d + \bar\psi_s\psi_s - 3\bar\psi_c\psi_c \end{aligned}$$

where O_0 transforms as a SU(4) flavor-singlet to be identified with the fermionic singlet operator O_F in eq. (5.75), and $O_{i=3,8,15}$ are the flavor quantum-number carrying non-singlet operators related to the NS structure functions in eq. (5.63). Defining the parton distributions as in eq. (5.11), the amplitudes with specific singlet and non-singlet SU(4) transformation properties are given by

$$\begin{aligned} \Sigma &\equiv \langle p|O_0|p\rangle = u + \bar u + d + \bar d + s + \bar s + c + \bar c = u_V + d_V + 6\xi + 2\xi' \\ A_3 &\equiv \langle p|O_3|p\rangle = u + \bar u - (d + \bar d) = u_V - d_V \\ A_8 &\equiv \langle p|O_8|p\rangle = u + \bar u + d + \bar d - 2(s + \bar s) = u_V + d_V \\ A_{15} &\equiv \langle p|O_{15}|p\rangle = u + \bar u + d + \bar d + s + \bar s - 3(c + \bar c) = u_V + d_V + 6\xi - 6\xi' \end{aligned} \tag{5.89}$$

with $\Sigma = \Sigma(x, Q_0^2)$, $A_i = A_i(x, Q_0^2)$, $u = u(x, Q_0^2)$ etc., and where we have also used the SU(3) symmetric ansatz (5.28) and for the charmed parton distributions we have taken

$$\xi' \equiv c \simeq \bar c. \tag{5.90}$$

Solving eq. (5.89) for the parton distributions we get the desired result

$$\begin{aligned} u_V &= \tfrac{1}{2}(A_8 + A_3), \qquad & \xi &= \tfrac{1}{6}(\tfrac{3}{4}\Sigma - A_8 + \tfrac{1}{4}A_{15}) \\ d_V &= \tfrac{1}{2}(A_8 - A_3), \qquad & \xi' &= \tfrac{1}{8}(\Sigma - A_{15}). \end{aligned} \tag{5.91}$$

This allows us to calculate the Q^2 dependence in a rather straightforward way since the Q^2 evolution of the A_i is given by eq. (5.63) whereas the singlet combination Σ evolutes according to the (±)-component in eq. (5.76), using eq. (5.75), to which we will now turn.

For completeness let us first state the result of the above decomposition for a three-flavor SU(3) theory (u, d, s quarks): Instead of eqs. (5.89) and (5.91) we have

$$\begin{aligned} \Sigma &= u + \bar u + d + \bar d + s + \bar s = u_V + d_V + 6\xi \\ A_3 &= u + \bar u - (d + \bar d) = u_V - d_V \\ A_8 &= u + \bar u + d + \bar d - 2(s + \bar s) = u_V + d_V \end{aligned} \tag{5.92}$$

and

$$u_V = \tfrac{1}{2}(A_8 + A_3), \qquad \xi = \tfrac{1}{6}(\Sigma - A_8)$$
$$d_V = \tfrac{1}{2}(A_8 - A_3). \tag{5.93}$$

Because of eq. (5.75) the Q^2 evolution of the fermionic singlet structure function Σ will be influenced by the gluon distribution $G(x, Q^2)$ in the nucleon: since

$$x\,\Sigma(x, Q_0^2) \equiv \langle p|O_F|p\rangle, \qquad x\,G(x, Q_0^2) \equiv \langle p|O_V|p\rangle \tag{5.94}$$

eq. (5.75) implies

$$\langle F_\pm(Q_0^2)\rangle_n = \begin{pmatrix} 1-\alpha_n \\ \alpha_n \end{pmatrix} \langle x\,\Sigma(Q_0^2)\rangle_n \mp \beta_n \langle xG(Q_0^2)\rangle_n \tag{5.95}$$

where we have used eqs. (5.70) and (5.72). Solving these equations for $\langle x\Sigma\rangle_n$ and $\langle xG\rangle_n$ and using the RG exponents in eq. (5.76) for $\langle F_\pm(Q^2)\rangle_n$ we can reexpress the Q^2-evolution for singlet components entirely in terms of parton distributions: remember that generically we had

$$\left.\begin{aligned} O_- &= \alpha_n O_F + \beta_n O_V \\ O_+ &= (1-\alpha_n)O_F - \beta_n O_V \end{aligned}\right\} \Rightarrow \begin{aligned} O_F &= O_- + O_+ \\ \beta_n O_V &= (1-\alpha_n)O_- - \alpha_n O_+ \end{aligned} \tag{5.96}$$

from which we can directly read off the Q^2-evolution of Σ and G:

$$\begin{aligned} \langle x\Sigma(Q^2)\rangle_n = {} & [\alpha_n \langle x\Sigma(Q_0^2)\rangle_n + \beta_n \langle xG(Q_0^2)\rangle_n] \exp\{-sa_-(n)\} \\ & + [(1-\alpha_n)\langle x\Sigma(Q_0^2)\rangle_n - \beta_n \langle xG(Q_0^2)\rangle_n] \exp\{-sa_+(n)\} \end{aligned} \tag{5.97}$$

$$\begin{aligned} \langle xG(Q^2)\rangle_n = {} & \left[(1-\alpha_n)\langle xG(Q_0^2)\rangle_n + \frac{\alpha_n(1-\alpha_n)}{\beta_n}\langle x\Sigma(Q_0^2)\rangle_n\right] \exp\{-sa_-(n)\} \\ & + \left[\alpha_n \langle xG(Q_0^2)\rangle_n - \frac{\alpha_n(1-\alpha_n)}{\beta_n}\langle x\Sigma(Q_0^2)\rangle_n\right] \exp\{-sa_+(n)\} \end{aligned} \tag{5.98}$$

and the non-singlet pieces evolute according to

$$\langle xA_{i=3,8,15}(Q^2)\rangle_n = \langle xA_{i=3,8,15}(Q_0^2)\rangle_n \exp\{-sa_{NS}(n)\}. \tag{5.99}$$

Equations (5.97)–(5.99) are the basic predictions for scaling violations in structure functions according to QCD as well as to conventional fixed point theories with $a_i(n)$ and s given by eqs. (5.77) and (5.78), respectively, and α_n and β_n defined in eq. (5.72). The basic algorithm for comparing eqs. (5.97)–(5.99) with experiment is the following:

(i) parametrize the parton distributions at a fixed value of Q_0^2 according to some power law $u_v(x, Q_0^2) \sim x^a(1-x)^b$, etc. and fit these x-dependences to experiment at $Q^2 = Q_0^2$ using the naive parton model relations (5.12) and (5.13), for example;

(ii) calculate via eq. (5.89) the input amplitudes $\Sigma(x, Q_0^2)$ and $A_i(x, Q_0^2)$;

(iii) insert these expressions into eqs. (5.97)–(5.99) in order to obtain their Q^2-dependence;

(iv) these Q^2 dependent moments of $\Sigma(x, Q^2)$ and $A_i(x, Q^2)$ allow us to calculate the Q^2 dependent parton distributions using eq. (5.91);

(v) the connection with measured structure functions at $Q^2 \neq Q_0^2$ is then again given by the parton model relations such as eqs. (5.12) and (5.13).

Equation (5.97) is of utmost importance since it allows us to determine the gluon content of the nucleon from the measured Q^2 dependence of structure functions: For this purpose we use, for example,

$$F_2^{e(\mu)p}(x, Q^2) = \tfrac{5}{18} x\Sigma(x, Q^2) + \tfrac{1}{6} x[u + \bar{u} - d - \bar{d} - s - \bar{s} + c + \bar{c}] \tag{5.100}$$

$$F_2^{\nu N}(x, Q^2) = x\Sigma(x, Q^2) \tag{5.101}$$

with $N = (p+n)/2$, $u = u(x, Q^2)$, etc. and where we have assumed $s \simeq \bar{s}$ and $c \simeq \bar{c}$ in $F_2^{\nu N}$; the NS expression in square-brackets in eq. (5.100) evolutes according to eq. (5.99). Then the only unknown in eq. (5.97) is $\langle xG(Q_0^2)\rangle_n$, besides of course the scale parameter Λ in s, which can be fitted to the measured Q^2 dependence of $F_2(x, Q^2)$ or of $\langle F_2(Q^2)\rangle_n$.

Since the input parton distributions, which describe the bound states of the considered hadron, are so far theoretically not calculable one usually refers to theoretical prejudices as far as their x-dependence is concerned. At small values of x one uses the Regge constraints (5.26) and (5.27) whereas at large x one resorts to naive dimensional counting rules [59–61] to fix their threshold suppression which tell us that

$$q(x, Q_0^2) \sim (1-x)^{2n-3} \qquad \text{as } x \to 1 \tag{5.102}$$

where n is the minimum number of the possible hard constituents in the hadron. The value of Q_0^2 where these rules apply is unknown but optimistically we may expect (5.102) to be valid at distances where the naive parton model starts to make sense ("precocious scaling"), i.e. $Q_0^2 \simeq 2$–$5\ \mathrm{GeV}^2$. As an example let us consider the most important case of parton distributions in the nucleon:

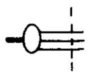 : $u_v, d_v \sim (1-x)^{2\times 3-3} = (1-x)^3$

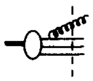 : $G \sim (1-x)^{2\times 4-3} = (1-x)^5$ (5.103)

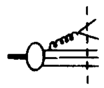 : $\xi \sim (1-x)^{2\times 5-3} = (1-x)^7.$

Needless to say that any other input parametrization which fits the data will do as well. However, because of momentum conservation, the parton distributions are expected to have in general the qualitative structure as shown in fig. 5.9. This is obvious from fig. 5.3 where, because of the gluon bremsstrahlung, the sea quark ($q\bar{q}$) will carry the least amount of large (hard) momentum in contrast to valence quarks, with the gluons lying in between. The charmed sea distribution $\xi' \equiv c \simeq \bar{c}$ in fig. 5.9 is always expected to be much steeper ("softer") than the SU(3) sea ξ since heavy quarks carry on the

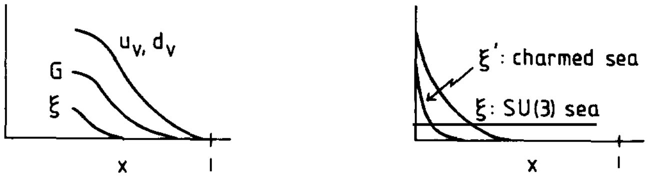

Fig. 5.9. Qualitative behavior of parton distributions at large and small values of x.

average less large momenta than the light SU(3) quarks. Finally, for practical purposes, the moments in eqs. (5.97)–(5.99) of a given parametrization of an input parton distribution $xq(x, Q_0^2) = x^a(1-x)^b$, say, can be simply calculated by

$$\langle xq(Q_0^2)\rangle_n = \langle x^a(1-x)^b\rangle_n = B(a+n-1, b+1) \tag{5.104}$$

with the Euler beta function $B(x, y) = \Gamma(x)\,\Gamma(y)/\Gamma(x+y)$. Later we shall use this equation to analytically continue our real-n moments to complex values of n which will be necessary to obtain, via a Mellin inversion technique, the explicit x-dependence of structure functions from their moments in eqs. (5.97)–(5.99).

In the next two subsections we shall discuss how to compare the predictions (5.97)–(5.99) for scaling violations with experiment.

5.5. *Comparing moments of structure functions with experiment*

The most straightforward and simple, although in many cases not very stringent and instructive, tests of field theories are to compare just moments of structure functions with experiment which, as we have seen, are directly predicted by any field theory. However, it should be noted that even the experimental determination of moments, defined in eq. (5.45), is problematic since for a given value of Q^2 one has so far measurements of $F(x, Q^2)$ available only in a limited region of x; therefore in order to calculate the moments in (5.45) one has to make one or another ad hoc extrapolation into regions of x experimentally not yet accessible.

Let us start with the theoretically most simple case of *non-singlet* structure functions, i.e. with eq. (5.63) which, for QCD, tells us that

$$\langle F_{NS}(Q^2)\rangle_n^{-1/a_{NS}(n)} \sim \ln(Q^2/\Lambda^2) \tag{5.105}$$

i.e., the $(-1/a_{NS})$th power of the nth moments are expected to lie along straight lines when plotted against $\ln Q^2$ with a common intercept $\ln Q^2 = \ln \Lambda^2$. These predictions have been found to be in very good agreement [62] with the data of $F_{NS} = xF_3^{\nu N}$ for $\Lambda \simeq 0.5$ GeV as shown in fig. 5.10(a). Similar conclusions have been reached from analyzing the BEBC data [43] but it should be emphasized, however, that these latter results rely heavily on measurements between $Q^2 = 0.6$ and $2\ \mathrm{GeV}^2$ – a region neither appropriate for the parton model nor for the legitimacy of perturbative calculations. Even in the CDHS experiment [62], where $Q^2 \gtrsim 6.5\ \mathrm{GeV}^2$, ill understood kinematical target mass effects $(\sim x^2 m_N^2/Q^2)$ play a non-negligible role: Assuming that these effects can be in part accounted for by "Nachtmann moments" [63, 64]

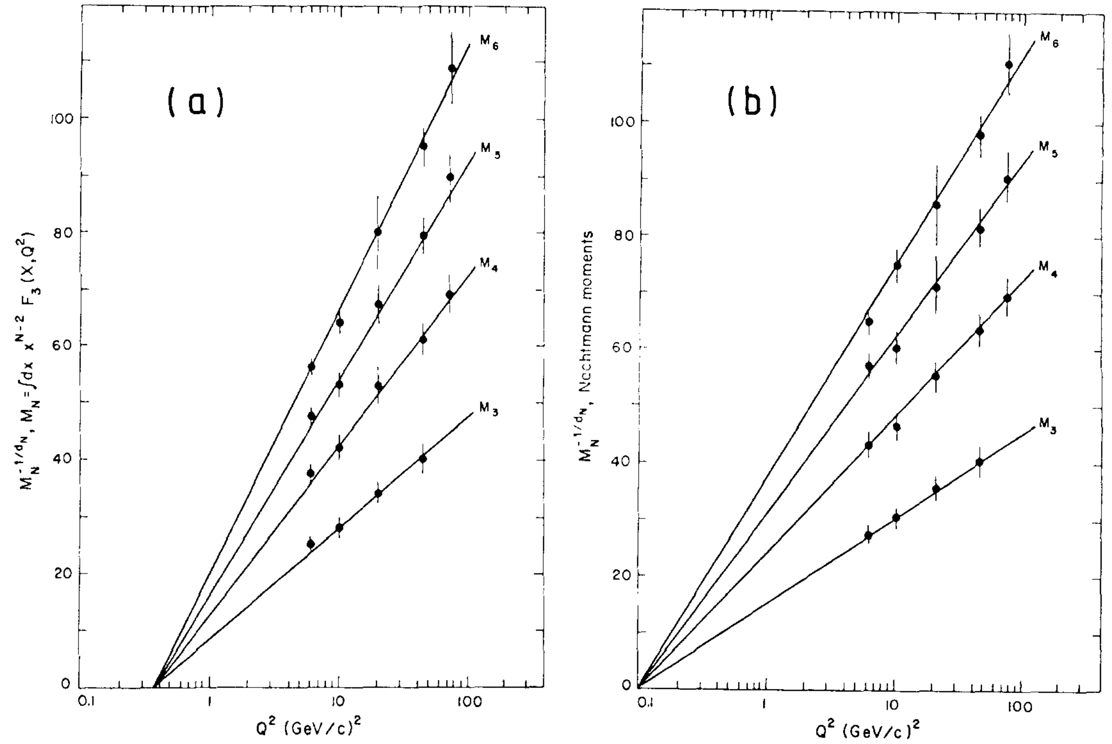

Fig. 5.10. Fit to the Q^2 dependence of (a) ordinary Cornwall–Norton x-moments $M_n \equiv \langle xF_3^{\nu N}(Q^2)\rangle_n$ and (b) Nachtmann moments according to QCD. The figures are taken from ref. [62].

$$\int_0^1 dx\, \frac{\xi^{n+1}}{x^3} \frac{1+(n+1)\sqrt{1+4x^2 m_N^2/Q^2}}{n+2}\, x F_3(x, Q^2) \tag{5.106}$$

with

$$\xi = \frac{2x}{1+\sqrt{1+4x^2 m_N^2/Q^2}}, \tag{5.107}$$

then the fitted slopes *decrease* by more than 10% as shown in fig. 5.10(b). The importance of this statement will become clear in a moment. The target mass effects in eq. (5.106) result from the trace-terms in the NS Wilson operator of twist 2 and with definite spin in eq. (5.60), i.e. from the $g^{\mu\nu}$ terms indicated in eq. (5.40). (Higher twist $\tau > 2$ effects as in eq. (5.41) are of course still neglected.) Besides using the rather heavy artillery of the operator product expansion, the Georgi–Politzer [65, 31] ξ-scaling variable in eq. (5.107) can be derived in a physically more transparent way by using the on-mass shell covariant parton model [66]. The parton language is a useful mnemonic for the form [67, 65] of ξ in eq. (5.107): If a massless quark carries a fraction ξ of the proton momentum and is kicked onto its mass shell by the collision, then $(\xi p + q)^2 = 0 = \xi^2 m_N^2 + 2\xi p \cdot q + q^2$ and the positive solution of this quadratic equation gives (5.107). It should be emphasized that these kinematical rescaling effects due to target masses alone cannot adequately describe [66] scaling violations and therefore the renormalization group improved QCD effects (radiative gluon corrections) discussed so far are significant and probably dominant in explaining the observed deviations from exact scaling. Since $n \gtrsim 3$ moments weigh mainly the large x region, one has to choose rather large values for Q^2 ($\gtrsim 10\,\text{GeV}^2$, say) in order to suppress subasymptotic kinematical terms since

$$\xi = x - x^3 m_N^2/Q^2 + O(m_N^4/Q^4), \tag{5.108}$$

or for the purely phenomenological Bloom–Gilman scaling variable [68] we would have

$$x' \equiv \frac{x}{1 + x m_N^2/Q^2} \simeq x - x^2 \frac{m_N^2}{Q^2} + O\left(\frac{m_N^4}{Q^4}\right). \tag{5.109}$$

These differences between the rescaling effects of $\xi, x', \ldots$ and the truly asymptotic Bjorken scaling variable x can be suppressed by directly studying $F(x, Q^2)$ for $x \lesssim 0.6$ and $Q^2 \gtrsim 5\,\text{GeV}^2$, say, since a transition from x to ξ or x' amounts practically to adding $O(m_N^2/Q^4)$ terms to the slopes of structure functions as is immediately evident from the following relation

$$\left.\frac{\partial F(x, Q^2)}{\partial Q^2}\right|_x = \left.\frac{\partial F(\bar{x}, Q^2)}{\partial Q^2}\right|_{\bar{x}} + \left.\frac{\partial F(\bar{x}, Q^2)}{\partial \bar{x}}\right|_{Q^2} \left.\frac{\partial \bar{x}}{\partial Q^2}\right|_x \tag{5.110}$$

for $\bar{x} = \xi, x'$, etc.

The measured NS moments of $F_3^{\nu N}$ in fig. 5.10(a), however, can be equally well explained by conventional fixed point field theories [69]. For an abelian vector-gluon theory eqs. (4.4), (4.17), (5.61), (5.64) and (5.78) tell us that (for $N_f = 4$)

$$a_{NS}^{\text{vector}} = \frac{25\alpha^*}{16\pi} a_{NS} \tag{5.111}$$

and thus eq. (5.63) predicts, in contrast to eq. (5.105),

$$\langle F_{NS}(Q^2)\rangle_n^{-1/a_{NS}(n)} = C_n(Q_0^2)(Q^2/Q_0^2)^{25\alpha^*/16\pi} \tag{5.112}$$

where the unknown normalization constants $C_n(Q_0^2) \equiv \langle F_{NS}(Q_0^2)\rangle_n^{-1/a_{NS}}$ have to be fitted to the data at an arbitrary value of $Q^2 = Q_0^2$. A similar power-like behavior in Q^2 is predicted by, for example, non-abelian scalar-gluon theories where, according to eqs. (4.18), (5.78) and (5.83),

$$a_{NS}^{\text{scalar}} = \frac{\alpha^*}{8\pi} \tilde{a}_n \tag{5.113}$$

with $\tilde{a}_n = \frac{4}{3}[1 - 2/\{n(n+1)\}]$ which gives for eq. (5.63)

$$\langle F_{NS}(Q^2)\rangle_n^{-1/\tilde{a}_n} = \tilde{C}_n(Q_0^2)(Q^2/Q_0^2)^{\alpha^*/8\pi}. \tag{5.114}$$

The predictions of abelian scalar-gluon theories are as in eq. (5.114) with α^* multiplied by a factor of 3/4, which follows from eqs. (4.17), (4.18) and (5.83). From fig. 5.11 it can be seen that the predictions

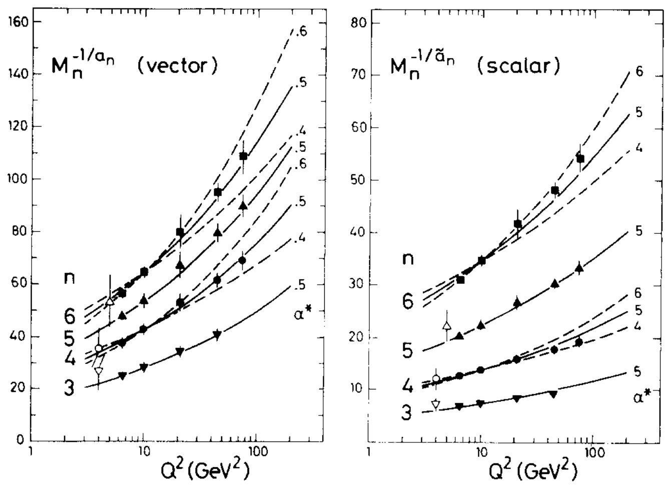

Fig. 5.11. Comparison of measured [62] moments $M_n \equiv \langle xF_3^{\nu N}(Q^2)\rangle_n$ with the predictions [69] of abelian vector-gluon theories ($a_n \equiv a_{NS}(n)$), eq. (5.112) and non-abelian scalar-gluon theories, eq. (5.114) for various choices of the fixed point α^*. The low-statistics data (open circles and triangles) are from ref. [43].

according to eqs. (5.112) and (5.114) are in equally good agreement [69] with experiment as are the straight line fits in fig. 5.10. Thus non-singlet quantities can only provide us with a consistency check of a given theory but cannot discriminate between QCD and other finite fixed point theories of strong interactions [70] (unless precision measurements can be extended to $Q^2 = 200$ or $300\,\mathrm{GeV}^2$, as it is evident from fig. 5.11). This, however, is not too surprising since the Q^2 dependence of NS moments is uniquely determined by just *one* anomalous dimension and, therefore, quantities such as $\langle F_{NS}(Q^2)\rangle_n^{-1/a_{NS}}$ are mainly sensitive to differences in a logarithmic and a power-like behavior in Q^2. This is in contrast to structure functions which receive also contributions from flavor-*singlet* Wilson operators, such as F_2, the Q^2 dependence of which is determined by *three* different anomalous dimensions in eq. (5.76): These subtleties of singlet-mixing will play a crucial role in discriminating between different field theories which will be discussed in a moment.

Another theoretically very attractive test of field theories, which measures ratios of anomalous dimensions directly, is obtained [43] by comparing the logarithms of two moments $\langle F_{NS}\rangle_n$ and $\langle F_{NS}\rangle_{n'}$ which, according to eq. (5.63), should result in straight lines (in the 1-loop order) with slopes $a_{NS}(n)/a_{NS}(n')$:

$$\frac{\mathrm{d}\ln\langle F_{NS}(Q^2)\rangle_n}{\mathrm{d}\ln\langle F_{NS}(Q^2)\rangle_{n'}} = \frac{a_{NS}(n)}{a_{NS}(n')}. \tag{5.115}$$

These slopes are obviously independent of Λ and α^*, as well as of the number of flavors. Moreover it should be emphasized that eq. (5.115) can discriminate only between vector and scalar gluons, but not between subtleties such as their abelian or non-abelian group structure: This is because the only difference between an abelian and non-abelian structure of the qqg-coupling in vector-gluon theories is due to the "color charge of a quark" $C_2(R)$ in eq. (5.61) which cancels in the ratio in eq. (5.115); and similarly for scalar-gluon theories. For illustration we compare in table 5.1 a typical prediction for the ratio of anomalous dimensions, according to eq. (5.61), with the measured [62, 43] $F_3^{\nu N}$-moments. As we can see, the measured slope [71] of ordinary x-moments $\langle xF_3^{\nu N}(Q^2)\rangle_n$ is in good agreement with the

Table 5.1
Comparison of the theoretical predictions for the $n/n' = 6/4$ moment ratio with CDHS measurements [62, 71]; the ordinary x-moments are defined in eq. (5.45) and Nachtmann moments in eq. (5.106)

	experiment		theory	
	$\langle xF_3^{\nu N}\rangle_n$	Nachtmann	vector	scalar
$a_{NS}(6)/a_{NS}(4)$	1.34 ± 0.07	1.18 ± 0.09	1.29	1.06

predictions of vector-gluon theories. However, as in the previous case, target mass effects (Nachtmann moments) play a non-negligible role, although $Q^2 \geq 6.5\,\text{GeV}^2$ for the CDHS experiment [62], which *decrease* the slopes by more than 10% as compared to our ordinary moments. On the other hand the slope predictions of scalar theories are typically 20% smaller than those of vector theories. Thus, at present, not even scalar-gluon theories can be ruled out within 1σ on the basis of this non-singlet moment-slope test in eq. (5.115).

In order to proceed we should make use of the full content of the theoretical predictions in eq. (5.76) or eqs. (5.97)–(5.99) by studying structure functions such as $F_2(x, Q^2)$ which contain dominant *singlet* components. This should prove more awarding since fixed point theories differ from QCD mainly in their singlet mixing properties, because of their very different gluonic anomalous dimensions as implied by eqs. (5.68) and (5.83) together with eqs. (4.4), (4.17) and (4.18). The most important and instructive moment to study [72] is the lowest $n = 2$ moment of F_2, i.e. the area under $F_2(x, Q^2)$. From eqs. (5.100) and (5.101) we have for $\langle F_2(Q^2)\rangle_2 \equiv \int_0^1 F_2(x, Q^2)\,dx$

$$\langle F_2^{\mu p}(Q^2)\rangle_2 = \tfrac{5}{18}\langle x\,\Sigma(Q^2)\rangle_2 + \tfrac{1}{6}\langle x[u_v(Q_0^2) - d_v(Q_0^2) - 2\xi(Q_0^2) + 2\xi'(Q_0^2)]\rangle_2 \exp\{-s a_{NS}(2)\} \tag{5.116}$$

$$\langle F_2^{\nu N}(Q^2)\rangle_2 = \langle x\,\Sigma(Q^2)\rangle_2 \tag{5.117}$$

where the non-singlet component in eq. (5.116) can be estimated to be small [72], and the Q^2 dependence of the singlet piece follows from eq. (5.97)

$$\langle x\,\Sigma(Q^2)\rangle_2 = \alpha_2 + [\langle x\,\Sigma(Q_0^2)\rangle_2 - \alpha_2]\exp\{-s a_+(2)\} \tag{5.118}$$

where we have used $\alpha_2 = \beta_2$, $a_-(2) = 0$ and

$$\langle xG\rangle_2 = 1 - \langle x\Sigma\rangle_2 \tag{5.119}$$

which, by momentum conservation (see eq. (5.16)), holds for all values of Q^2. The physical interpretation of eq. (5.118) is obvious: α_2 is the asymptotic value of the total fractional momentum carried by the fermionic constituents of the nucleon in the limit $Q^2 \to \infty$; because of the gluon self-couplings, quarks are much more effective in radiating gluons and can therefore easier transmit their momentum to gluons in QCD than in conventional fixed point theories which naively implies

$$\alpha_2^{\text{QCD}} < \alpha_2^{\text{fixed-point}}.$$

Thus eq. (5.118) plays a unique role [72] in discriminating between QCD and all other conventional fixed point field theories. This comes about as follows. At moderate $Q^2 \simeq 2$–$4\,\mathrm{GeV}^2$, corresponding to our input Q_0^2, experiment tells us [43–45] that the total fractional momentum carried by quarks is $\langle x\Sigma(Q_0^2)\rangle_2 \simeq 0.52$ and hence, according to eq. (5.118) and since $a_+(2) = 56/75 > 0$ (using $N_f = 4$), $\langle x\Sigma(Q^2)\rangle_2$ is an increasing or decreasing function of Q^2 depending on whether α_2 is larger or smaller than 1/2, respectively. Substituting the different possible values of the group invariants of eqs. (4.4), (4.17) and (4.18) into eq. (5.72), it turns out that $\alpha_2 < 1/2$ *only* for QCD where $\alpha_2 = 3/7$ (see eq. (5.74)). It is a unique feature of *all* other presently known field theories that $\alpha_2 > 1/2$ (specifically [72] $\alpha_2 = 6/7$, 9/10 and 72/73 for abelian vector-gluon, non-abelian scalar-gluon and abelian scalar-gluon theories, respectively) which forces $\int_0^1 F_2(x, Q^2)\,dx$ to *increase* with Q^2. Since $\int_0^1 F_2(x, Q^2)\,dx$ is experimentally observed [43, 44, 73, 74] to *decrease* with Q^2 (or at most to be constant), all theories except QCD are already excluded on the basis of this single *qualitative* observation! In fig. 5.12 we compare these predictions with experiment, where for the abelian vector-gluon theory we have taken the fixed point α^* to be 0.5 in agreement with our analysis [69] of NS moments in fig. 5.11. The predictions of scalar-gluon theories are in even worse agreement with the data since their values for α_2 are always larger than 6/7. Similar conclusions have been already reached some time ago by a more detailed quantitative analysis [75, 76] of $F_2^{e(\mu)N}(x, Q^2)$ and also by studying the timelike q^2 [77, 78]. It should, however, be noted that, although for $n = 2$ we have (using $\gamma_-(2) = 0$ in eq. (5.71) and eq. (5.72))

$$\alpha_2 = \frac{\gamma^{V}_{VV}(2)}{\gamma^{F}_{FF}(2) + \gamma^{V}_{VV}(2)} = \tag{5.120}$$

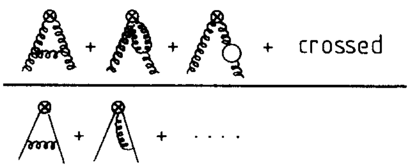

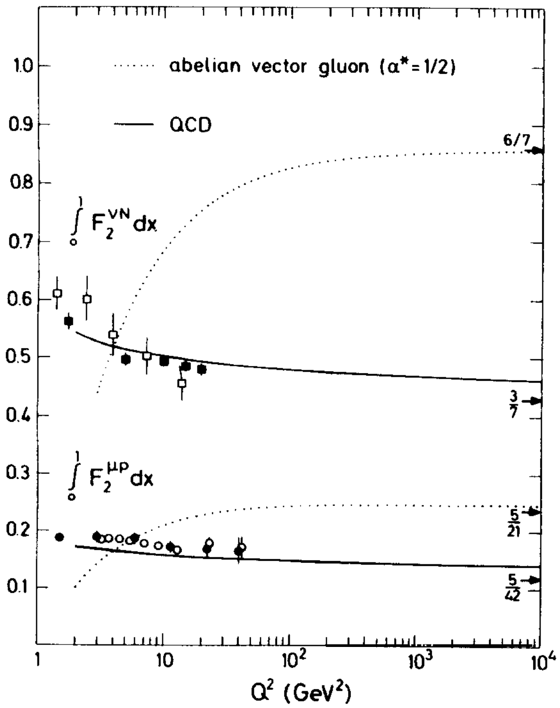

Fig. 5.12. Comparison [72] of the Q^2 evolution of the area under F_2, predicted by vector-gluon theories, with the νN data of refs. [43, 45] and with the μp data of ref. [73].

Table 5.2
Values for the renormalization group exponents $a_i(n)$ and for the projection matrix elements $\alpha_n \equiv p_{\bar{1}1}(n)$ and $\beta_n \equiv p_{\bar{2}1}(n)$ in eq. (5.72) for a four flavor QCD ($N_f = 4$)

n	$a_{NS}(n)$	$a_-(n)$	$a_+(n)$	α_n	β_n
2	0.427	0	0.747	0.429	0.429
3	0.667	0.609	1.39	0.925	0.288
4	0.837	0.817	1.85	0.98	0.17
5	0.971	0.960	2.19	0.992	0.119
6	1.08	1.07	2.46	0.996	0.091

the Q^2 dependence of $\langle x\,\Sigma(Q^2)\rangle_2$ in eq. (5.118) is *not* directly sensitive to the triple gluon coupling since the coefficient of $C_2(G)$ in $\gamma^{V}_{VV}(2)$ in eq. (5.68) vanishes. Therefore the whole contribution to $\gamma^{V}_{VV}(2)$ is due to the term proportional to $T(R)$ in eq. (5.68), i.e. to the external wave function renormalization () corresponding to the last term in eq. (5.52). Thus, α_2 measures mainly the color charge of quarks, i.e. the quark–gluon coupling in (3.6) but not the self-interactions (2.5) of gluons, i.e. the Yang–Mills structure of eq. (2.3). Needless to say that gluon self-couplings are required in order to render a non-abelian vector-gluon theory renormalizable leaving QCD unrivalled.

Since higher $n(\gtrsim 3)$ moments weigh mainly the large x region ($x \gtrsim 0.3$), the study of $n > 2$ moments of any structure function cannot provide us with additional information on the gluon structure of QCD. This is so because from eq. (5.71) one obtains

$$\left.\begin{aligned} &\gamma_-(n) = \gamma^{F}_{FF}(n) - O\left(\frac{1}{n^2 \ln n}\right) \\ &\gamma_+(n) \gg \gamma_-(n) \end{aligned}\right\} \quad \text{for} \quad n > 2 \tag{5.121}$$

and thus always just one anomalous dimension $\gamma_{NS} \equiv \gamma^{F}_{FF}$ in eq. (5.76) dominates: any structure function such as $F_2(x, Q^2)$ will, for $x \gtrsim 0.3$ (i.e. $n \gtrsim 3$), essentially behave as the non-singlet function in eq. (5.63). Table 5.2 illustrates how well (5.121) is already satisfied for $n \gtrsim 3$. Therefore, the subtle and very important singlet-mixing properties of the theory, which allows us to study the detailed gluon structure, is only effective for small n, i.e. in the small x-region, not accessible to any moment analysis. We will therefore try to extract from the predicted moments of structure functions in eqs. (5.76) or (5.97)–(5.99) the explicit x-dependence of $F(x, Q^2)$ which is after all the quantity directly accessible experimentally.

5.6. *Inverting moments*

The general procedure to obtain $F(x, Q^2)$ from given moments $\langle F(Q^2)\rangle_n \equiv \int_0^1 dx\, x^{n-2} F(x, Q^2)$ is to perform a Mellin inversion [79]

$$F(x, Q^2) = \frac{1}{2\pi i} \int_{c-i\infty}^{c+i\infty} dn\, x^{-n+1} \langle F(Q^2)\rangle_n \tag{5.122}$$

where the integration contour has to lie to the right of the rightmost singularity of $\langle F(Q^2)\rangle_n$ in the complex

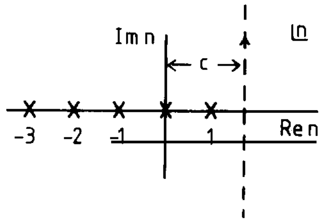

Fig. 5.13. The integration contour for the inversion of the Mellin transform $\langle F(Q^2)\rangle_n = \langle F(Q_0^2)\rangle_n \exp\{-sa(n)\}$ in eq. (5.122). The crosses (×) denote the singularities of $\langle F(Q^2)\rangle_n$ which are either simple poles (stemming from the input distributions $\langle F(Q_0^2)\rangle_n \sim B(a+n-1, b+1)$ in eq. (5.104)) or essential singularities (stemming from $\exp\{-sa(n)\}$ due to the poles of $a(n)$).

n plane as indicated in fig. 5.13. The inversion of asymptotic approximations (leading log's) of moments, like eqs. (5.63) or (5.76), via the continuation in n is certainly suspect. By inverting the moments to deduce the behavior of $F(x, Q^2)$ one must assume that all possible subdominant higher-order terms in anomalous dimensions and Wilson coefficients are negligible uniformly in n. Thus, all subdominant terms on the right-hand side of eqs. (5.63) or (5.76) have to be negligible once Q^2 exceeds a certain limit, call it Q_0^2, where Q_0^2 is independent of n. These corrections are indeed negligible provided [80, 6]

$$\alpha_s\left[\ln\frac{4G\ln\alpha_s}{\ln x}\right]^3 \ll 1 \qquad \text{for} \quad x \simeq 1$$

$$\alpha_s\left[\frac{\ln x}{9G\ln\alpha_s}\right]^{3/2} \ll 1 \qquad \text{for} \quad x \ll 1 \tag{5.123}$$

with

$$G \equiv \frac{C_2(R)}{16\pi^2 b} = \frac{4}{33-2N_f}. \tag{5.124}$$

For general (singlet) structure functions, eq. (5.122) can only be calculated numerically [56] but for special cases, such as NS structure functions or for $x \to 1$, one can handle eq. (5.122) analytically which we shall do first.

Although for practical purposes it turns out that the numerical evaluation of the integral in (5.122) is the most efficient one, it is possible and also instructive to reduce this complicated integral to a more simple expression for *non-singlet* structure functions. We start from the NS-moment prediction in eq. (5.63)

$$\langle F_{NS}(Q^2)\rangle_n = \langle F_{NS}(Q_0^2)\rangle_n \exp\{-sa_{NS}(n)\} \tag{5.63}$$

and use the following convolution theorem of Mellin transforms: If two moments are given by

$$\int_0^1 dx\, x^{n-2} f_i(x) = g_i(n)$$

then

$$\int_0^1 dx\, x^{n-2} f_1 * f_2 = g_1(n)\, g_2(n)$$

where

$$f_1 * f_2 = \int_x^1 \frac{dx'}{x'} f_1(x') f_2\left(\frac{x}{x'}\right). \tag{5.125}$$

From this one simply obtains for eq. (5.63)

$$F_{NS}(x, Q^2) = \int_x^1 \frac{dx'}{x'} F_{NS}\left(\frac{x}{x'}, Q_0^2\right) T(x', Q^2) \tag{5.126}$$

with the Mellin-inverse of the RG exponent given by

$$T(x', Q^2) = \frac{1}{2\pi i} \int_{c-i\infty}^{c+i\infty} dn\, x'^{1-n} \exp\{-s a_{NS}(n)\}. \tag{5.127}$$

For the general $a_{NS}(n)$ in eq. (5.61) this kernel T cannot be evaluated exactly because of the exponential. Therefore one should instead differentiate [81] eq. (5.63)

$$\frac{d\langle F_{NS}(Q^2)\rangle_n}{ds} = -a_{NS}(n) \langle F_{NS}(Q^2)\rangle_n \tag{5.128}$$

which upon using the above convolution theorem (5.125) gives

$$\frac{dF_{NS}(x, Q^2)}{ds} = \int_x^1 \frac{dx'}{x'} F_{NS}\left(\frac{x}{x'}, Q^2\right) \frac{1}{2\pi i} \int_{c-i\infty}^{c+i\infty} dn\, x'^{1-n}(-a_{NS}(n)). \tag{5.129}$$

Now the relevant integrals over n can be done explicitly [79] to give (note that this would not be possible for the singlet structure functions $F_\pm$ because of the square-root terms in $a_\pm(n)$ in eq. (5.71))

$$\frac{dF_{NS}(x, Q^2)}{ds} = G\Big\{[3 + 4\ln(1-x)]\, F_{NS}(x, Q^2) + \int_x^1 dx'\,(2-2x')\, F_{NS}\left(\frac{x}{x'}, Q^2\right)$$
$$+ 4\int_x^1 \frac{dx'}{1-x'}\left[x' F_{NS}\left(\frac{x}{x'}, Q^2\right) - F_{NS}(x, Q^2)\right]\Big\}. \tag{5.130}$$

This is Parisi's integro-differential equation [81] which can be solved [82] for the scaling violations of $F_{NS}(x, Q^2)$. Figure 5.14 shows the QCD predictions [83] for $F_{NS} = F_1^{ep} - F_1^{en}$ taking the measured values for F_1^{en} as input [84]. The agreement with the data is good.

Furthermore, eq. (5.126) allows us to derive an explicit analytic expression for the threshold behavior of any structure function [85], i.e. for the Q^2 dependence of $F(x, Q^2)$ at large x, because of (5.121) the Q^2 evolution of *any* (singlet or non-singlet) structure function will be dominated by just one anomalous

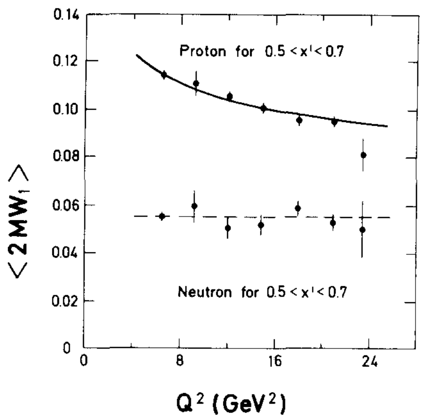

Fig. 5.14. Comparison of the experimental data [84] with the predicted variation of $F_{NS} = F_1^{ep} - F_1^{en}$ in eq. (5.63), using the neutron data as input [83].

dimension $\gamma_{NS} \equiv \gamma_{FF}^{F}$ for large n (i.e. large x). In this region we can therefore use the asymptotic expression for the ψ-function in eq. (5.62),

$$\psi(z) = \ln z + O(1/z) \qquad \text{for} \quad z \to \infty,$$

which, inserted into eqs. (5.61) and (5.64), yields

$$a_{NS}(n) \simeq G(c_1 \ln n + c_2) + O(1/n) \tag{5.131}$$

where $c_1 = 4$, $c_2 = -0.69$ and G is given in eq. (5.124). Note that the $\ln n$ term stems from the second and third diagram of fig. 5.7. For this simple case the kernel in eq. (5.127) can be calculated with the result

$$T(x', Q^2) \simeq \exp(-c_2 Gs) \frac{x(\ln(1/x))^{P-1}}{\Gamma(P)}, \qquad P = c_1 Gs. \tag{5.132}$$

Assuming now an input distribution in (5.126) of the form $F(x, Q_0^2) \simeq (1-x)^d$ we finally get

$$F(x, Q^2) \simeq (1-x)^d \left(\ln \frac{1}{x}\right)^P \exp(-c_2 Gs) \frac{\Gamma(d+1)}{\Gamma(d+1+P)}. \tag{5.133}$$

This is the famous Gross inversion formula [85] for large x, which for practical purposes is sufficiently accurate for $0.3 \lesssim x \lesssim 1$. A similar expression can be derived for just the F_+ amplitude, $\langle F_+(Q^2)\rangle_n = \langle F_+(Q_0^2)\rangle_n \exp(-sa_+(n))$: In this case one obtains [56] $c_1 = 9$ and $c_2 = -1.06$, which clearly shows that $F_+(x, Q^2)$ is much stronger suppressed in $(1-x)$ as $x \to 1$ than eq. (5.133). Since for non-gauge (scalar-gluon) theories only the first diagram in fig. 5.7 contributes to γ_{FF}^{F} in eq. (5.83), there will be no $\ln n$ term in eq. (5.131); thus P in eq. (5.133) vanishes which implies that $F(x, Q^2) \sim (1-x)^d$ has the same power behavior in $(1-x)$ as the input $F(x, Q_0^2) \sim (1-x)^d$. This is in contrast to gauge (vector-gluon) theories where the input $(1-x)^d$ will be changed to $F(x, Q^2) \sim (1-x)^{d+P}$ according to (5.133). First attempts [86] to compare the scaling violations predicted by eq. (5.133) with data for F_1^{ep} in the large x-region resulted in a good agreement between QCD and experiment. Equation (5.133) will also be useful for describing the scaling violations of fragmentation functions $D_q^h(z, Q^2)$ for large values of z to which we shall turn in section 10.

Similar analytic expressions for $F(x, Q^2)$ can be derived [56, 87] in the *small-x* region where only the contributions of the rightmost singularities of the anomalous dimensions are assumed to dominate. For these one can use the saddle-point method to evaluate their contributions to the inverse Mellin transforms (5.122) as done in ref. [87], or even better one can perform the inversions exactly [56] which allows $F(x, Q^2)$ to be expressed by modified Bessel functions. Unfortunately, for x even as small as 0.02, these results deviate by about 20%–30% from the results obtained from exact inversion procedures [56] for presently available values of Q^2.

In general one has therefore to perform the Mellin inversion (5.122) numerically [56] in order to obtain the required accuracy. For this it is convenient to rewrite eq. (5.122)

$$F(x, Q^2) = \frac{1}{\pi} \int_0^\infty dz \, \mathrm{Re}\{x^{1-c-iz} \langle F(Q^2) \rangle_{n=c+iz}\}. \tag{5.134}$$

Choosing $c \simeq 2.5$, which is appropriate for all structure functions and field theories studied so far [56], an upper limit of integration in (5.134) of about 50 suffices to guarantee an accuracy of 10^{-3}. It is now

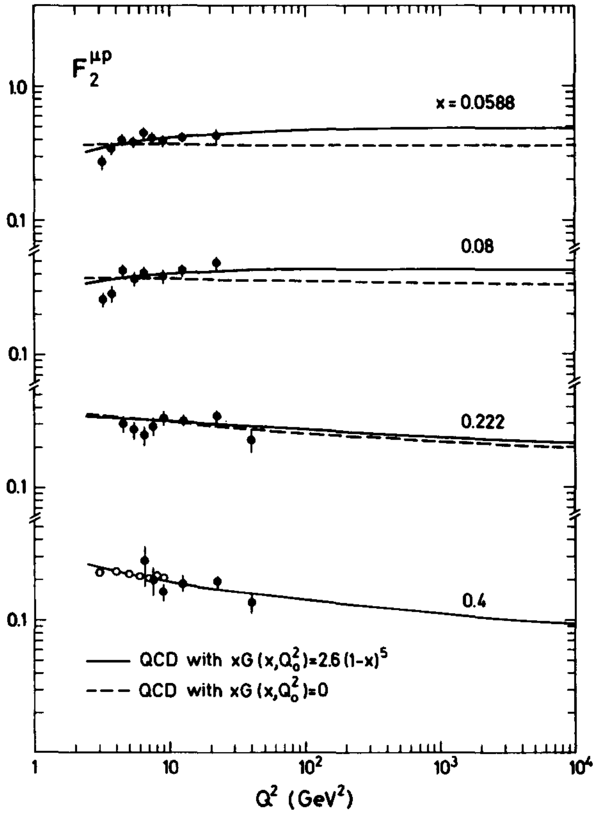

Fig. 5.15. Comparison of the predictions [72] for scaling violations with μp data [73] (solid points) and ep data [94] (open points).

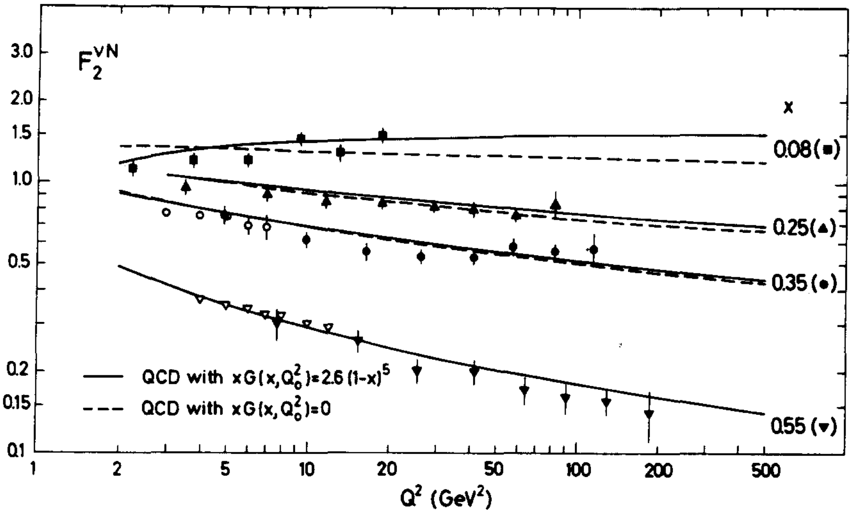

Fig. 5.16. Predictions [72] of scaling violations according to QCD as compared with neutrino data [44, 45] (solid points) and ed data [94] multiplied by the average valence quark charge 9/5 (open points).

straightforward to invert the moments in eqs. (5.97)–(5.99), for example, once we have fitted the parton distributions to experiment at Q_0^2 and using eq. (5.104) to calculate their analytically continued moments needed in (5.134). Scaling violations in $F_2(x, Q^2)$ have been studied in the past using a variety of different input distributions [88, 56, 76, 89–93]. As an example, we compare in figs. 5.15 and 5.16 the predicted scaling violations [72] in $F_2^{\mu p}$ and $F_2^{\nu N}$ with recent data [44, 45, 73, 94] using $\Lambda = 0.5$ GeV and the following input quark distributions at $Q_0^2 = 4\ \text{GeV}^2$, with the decomposition (5.28),

$$\begin{aligned} x(u_v + d_v) &= 4.546x^{0.624}(1-x)^{2.657} \\ xd_v &= 2.715x^{0.773}(1-x)^{3.7} \\ x\xi &= 0.17(1-x)^7 \\ x\xi' &= 0.05(1-x)^{30}. \end{aligned} \tag{5.135}$$

The steep charm distribution ξ' results from the virtual Bethe–Heitler process $\gamma^* g \to Q\bar{Q}$ which, due to the large mass of heavy quark flavors Q = c, b, . . . , is expected [95] to be the dominant contribution for heavy quark production [96, 97] and is directly proportional to the gluon content $G(x, Q^2)$ of the nucleon (fig. 5.17). To demonstrate the sensitivity of the predicted scaling violations to the choice of $G(x, Q_0^2)$ in eq. (5.97), we have performed the calculations once with the "standard" counting-rule-like

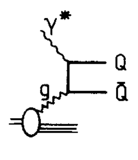

Fig. 5.17. Bethe–Heitler process for heavy-quark production.

gluon distribution

$$xG(x, Q_0^2) = 2.6(1-x)^5 \tag{5.136}$$

implied by eq. (5.103), and once with $G(x, Q_0^2) = 0$. This latter choice obviously violates the energy-momentum sum rule,

$$\langle x\Sigma(Q^2)\rangle_2 + \langle x\,G(Q^2)\rangle_2 = 1,$$

and is intended only as a check on the above mentioned sensitivity to $G(x, Q_0^2)$. As one can see from figs. 5.15 and 5.16 the scaling violations with the "standard" counting-rule gluon distribution (full lines) do not differ significantly from the ones with a zero input gluon distribution (dashed lines). Within a few percent these "standard" predictions in figs. 5.15 and 5.16 (solid curves) remain unchanged if one uses a broad gluon

$$x\,G(x, Q_0^2) = 0.88(1+9x)(1-x)^4 \tag{5.137}$$

as suggested by the Caltech group [98]. This huge gluon distribution with an abundance of hard gluons in the large-x region appears to be in better agreement with recent deep inelastic experiments [43, 44, 74]; especially it seems to be required by deep inelastic J/ψ production [99] and for explaining the hard transverse momentum spectrum ($p_T \gtrsim 1$ GeV) of Drell–Yan dilepton pairs to be discussed in section 8.1. The fact that the predictions for scaling violations in F_2 are insensitive to the gluon content of the nucleon for large x ($\gtrsim 0.3$) can be easily understood from the explicit values of the projection matrix elements α_n and β_n and how they enter eq. (5.97): From table 5.2 we see that $\alpha_n \simeq 1$ and $\beta_n \ll 1$ for $n > 3$ and therefore $\langle x\,G(Q_0^2)\rangle_n$ in eq. (5.97) is strongly suppressed for large n (i.e., large x). Thus any moment analysis of F_2 with $n \gtrsim 4$ for testing QCD and determining the gluon distribution via eq. (5.97), using presently available data, is rendered meaningless and statistically insignificant. Only future high-statistics measurements of F_2 for $0.05 \lesssim x \lesssim 0.3$ (heavy quark production should become important [96] only for smaller values of x) and for Q^2 up to 100–200 GeV^2, say, should shed further light on $G(x, Q^2)$. Needless to say that this small-x region is not accessible to any $n > 3$ moment analysis.

The general pattern of scaling violations, illustrated in figs. 5.15 and 5.16, is generally expected from any field theory: $F(x, Q^2)$ decreases with Q^2 at large values of x, whereas it increases with Q^2 at small x. This qualitative behavior can be easily understood because of the radiative gluon corrections (figs. 5.3 and 5.4(b)) and momentum conservation: increasing Q^2, the hard valence quarks will loose momentum by radiating gluons (fig. 5.3) and thus the valence distributions have to decrease at large x and increase at small x as illustrated in fig. 5.18(a); on the other hand, the larger Q^2 the more $q\bar{q}$ pairs can be

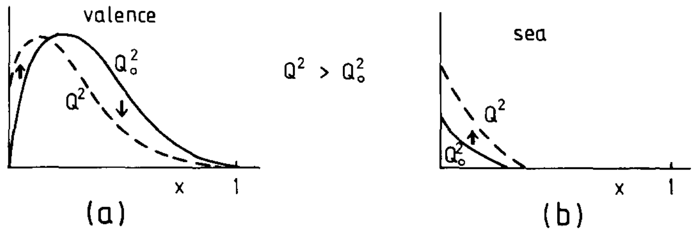

Fig. 5.18. Qualitative pattern for scaling violations for (a) valence distributions (xu_v, xd_v, $F_{NS} = F_2^{ep} - F_2^{en}$, etc.) and (b) for singlet "sea" distributions ($x\xi$, xG, etc.).

produced by the radiated gluons (fig. 5.3) and thus the sea distribution, which dominates $F(x, Q^2)$ at small x, has to increase at small x as shown in fig. 5.18(b). This qualitative interpretation of the pattern for the scaling violations in F_2 follows of course directly from our formal calculations of radiative QCD corrections to moments of F_2: from eqs. (5.116), (5.118), (5.73) and (5.63) we obtain

$$\lim_{Q^2\to\infty} \int_0^1 F_2^{\mathrm{ep,en}}(x, Q^2)\,\mathrm{d}x = \frac{5}{18}\alpha_2 = \frac{5}{18}\frac{3N_f}{16+3N_f} \tag{5.138}$$

$$\lim_{Q^2\to\infty} \int_0^1 (F_2^{\mathrm{ep}} - F_2^{\mathrm{en}})\,\mathrm{d}x = 0. \tag{5.139}$$

From eq. (5.138) we conclude that asymptotically the total area under F_2 remains constant, but it squeezes progressively into smaller and smaller x as indicated in fig. 5.18. Since the difference (5.139) of structure functions vanishes asymptotically, it seems that valence quarks are gradually disappearing as $Q^2\to\infty$; the asymptotic constancy of the singlet moment (5.138) suggests that everything finishes up in the "sea" (fig. 5.18(b)), which however also changes its shape, shrinking towards $x = 0$ at $Q^2\to\infty$.

Having fixed all input parton distributions and $\Lambda \simeq 0.5\,\mathrm{GeV}$, it is now straightforward to calculate further, essentially parameter-free scale-breaking predictions for deep inelastic neutrino reactions such as $\sigma^{\bar\nu}/\sigma^{\nu}$, $\langle y\rangle^{\bar\nu}$, explicit y distributions etc. [57, 100, 76, 89, 101–104]. Again the agreement with experiment is good [103, 104] by using the weak quark couplings implied by the standard Weinberg–Salam model. Since σ^{ν} receives its dominant contributions from valence quarks, we expect it to be governed, at presently measured energies, by the decrease of the valence quark distributions, i.e. σ^{ν}/E is expected to fall with increasing energy (see eq. (5.5)). For $\bar\nu$ scattering the decrease of the valence quark contribution is roughly compensated by the increase of the sea (fig. 5.18); thus $\sigma^{\bar\nu}/E$ is expected to be approximately constant at moderate energies, and to rise slowly at higher energies where charm production is at full strength. Asymptotically, $\sigma^{\bar\nu}/E$ should approach σ^{ν}/E and consequently $\sigma^{\bar\nu}/\sigma^{\nu}$ is predicted to increase. All these general expectations implied by QCD are confirmed by recent high energy experiments.

For alternative, non-field-theoretic (Regge-like) approaches to scaling violations we refer, for example, to refs. [105–108]. However, such (generalized) vector-meson dominance models can be "trusted" mainly in the small x-region. The power and beauty of explaining scaling violations with field theoretic methods (i.e., radiative corrections in QCD) remains, however, unchallenged in as much as they provide us with a framework for the *whole* x-region with essentially only *one* free parameter Λ. Furthermore, it appears to be a unique feature of the parton model combined with QCD to predict in terms of a single set of distribution functions (and decay functions) together with all possible α_s corrections and without invoking new free parameters, *all* known inclusive processes *simultaneously* such as $\mu p\to\mu\pi + X$, $pp\to\mu^+\mu^- + X$ (Drell–Yan), $pp\to$(heavy quark pair)$+ X$, $pp\to$(high-p_T jet)$+ X$, $\gamma p\to$(heavy quark pair)$+ X$, $e^+e^-\to q\bar q$-, $q\bar q g$- and 3g-jets, and many others more [109, 110].

5.7. Dynamical calculation of parton distributions

An intriguing possibility to determine the theoretically ill understood singlet parton distributions is to calculate the sea and gluon distributions dynamically [88, 111, 112] using the RG equations (5.97)–

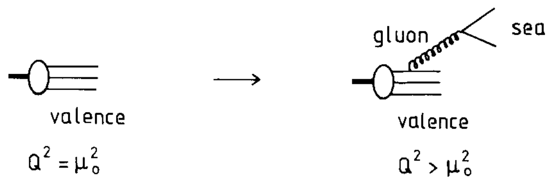

Fig. 5.19. Valence quarks at $Q^2=\mu_0^2$ generate dynamically sea quarks through gluons at $Q^2>\mu_0^2$.

(5.99). This idea [88] is based on the observation that setting $\langle x\,\xi(\mu_0^2)\rangle_n=0$ and $\langle x\,G(\mu_0^2)\rangle_n=0$ at $Q^2=\mu_0^2$ in (5.97) and (5.98), then at $Q^2>\mu_0^2$ we have $\langle x\,\xi(Q^2)\rangle_n\neq 0$ and $\langle x\,G(Q^2)\rangle_n\neq 0$. Thus all the glue and q$\bar{\text{q}}$ pairs seen in the nucleon are produced via gluon bremsstrahlung off the valence quark system. This situation is exemplified in fig. 5.19. To illustrate this in more detail let us consider [112] a three-flavor ($N_f=3$) QCD and using the parton decomposition of eq. (5.28). We start with the assumption that at "large" distances $Q^2=\mu_0^2\simeq 0.1$–$0.5\ \text{GeV}^2$ the nucleon consists of valence quarks only, i.e.

$$x\,\xi(x,\mu_0^2)=x\,G(x,\mu_0^2)=0 \tag{5.140}$$

which allows us to calculate all parton distributions at $Q^2=Q_0^2\gg\mu_0^2$, using eqs. (5.97)–(5.99), in terms of $u_v(x,\mu_0^2)$ and $d_v(x,\mu_0^2)$ only:

$$\langle x\,u_v(Q_0^2)\rangle_n=\langle x\,u_v(\mu_0^2)\rangle_n\,L_0^{-a_{NS}} \tag{5.141a}$$

$$\langle x\,d_v(Q_0^2)\rangle_n=\langle x\,d_v(\mu_0^2)\rangle_n\,L_0^{-a_{NS}} \tag{5.141b}$$

$$\langle x\,\xi(Q_0^2)\rangle_n=\tfrac{1}{6}\langle x\,u_v(\mu_0^2)+x\,d_v(\mu_0^2)\rangle_n\,[\alpha_n L_0^{-a_-}+(1-\alpha_n)L_0^{-a_+}-L_0^{-a_{NS}}] \tag{5.141c}$$

$$\langle x\,G(Q_0^2)\rangle_n=\langle x\,u_v(\mu_0^2)+x\,d_v(\mu_0^2)\rangle_n\,(1-\alpha_n)\frac{\alpha_n}{\beta_n}\,[L_0^{-a_-}-L_0^{-a_+}] \tag{5.141d}$$

where $L_0\equiv L(Q_0^2)$ with

$$L\equiv L(Q^2)\equiv\frac{\alpha_s(\mu_0^2)}{\alpha_s(Q^2)}=\frac{\ln(Q^2/\Lambda^2)}{\ln(\mu_0^2/\Lambda^2)}.$$

The theoretically unknown valence distributions at $Q^2=\mu_0^2$ can now be related to the measured deep inelastic structure functions $F_2^{ep,n}$ at $Q^2=Q_0^2\simeq 2$–$4\ \text{GeV}^2\gg\mu_0^2$, using eqs. (5.141a,b): Recalling

$$F_2^{eN}\equiv\tfrac{1}{2}(F_2^{ep}+F_2^{en})=\tfrac{5}{18}(xu_v+xd_v)+\tfrac{4}{3}x\xi$$

and sustituting eqs. (5.141a–c) into it, one obtains

$$\langle x\,u_v(\mu_0^2)+x\,d_v(\mu_0^2)\rangle_n=\frac{18\langle F_2^{eN}(Q_0^2)\rangle_n}{4\alpha_n L_0^{-a_-}+4(1-\alpha_n)L_0^{-a_+}+L_0^{-a_{NS}}}. \tag{5.142}$$

Thus, according to eqs. (5.141c,d), $\xi(x, Q_0^2)$ and $G(x, Q_0^2)$ are uniquely determined in terms of $F_2^{eN}(x, Q_0^2)$ once L_0 (or μ_0^2) is given. L_0 follows from eq. (5.142) for $n = 2$ by using the energy-momentum sum rule (5.119) at $Q^2 = \mu_0^2$, i.e. $\langle x\, u_v(\mu_0^2) + x\, d_v(\mu_0^2)\rangle_2 = 1$:

$$\langle F_2^{eN}(Q_0^2)\rangle_2 = \tfrac{2}{9}(\tfrac{9}{25} + \tfrac{16}{25}L_0^{-50/81}) + \tfrac{1}{18}L_0^{-32/81}. \tag{5.143}$$

Experimentally [73, 74, 48] $\langle F_2^{eN}(Q_0^2 \simeq 3\,\mathrm{GeV}^2)\rangle_2 = 0.15 \pm 0.01$ which implies $L_0 = 7 \pm 2$. (For example, $Q_0^2 = 3\,\mathrm{GeV}^2$ and $\Lambda^2 = 0.1\,\mathrm{GeV}^2$ implies $\mu_0^2 \simeq 0.16\,\mathrm{GeV}^2$ where our boundary condition (5.140) is supposed to hold.) To separate $u_v(x, \mu_0^2)$ from $d_v(x, \mu_0^2)$ one further uses

$$F_2^{ep}(x, Q_0^2) - F_2^{en}(x, Q_0^2) = \tfrac{1}{3}[x\, u_v(x, Q_0^2) - x\, d_v(x, Q_0^2)]$$

together with eqs. (5.141a,b) and (5.142). The distributions at $Q^2 > Q_0^2$ are now obtainable by replacing in eq. (5.141) $Q_0^2 \to Q^2$, $L_0 \to L = L_0 \ln(Q^2/\Lambda^2)/\ln(Q_0^2/\Lambda^2)$.

Figure 5.20 shows the predictions [112] for the momentum distributions within the nucleon. Already for $Q^2 \simeq 1\,\mathrm{GeV}^2$ we obtain a reasonable agreement with the experimental result [43–45, 113] that at low values of Q^2 about 50% of the nucleon momentum is carried by gluons. This gives us some confidence in these dynamical predictions as long as $Q^2 \gtrsim 1\,\mathrm{GeV}^2$, whereas predictions for $Q^2 < 1\,\mathrm{GeV}^2$ are clearly not to be taken seriously due to the strong variations in this region as shown in fig. 5.20. Inverting the moments in eq. (5.141) numerically, as discussed in the previous subsection, we compare in fig. 5.21 our predictions for the quark- and antiquark-densities $q(x, Q^2)$ and $\bar{q}(x, Q^2)$, respectively, at $Q^2 = 3\,\mathrm{GeV}^2$ with the Gargamelle experiment [113]. Note that the sea distribution $\bar{q}$ is now a genuine parameter-free prediction of QCD. Comparing, however, these dynamically predicted sea and gluon distributions, $\xi(x, Q^2)$ and $G(x, Q^2)$, with the ones expected by the naive counting rules (5.103) and also with more recent neutrino experiments [45] and with Drell–Yan dilepton production [112], for example, we find that in the intermediate x-range $(0.2 \lesssim x \lesssim 0.5)$ these dynamical distributions underestimate the required sea distributions by about a factor of 2 [112, 114]; this is not entirely unexpected in view of the boundary conditions (5.140). In the small x-region, however, these dynamical predictions agree [112, 114] with most ad hoc sea and gluon parametrizations and with the data, and confirm roughly also the naive counting rules (5.102) in the large x-region [112] where they are supposed to hold. For more

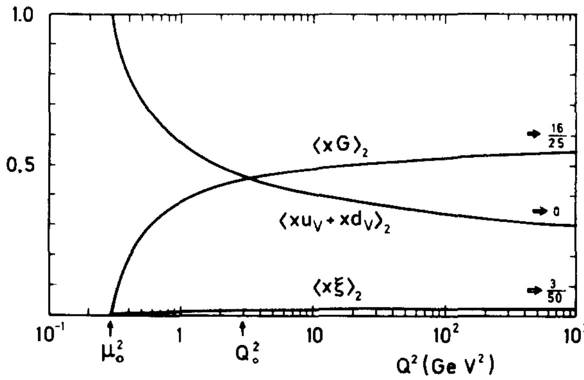

Fig. 5.20. Dynamical QCD predictions for the momentum distributions within the nucleon. The 'static point' $\mu_0^2 = 0.3\,\mathrm{GeV}^2$, where the nucleon consists of valence quarks only, corresponds to $\Lambda = 0.45\,\mathrm{GeV}$, for a given $L_0 = 7$ and $Q_0^2 = 3\,\mathrm{GeV}^2$.

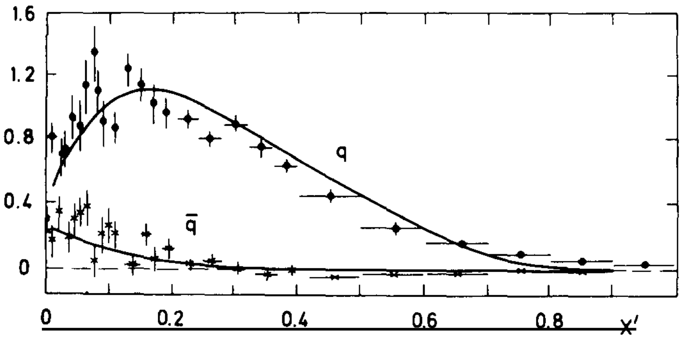

Fig. 5.21. Comparison of the dynamically predicted [112] amounts of quarks $q = x(u+d) = x(u_v + d_v + 2\xi)$ and antiquarks (sea) $\bar{q} = x(\bar{u} + \bar{d}) = 2x\xi$ at $Q^2 = Q_0^2 = 3\,\mathrm{GeV}^2$ with the Gargamelle data [113].

details and also for explicit analytic parametrizations of the predicted x- as well as Q^2-dependence of parton distributions we refer the interested reader to refs. [112] and [114].

The same techniques can be applied to calculate parton distributions for the pion [112, 114] where these dynamical predictions might be a useful guide to the 'real truth', since even less is experimentally known about pionic sea and gluon distributions than in the case of nucleons.

5.8. *The ratio of the longitudinal to transverse cross sections*: $R = \sigma_L/\sigma_T$

One of the most fundamental and cleanest tests of "finite" (i.e. non-logarithmic) terms, and thus of QCD itself, is provided by the measurement of the longitudinal cross section σ_L, or in other words by deviations from the Callan–Gross relation $F_2 = 2xF_1$ in (5.14) since [40, 38, 5]

$$R \equiv \frac{\sigma_L}{\sigma_T} = \frac{F_2 - 2xF_1}{F_2} \equiv \frac{F_L}{F_2} \ . \tag{5.144}$$

Remember that $F_L = 0$ is a simple consequence of helicity conservation in the naive (massless) quark model in the limit of vanishing transverse momenta p_T of quarks in the nucleon: in the frame where the spacelike current carries no energy, $q = (0, Q, 0, 0)$, the hit quark reverses its momentum and also its spin (since vector- and axial-vector interactions of massless fermions imply helicity conservation); therefore angular momentum conservation forces the current to carry one unit of spin, since the process is collinear, and hence $\sigma_L = 0$. Apart from the small quark masses, a finite σ_L is due to $p_T \neq 0$ which can be either generated perturbatively (dynamically) by radiating a hard gluon off a collinear quark, say, or stems from non-perturbative effects of finite "intrinsic" transverse momenta of quarks in the nucleon wave function. Let us consider the former perturbative case first.

The fundamental parton processes $\mathrm{Vq} \to \mathrm{gq}$ and $\mathrm{Vg} \to \mathrm{q\bar{q}}$ with $\mathrm{V} = \gamma^*$ or W, as shown in fig. 5.22, imply [115, 116] that $F_L \sim O(\alpha_s)$. Furthermore, since differences of structure functions appear in eq. (5.144), the longitudinal cross section $\sigma_L \sim F_L$ is well defined even in the massless theory, i.e. is independent of any infrared cut-off. Disregarding the electromagnetic and weak charges of quarks, the longitudinal projections of the fundamental parton processes in fig. 5.22 are given by [115, 31, 89]

$$F_L^q(x) = \frac{4\alpha_s}{3\pi} x^2, \qquad F_L^g(x) = \frac{2\alpha_s}{\pi} x^2(1-x) \tag{5.145}$$

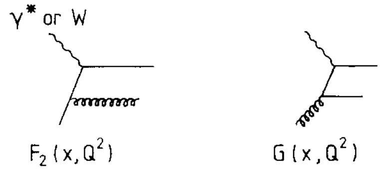

Fig. 5.22. Lowest order-α_s contributions to the longitudinal structure function F_L, and to jets in leptoproduction (crossed diagrams are not shown).

where the superscripts q and g refer to the initial quark and gluon, respectively. (A detailed discussion of the calculation of these quantities will be given in section 6.1.) The moments $C_n^i \equiv \int_0^1 dx\, x^{n-2} F_L^i(x)$ are then simply

$$C_n^q = \frac{4\alpha_s(Q^2)}{3\pi(n+1)}\,, \qquad C_n^g = \frac{2\alpha_s(Q^2)}{\pi(n+1)(n+2)}\,. \tag{5.146}$$

The results for an arbitrary physical scattering process are then obtained from convoluting eq. (5.145) with the appropriate RG-improved wave functions, i.e. with the probabilities of finding quarks and gluons in the initial state as indicated in fig. 5.22:

$$F_L(x, Q^2) = \frac{4\alpha_s(Q^2)}{3\pi} \int_x^1 \frac{dy}{y} \left(\frac{x}{y}\right)^2 F_2(y, Q^2) + a\, \frac{2\alpha_s(Q^2)}{\pi} \int_x^1 \frac{dy}{y} \left[\left(\frac{x}{y}\right)^2 - \left(\frac{x}{y}\right)^3\right] y\, G(y, Q^2) \tag{5.147}$$

or, in terms of moments where parton cross sections and parton distributions always factorize,

$$\langle F_L(Q^2)\rangle_n = C_n^q \langle F_2(Q^2)\rangle_n + a C_n^g \langle xG(Q^2)\rangle_n \tag{5.148}$$

with $a = \Sigma_q e_q^2$ (=6/9 for $N_f = 3$) for electroproduction and $a = 4$ for ν and $\bar{\nu}$ scattering on matter. Remember that the convolution (5.147) with parton distributions, having the same form as eq. (5.126), corresponds to integrating over all possible parton momenta by imposing momentum conservation:

$$\begin{aligned} F(x, Q^2) &= \int_0^1 dy \int_0^1 dz\, \delta(x - zy)\, f(z)\, q(y, Q^2) \\ &= \int_x^1 \frac{dy}{y} f\left(\frac{x}{y}\right) q(y, Q^2) \end{aligned} \tag{5.149}$$

where y is the fractional momentum of the primary parton which fragments into a parton carrying momentum zy. Equation (5.147) is the fundamental prediction of QCD for σ_L which tells us that

$$R^{QCD}(x, Q^2) = F_L(x, Q^2)/F_2(x, Q^2) \sim \alpha_s(Q^2) \sim 1/\ln Q^2 \tag{5.150}$$

vanishes only logarithmically as $Q^2 \to \infty$. This is a purely dynamical (perturbative) prediction and since F_L vanishes in zeroth order, in contrast to F_2 say, non-perturbative effects such as kinematical target mass effects will play a dominant role for subasymptotic values of Q^2. Simple kinematics give the well known relation of the naive parton model [38, 40]

$$R^{\text{intrinsic}} \simeq 4\frac{\langle k_T^2\rangle + m_q^2}{Q^2} \tag{5.151}$$

where the 'intrinsic' or primordial transverse momentum k_T refers to the parton momentum transverse relative to the direction of the virtual γ^* or W and which does not originate from the dynamical gluon radiation effects (fig. 5.22). Equation (5.151) can be also obtained from the on-shell version [65, 66, 31] of the covariant parton model [117]. Although the intrinsic k_T of a parton is a purely non-perturbative component of the nucleon's wave function we can try to estimate its size using the on-shell covariant parton model [118] which allows us to express $\langle k_T^2\rangle$ entirely in terms of the well known (longitudinal) structure functions by considering just the handbag diagram of fig. 5.2. An analysis similar to the famous ξ-scaling analysis [65, 66, 31] then yields [118], to leading order in m_N^2/Q^2,

$$\langle k_T^2(x, Q^2)\rangle \simeq \frac{m_N^2 x^3}{F_2(x, Q^2)} \int_x^1 \frac{dy}{y^2} F_2(y, Q^2) \tag{5.152}$$

which determines $R^{\text{intrinsic}}$ in eq. (5.151). For the measured values of F_2 the corresponding intrinsic transverse momentum per parton turns out to be [118] $\sqrt{\langle k_T^2\rangle} \lesssim 0.3\,\text{GeV}$ in agreement with naive expectations $\sqrt{\langle k_T^2\rangle} \simeq m_N/3$. Any estimate of the ill understood non-perturbative effects is, however, strongly model dependent and one can easily arrive at drastically different results [119, 120] using the off-shell parton model [117]. All we can say is that non-perturbative contributions to R fall off like powers of Q^2, eq. (5.151), in contrast to the perturbative α_s corrections predicted in eq. (5.147). Therefore at high enough values of Q^2 ($\gtrsim 20\,\text{GeV}^2$, hopefully) it should be possible to test eq. (5.147) with the non-perturbative contribution (5.151) being suppressed.

Good data on $F_L(x, Q^2)$ would allow us to test the prediction (5.147), or (5.148), in to two different ways. Either we assume $F_2(x, Q^2)$ and $G(x, Q^2)$ to be known, the latter could for example be determined from the Q^2-dependence of F_2 using eq. (5.97), then F_L can be predicted. Using a "standard" gluon distribution $x\,G(x, Q_0^2) \simeq 2.6(1-x)^5$ as *input* the detailed predictions for R^{QCD} have been studied by several authors [31, 89, 92, 121]. To illustrate the expected [118] x- and Q^2-dependence of $R(x, Q^2) = R^{\text{intrinsic}} + R^{\text{QCD}}$ we give a few predictions in table 5.3. These values can be increased if one chooses a harder (flatter) gluon distribution than our "standard" choice. Although one cannot draw any definite conclusions from the presently available scarce measurements of R, it appears that at least the expected qualitative trend (R increases for decreasing x) in table 5.3 is not inconsistent with the data: The SLAC ep measurements ($0.3 \lesssim x \lesssim 0.8$, $3\,\text{GeV}^2 \lesssim Q^2 \lesssim 18\,\text{GeV}^2$) give on the average [122] $R = 0.21 \pm 0.1$, whereas the Fermilab μp experiment ($0.003 < x < 0.1$, $1\,\text{GeV}^2 \lesssim Q^2 \lesssim 30\,\text{GeV}^2$) gives an average value of [74] $R = 0.52 \pm 0.35$. We stress again that the verification of the QCD prediction (5.147) is of utmost importance since it represents one of the cleanest and most direct tests of "finite" terms due to gluon bremsstrahlung (fig. 5.22).

On the other hand we can use eq. (5.147), or (5.148), to determine the gluon content of the nucleon in a most direct way: measuring $F_L(x, Q^2)$ in addition to $F_2(x, Q^2)$ gives us directly $G(x, Q^2)$. Comparing the Q^2-dependence of this measured gluon distribution with the RG prediction in eq. (5.98) would then provide us with a direct and sensitive test of the triple-gluon vertex [123], i.e. of the Yang–Mills

Table 5.3
Predicted values [118] for $R(x, Q^2) = R^{\rm intrinsic} + R^{\rm QCD}$ for electroproduction according to eqs. (5.147) and (5.152). The Q^2 dependent parton distributions of ref. [114] have been used with the standard gluon input $x\,G(x, Q_0^2) = 2.6(1-x)^5$. The predictions at $Q^2 = 2\,\mathrm{GeV}^2$ correspond to naive (Q^2-independent) parton distributions

$Q^2(\mathrm{GeV}^2)$	x	R	$R^{\rm intrinsic}$	$R^{\rm QCD}$
	0.8	0.1	0.08	0.02
2	0.5	0.16	0.1	0.06
	0.2	0.19	0.04	0.15
	0.02	0.53	0.0	0.53
	0.8	0.025	0.015	0.01
10	0.5	0.05	0.02	0.03
	0.2	0.08	0.01	0.07
	0.02	0.23	0.0	0.23
	0.8	0.014	0.006	0.008
20	0.5	0.035	0.01	0.025
	0.2	0.063	0.003	0.06
	0.02	0.18	0.0	0.18
	0.8	0.007	0.002	0.005
100	0.5	0.02	0.002	0.018
	0.2	0.04	0.0	0.04
	0.02	0.12	0.0	0.12

structure of QCD: Since $\alpha_n \simeq 1$ and $\beta_n \ll 1$ for $n \gtrsim 3$ (see table 5.2), eq. (5.98) tells us that $\langle x\,G(Q^2)\rangle_n \simeq \langle x\,G(Q_0^2)\rangle_n \exp(-s a_+(n))$ with $a_+(n)$ being critically dependent on [123] $\gamma^{\rm V}_{\rm VV}(n)$ in eq. (5.68) and thus on the triple-gluon vertex. All tests of QCD studied so far are mainly sensitive to the quark–gluon coupling but not to the gluon self-couplings which are so very essential for asymptotic freedom. It should be emphasized that the predictions (5.98) for $\langle x\,G(Q^2)\rangle_n$ cannot serve as an independent test of QCD if one determines [43, 44] the gluon distribution from fitting to the scaling violations of F_2 predicted by (5.97) since, once $\langle x\,\Sigma(Q_0^2)\rangle_n$ and $\langle x\,G(Q_0^2)\rangle_n$ are fixed by experiment via $\langle x\,\Sigma(Q^2)\rangle_n$ in (5.97), eq. (5.98) is trivially satisfied.

5.9. Jets in leptoproduction

A closely related consequence follows from the above discussion for the $p_{\rm T}$ distribution of jets. Neglecting the intrinsic $p_{\rm T}$ spread of quarks in the nucleon which is damped by the wave function and does not increase with Q^2 (see eq. (5.152)), we expect in the naive parton model two hadronic opposite side jets (fig. 5.4(a)) arising from the fragmentation of the quark on one side (current region) and from the remaining nucleon on the other side (target fragmentation region). In QCD, the existence of hard gluon interactions in fig. 5.22 provides the quark with a hard tail in its $p_{\rm T}$ distribution which, unlike the intrinsic component, increases with Q^2 at fixed x. Intuitively this can be easily understood since

$$\langle p_{\rm T}^2\rangle \sim \alpha_{\rm s} \int^{\sim Q^2} p_{\rm T}^2 \frac{{\rm d}p_{\rm T}^2}{p_{\rm T}^2} \sim \alpha_{\rm s} Q^2 + \text{const.} \tag{5.153}$$

where the factor $1/p_T^2$ results from the quark propagator in fig. 5.22, while the constant term refers to the intrinsic wave function effects and cannot be evaluated. We thus expect a fraction of events of order α_s to have a three jet structure [124, 125]: The target fragmentation jet with small p_T aligned along the collision axis, and two jets with large and almost opposite p_T due to the fragmenting quark–gluon and quark–antiquark final states (figs. 5.22 or 5.4(b)). For the time being we will consider a jet as being just a quark or the gluon itself and neglect the small non-perturbative transverse momenta of hadrons in the jet which arise from the decay of partons into observed hadrons (jet broadening).

For a more quantitative discussion of p_T distributions one has now to evaluate just the differential angular distributions $d\sigma/dp_T^2$ of the fundamental hard parton scattering processes in fig. 5.22 (in contrast to the phase-space integrated total cross sections (5.145) for obtaining F_L) which have to be convoluted with the appropriate parton distributions, as was done in eq. (5.147), in order to obtain measurable physical quantities [124, 126–132]. In this way one obtains for the average p_T^2 of the final parton jet [126]

$$\frac{\langle p_T^2\rangle}{Q^2} = \frac{\alpha_s(Q^2)}{2\pi}\frac{x}{F_2(x,Q^2)}\int_x^1 \frac{dz}{z^2}\left\{\frac{4}{3}\frac{4(x/z)^2-2x/z+7}{12x/z}F_2(z,Q^2)\right.$$
$$+\left(\sum_q e_q^2\right)\frac{1-x/z}{3x/z}\left[\left(\frac{x}{z}\right)^2+\left(1-\frac{x}{z}\right)^2\right]z\,G(z,Q^2)+\frac{1-y}{1-y+y^2/2}\left[\frac{4}{9}\left(1-\frac{x}{z}\right)F_2(z,Q^2)\right.$$
$$\left.\left.+\left(\sum_q e_q^2\right)\frac{2}{3}\left(1-\frac{x}{z}\right)^2 z\,G(z,Q^2)\right]\right\}. \tag{5.154}$$

The y-dependence of this expression turns out to be almost negligible, while the marked x-dependence is mostly related to the variation of the invariant mass squared W^2 of the hadrons (eq. (5.7)) for x not too small. This x-dependence can almost completely be taken into account by the empirical formula

$$\langle p_T^2\rangle \simeq 0.031\alpha_s(Q^2)W^2. \tag{5.155}$$

It should be also noted that the naive parton model relation (5.151), $F_L/F_2 \simeq 4\langle p_T^2\rangle/Q^2$, is not reproduced even approximately in QCD by comparing eqs. (5.147) and (5.154) quantitatively [126]. At given values of Q^2 and x, the predicted tail of the perturbative p_T distribution in (5.154) should be clearly visible above the intrinsic component [124, 128–130] which does not increase with Q^2 (see for example eq. (5.152)). This is illustrated in fig. 5.23 where an exponential fall-off of the intrinsic k_T distribution has been assumed; this latter assumption, however, is questionable within the framework of the covariant parton model [117] where one expects [133] at most a power like fall-off ($\sim k_T^{-8}$ for valence quarks $\sim(1-x)^3$). Although this tail extends up to $p_T^2 \sim Q^2$, it is rather small (of order α_s) and therefore hard to observe apart from uncalculable contributions due to the fragmentation properties of the parton into the observed hadrons. In other words, since the slope in W^2 of the linearly rising $\langle p_T^2\rangle$ in (5.155) is small, it is not very surprising that at present energies ($W^2 \lesssim 200\,\text{GeV}^2$) the presence of this hard component is still not clearly visible [134, 130]: The increase of $\langle p_T^2\rangle$ with W^2 is observed in ν scattering, while the same effect is not visible in $\bar\nu$ scattering where the statistics is more limited.

Further tests of QCD involving three jet events, and which depend also on the transverse momentum of the active quark in the interaction, concern azimuthal corrections between the final lepton and the jet axis. These so-called ϕ-asymmetries have been originally suggested by Georgi and Politzer [135] and result from the differential parton cross sections for the processes in fig. 5.22 which are of the form

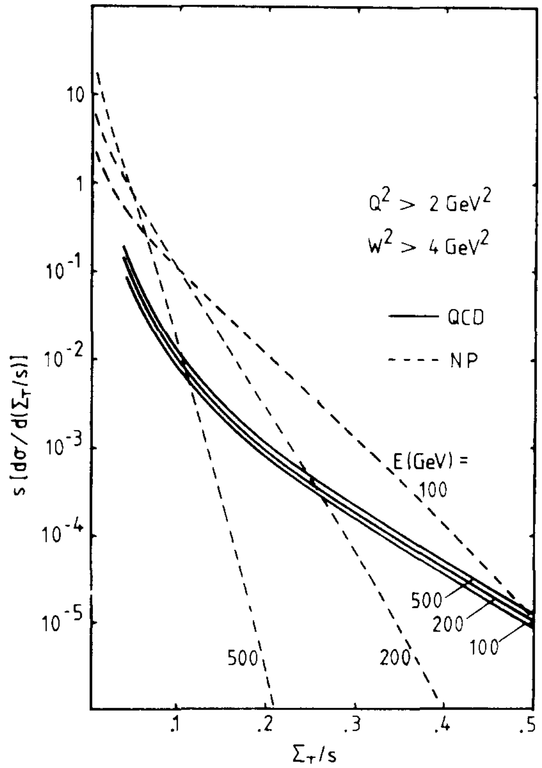

Fig. 5.23. Predictions [128] for the transverse momentum distributions in the variable $\Sigma_T \equiv (\Sigma_i |p_T^i|)^2$, where i runs over all final hadrons, for μp interactions at various beam energies. Note that Σ_T is insensitive to fragmentation dynamics since it allows in principle to reconstruct the p_T of the decaying parton itself. The dashed curves are estimates of the intrinsic, non-perturbative (NP) components.

[127, 135–137]

$$\frac{d\sigma}{dx\, dy\, dz\, d\phi} = A_0 + A + B \cos\phi + C \cos 2\phi \tag{5.156}$$

where A_0 is the zeroth order (naive) parton cross section, and with the QCD contributions A, B, $C \sim O(\alpha_s)$ and z being the momentum fraction of the decaying quark carried by the observed outgoing hadron. (A detailed discussion of fragmentation functions can be found in section 10.) Convoluting eq. (5.156) with the appropriate parton distributions and fragmentation functions allows us to calculate the average values $\langle\cos\phi\rangle$ and $\langle\cos 2\phi\rangle$ which have, according to fig. 5.24, a straightforward physical interpretation: The first quantity $\langle\cos\phi\rangle$ measures the front-to-back asymmetries of hadrons, whereas $\langle\cos 2\phi\rangle$ measures the accumulation of hadrons at the lepton scattering plane. Detailed analyses [127, 135, 137] of these quantities show, for beam energies $E \simeq 200$ GeV and in the current fragmentation region, that they are of the order

$$\langle\cos\phi\rangle^{\mu N, \nu N} \simeq -0.1, \quad \langle\cos\phi\rangle^{\bar\nu N} \simeq -0.2 \quad \text{and} \quad \langle\cos 2\phi\rangle^{\nu N} \simeq +0.01.$$

Although $\langle\cos\phi\rangle$ is rather sizeable, it will not be easy to disentangle these perturbatively predicted correlations from the data, because the same sort of effect can be also produced within the naive parton

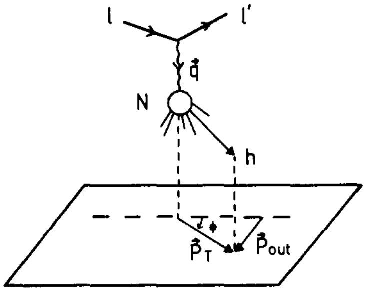

Fig. 5.24. Kinematical configuration of the process $\ell \to \ell' hX$ in the nucleon's lab system.

model by the presence of non-perturbative intrinsic k_T's of partons in the nucleon [138]:

$$\begin{aligned} \langle \cos \phi \rangle &\sim 2\langle k_T \rangle / \sqrt{Q^2} \\ \langle \cos 2\phi \rangle &\sim 4\langle k_T^2 \rangle / Q^2 . \end{aligned} \tag{5.157}$$

These ill understood non-perturbative effects can, however, be suppressed by making p_T-cuts in the data ($p_T \gtrsim 1.5$ GeV) which practically eliminates the intrinsic smearing (5.157) in azimuth due to the fragmentation process [139]. Furthermore, experimentally it should be easier to determine p_{out}-distributions [127] (fig. 5.24)

$$\langle p_{out}^2 \rangle = \langle p_T^2 \sin^2 \phi \rangle = \tfrac{1}{2}\langle p_T^2 \rangle - \tfrac{1}{2}\langle p_T^2 \cos 2\phi \rangle$$

since their measurement requires only the knowledge of the leptonic scattering plane. This is in contrast to the ϕ-asymmetries about the momentum transfer direction and to p_T measurements which depend on the accurate determination of the q direction in the leptonic plane (see fig. 5.24).

Finally we would like to emphasize the importance of those three jet events where one of the hadronic jets is replaced by a hard real photon [140] as shown in fig. 5.25(a). The theoretical beauty of this 'direct photon' process is that even its *absolute* magnitude can be calculated and not just the Q^2-evolution of an uncalculable input wave function as has been done so far and as would be the case for the additional hadronic contribution to the hard photon jet in fig. 5.25(b). This latter hadronic background should be suppressed relative to the Born-term of fig. 5.25(a) in the region where the (hard) photon carries most of the fractional momentum z of the original quark ($z \gtrsim 0.6$). The quark $\to$ photon input fragmentation function $D_q^\gamma(z, Q^2)^{Born}$ can be simply calculated from the Born diagram in fig.

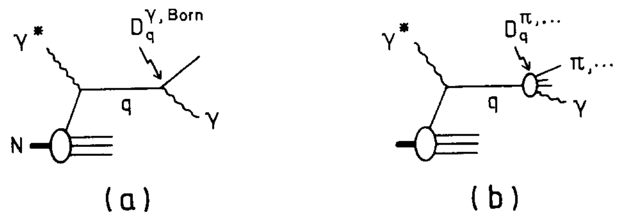

Fig. 5.25. Diagrams which contribute to the fragmentation into real photons: (a) uniquely calculable Born term which dominates hard 'direct' photon emission, and (b) hadronic contribution with the theoretically unknown input fragmentation function $D_q^\pi(z, Q_0^2)$.

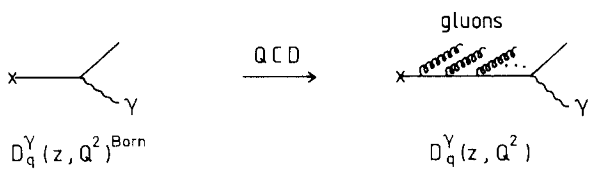

Fig. 5.26. QCD corrections to the $q\to\gamma$ Born term.

5.25(a),

$$D_q^\gamma(z,Q^2)^{Born}=e_q^2\frac{\alpha}{2\pi}\frac{1+(1-z)^2}{z}\ln\frac{Q^2}{\Lambda^2} \tag{5.158}$$

and the leading logarithmic QCD corrections to it (fig. 5.26) can be resummed to all orders in α_s using renormalization group techniques (or using physically more intuitive approaches to be discussed in the next section) which yield [140, 141]

$$\langle zD_q^\gamma(Q^2)\rangle_n=\left[\frac{e_q^2-\frac{5}{18}}{1+a_{NS}}+\frac{5}{18}\frac{1+a_{VV}^V}{K_n}\right]\left\langle\frac{1}{e_q^2}zD_q^\gamma(Q^2)^{Born}\right\rangle_n \tag{5.159}$$

with $K_n=1+a_{NS}+a_{VV}^V+a_{NS}a_{VV}^V-a_{FF}^V a_{VV}^F$ and where the anomalous dimensions are defined by eqs. (5.64), (5.68) and (5.77). A similar expression can be derived [140] for the much softer gluon$\to$photon decay function $D_g^\gamma(z,Q^2)$. The predicted z-dependence [140] of the observed hard photons in (5.159), which is significantly different from the one of the input Born term in eq. (5.158), will provide us with a clear cut test of QCD especially in the large-z region where the hadronic background is suppressed.

Of similar importance for testing the existence of gluon jets are those 3-jet events which are initiated by a real photon [142] (QCD Compton effect) such as $\gamma N\to$ (large-p_T jets) + X. This process is depicted in fig. 5.27(a) and is proportional to $\alpha_s q(x)$. It should be possible to select experimentally these three-jet events from those (non-gluonic) four quark-jet events which originate from the hadronic component of the photon (ρ meson, etc.) as shown in fig. 5.27(b): The additional fourth jet in the forward direction is thus produced by the constituents of the vector mesons which do not take part in the hard scattering process and this process is proportional to $\alpha_s^2 q^\gamma q$ with q^γ being the quark distribution inside the photon [140]. Thus the observation of *three*-jet events in γN collisions would provide us with direct evidence for the existence of gluons! The cross section for these gluon-jet events can be easily estimated [142] to be

$$\left(E'\frac{d\sigma^{3\text{-jet}}}{dE'\,d\Omega'}\right)_{E'=4\,\text{GeV},\,\theta'=90^\circ}\simeq 12\alpha_s\,\text{nb} \tag{5.160}$$

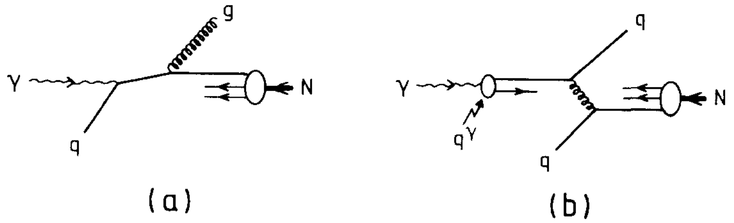

Fig. 5.27. QCD Compton effect giving rise to (a) 3-jet events and to (b) non-gluonic 4-jet events due to the hadronic component of the real photon.

for $E^{\gamma}_{\rm lab} \simeq 200$ GeV ($E^{\gamma}_{\rm c.m.} = 10$ GeV) and where the primed quantities refer to the c.m. kinematics of the gluon in fig. 5.27(a). Thus $\sigma^{\text{3-jet}} \simeq 10^{-4}\,\sigma^{\gamma N}_{\rm tot}$, i.e., the cross section for events due to the QCD Compton effect where a gluon and a quark jet carrying a few GeV each emerge at large angles in the c.m. system is about 10^{-4} of the total photon–nucleon cross section for $E^{\gamma}_{\rm lab} \simeq 200$ GeV.

5.10. Non-leading corrections: 2-loops and "finite terms"

Before closing this section, I finally would like to comment briefly on various recent analyses concerning subleading α_s corrections to Wilson coefficients ("finite terms") and 2-loop α_s^2 contributions to anomalous dimensions and to the β-function. So far we have considered only the leading order contributions to Wilson coefficients, i.e. $C^n_{\rm F}(1, \bar{g}) = 1$ and $C^n_{\rm G}(1, \bar{g}) = 0$ in eq. (5.56), and the leading 1-loop contribution to anomalous dimensions $\gamma \sim \alpha_s$. Taking into account non-leading terms we have to consider the following terms in the power expansions of β, γ^n_i and C^n_i:

$$\beta(\bar{g}) = -\beta_0 \frac{\bar{g}^3}{16\pi^2} - \beta_1 \frac{\bar{g}^5}{(16\pi^2)^2} \tag{5.161}$$

$$\gamma^n_i(\bar{g}) = \gamma^n_{i,0} \frac{\bar{g}^2}{16\pi^2} + \gamma^n_{i,1}\left(\frac{\bar{g}^2}{16\pi^2}\right)^2 \tag{5.162}$$

$$C^n_i(1, \bar{g}) = \delta_i + c^n_i \frac{\bar{g}^2}{16\pi^2} \tag{5.163}$$

with $\delta_{\rm F} = 1$ and $\delta_{\rm G} = \delta_{\rm L} = 0$. (L stands for longitudinal structure functions.) Inserting eqs. (5.161)–(5.163) into the renormalization group solution (5.55),

$$C^n_i(Q^2/\mu^2, g(\mu^2)) = C^n_i(1, \bar{g}(Q^2)) \exp\left[-\int_g^{\bar{g}} \frac{\gamma^n_i(g')}{\beta(g')} \mathrm{d}g'\right], \tag{5.164}$$

and expanding in $\bar{g}^2(Q^2)$, the Q^2 dependence of moments of non-singlet structure functions in eq. (5.63) is now predicted to be

$$\langle F_{\rm NS}(Q^2)\rangle_n = \langle F_{\rm NS}(Q_0^2)\rangle_n \left\{1 + \frac{\alpha_s(Q^2) - \alpha_s(Q_0^2)}{4\pi}\left[c^n_{\rm NS} + \frac{\gamma^n_{\rm NS,1}}{2\beta_0} - \frac{\gamma^n_{\rm NS,0}}{2\beta_0^2}\beta_1\right]\right\}\left[\frac{\alpha_s(Q_0^2)}{\alpha_s(Q^2)}\right]^{-\gamma^n_{\rm NS,0}/2\beta_0} \tag{5.165}$$

and the corrected form of α_s is

$$\frac{\alpha_s(Q^2)}{4\pi} = \frac{1}{\beta_0 \ln(Q^2/\Lambda^2)} - \frac{\beta_1}{\beta_0^3}\frac{\ln\ln(Q^2/\Lambda^2)}{\ln^2(Q^2/\Lambda^2)} + O\left(\frac{1}{\ln^3(Q^2/\Lambda^2)}\right) \tag{5.166}$$

where Λ has been arbitrarily chosen so that there are no further terms of order $1/(\ln^2(Q^2/\Lambda^2))$ with

$$\Lambda^2 \equiv \mu^2 \exp\left[-\frac{16\pi^2}{\beta_0 g^2} + \frac{\beta_1}{\beta_0^2}\ln\frac{16\pi^2}{\beta_0 g^2}\right]. \tag{5.167}$$

Because of the freedom we have in defining $\alpha_s(Q^2)$ when solving the renormalization group equation, this choice of Λ is clearly not unique and one could use other definitions of Λ as well. For a detailed discussion of other choices as well as of non-leading contributions to singlet structure functions we refer the interested reader to the comprehensive review of Buras [11]. It is clear from eq. (5.165) that $O(\alpha_s)$ corrections to the Wilson coefficients C_i^n have to be taken into account once the 2-loop contributions β_1 and $\gamma_{i,1}^n$ to β and γ_i^n are considered, in order to include consistently all contributions in a given order of perturbation theory. It should be emphasized that only the *whole* eq. (5.164) corresponds to a physical measurable quantity, whereas the individual quantities $C_i^n(1, \bar{g})$ and exp[. . .] depend upon the precise definition of the Wilson operator (the renormalization prescription): Although the parameters $\gamma_{i,0}^n$, $\beta_0 = 11 - \frac{2}{3}N_f$ and [143] $\beta_1 = 102 - \frac{38}{3}N_f$ are gauge and renormalization prescription independent, the quantities c_i^n and $\gamma_{i,1}^n$ depend on the renormalization prescription and on the gauge chosen. Thus c_i^n and $\gamma_{i,1}^n$ must be calculated in the *same* renormalization scheme in order to obtain a physical, convention independent answer for eq. (5.165): In this case the quantity $c_{NS}^n + \gamma_{NS,1}^n/2\beta_0$ in eq. (5.165) is renormalization prescription independent. The 2-loop contribution $\gamma_{i,1}^n$ for non-singlet structure functions (i = NS) have been calculated in ref. [144] and the ones for singlet structure functions in ref. [145] using 't Hooft's minimal subtraction scheme to renormalize the amplitudes. The appropriate Wilson coefficients ("finite terms") c_i^n have been evaluated in ref. [146] within the same dimensional regularization scheme. Calculations of the finite terms c_i^n in different renormalization schemes have been performed in refs. [31] and [147–149]; needless to say that these results differ from each other due to the different renormalization schemes used.

As in the case of leading order contributions, the most useful and reliable quantitative comparison of subleading contributions with experiment is achieved by studying the explicit x- and Q^2-dependence of structure functions: Studies of non-singlet [121] structure functions $F_2^{\mu p}(x \gtrsim 0.4, Q^2)$ as well as singlet [150] contributions in $F_2(x, Q^2)$ have shown that the 2-loop approximation gives also an equally good agreement with experiment as does the 1-loop approximation, provided the scale Λ of the effective coupling constant is changed by about 20–30% as compared to the value of Λ obtained by fitting the leading order (1-loop) expressions to experiment. At the present state of art, the most sensible and reliable way to study the effects of higher order QCD corrections is to consider [151] combinations of structure functions which are *independent of the renormalization scheme* used to define α_s: the effect of these corrections are found to be very small, generally smaller than the errors in the existing data! Therefore, although further detailed analyses are certainly required before we can draw definite conclusions, it appears that non-leading terms do not significantly alter the successful quantitative results based on the 1-loop approximation; this gives us some additional confidence in the usefulness and validity of perturbative lowest order calculations in QCD.

Based on moment analyses of F_2 there have, however, been made recent claims that data on $\langle F_2^{\mu p,n}\rangle_n$ require [74] the non-leading 2-loop corrections, or that the non-singlet data for $\langle F_2^{\mu p} - F_2^{\mu n}\rangle_n$ are not in good accord [152] with either leading or non-leading order predictions of QCD. It should be emphasized that these conclusions rely entirely on $n \gtrsim 5$ moments, which weigh the large-x region only, and therefore should not be taken too seriously. The reason for this is twofold: The experimental determination of $n \gtrsim 5$ moments depends heavily on the ill understood elastic and quasi-elastic contributions at large x; theoretically large-n moments receive sizeable contributions from ill understood target mass effects at moderate values of Q^2 and in addition can be totally contaminated by the theoretically even less understood higher twist contributions [153] to eq. (5.41). Note that higher twist contributions to moments are expected [31] to be proportional to na/Q^2 with $a \simeq \langle k_T^2\rangle^{\text{intrinsic}} \simeq 0.1\ \text{GeV}^2$. The only sensible way to avoid these difficulties related to ill understood $1/Q^2$ contributions encountered in ref. [153] is, of course, to study not high-n moments or equivalently just non-singlet structure functions, but instead to consider the Q^2 dependence of the general structure functions $F_2^{\mu p}$, $F_2^{\nu N}$, etc. in the *whole* x-region where all singlet components fully contribute; only these general structure functions provide us with decisive tests of QCD and do not allow for the presence of large $1/Q^2$ contributions [72, 75, 76, 154].

For illustrative purposes let us briefly consider the ratio of slopes of the logarithms of two different moments in eq. (5.115). In the non-leading approximation (5.165), these quantities will now depend on the specific choice of Q^2 and Λ: For $F_{NS} = F_2^{\mu p} - F_2^{\mu n}$ one expects $d\ln\langle F_{NS}\rangle_6 / d\ln\langle F_{NS}\rangle_4$ to change from 1.29 in the 1-loop order to 1.33 in the 2-loop order (for [145] $Q_0^2 = 4\,\mathrm{GeV}^2$, $Q^2 = 50\,\mathrm{GeV}^2$ and $\Lambda = 0.5\,\mathrm{GeV}$), to be compared with the measured value of [74] 1.6 ± 0.2. Similarly $d\ln\langle xF_3^{\nu N}\rangle_6 / d\ln\langle xF_3^{\nu N}\rangle_4$ is expected [153] to change to about 1.45 (as compared to 1.29 in leading order) which is not in disagreement with the observed value of [62] 1.34 ± 0.07.

For practical applications a very convenient definition of parton distributions has been suggested [149] to facilitate the study of "finite" α_s terms in C_i^n: The effective Q^2-dependent parton distributions are defined relative to F_2, i.e., by demanding that $F_2(x, Q^2)$ expressed in terms of them should have the same form as in the naive quark model (F_2 is given a special status because it satisfies the fundamental Adler sum rule (5.17) which is exactly valid at all Q^2):

$$\langle q(Q^2)\rangle_n \equiv C_2^n(1, \alpha_s(Q^2))\, A_{NS}^n \exp[\ldots] \tag{5.168}$$

instead of the usual definition $\langle \tilde{q}(Q^2)\rangle_n \equiv A_{NS}^n \exp[\ldots]$ where $\exp[\ldots]$ is our general RG exponent in eq. (5.164) and A_{NS}^n are the matrix elements of the local Wilson operators between target states (see eqs. (5.40) and (5.57)). Similar definitions [149] apply to singlet (gluon) densities. Thus, once the input parton distributions $q(x, Q_0^2)$ are fitted at $Q^2 = Q_0^2$ to $F_2(x, Q^2)$, using eqs. (5.100) and (5.101) for example, one can study the effects of finite terms in structure functions (or processes) *other* than F_2 since

$$\begin{aligned}\langle F_i(Q^2)\rangle_n &= \frac{C_i^n(1, \alpha_s(Q^2))}{C_2^n(1, \alpha_s(Q^2))} C_2^n(1, \alpha_s(Q^2)) A_i^n \exp[\ldots] \\ &\equiv \frac{C_i^n(1, \alpha_s(Q^2))}{C_2^n(1, \alpha_s(Q^2))} \langle q(Q^2)\rangle_n\end{aligned} \tag{5.169}$$

which is of course a fully gauge invariant and renormalization prescription independent procedure and where $\langle q(Q^2)\rangle_n$ generically denotes the moments of the appropriate combinations of quark and antiquark distributions. Thus, expanding in α_s, we get always *differences* $c_i^n - c_2^n$ of "finite" terms contributing to F_i with $i \neq 2$:

$$\langle xF_3(Q^2)\rangle_n = (-\langle xq(Q^2)\rangle_n + \langle x\bar{q}(Q^2)\rangle_n)\,[1 + \alpha_s(Q^2)(c_{3,q}^n - c_{2,q}^n)], \text{ etc.} \tag{5.170}$$

where the fermionic Wilson coefficients $c_{i,q}^n$ result from [146, 149]

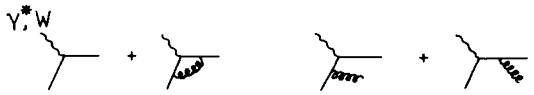

and gluonic Wilson coefficients $c_{i,G}^n$ are calculated from

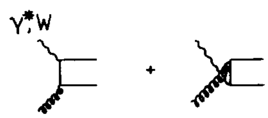

The importance of these "finite" $\alpha_s(Q^2)$ corrections for phenomenological applications are obvious: For example their effect in total neutrino cross sections and their y-dependence is sizeable [149, 154] and therefore the effect of "finite" (gluon) corrections cannot be neglected for a precise quantitative determination of sea densities. Similarly, one has to check *simultaneously*, using the same parton distributions determined in deep inelastic reactions, the importance of "finite" terms in other reactions such as Drell–Yan dimuon production [149] ($pp \to \mu^+\mu^- + X$) as we shall discuss later. Here "finite" terms are obtained [148, 149, 155–159] from the same, but crossed diagrams which yielded the above quantities $c^n_{i,q}$ and $c^n_{i,G}$.

6. Scaling violations à la Altarelli–Parisi and Bethe–Salpeter ladders

So far the discussion of the Q^2 dependence of structure functions was based on the rather formal approach using renormalization group techniques. We will now turn to an alternative method of calculating scaling violations which is not only physically more transparent but also shows that the (logarithmic) Q^2 dependencies of parton distributions considered so far have universal validity, i.e. are process independent and remain the same whether Q^2 is space- or time-like. This physically transparent method is, as a generalization of the Weizsäcker–Williams equivalent photon approximation [160, 161, 4] in QED, based on the intuitive parton picture of Kogut and Susskind [162] which imagines to find partons in partons in ... by resolving the nucleon at smaller and smaller distances (fig. 5.1(d)): By increasing the power of our "microscope" from Q_0^2 to $Q^2 > Q_0^2$ we can resolve a quark with momentum fraction x into a quark with $x' < x$ and a gluon with $x'' = x - x'$ as illustrated in fig. 6.1(a). Similarly a gluon with momentum fraction x can be resolved into a $q\bar{q}$ pair as shown in fig. 6.1(b), and there exists also the process of fig. 6.1(c) which can be interpreted as resolving a gluon into a gluon pair. On account of these decay processes we then can define probabilities $P_{ij}(x)$ for finding a parton i in a given parton j, with x being the longitudinal momentum fraction carried by i. These decay probabilities will then determine the structure of a nucleon at a given momentum scale or, equivalently, parton distributions will depend on Q^2. Quantitatively this picture has been developed by Altarelli and Parisi [163, 4] who derived integro-differential equations describing the Q^2 dependence of parton distributions. These $\alpha_s \ln Q^2$ terms can be also resummed by the closely related and physically even more transparent method of summing Bethe–Salpeter ladders which will be discussed at the end of this section.

Before writing down the most general form of the Altarelli–Parisi evolution ("master") equations, let us first discuss the basic physical ideas which lead to these equations. This is easiest done by considering first the nucleon to consist of valence quarks only [8], i.e. neglecting for the time being the gluon content of the nucleon. In the naive parton model (fig. 5.4(a)) the structure function is then formally given by

$$\frac{1}{x}F_2(x) = \left| \quad \right|^2$$

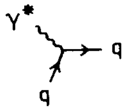

$$= \int_0^1 dy\, dz\, \delta(x - zy)\, q(y)\, \sigma_2^{\text{point}}(z) \qquad (6.1)$$

$$= e_q^2 q(x)$$

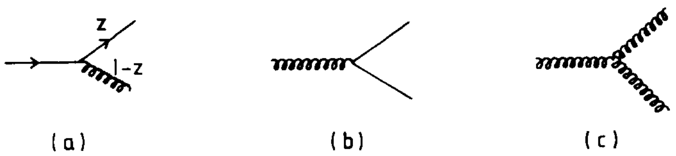

Fig. 6.1. Basic processes describing the decay probabilities ("splitting" functions) of (a) P_{qq} and P_{gq}, (b) P_{qg} and (c) P_{gg}.

since the F_2-projection of the pointlike fundamental parton cross section is given by $\sigma_2^{\text{point}}(z) = e_q^2\delta(1-z)$. The δ-function occurs because of momentum conservation since the original parton cannot loose momentum since no gluon emission exists in the naive parton model. This situation changes of course when we consider the parton model in the context of QCD where the quark–gluon interactions modify eq. (6.1) to

$\frac{1}{x}F_2 =$

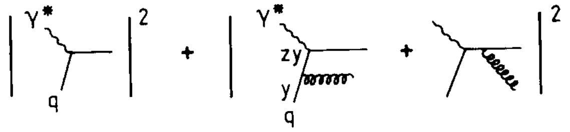

$$= \int_0^1 \mathrm{d}y\, \mathrm{d}z\, \delta(x - zy)\, q(y)\, [e_q^2\, \delta(1-z) + \sigma_2^{\gamma^* q\to gq}(z, Q^2)] \tag{6.2}$$

$$= \int_x^1 \frac{\mathrm{d}y}{y} q(y) \left[e_q^2\, \delta\left(1-\frac{x}{y}\right) + \sigma_2^{\gamma^* q\to gq}\left(\frac{x}{y}, Q^2\right)\right]$$

where the fundamental parton cross section has the following general form

$$\sigma_2^{\gamma^* q\to gq}(z, Q^2) = e_q^2 \frac{\alpha_s}{2\pi}\left[P_{qq}(z)\ln\frac{Q^2}{\mu^2} + f(z) + \mathrm{O}(1/Q^2)\right] \tag{6.3}$$

with μ being some convenient but arbitrary normalization mass. While the function $P(z)$ is uniquely defined as the coefficient of $\ln Q^2$, the definition of the "finite" (scaling) term $f(z)$ depends on μ^2 and does not depend on $\ln Q^2$: changing μ^2 to m^2 adds to f a term $P\ln(m^2/\mu^2)$. The neglected terms of order $1/Q^2$ correspond to the already neglected non-leading singularities on the light cone in eq. (5.41). The origin of the structure of eq. (6.3) is easily understood by recalling that any differential cross section involving one fermion propagator as in the diagrams of eq. (6.2) is of the form $\mathrm{d}\sigma/\mathrm{d}t \sim 1/t$ with the usual Mandelstam variable $-t \sim p_T^2$. Thus the total phase-space integrated cross section becomes

$$\int \frac{\mathrm{d}\sigma}{\mathrm{d}t}\mathrm{d}t \sim -\int_{m^2}^{\sim Q^2} \frac{\mathrm{d}t}{t} \sim \ln\frac{Q^2}{m^2} + \cdots \tag{6.4}$$

where we have cured the infrared divergence at the lower (soft) limit of integration by integrating only from m^2, i.e. by working with off mass shell quarks with zero rest mass. Different choices of infrared regularization schemes will only affect the "finite" term $f(z)$ in eq. (6.3) whereas the $\ln Q^2$ term, i.e. $P(z)$ is well defined even in the massless theory.

Whenever there are well identified partons in the initial or final state, the zero mass limit $m^2 \to 0$ will not be regular in perturbation theory in the sense that $\ln(Q^2/m^2)$ singularities will show up. (This is in contrast to a fully inclusive process with no well identified parton lines in the initial and final state, as is the case for the ratio $R_{e^+e^-}$ of hadronic to leptonic yield in e^+e^- collisions in eq. (1.9).) The physical origin of these so called "mass singularities" is easily understood by observing that a massless quark can emit a hard collinear massless gluon and still remains on its mass shell. This process is kinematically allowed and will produce a divergence if the phase space is large enough. Indeed, if we consider the process quark(p) → quark(p′) + gluon(k) we obtain for the virtual mass of the outgoing quark

$$p'^2 = (p-k)^2 = -2p\cdot k = -2p_0k_0(1-\cos\theta) \tag{6.5}$$

with θ being defined as the angle of emission of the gluon with respect to the direction of the incoming quark. Clearly, if the emission is collinear ($\theta = 0$) the outgoing quark is on its mass shell. Therefore, collinear emission of hard gluons induces dangerous propagators which are responsible for the logarithmic mass singularities in eq. (6.4). Since these $\ln(Q^2/m^2)$ terms will spoil any naive use of perturbation theory for light partons, $m^2 \ll Q^2$, all leading powers of logarithms of the form $\alpha_s^n(Q^2)\ln^n(Q^2/m^2)$ have to be summed up in order to reestablish an improved perturbation theory which constitutes the so called "leading log approximation". This will be done in the remainder of this subsection and leads of course to the same results obtained using the rather formal renormalization group techniques.

Let us return to eq. (6.3), the essential feature of it is the presence of the factor of $\ln Q^2$. This term violates scaling and indicates the failure of the naive parton model in QCD. (For the naive parton model to work, a decrease in $-t \sim p_T^2$ faster than $1/p_T^2$ in eq. (6.4) would be necessary in order to avoid large logarithms in (6.4).) Since $\alpha_s\ln(Q^2/\mu^2) \not\ll 1$ in (6.3), eq. (6.2) is certainly insufficient as it stands. In order to proceed let us try to absorb this anomalous term into a modified parton distribution. To this end we rewrite eq. (6.2) in the following form

$$\begin{aligned}\frac{1}{x}F_2 &= e_q^2\int_x^1 \frac{dy}{y}\,q(y)\left[\delta\left(1-\frac{x}{y}\right)+\frac{\alpha_s}{2\pi}P_{qq}\left(\frac{x}{y}\right)\ln\frac{Q^2}{\mu^2}+\cdots\right]\\ &\equiv e_q^2\int_x^1\frac{dy}{y}\,[q(y)+\Delta q(y,Q^2)]\,\delta\left(1-\frac{x}{y}\right)\\ &= e_q^2[q(x)+\Delta q(x,Q^2)]\end{aligned} \tag{6.6}$$

where

$$\Delta q(x,Q^2) \equiv \frac{\alpha_s}{2\pi}\ln\frac{Q^2}{\mu^2}\int_x^1\frac{dy}{y}\,q(y)\,P_{qq}\left(\frac{x}{y}\right)+\cdots\,. \tag{6.7}$$

We see that lowest order perturbation theory suggests to replace the naive (Q^2-independent) parton densities inside the nucleon by effective densities as seen by the photon (with momentum $q^2 \equiv -Q^2$)

which depend now on Q^2:

$$q(x) \to q(x, Q^2) = q(x) + \Delta q(x, Q^2). \tag{6.8}$$

Thus, the Q^2 dependence is due to the fact that a photon with larger Q^2 explores a wider range of p_T^2 inside the nucleon, i.e., resolves the "fine structure" of a nucleon at smaller distances (see fig. 5.1(d)). The variation of $q(x, Q^2)$ for an increase $\mathrm{d} \ln Q^2$, which is due to probing a new infinitesimal interval of $Q^2 \sim p_T^2$, follows from eq. (6.7) to be

$$\frac{\mathrm{d}q(x, Q^2)}{\mathrm{d} \ln Q^2} = \frac{\alpha_s}{2\pi} \int_x^1 \frac{\mathrm{d}y}{y} q(y, Q^2) P_{qq}\left(\frac{x}{y}\right). \tag{6.9}$$

Note that this equation is insensitive to the non-leading "finite" terms $f(z)$ in eq. (6.3) and is exact up to terms of order α_s^2. Since so far we have been dealing only with "bare" (skeleton) diagrams in eq. (6.2), we still have a *constant* strong coupling $\alpha_s = \alpha_s(\mu^2)$ renormalized at an arbitrary but fixed Euclidean momentum $p^2 = -\mu^2$ (see eq. (3.11)). Adding the appropriate vertex and propagator insertions (4.1) to the diagrams of eq. (6.2) just amounts to changing $\alpha_s \to \alpha_s(Q^2)$ in eqs. (6.3)–(6.9) with the running coupling constant given as usual by eq. (4.9). Our basic equation (6.9), which describes the Q^2 evolution of a non-singlet (valence) quark distribution, then finally becomes

$$Q^2 \frac{\mathrm{d}q(x, Q^2)}{\mathrm{d}Q^2} = \frac{\alpha_s(Q^2)}{2\pi} \int_x^1 \frac{\mathrm{d}y}{y} q(y, Q^2) P_{qq}\left(\frac{x}{y}\right). \tag{6.10}$$

An important property of this integro-differential equation is that it reduces to a simple differential equation for the moments of parton densities: Taking the $(n-1)$th x-moment of eq. (6.10) yields

$$\begin{aligned} Q^2 \frac{\mathrm{d}}{\mathrm{d}Q^2} \int_0^1 \mathrm{d}x\, x^{n-1} q(x, Q^2) &= \frac{\alpha_s(Q^2)}{2\pi} \int_0^1 \mathrm{d}x\, x^{n-1} \int_x^1 \frac{\mathrm{d}y}{y} q(y, Q^2) P_{qq}\left(\frac{x}{y}\right) \\ &= \frac{\alpha_s(Q^2)}{2\pi} \int_0^1 \mathrm{d}x\, x^{n-1} \int_0^1 \mathrm{d}y\, \mathrm{d}z\, \delta(x - zy) q(y, Q^2) P_{qq}(z) \\ &= \frac{\alpha_s(Q^2)}{2\pi} \int_0^1 \mathrm{d}y\, y^{n-1} q(y, Q^2) \int_0^1 \mathrm{d}(z)\, (z)^{n-1} P_{qq}(z) \\ &= -\frac{a_{NS}(n)}{\ln(Q^2/\Lambda^2)} \langle y q(y, Q^2) \rangle_n \end{aligned} \tag{6.11}$$

where in the last line we used eqs. (4.8) and (5.64), and

$$\int_0^1 \mathrm{d}z\, z^{n-1} P_{qq}(z) = -\frac{\pi}{\alpha_s} \gamma_{FF}^F \tag{6.12}$$

which will be proven in the next subsection. (We have to take the $(n-1)$-moments since P_{ij} is defined relative to $(1/x)F_2$ and not to F_2.) Since eq. (6.11) coincides with eq. (5.128), the evolution equation (6.10) is nothing else but Parisi's equation (5.129) or (5.130) for non-singlet structure functions derived from the general renormalization group analysis [81]; thus our present approach to calculate the Q^2 dependence of parton distributions is entirely equivalent to the rather abstract method using the renormalization group in as far as it sums all leading logarithmic contributions of parton cross sections to all orders in α_s.

The physical interpretation of eq. (6.10) is now straightforward. Probing a nucleon at a momentum scale $\ln Q^2 + \mathrm{d}\ln Q^2$ the variation of a (valence) quark density is given by the probability of finding a quark at the original momentum scale $\ln Q^2$ carrying fractional momentum y, $q(y, Q^2)$, times the lowest order variation $(\alpha_s/2\pi)P_{qq}(x/y)$ of the probability of finding a quark inside the original quark [164] with momentum smaller by a fraction x/y. According to the basic vertices in fig. 6.1, we therefore specify in general a "splitting function" $P_{ij}(z)$ as the probability of parton j emitting a parton i with longitudinal momentum fraction $z(<1)$ of the parent parton j when $\ln Q^2 \to \ln Q^2 + \mathrm{d}\ln Q^2$. At $z = 1$, which corresponds to no real gluon emission, the quantities P_{qq} and P_{gg} will of course include $\delta(1-z)$ contributions arising from the virtual gluon radiative corrections to the (elastic) quark and gluon lines. It is therefore clear that in general the real positive definite probability densities will be

$$P_{ij}(z, Q^2) = \delta(1-z)\delta_{ij} + \frac{\alpha_s}{2\pi} P_{ij}(z) \ln(Q^2/\mu^2) \tag{6.13}$$

and not $P_{ij}(z)$. The situation in QCD is analogous to that in QED, where in the Weizsäcker–Williams equivalent photon approximation [160, 161] we talk in terms of the photon density inside an electron with energy $E = p$ being

$$\frac{\mathrm{d}N_\gamma(z, E)}{\mathrm{d}z} = \frac{\alpha}{2\pi}\left[\frac{1+(1-z)^2}{z}\right] \ln\left(\frac{E}{m_e}\right)^2 \tag{6.14}$$

corresponding to

$$P_{\gamma e}(z) = \frac{1+(1-z)^2}{z}: \tag{6.15}$$

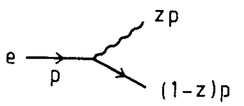

and similarly for the probability P_{ee} of finding e's in e. The density of gluons in a quark is analogous to eq. (6.15), the only difference being the group theoretical factor for the color coupling in eq. (2.6), i.e. $C_2(R) = 4/3$.

We now drop the restriction to one flavor and to non-singlet distributions. Thus, in addition to the quark initiated processes in eq. (6.2), also gluon initiated processes such as shown in fig. 5.4(b) will now contribute. These latter reactions, being proportional to the gluon density $G(y, Q^2)$, will then also depend on the gluon $\to$ quark and gluon $\to$ gluon splitting functions as it is obvious from the last diagram in fig. 5.4(b) and from the QCD vertices in fig. 6.1. Keeping in mind the above discussion and eq. (6.10), we can now directly write down just by inspection the integro-differential equations which describe the Q^2 dependence of parton distributions in the general case [4, 163]

$$Q^2 \frac{\mathrm{d}q(x, Q^2)}{\mathrm{d}Q^2} = \frac{\alpha_s(Q^2)}{2\pi} \int_x^1 \frac{\mathrm{d}y}{y} \left[q(y, Q^2) P_{qq}\left(\frac{x}{y}\right) + G(y, Q^2) P_{qg}\left(\frac{x}{y}\right) \right]$$

$$Q^2 \frac{\mathrm{d}G(x, Q^2)}{\mathrm{d}Q^2} = \frac{\alpha_s(Q^2)}{2\pi} \int_x^1 \frac{\mathrm{d}y}{y} \left[\sum_i^{2N_f} q_i(y, Q^2) P_{gq}\left(\frac{x}{y}\right) + G(y, Q^2) P_{gg}\left(\frac{x}{y}\right) \right]. \tag{6.16}$$

These are the general evolution- or master-equations of Altarelli and Parisi [4, 163] where the sum runs over quarks and antiquarks of all flavors. The number of quarks as seen by the electromagnetic or weak current changes by two mechanisms: a quark originally at momentum scale Q^2 and with higher momentum y may loose momentum by radiating a gluon and/or a gluon inside the nucleon may produce a $q\bar{q}$ pair. Similarly the number of gluons changes because a quark may radiate a gluon and/or a gluon may split into a $q\bar{q}$ pair or into two gluons. This latter possibility is typical for non-abelian gauge theories (QCD) where a three-gluon vertex exists to order g. The splitting functions are given by

$$P_{qq}(x) = \frac{4}{3} \frac{1+x^2}{(1-x)_+} + 2\delta(1-x) \tag{6.17}$$

$$P_{qg}(x) = \tfrac{1}{2}[x^2 + (1-x)^2] \tag{6.18}$$

$$P_{gq}(x) = \frac{4}{3} \frac{1+(1-x)^2}{x} \tag{6.19}$$

$$P_{gg}(x) = 6\left[\frac{x}{(1-x)_+} + \frac{1-x}{x} + x(1-x) + \left(\frac{11}{12} - \frac{N_f}{18} \right) \delta(1-x) \right] \tag{6.20}$$

with the distribution $(1-x)_+^{-1}$ being defined by

$$\int_0^1 \mathrm{d}x \frac{f(x)}{(1-x)_+} \equiv \int_0^1 \mathrm{d}x \frac{f(x) - f(1)}{1-x} \tag{6.21}$$

and $(1-x)_+ = (1-x)$ for $x < 1$. For practical quantitative calculations it is useful to get rid of terms $(1-x)_+^{-1}$ in eq. (6.16) by employing the following formula

$$\int_x^1 \frac{\mathrm{d}y}{y} \frac{f(y)}{(1-x/y)_+} = f(x) \ln \frac{1-x}{x} + \int_x^1 \frac{\mathrm{d}y}{y} \frac{f(y) - f(x)}{1-x/y} \tag{6.22}$$

where $f(y)$ is any function regular at the end points. The decay functions in eqs. (6.17)–(6.20) satisfy the following relations: by charge conjugation we have

$$P_{\bar{q}g} = P_{qg}, \qquad P_{g\bar{q}} = P_{gq}; \tag{6.23}$$

furthermore charge conservation requires (see eq. (5.79))

$$\int_0^1 \mathrm{d}x\, P_{\mathrm{qq}}(x) = 0 \tag{6.24}$$

which implies via eq. (6.12) that $\gamma_{\mathrm{FF}}^{\mathrm{F}}(n=1)=0$ and therefore the sum rules (5.15) hold at all values of Q^2, i.e. the charges are Q^2 independent. Finally, momentum conservation at the vertices in fig. 6.1 requires (for $z<1$)

$$\begin{aligned} P_{\mathrm{qq}}(x) &= P_{\mathrm{gq}}(1-x) \\ P_{\mathrm{qg}}(x) &= P_{\mathrm{qg}}(1-x) \\ P_{\mathrm{gg}}(x) &= P_{\mathrm{gg}}(1-x) \end{aligned} \tag{6.25}$$

whereas total momentum conservation implies

$$\begin{aligned} &\int_0^1 \mathrm{d}x\, x[P_{\mathrm{qq}}(x)+P_{\mathrm{gq}}(x)] = 0 \\ &\int_0^1 \mathrm{d}x\, x[2N_{\mathrm{f}}P_{\mathrm{qg}}(x)+P_{\mathrm{gg}}(x)] = 0. \end{aligned} \tag{6.26}$$

The connection with our familiar results for the moments of densities, obtained by the more sophisticated field theoretic renormalization group calculations, is made by noting that the splitting functions are related to the anomalous dimensions of Wilson operators in eqs. (5.61) and (5.68) in the following way (the proof can be found in the next subsection)

$$\int_0^1 \mathrm{d}x\, x^{n-1}\begin{pmatrix} P_{\mathrm{qq}}(x) & P_{\mathrm{gq}}(x) \\ 2N_{\mathrm{f}}\, P_{\mathrm{qg}}(x) & P_{\mathrm{gg}}(x) \end{pmatrix} = -\frac{\pi}{\alpha_{\mathrm{s}}}\begin{pmatrix} \gamma_{\mathrm{FF}}^{\mathrm{F}} & \gamma_{\mathrm{FF}}^{\mathrm{V}} \\ \gamma_{\mathrm{VV}}^{\mathrm{F}} & \gamma_{\mathrm{VV}}^{\mathrm{V}} \end{pmatrix}. \tag{6.27}$$

Taking now the $(n-1)$th x-moments of eq. (6.16), exactly in the same way as we proceeded in eq. (6.11), it is a simple exercise [11] to arrive at the renormalization group predictions (5.97) and (5.98). This proves the equivalence of the intuitive Altarelli–Parisi approach and the formal renormalization group analysis. Apart from being physically more transparent, the main virtue of the Altarelli–Parisi approach is that the fundamental decay functions P_{ij} are *independent* of the *probe* (i.e., lepton beams or hadron beams) and *depend only* on the *target* considered, i.e. on the strong quark–gluon and gluon–gluon interaction vertices [163]. (This is of course in contrast to our previous renormalization group analysis which heavily relied on the light-cone expansion appropriate only for deep inelastic lepton–nucleon scattering processes.) Therefore we expect that the Q^2 dependences of parton distributions described by eq. (6.16) to have universal validity and that they should be the same for any leptonic or hadronic reaction considered; moreover, this suggests that the IR factorization found in eqs. (5.58) and (5.97)–(5.99) holds to all leading orders in α_{s} for any process, i.e. the wave function at Q_0^2 factorizes from the $\ln Q^2$ terms in a process independent way. In the meantime these conjectures have been proven to be correct using various different field theoretic techniques which will be discussed in section 7.

6.1. Calculating the splitting functions P_{ij} and anomalous dimensions

Although the P_{ij}'s can be calculated in a probe independent way just from the basic QCD vertices in fig. 6.1 using "old fashioned" perturbation theory [163], we will consider the deep inelastic electroproduction process in order to keep the calculation of these functions as transparent as possible. Since the P-functions are defined as the coefficients of the leading $\ln Q^2$ terms of cross sections, eq. (6.3), we simply have to calculate the fundamental parton cross sections for $\gamma^* q \to gq$ and $\gamma^* g \to q\bar{q}$, and to extract their $\ln Q^2$ contributions. By convention we have defined P_{ij} relative to F_2 in eq. (6.2) and therefore we first need the projection of the parton cross sections onto F_2. This can be easily obtained from the general definition of the hadronic tensor in eq. (5.2) where, since we consider electromagnetic currents, only the W_1 and W_2 structure functions are present. In the Bjorken limit (5.8), eq. (5.2) yields the following contractions:

$$g^{\mu\nu} W_{\mu\nu} = \frac{1}{2x}(F_2 - 6xF_1) \tag{6.28}$$

$$p^\mu p^\nu W_{\mu\nu} = \frac{Q^2}{4x^2}\frac{1}{2x}(F_2 - 2xF_1) \equiv \frac{Q^2}{4x^2}\frac{1}{2x}F_L \tag{6.29}$$

from which we obtain

$$\frac{1}{x}F_2 = \frac{12x^2}{Q^2}p^\mu p^\nu W_{\mu\nu} - g^{\mu\nu}W_{\mu\nu} \tag{6.30}$$

$$F_L = \frac{8x^3}{Q^2}p^\mu p^\nu W_{\mu\nu}\ . \tag{6.31}$$

Note that for extracting just the leading $\ln Q^2$ contribution to F_2 we do not have to calculate $p^\mu p^\nu W_{\mu\nu} \sim F_L$ since the contraction with p^μ will compensate the appropriate propagators in the amplitude and therefore the phase space integration does not give rise to $\ln Q^2$ mass singularities; thus F_L is down by a power of $\alpha_s(Q^2) \sim 1/\ln Q^2$ relative to F_2. The relation between the usual cross sections and $W_{\mu\nu}$ is then given by

$$\int |M|^2\, dR_n = 4\pi \varepsilon_\mu^* \varepsilon_\nu W^{\mu\nu} \tag{6.32}$$

with the photon polarizations ε given by $\varepsilon_\mu^*\varepsilon_\nu = g_{\mu\nu}$ or $p_\mu p_\nu$ depending on the required contraction (6.28) or (6.29). The normalization of the spin averaged scattering amplitude M is that of Bjorken and Drell [165] except that our spinor normalization is $\bar{u}u = 2m$. The factor 4π in (6.32) results from considering the naive parton model vertex $\gamma^* q \to q$, see eq. (6.1), in which case the right hand side of eq. (6.32) is well known: $F_2^q = 2xF_1^q = e_q^2\delta(1-x)$. (The structure functions and all kinematic quantities in this subsection refer of course always to the fundamental photon–parton system, e.g. to the quantities inside the square brackets in eq. (6.2).) Furthermore, the two-particle phase space integral we shall subsequently need is given by (we are working with massless quarks and gluons throughout)

$$\int \mathrm{d}R_2 = \frac{1}{8\pi}\frac{1}{s+Q^2}\int_{-s-Q^2}^{0} \mathrm{d}t \tag{6.33}$$

with $Q^2 \equiv -q^2$ and s, t and u being the usual Mandelstam variables. As an IR cut-off we shall simply use

$$\int^{0} \mathrm{d}t \to \int^{-m^2} \mathrm{d}t \tag{6.34}$$

but any other choice would do as well since the coefficients of the leading $\ln Q^2$ terms are convention independent.

Let us start with the process $\gamma^* \mathrm{q} \to \mathrm{q}\bar{\mathrm{q}}$ as shown in fig. 6.2 which allows us to calculate P_{qg}. The spin and color averaged amplitude squared for this process reads [166]

$$|M^{\gamma^* \mathrm{g}\to \mathrm{q}\bar{\mathrm{q}}}|^2_{\varepsilon^*_\mu \varepsilon_\nu = g_{\mu\nu}} = \tfrac{1}{2} e_{\mathrm{q}}^2 4g^2\left[-\frac{u}{t}-\frac{t}{u}+\frac{2sQ^2}{tu}\right] \tag{6.35}$$

where the color factor $\frac{1}{2}$ for a given flavor ($N_{\mathrm{f}} = 1$) can be read off eqs. (4.3) and (4.4):

$$\frac{1}{8}\sum_{c=1}^{8}\sum_{i=1}^{3}(T_c T_c)_{ii} = \frac{1}{2}.$$

Using the following kinematic relations

$$\begin{aligned} &s+t+u = -Q^2 \\ &s+Q^2 = Q^2/x, \qquad x \equiv Q^2/2p\cdot q \end{aligned} \tag{6.36}$$

the phase space integral in (6.33) together with (6.34) gives for eq. (6.32), keeping the dominant $\ln Q^2$ terms only,

$$-2e_{\mathrm{q}}^2\alpha_{\mathrm{s}}[x^2+(1-x)^2]\ln(Q^2/m^2) = 4\pi g_{\mu\nu}W^{\mu\nu}. \tag{6.37}$$

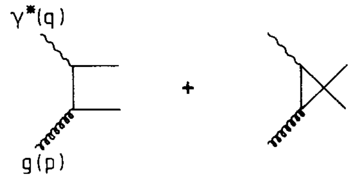

Fig. 6.2. Diagrams giving rise to $F_2^{\mathrm{g}} \sim P_{\mathrm{qg}}$ and $F_{\mathrm{L}}^{\mathrm{g}}$.

Using eq. (6.30) and the definition (6.3) for the P's we obtain in the leading ln Q^2 approximation

$$\frac{1}{x} F_2^g \simeq -g^{\mu\nu} W_{\mu\nu} = e_q^2 \frac{\alpha_s}{2\pi} [x^2 + (1-x)^2] \ln \frac{Q^2}{m^2} \equiv e_q^2 \frac{\alpha_s}{2\pi} 2P_{qg}(x) \ln \frac{Q^2}{m^2} \tag{6.38}$$

which gives eq. (6.18). Note that in the last line we have by convention included a factor of 2 in order to account for the fact that two quarks ($q\bar{q}$) couple to the gluon vertex in fig. 6.2 whereas the decay functions P_{ij} are always defined to describe the transition form j to *one* species i. Furthermore, taking the $(n-1)$th moment of P_{qg} we obtain the appropriate anomalous dimension in eq. (5.68)

$$2N_f \int_0^1 dx\, x^{n-1} P_{qg}(x) = \frac{n^2+n+2}{n(n+1)(n+2)} N_f = -\frac{\pi}{\alpha_s} \gamma_{\text{VV}}^{\text{F}}(n). \tag{6.39}$$

That P_{qg} yields $\gamma_{\text{VV}}^{\text{F}}$ becomes obvious by comparing the relevant diagrams in eq. (5.67) with fig. 6.2.

On the other hand, if we take $\varepsilon_\mu^* \varepsilon_\nu = p_\mu p_\nu$ in eq. (6.32) we can calculate, according to eq. (6.31), the "finite" term F_L^g. In this case we have

$$|M^{\gamma^* g \to q\bar{q}}|^2_{\varepsilon_\mu^* \varepsilon_\nu = p_\mu p_\nu} = \tfrac{1}{2} e_q^2 4 g^2 s \tag{6.40}$$

which gives, using (6.31)–(6.33) and (6.36), F_L^g in eq. (5.145).

Next, let us consider the reaction $\gamma^* q \to gq$ shown in fig. 6.3 which allows us to calculate P_{qq} and P_{gq}. Taking $\varepsilon_\mu^* \varepsilon_\nu = g_{\mu\nu}$ in eq. (6.32) the spin and color averaged amplitude squared becomes

$$|M^{\gamma^* q \to gq}|^2_{\varepsilon_\mu^* \varepsilon_\nu = g_{\mu\nu}} = \frac{4}{3} e_q^2 4 g^2 \left[\frac{u}{s} + \frac{s}{u} + \frac{2tQ^2}{su}\right] \tag{6.41}$$

which, inserted into eq. (6.32), gives (note that only the second and third term in square brackets give rise to ln Q^2 terms [164])

$$-\frac{4}{3} 2 e_q^2 \alpha_s \frac{1+x^2}{1-x} \ln \frac{Q^2}{m^2} = 4\pi g_{\mu\nu} W^{\mu\nu}. \tag{6.42}$$

Using again eq. (6.30) we finally have for the leading log terms

$$\frac{1}{x} F_2^q = e_q^2 \frac{\alpha_s}{2\pi} \frac{4}{3} \frac{1+x^2}{1-x} \ln \frac{Q^2}{m^2} \equiv e_q^2 \frac{\alpha_s}{2\pi} P_{qq}(x) \ln \frac{Q^2}{m^2} \tag{6.43}$$

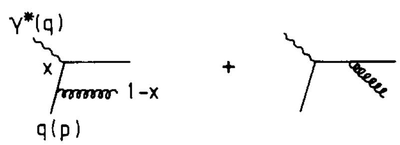

Fig. 6.3. Diagrams giving rise to $F_2^q \sim P_{qq}$, P_{gq} and F_L^q.

i.e.

$$P_{qq}(x) = \frac{4}{3}\frac{1+x^2}{1-x} \qquad (x<1). \tag{6.44}$$

This result is of course only correct for $x<1$ since the diagrams in fig. 6.3 do not account for the elastic case with no gluon emission ($x=1$). These radiative corrections to P_{qq} at $x=1$ can be easily calculated by first regularizing the singularity at $x=1$ in (6.44) by reinterpreting [163] the factor $(1-x)^{-1}$ as a distribution $(1-x)_+^{-1}$defined in eq. (6.21), and then adding to (6.44) a $\delta(1-x)$ function,

$$P_{qq}(x) = \frac{4}{3}\frac{1+x^2}{(1-x)_+} + c\,\delta(1-x), \tag{6.45}$$

with the coefficient determined by the charge conservation constraint (6.24): $c=2$. This is eq. (6.17). The diagonal anomalous dimension γ_{FF}^{F} in eq. (5.61) is then obtained from

$$\int_0^1 dx\, x^{n-1} P_{qq}(x) = \frac{4}{3}\left[-\frac{1}{2} + \frac{1}{n(n+1)} - 2\sum_{j=2}^{n}\frac{1}{j}\right] = -\frac{\pi}{\alpha_s}\gamma_{FF}^{F}(n) \tag{6.46}$$

where we have used

$$\begin{aligned}\int_0^1 dx\,\frac{x^{n-1}}{(1-x)_+} &\equiv \int_0^1 dx\,\frac{x^{n-1}-1}{1-x} = \int_0^1 \frac{dz}{z}\left[(1-z)^{n-1}-1\right] \\ &= \sum_{j=1}^{n-1}(-)^j\binom{n-1}{j}\int_0^1 dz\, z^j = -\sum_{j=1}^{n-1}\frac{1}{j}\end{aligned} \tag{6.47}$$

where the last equality can be easily proved by induction. The decay function P_{gq} can now be easily obtained from (6.44) using the momentum conservation constraint (6.25) (see also fig. 6.3):

$$P_{gq}(x) = P_{qq}(1-x) = \frac{4}{3}\frac{1+(1-x)^2}{x} \tag{6.48}$$

which is eq. (6.19) and which allows us to calculate γ_{FF}^{V} in eq. (5.68):

$$\int_0^1 dx\, x^{n-1} P_{gq}(x) = \frac{4}{3}\frac{n^2+n+2}{n(n^2-1)} = -\frac{\pi}{\alpha_s}\gamma_{FF}^{V}(n). \tag{6.49}$$

Comparing the appropriate diagrams in eq. (5.67) with those in fig. 6.3 it becomes immediately obvious that $P_{qq} \leftrightarrow \gamma_{FF}^{F}$ and $P_{gq} \leftrightarrow \gamma_{FF}^{V}$.

Again if we take $\varepsilon_\mu^* \varepsilon_\nu = p_\mu p_\nu$ in eq. (6.32) we can calculate, using eq. (6.31), the "finite" term F_L^q in eq. (5.145). In this case we have

$$|M^{\gamma^* q \to gq}|^2_{\varepsilon^*_\mu \varepsilon_\nu = p_\mu p_\nu} = \tfrac{4}{3} e_q^2 2 g^2 (-t) \tag{6.50}$$

which gives, using eqs. (6.31)–(6.33) and (6.36), F_L^q in (5.145).

A similar calculation [163] gives P_{gg} in eq. (6.20).

6.2. Bethe–Salpeter ladders

An alternative way to understand the physics behind the leading log summation via the integro-differential equations (6.16) of Altarelli and Parisi is based on an iterative summation of Bethe–Salpeter ladders. Based on the original calculations for pseudoscalar [167] and on the pioneering work of Gribov and Lipatov [168] for abelian vector–gluon theories, this method has been extended to QCD by several authors [169–172]. Apart from being physically most intuitive, this approach can be easily extended to processes other than deep inelastic reactions where no operator product expansion exists, such as to fragmentation functions in semi-inclusive processes ($\mu p \to \mu \pi + X$, $e^+ e^- \to \pi + X$, etc.), to Drell–Yan dilepton production ($pp \to \mu^+ \mu^- + X$), to high-p_T processes ($pp \to \pi + X$), and many other more. Since we have discussed in great detail two methods of summing leading logs, we shall limit ourselves here to sketch the main line of the ideas and to the calculation of flavor non-singlet structure functions.

So far our calculations have been always performed in a covariant (Lorentz–Feynman or Landau) gauge where the sum over gluon polarizations ε'_μ,

$$\sum_{\text{pol.}} \varepsilon'^*_\mu \varepsilon'_\nu = -g_{\mu\nu} \tag{6.51}$$

includes also unphysical longitudinal states. In this case, squaring the diagrams of fig. 6.3 as shown in fig. 6.4, not only the ladder-like u-channel graph in fig. 6.4(a) gives rise to leading logarithms but also the s–u interference term [164] in fig. 6.4(b). As was first noticed by Lipatov [173], a clever choice of gauge helps to minimize the number of diagrams contributing to the leading log approximation. This is achieved by summing only over the two transverse polarization states of the gluon with $\varepsilon' \cdot k = 0$, and instead of (6.51) we have

$$\sum_{\text{pol.}} \varepsilon'^*_\mu \varepsilon'_\nu = -g_{\mu\nu} + \frac{n_\mu k_\nu + n_\nu k_\mu}{n \cdot k} - \frac{k_\mu k_\nu}{(n \cdot k)^2} n^2 \tag{6.52}$$

where the arbitrary four-vector $n^\mu (n^2 \neq 0)$ indicates which components of the gluon field A^μ is set to

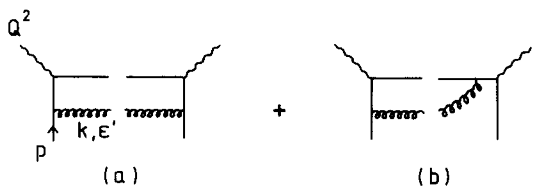

Fig. 6.4. The squared amplitudes of fig. 6.3 which give rise to leading logs in a covariant gauge. In the physical axial gauge *only* the "ladder" (a) contributes ln Q^2 terms.

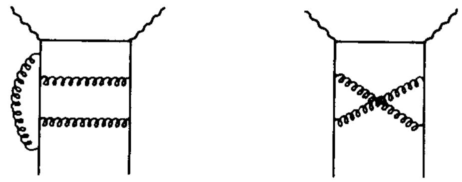

Fig. 6.5. A sample of diagrams which do not contribute to the leading log approximation.

zero ($n \cdot A = 0$). This physical transverse gauge is the so called "axial gauge". Now only the ladder-like parton cross section in fig. 6.4(a) gives rise to leading $\ln Q^2$ terms, but not the crossed interference term in fig. 6.4(b); more generally, crossed (nonplanar) diagrams exhibited in fig. 6.5 do not contribute to the leading log approximation. The smallness of the nonplanar diagrams in the axial gauge is related to the fact that the gluon propagator $D_{\mu\nu}(k) = \mathrm{i}\Delta_{\mu\nu}/k^2$ with $\Delta_{\mu\nu} \equiv \Sigma_{\rm pol.}\, \varepsilon_\mu'^* \varepsilon_\nu'$ can now propagate only the two physical transverse polarization states. Indeed, as the gluon goes on shell ($k^2 \to 0$) we have

$$-g^{\mu\nu}\Delta_{\mu\nu}(k) \to 2, \qquad k^\mu \Delta_{\mu\nu}(k) \to 0. \tag{6.53}$$

(For comparison, in the Feynman gauge we have according to eq. (6.51) $-g^{\mu\nu}\Delta_{\mu\nu} = 4$ and $k^\mu\Delta_{\mu\nu} = k_\nu \neq 0$.) Technically, the smallness of the nonplanar diagrams in the axial gauge is related to the following property of the propagator [169]: $p^\mu \Delta_{\mu\nu}(k) = O(k_{\rm T})$.

It is now straightforward to determine [171] the leading log contributions stemming from ladder diagrams depicted in fig. 6.4(a). If Q^2 is large enough, each subsequent quark below the first radiated hard gluon can itself radiate a hard collinear gluon (thus giving rise to one power of $\ln Q^2$) as long as $|t_j|$ is large enough to ensure perturbative calculations; in this way the Bethe–Salpeter ladder in fig. 6.6 builds up with n rungs and we can sum all mass singularities by iteration. The lower non-perturbative part of the ladder where $|t_{j+1}| < Q_0^2$ with $\alpha_s(Q_0^2)/\pi \not\ll 1$ can be factorized [171] from the leading perturbative contributions and describes the uncalculable nucleon wave function probed at Q_0^2 which has to be fitted to experiment. In the leading log configuration the connection between the jth and $(j-1)$th rung in fig. 6.6 is easily obtained to be [171]

$$M_j = \frac{2g^2}{yt_j} P_{\rm qq}(y)\, {\rm Tr}(\not{p}' M_{j-1}). \tag{6.54}$$

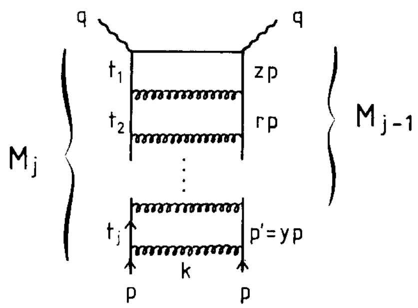

Fig. 6.6. Bethe–Salpeter ladder giving rise to leading mass singularities in non-singlet structure functions whenever the gluon is collinear to the incoming quark.

In the region where $\boldsymbol{k}$ is almost parallel to $\boldsymbol{p}$, $\boldsymbol{k} = (1-y)\boldsymbol{p}$, we can write the phase space factor

$$\frac{d^3k}{2k_0(2\pi)^3} \simeq \frac{dy\, dt_j}{16\pi^2}$$

where we used eq. (6.5) for $t_j = p'^2$. Hence the contribution to the j particle cross section is given by

$$\sigma_j(p, q, p^2 = m^2) = \int \frac{dy}{y} \frac{dt_j}{t_j} \frac{\alpha_s}{2\pi} P_{qq}(y)\, \sigma_{j-1}(yp, q, p'^2 = t_j). \tag{6.55}$$

So far we have been dealing only with bare ladder diagrams ("skeletons") and therefore the strong coupling α_s is *constant* – not yet running. If we dress these bare ladders by including all virtual radiative corrections essentially amounts to [169, 171] $\alpha_s \to \alpha_s(t_n)$, with $\alpha_s(t)$ being the usual running coupling, as shown in fig. 6.7. Moreover, it follows from simple kinematical considerations that the invariant masses t_i in fig. 6.6 are ordered

$$p^2 \leq |t_j| \leq |t_{j-1}| \leq \cdots \leq |t_1| \leq Q^2. \tag{6.56}$$

Therefore, in the leading log approximation, the iteration of (6.55) for the whole ladder in fig. 6.6 gives, using eq. (4.8) for $\alpha_s(t_i) \simeq (4\pi b \ln t_i)^{-1}$,

$$\sigma_j = \frac{1}{(8\pi^2 b)^j} \int\limits_{m^2}^{Q^2} \frac{dt_1}{t_1 \ln t_1} \int\limits_{m^2}^{t_1} \frac{dt_2}{t_2 \ln t_2} \cdots \int\limits_{m^2}^{t_{j-1}} \frac{dt_j}{t_j \ln t_j} \int\limits_0^1 \frac{dy}{y} P_{qq}(y) \int\limits_0^y \cdots \int\limits_0^r \frac{dz}{z} P_{qq}\left(\frac{z}{r}\right) \delta\left(1 - \frac{x}{z}\right) \tag{6.57}$$

where again m^2 denotes a suitably chosen IR cut-off. Thus each (collinear) gluon emission in fig. 6.6 will give rise to a logarithmic contribution for which the t-integrals in eq. (6.57) give $(1/j!)(\ln \ln Q^2/m^2)^j$ since $dt/t \ln t = d(\ln \ln t)$. The nested integrals involving P_{qq} can be decoupled by taking moments which give

$$\int\limits_0^1 dx\, x^{n-1} \sigma_j = \frac{1}{(8\pi^2 b)^j} \frac{1}{j!} \left(\ln \ln \frac{Q^2}{m^2}\right)^j \left[\int\limits_0^1 dy\, y^{n-1} P_{qq}(y)\right]^j = \frac{1}{j!} \left[-a_{NS}(n) \ln \ln \frac{Q^2}{m^2}\right]^j \tag{6.58}$$

where we have used eqs. (6.12) and (5.64) to obtain the non-singlet anomalous dimension $a_{NS}(n)$. Since

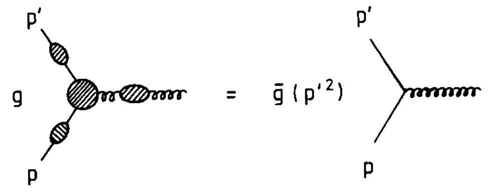

Fig. 6.7. Virtual corrections that make the coupling constant run.

a structure function is defined as a sum over all possible j-rungs in fig. 6.6, we finally get

$$\int_0^1 \mathrm{d}x\, x^{n-2} F_2^{\mathrm{NS}}(x, Q^2) \sim \sum_j \int_0^1 \mathrm{d}x\, x^{n-1} \sigma_j$$
$$= \exp[-a_{\mathrm{NS}}(n) \ln \ln(Q^2/m^2)] = (\ln Q^2/m^2)^{-a_{\mathrm{NS}}(n)} \qquad (6.59)$$

which is our desired result. Similarly, generalized ladders such as shown in fig. 6.8 allow us to calculate [169, 171] also the correct Q^2 dependence of the moments of flavor singlet structure functions.

Note that for a fixed point theory where $\alpha_s \equiv \alpha^* = \text{const.}$ in eq. (6.55), we get $\mathrm{d}t/t = \mathrm{d}\ln t$ in place of $\mathrm{d}t/t \ln t = \mathrm{d}(\ln \ln t)$ in eq. (6.57). Thus we have one ln less in (6.58) which implies, instead of eq. (6.59),

$$\int_0^1 \mathrm{d}x\, x^{n-2} F_2^{\mathrm{NS}}(x, Q^2) \sim \exp[-a_{\mathrm{NS}}(n) \ln Q^2] = (Q^2)^{-a_{\mathrm{NS}}(n)} \qquad (6.60)$$

which is the power-like behavior obtained previously for abelian vector gluon theories in eq. (5.59) with the anomalous dimension now given by

$$a_{\mathrm{NS}}(n) = -\frac{\alpha^*}{2\pi} \int_0^1 \mathrm{d}y\, y^{n-1} P_{\mathrm{qq}}(y) = \frac{1}{2} \gamma_{\mathrm{FF}}^{\mathrm{F}}(n)$$

in agreement with eqs. (5.78), (5.61) and (6.46); of course we have now $C_2(R) = 1$ instead of 4/3.

We just have demonstrated in a rather transparent way how the dominant $\ln Q^2$ terms can be summed to all orders in α_s by iterating all possible hard collinear gluon emissions in a given Bethe–Salpeter ladder. As we have already seen these leading mass singularities *factorize*, to all orders in α_s, from the non-perturbative hadronic wave function (parton distribution) at, say, $Q^2 = Q_0^2$. Moreover, they are *universal* in the sense that they are independent of the particular hard process under consideration which is intuitively clear since one can iterate $\ln Q^2$ terms stemming from the emission of hard gluons off any parton line relevant to a given process. The same result is true for hard processes containing well identified partons in the final state: In this case the same $\ln Q^2$ terms govern the Q^2 dependence of parton decay or fragmentation functions to which we will turn in section 10.

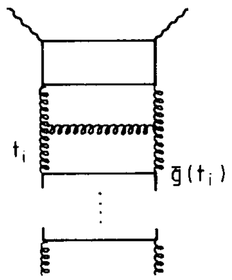

Fig. 6.8. Bethe–Salpeter ladder contributing to the Q^2 dependence of singlet structure functions.

7. Factorization and the universal validity of the Q^2-dependence of parton distributions

So far we have discussed three methods of calculating the leading logarithmic Q^2-dependence of parton distributions in deep inelastic lepton–nucleon scattering processes. Moreover we have found that all non-perturbative pieces (matrix elements of local operators to be interpreted as hadronic wave functions or parton distributions at a fixed $Q^2 = Q_0^2$) factorized to all orders in $\alpha_s(Q^2)$ and in all logarithms of Q^2. We now turn to the question whether these results are of universal validity in the sense that the (infrared) factorization properties as well as the Q^2-dependencies obtained so far are the same for any other hard scattering process. Although it will be obvious from our discussion in the previous section that this is indeed the case, we will briefly illustrate the basic ideas which led to this conclusion in as simple terms as possible following the original suggestions and conjectures of Politzer [174].

Electroproduction serves as a simple example of the method. Let us begin with the parton description of the ep cross section $d\sigma$ (see fig. 5.4 and eq. (6.2) for $d\sigma \sim F_2$)

$$d\sigma(x, Q^2) = \int_x^1 dy\, q(y)\, d\sigma_{\text{parton}}\left(\frac{x}{y}, Q^2\right) \tag{7.1}$$

where in general (apart from obvious factors such as quark charges)

$$d\sigma_{\text{parton}}\left(\frac{x}{y}, Q^2\right) \sim \delta\left(1 - \frac{x}{y}\right) - \alpha_s a\left(\frac{x}{y}\right) \ln \frac{Q^2}{-p^2} - \alpha_s f\left(\frac{x}{y}\right) + \cdots \tag{7.2}$$

with $a(x/y)$ being straightforwardly related to the anomalous dimensions (or splitting functions). In (7.2) we have assumed that the calculations have been performed for incoming (massless) quarks slightly off-shell ($p^2 < 0$). We could, of course, also work with $p^2 = 0$ but keep the quark mass $m^2 \neq 0$: In this case the finite terms $f(x/y)$ will be different but the dominant contribution $a(x/y) \ln(Q^2/m^2)$ remains the same. Equations (7.1) and (7.2) do not make sense as they stand since terms like $\ln(Q^2/-p^2)$, for $-p^2 \ll Q^2$, spoil any naive use of perturbation theory which reflects the general desease of "infrared" divergences present for light or massless quarks and gluons.

The key observation [174] in handling the $\ln(Q^2/-p^2)$ as $p^2 \to 0$ is that $d\sigma_{\text{parton}}$ factorizes into a Q^2 dependent well behaved piece times a Q^2 independent infrared divergent piece. The latter should then be absorbed into the parton distribution $q(y)$, where it really belongs.

Because of the convolution (7.1), this factorization is somewhat complicated by the x dependence of $d\sigma_{\text{parton}}$ in (7.2). The essential trick to circumvent this problem is to take *x-moments*, in terms of which the convolution (7.1) factorizes (see eq. (6.11)):

$$\int_0^1 dx\, x^{n-2}\, d\sigma(x, Q^2) = \int_0^1 dy\, y^{n-2}\, y\, q(y) \int_0^1 dz\, z^{n-2}\, d\sigma_{\text{parton}}(z, Q^2) \tag{7.3}$$

with

$$\int_0^1 dz\, z^{n-2}\, d\sigma_{\text{parton}}(z, Q^2) \sim 1 - \alpha_s a_n \ln \frac{Q^2}{-p^2} + \cdots$$
$$= \left(1 - \alpha_s a_n \ln \frac{Q_0^2}{-p^2} + \cdots\right)\left[1 - \alpha_s a_n \ln \frac{Q^2}{Q_0^2} + \cdots\right] \tag{7.4}$$

where $a_n = \int_0^1 dz\, z^{n-2}\, a(z)$, and we have factorized the dangerous piece ($p^2 \to 0$) at the expense of introducing a new arbitrary but *finite* momentum scale Q_0^2. All the infrared difficulties reside in the first factor (if we choose $Q_0^2 \sim O(Q^2)$) which is independent of Q^2. So the infrared sensitivity can be factored and reabsorbed into $q(y)$ in eq. (7.3):

$$\int_0^1 dx\, x^{n-2}\, d\sigma(x, Q^2) \sim \int_0^1 dy\, y^{n-2} y\, q(y, Q_0^2)\left[1 - \alpha_s a_n \ln \frac{Q^2}{Q_0^2} + \cdots\right] \tag{7.5}$$

which now admits a well-behaved power series expansion in α_s and allows us to compute the Q^2 dependence reliably. The renormalized, measurable wave function (to be extracted from experiment) is given by

$$\int_0^1 dy\, y^{n-2} y\, q(y, Q_0^2) \equiv \int_0^1 dy\, y^{n-2} y\, q(y)\left(1 - \alpha_s a_n \ln \frac{Q_0^2}{-p^2} + \cdots\right). \tag{7.6}$$

The fact that the logarithmic terms make no sense as $p^2 \to 0$ is irrelevant because it is only $q(y, Q_0^2)$, and *not* $q(y)$, that is experimentally observable. Having used this algorithm of extracting and factorizing infrared divergent pieces via moments, we can invert our well-behaved moment prediction to give simple results for the x and Q^2 dependence of cross sections (structure functions)

$$d\sigma(x, Q^2) \sim \int_x^1 dy\, q(y, Q_0^2)\left[\delta\left(1 - \frac{x}{y}\right) - \alpha_s a\left(\frac{x}{y}\right) \ln \frac{Q^2}{Q_0^2} + \cdots\right]. \tag{7.7}$$

Taking moments is of course not only a theoretical tool used to justify eq. (7.7) but is also a very practical calculational tool since in general $a(z)$ is not well behaved for $z \to 1$ (see eq. (6.45)) and hence its meaning is made precise only by integrals (such as in eq. (6.46)).

Although the factorization of the Q^2 dependence from the p^2 dependence in eq. (7.4) is almost trivial to order α_s, it is a far more complex issue in higher orders: It was the essential content of the renormalization group improved operator product expansion, discussed in section 5, to prove that the factorization in (7.5) persists to *all* orders in $\alpha_s(Q^2)$ and to all logarithms of Q^2. Of course, (7.5) will turn into a matrix equation if gluonic singlet initial states are considered as well (singlet mixing!).

We can now apply our method to any parton process which is not necessarily dominated by the leading light-cone singularity of an operator product expansion, as was the case for electroproduction. Let us first study the order α_s corrections [174–176] to the Drell–Yan mechanism [177] for producing heavy lepton pairs in hadronic collisions, $h_1 h_2 \to \mu^+\mu^- + X$. Here one imagines a parton (antiparton) with

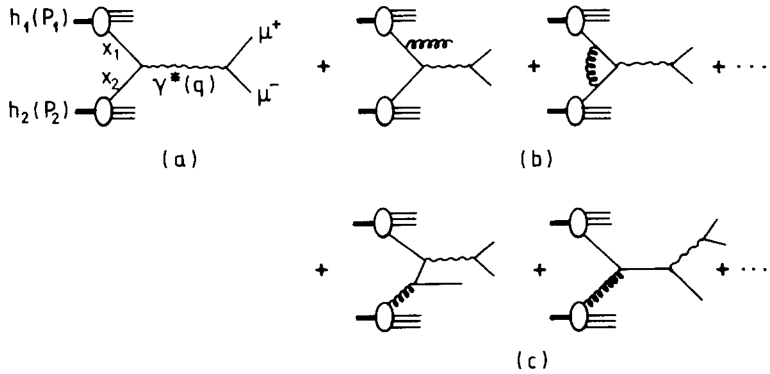

Fig. 7.1. Sample diagrams contributing to the Drell–Yan process in (a) the naive parton model and (b), (c) to the α_s corrections in QCD.

fraction x_1 of the incoming hadron h_1 annihilating an antiparton (parton) of fractional momentum x_2 in the target h_2, thereby creating a heavy virtual photon which then decays into the lepton pair (fig. 7.1(a)). The cross section for creating in this way dileptons of invariant mass-squared $Q^2 \equiv +q^2$,

$$Q^2 = (x_1P_1 + x_2P_2)^2 \simeq 2x_1x_2P_1 \cdot P_2 \simeq x_1x_2s, \tag{7.8}$$

is, in the naive parton model, formally given by [177, 178]

$$\mathrm{d}\sigma^{\mathrm{DY}} = \int \mathrm{d}x_1\, \mathrm{d}x_2\, q_1(x_1)\, \bar{q}_2(x_2)\, \mathrm{d}\sigma_{\mathrm{parton}} \tag{7.9}$$

where, in the free field case, $\mathrm{d}\sigma_{\mathrm{parton}} = \mathrm{d}\sigma^{q\bar{q}\to\mu^+\mu^-}(Q^2)$. (The detailed form of the Drell–Yan cross section together with all the relevant kinematics will be given in section 8.) In order to calculate the order α_s corrections to the naive Drell–Yan cross section we proceed in the same way as before for electroproduction and consider, for simplicity, the $q\bar{q}$ annihilation process first. As in eq. (7.2) we calculate $\mathrm{d}\sigma_{\mathrm{parton}}$ for $q\bar{q}\to\gamma^*g$ (fig. 7.1(b)) and keep the dominant log-contributions only which arise from gluon emissions parallel (collinear) to the quark lines in fig. 7.1(b) carrying momenta $p_1 = x_1P_1$ and $p_2 = x_2P_2$:

$$\mathrm{d}\sigma^{q\bar{q}} \sim \delta(1 - \tau/x_1x_2) - \alpha_s a(\tau/x_1x_2) \ln Q^2 \tag{7.10}$$

where the δ-function takes care of the constraint (7.8) for the naive $q\bar{q}\to\gamma^*$ vertex with $\tau = Q^2/s$ (≤ 1). The infrared singularities will be regulated by taking the quarks off shell $p_1^2 \neq 0$, $p_2^2 \neq 0$. We then take moments of eq. (7.9) in order to determine the factorizable infrared sensitive pieces which are to be absorbed into the unrenormalized naive wave functions $q(x)$, etc. Instead of the x-moments in eq. (7.3), the appropriate $\tau \equiv Q^2/s$ moments of (7.9) read [174–176]

$$\begin{aligned}\int_0^1 \mathrm{d}\tau\, \tau^{n-2}\, \mathrm{d}\sigma^{\mathrm{DY}}(\tau) &= \int_0^1 \mathrm{d}\tau\, \tau^{n-2} \int_\tau^1 \mathrm{d}x_1\, q_1(x_1) \int_{\tau/x_1}^1 \mathrm{d}x_2\, \bar{q}_2(x_2)\, \mathrm{d}\sigma^{q\bar{q}}(\tau_{12}) \\ &= \int_0^1 \mathrm{d}x_1\, x_1^{n-2} x_1\, q_1(x_1) \int_0^1 \mathrm{d}x_2\, x_2^{n-2} x_2\, \bar{q}_2(x_2) \int_0^1 \mathrm{d}\tau_{12}\, \tau_{12}^{n-2}\, \mathrm{d}\sigma^{q\bar{q}}(\tau_{12})\end{aligned} \tag{7.11}$$

where $\tau_{12} = \tau/x_1x_2$ and

$$\int_0^1 \mathrm{d}\tau_{12}\, \tau_{12}^{n-2}\, \mathrm{d}\sigma^{q\bar{q}}(\tau_{12}) \sim 1 - \alpha_s a_n \left(\ln \frac{Q^2}{-p_1^2} + \ln \frac{Q^2}{-p_2^2}\right)$$

$$= \left(1 - \alpha_s a_n \ln \frac{Q_0^2}{-p_1^2}\right)\left(1 - \alpha_s a_n \ln \frac{Q_0^2}{-p_2^2}\right)\left[1 - \alpha_s a_n \ln \frac{Q^2}{Q_0^2}\right]^2 ; \tag{7.12}$$

obvious factors stemming from the lowest order process $q\bar{q} \to \mu^+\mu^-$ in fig. 7.1(a) are suppressed. As in eq. (7.4) we again have been able to factorize the infrared dangerous pieces ($p_i^2 \to 0$) by introducing a new mass scale Q_0^2. Absorbing these pieces into $q_i(x_i)$ as was done in eq. (7.6),

$$\int_0^1 \mathrm{d}x_i\, x_i^{n-2} x_i\, q_i(x_i, Q_0^2) \equiv \int_0^1 \mathrm{d}x_i\, x_i^{n-2} x_i\, q_i(x_i) \left(1 - \alpha_s a_n \ln \frac{Q_0^2}{-p_i^2}\right), \tag{7.13}$$

we again obtain a perfectly well behaved prediction for the physical cross section in eq. (7.11)

$$\int_0^1 \mathrm{d}\tau\, \tau^{n-2}\, \mathrm{d}\sigma^{\mathrm{DY}}(\tau) \sim \int_0^1 \mathrm{d}x_1\, x_1^{n-2} x_1\, q_1(x_1, Q_0^2) \int_0^1 \mathrm{d}x_2\, x_2^{n-2} x_2\, \bar{q}_2(x_2, Q_0^2) \left[1 - \alpha_s a_n \ln \frac{Q^2}{Q_0^2}\right]^2 . \tag{7.14}$$

Thus, to leading order, the whole effect of gluon radiations in fig. 7.1(b) is to make the naive parton distributions in eq. (7.9) Q^2-dependent,

$$\int_0^1 \mathrm{d}x_i\, x_i^{n-2} x_i\, q_i(x_i, Q^2) = \int_0^1 \mathrm{d}x_i\, x_i^{n-2} x_i\, q_i(x_i, Q_0^2) \left[1 - \alpha_s a_n \ln \frac{Q^2}{Q_0^2}\right], \tag{7.15}$$

leaving us formally with the same expression for the Drell–Yan cross section as given by the naive parton model (eq. (7.9) and fig. 7.1a) but with $q_i(x_i) \to q_i(x_i, Q^2)$.

Apart from having established the infrared factorization property, the most significant observation originally made by Politzer [174] is that the coefficient a_n of the $\ln Q^2$ terms is exactly the *same* function which appears in the order α_s corrections to deep inelastic scattering on a quark, for example in eq. (7.5)! The same is true for corrections which result from the gluon initiated process [174–176] in fig. 7.1(c); in this case the logarithmic coefficient is proportional to $P_{qg} \sim \gamma_{\mathrm{VV}}^{\mathrm{F}}$ which turns out to be identical to the one stemming from the deep inelastic process in fig. 6.2. Therefore the scaling violating *Q^2-dependence* of parton distributions in eqs. (7.5) and (7.14) is the *same* regardless of probing the space-like ($q^2 < 0$ with $Q^2 \equiv -q^2$) or the time-like ($q^2 > 0$ with $Q^2 \equiv +q^2$) region – a statement which is equivalent to our previous remark that the splitting functions P_{ij} can be calculated in a probe independent way [163]. Or in other words:

The deviations from the naive Drell–Yan picture are intimately related to the violations of Bjorken scaling in deep inelastic scattering!

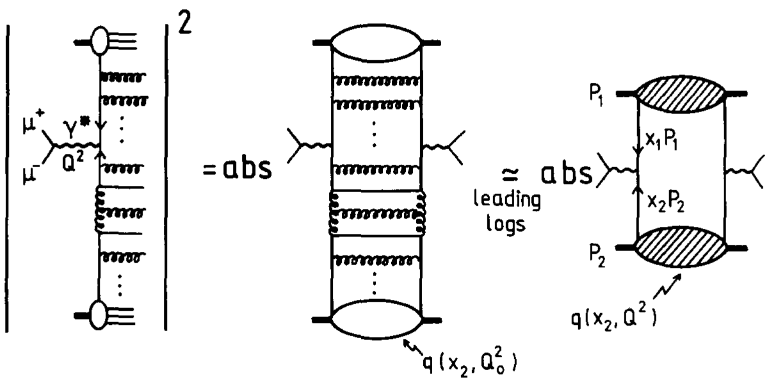

Fig. 7.2. Sample diagrams in the planar (axial) gauge giving rise to the leading logarithmic Q^2-dependences of parton distributions in the Drell–Yan process of massive dilepton production.

These results can be shown to hold to all logarithmic orders in perturbation theory [169–172, 179–184] where, in contrast to the above order α_s case, the proof of infrared factorization becomes a highly non-trivial matter. Here one essentially sums leading mass singularities (parallel gluon emission) of planar Bethe–Salpeter ladder diagrams shown in fig. 7.2, a technique similar to the one discussed in section 6.2 for deep inelastic processes (see, for example, figs. 6.6 and 6.8).

The same game can be played for any other hard scattering process such as "high-p_T" reactions where a pion, say, is produced with large transverse momentum relative to the beam axis of the colliding hadrons: $pp \to \pi + X$ etc. In the naive parton model approach the cross section for this reaction, as shown in fig. 7.3(a), is expected to be given by [185]

$$d\sigma^h = \int dx_a\, dx_b\, q_a(x_a)\, q_b(x_b)\, D_c^h(z)\, d\sigma_{\text{parton}}^{ab\to cd} \tag{7.16}$$

where the fragmentation function $D_c^h(z)$ describes the probability that the parton c decays into a hadron h ($=\pi$, K, ...) carrying fractional momentum z. (For more details we refer the interested reader to section 11.) Again, to all leading logarithmic orders in α_s, the contributions from all possible collinear gluon emissions as shown in fig. 7.3(b) do not alter the basic form of eq. (7.16), their only effect being to make the parton distributions Q^2-dependent [186], i.e. $q(x) \to q(x, Q^2)$ and $D(z) \to D(z, Q^2)$, and $d\sigma_{\text{parton}}$ becomes just the lowest order Born cross section for elastic $q_a q_b \to q_c q_d$ scattering in fig. 7.3a, calculated using the running coupling constant $\alpha_s(Q^2)$. The Q^2 dependence is of course the same as the one obtained for deep inelastic processes, a result which holds [169, 172, 179–181] to all orders in $\alpha_s(Q^2)$, but the choice of Q^2 is not unique: One usually chooses as a typical invariant mass scale

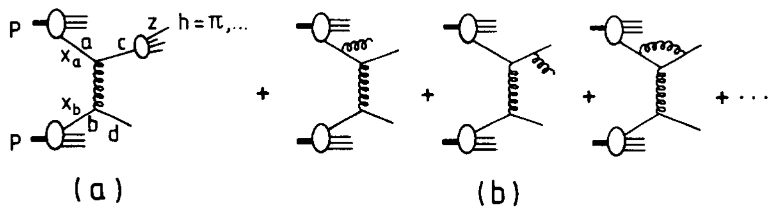

Fig. 7.3. High-p_T process in (a) the naive parton model and with (b) gluonic QCD corrections added.

$Q^2 = -\hat{t}$, $\sqrt[3]{\hat{s}\hat{t}\hat{u}}$ or $2\hat{s}\hat{t}\hat{u}/(\hat{s}^2 + \hat{t}^2 + \hat{u}^2)$, etc., where the differences are related to subleading contributions only, with $\hat{s}$, $\hat{t}$ and $\hat{u}$ being the usual Mandelstam variables of the partonic subprocess.

The same method can be applied to proof the factorization properties together with the universal validity of the leading logarithmic Q^2 dependence of any parton process, such as [169, 171, 172, 179–181]

$$e^+e^- \to \pi + X$$

$$\mu p \to \mu + \pi + X, \text{ etc.}$$

where again quark fragmentation functions are involved. Of course the "finite" terms, as discussed for deep inelastic processes in section 5.10 and shown for example in eq. (6.3), are process dependent and will provide us with additional important tests of QCD, i.e., with (in most cases small) deviations from the above factorization properties.

The moral of all this is that, apart from small non-factorization effects, the *same* parton distributions and fragmentation functions have to describe *all* hard scattering processes *simultaneously*. More explicitly, all expressions for observable cross sections derived in the naive parton model have to be modified by Q^2-dependent parton functions times, of course, the appropriate parton subprocesses. Thus QCD provides us with the only known rationale of the parton model and we will devote the remainder of this review to study several different processes in order to somewhat elucidate this ambitious program.

8. Hadronic production of massive lepton pairs: The Drell–Yan process

Let us first consider the hadronic production of massive lepton pairs via the Drell–Yan mechanism [177] depicted in fig. 7.1(a). That is, we consider the reaction

$$h_1 h_2 \to \mu^+\mu^- + X \tag{8.1}$$

where the beam particles are usually $h_1 = p, \bar{p}, \pi, K$ and the target consists commonly of nucleons, $h_2 = p$ or N. The invariant mass squared of the dileptons will be denoted by $Q^2 \equiv M^2 > 0$. The differential cross section for this process reads [177, 61, 187], taking into account the full leading QCD corrections as abundantly discussed in the previous section,

$$d\sigma = \frac{1}{3} \sum_{q=u,d,s,\ldots} [q_1(x_1, Q^2)\, \bar{q}_2(x_2, Q^2) + (1 \leftrightarrow 2)]\, \sigma^{q\bar{q}\to\mu^+\mu^-}(Q^2)\, dx_1\, dx_2\, dQ^2. \tag{8.2}$$

The factor 1/3 is due to color [61] and the fundamental parton annihilation cross section is well known from QED [165, 166]

$$\sigma^{q\bar{q}\to\mu^+\mu^-} = \frac{4\pi\alpha^2}{3Q^2}\, e_q^2. \tag{8.3}$$

Using eq. (7.8) we then simply obtain

$$\frac{d\sigma}{dQ^2}=\frac{1}{3}\frac{4\pi\alpha^2}{3Q^2}\int_0^1 dx_1\int_0^1 dx_2\,\delta(x_1x_2s-Q^2)\sum_q e_q^2\,[q_1(x_1,Q^2)\,\bar{q}_2(x_2,Q^2)+(1\leftrightarrow 2)]$$
$$=\frac{4\pi\alpha^2}{9Q^4}\int_\tau^1\frac{dx_1}{x_1}\,\tau\sum_q e_q^2\Big[q_1(x_1,Q^2)\,\bar{q}_2\Big(\frac{\tau}{x_1},Q^2\Big)+(1\leftrightarrow 2)\Big] \tag{8.4}$$

with $\tau=Q^2/s$ (≤ 1) and where the dominant contribution to the integral comes obviously from the region $x_1\simeq\sqrt{\tau}$. Since the Drell–Yan cross section is directly proportional to the sea distribution $\bar{q}$, it is clear that it will provide us with a most sensitive test of sea distributions extracted from deep inelastic reactions. Perhaps it should be noted that in the naive parton model with Q^2 independent quark distributions, the cross section in (8.4) would exhibit the naive dimensional scaling law $Q^4\,d\sigma/dQ^2=F(\tau)$; this is of course *not* true in QCD since eq. (8.4) implies $F=F(\tau,Q^2)$ with a highly non-trivial dependence on Q^2.

Instead of considering the electromagnetic production of $\mu^+\mu^-$ pairs in eq. (8.4), it is also straightforward to derive Drell–Yan-like cross sections for the production of weak intermediate vector bosons ($W^\pm$, Z^0). For example, the total cross section for W^+ production in pp collisions becomes

$$\sigma^{W^+}=\frac{\pi}{3}\sqrt{2}G_F\cos^2\theta_c\int_{\tau_W}^1\frac{dx_1}{x_1}\tau_W\Big[u_1(x_1,M_W^2)\,\bar{d}_2\Big(\frac{\tau_W}{x_1},M_W^2\Big)+\bar{d}_1(x_1,M_W^2)\,u_2\Big(\frac{\tau_W}{x_1},M_W^2\Big)\Big]$$
$$+\,[\mathrm{s,c},\ldots]\ \text{contributions} \tag{8.5}$$

where $\tau_W=M_W^2/s$. Total and differential production cross sections for heavy vector bosons have been already discussed abundantly and we refer the interested reader to the relevant literature [5, 89, 112, 188–193].

For many practical purposes one needs a more differential cross section than the one given in eq. (8.4). Neglecting the intrinsic transverse momenta of partons, then the lepton pair has, in the overall c.m. system, only longitudinal momentum, say Q_3, defined along the beam direction of h_1 in (8.1). Defining the Feynman variable $x_F\equiv 2Q_3/\sqrt{s}$, then the cross section for creating dileptons of invariant mass Q^2 and a definite longitudinal momentum Q_3 is given by [61]

$$\frac{d^2\sigma}{dQ^2\,dx_F}=\frac{1}{3}\frac{4\pi\alpha^2}{3Q^4}\frac{x_1x_2}{x_1+x_2}\sum_q e_q^2[q_1(x_1,Q^2)\,\bar{q}_2(x_2,Q^2)+(1\leftrightarrow 2)] \tag{8.6}$$

with $x_{1,2}=\frac{1}{2}[\pm x_F+(x_F^2+4Q^2/s)^{1/2}]$, i.e., $x_F=x_1-x_2$. In addition most of the experiments are performed at small c.m. rapidity y, where

$$y\equiv\frac{1}{2}\ln\frac{Q_0+Q_3}{Q_0-Q_3}=\tanh^{-1}\Big(\frac{Q_3}{Q_0}\Big)$$

and therefore

$$x_1=\sqrt{\tau}\,e^{y},\qquad x_2=\sqrt{\tau}\,e^{-y}. \tag{8.7}$$

Thus we obtain from eq. (8.6) for $y \to 0$

$$\left.\frac{d^2\sigma}{dQ^2\,dy}\right|_{y=0} = 2\sqrt{\tau}\left.\frac{d^2\sigma}{dQ^2\,dx_F}\right|_{x_F=0} = \frac{4\pi\alpha^2}{9Q^4}\,\tau \sum_q e_q^2[q_1(\sqrt{\tau}, Q^2)\,\bar{q}_2(\sqrt{\tau}, Q^2) + (1 \leftrightarrow 2)]. \tag{8.8}$$

As an illustrative example we compare in fig. 8.1 the predictions [118] of eq. (8.8) with recent data [194–196] using the "standard" SU(3) symmetric sea distribution in eq. (5.135) as input, i.e. $x\,\xi(x, Q_0^2) \simeq 0.15(1-x)^7$. Although the naive parton model predictions (Q^2-independent parton distributions) agree with the data in magnitude, the fully Q^2 dependent predictions of eq. (8.8) lie, by a factor 2–3, consistently below the pN data. One possible way to account for this discrepancy would be to double the above input sea distribution as suggested by the Caltech group [197, 198], but then it is difficult to reconcile the measurements *below* charm threshold for $\sigma^{\bar{\nu}}/\sigma^{\nu}$ – a quantity which is very sensitive to $\langle x\xi\rangle_2 \equiv \int_0^1 x\xi\,dx$: Since *below* charm threshold we have

$$\frac{\sigma^{\bar{\nu}}}{\sigma^{\nu}} = \frac{\frac{1}{2}\langle x(u_v + d_v)\rangle_2 + 4\langle x\xi\rangle_2}{2.82\,\frac{1}{2}\langle x(u_v + d_v)\rangle_2 + 4\langle x\xi\rangle_2} \tag{8.9}$$

we get, at $E_\nu \simeq 10\,\mathrm{GeV}$, $\sigma^{\bar{\nu}}/\sigma^{\nu} \simeq 0.43$ for the "standard" sea with $\langle x\xi\rangle_2 \simeq 0.02$ and $\sigma^{\bar{\nu}}/\sigma^{\nu} \simeq 0.5$ for $\langle x\xi\rangle_2 \simeq 0.04$ whereas experimentally [199, 43, 45] we have $\sigma^{\bar{\nu}}/\sigma^{\nu} \lesssim 0.43$ for $E_\nu \lesssim 20\,\mathrm{GeV}$.

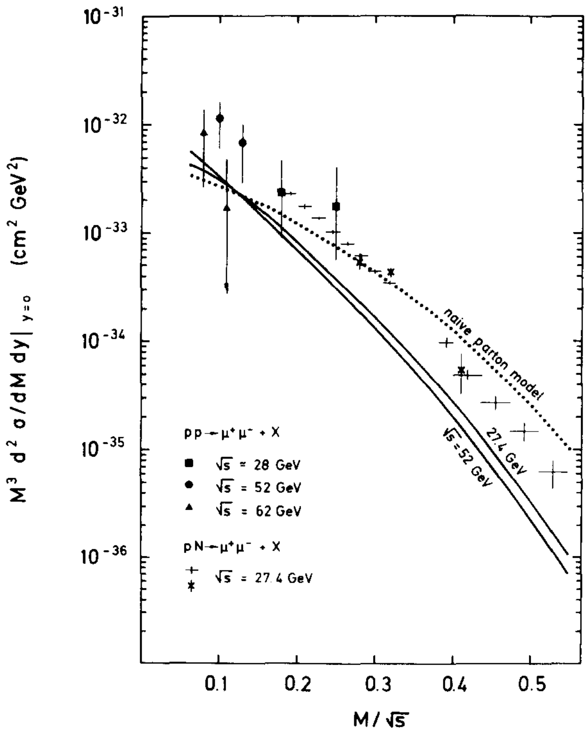

Fig. 8.1. The solid curves show the predictions [118] ($M^2 \equiv Q^2$) of eq. (8.8) using the fully Q^2 dependent parton distributions of ref. [114]; the input sea distribution corresponds to $x\xi(x, Q_0^2) = 0.15(1-x)^7$. This latter Q^2 independent distribution has been used to calculate the naive parton model prediction. The pp data are from ref. [194], and the pN data are taken from refs. [195] and [196].

Alternatively, "finite" α_s corrections to eq. (8.4) or (8.8) could also account for the above discrepancy. Although it is now generally agreed upon that the $gq \to \gamma^* q$ (fig. 7.1(c)) correction [149, 156, 159] and the contribution from the $O(\alpha_s^2)$ subprocess [156] $qq \to qq\gamma^*$ are small, the contributions from $q\bar{q} \to \gamma^* g$ in fig. 7.1(b) appear to be sizeable [159]! Although this latter $q\bar{q} \to \gamma^* g$ subprocess could partly account for the discrepancy in fig. 8.1 between theory and experiment, one might question the validity of perturbation theory in the present energy regime since it implies that α_s corrections are not small compared to 1. A discussion of other alternatives based on collective effects for *nuclear* targets can be found in refs. [118] and [112].

An immediate question arises whether massive lepton-pairs are indeed dominantly produced via the Drell–Yan mechanism of quark–antiquark annihilation. Several features of experimental data indicate that this is indeed the correct production mechanism. Let us denote the cross section for the reaction $h_1 N \to \mu^+\mu^- + X$ by σ^{h_1} for a specific beam particle h_1, then we expect the following qualitative features from eq. (8.4):

(i) For the π/p beam ratio we expect formally

$$\frac{\sigma^\pi}{\sigma^p} \sim \frac{v^\pi(u_v + d_v) + \text{sea}}{\xi(u_v + d_v) + \text{sea}} \sim \frac{1}{(1-x)^6} \gg 1 \quad \text{for } x \equiv \sqrt{\tau} \simeq 1 \tag{8.10}$$

to be compared with the experimental value [200–203] of about 200 at $\sqrt{\tau} = 0.5$! If the dileptons were produced by normal hadronic interactions, one may expect this ratio to be proportional to the corresponding total hadronic cross sections $\sigma_{tot}^{\pi N}/\sigma_{tot}^{pN} < 1$. In (8.10) we have used the same SU(3) symmetric decomposition for pionic quark distributions, using isospin and charge conjugation symmetry, as was done for the nucleonic ones in (5.28):

$$\begin{aligned} u^{\pi^+} &= \bar{d}^{\pi^+} = \bar{u}^{\pi^-} = d^{\pi^-} \equiv v^\pi + \xi^\pi \\ \bar{u}^{\pi^+} &= d^{\pi^+} = u^{\pi^-} = \bar{d}^{\pi^-} \simeq s^{\pi^\pm} = \bar{s}^{\pi^\pm} \equiv \xi^\pi . \end{aligned} \tag{8.11}$$

(ii) Remembering that $\pi^+ = (u\bar{d})$ and $\pi^- = (\bar{u}d)$, then the π^+/π^- beam ratio is expected to be

$$\begin{aligned} \frac{\sigma^{\pi^+}}{\sigma^{\pi^-}} \sim \frac{v_{\bar{d}}^{\pi}(\frac{1}{9}d_v) + \text{sea}}{v_{\bar{u}}^{\pi}(\frac{4}{9}u_v) + \text{sea}} &\simeq \tfrac{1}{4} \quad \text{for} \quad \sqrt{\tau} \simeq 1 \text{ (where } \xi \simeq \xi^\pi \simeq 0) \\ &\simeq 1 \quad \text{for } \sqrt{\tau} \ll 1 \text{ (where "valence"} \simeq 0) \end{aligned} \tag{8.12}$$

in good agreement with experiment [201–203].

(iii) Similarly the $\bar{p}$/p beam ratio should be

$$\frac{\sigma^{\bar{p}}}{\sigma^p} \sim \frac{(u_v + d_v)(u_v + d_v) + \text{sea}}{\xi(u_v + d_v) + \text{sea}} \approx \frac{\text{"valence"}}{\text{"sea"}} > 1, \tag{8.13}$$

and experimentally [203] this ratio is about 6 for $\sqrt{\tau} \simeq 0.4$.

Needless to say that, if $\mu^+\mu^-$ pairs are produced via π-beams for example, the Drell–Yan formula (8.4) or (8.8) provides us with a direct means to determine the structure function of the pion experimentally [204].

8.1. Transverse momenta of massive lepton pairs

Apart from the intrinsic transverse momenta of partons and other "soft" resummation mechanisms (see below) which are responsible for the small transverse momenta p_T ($\lesssim$1 GeV) of dileptons relative to the colliding beam axis, the hard p_T spectrum ($\gtrsim$1 GeV) of lepton pairs has to result [174, 175, 205–207] dominantly from the diagrams shown in figs. 7.1(b) and (c), i.e., from the $q\bar{q}\to(\mu^+\mu^-)g$ and $gq\to(\mu^+\mu^-)q$ subprocesses. The differential cross sections for these fundamental processes, as shown in fig. 8.2, are given by [206, 208]

$$\frac{d^2\sigma^{q\bar{q}}}{dQ^2\,d\hat{t}} = \frac{8\alpha^2\alpha_s}{27Q^2}\frac{1}{\hat{s}^2}\left(\frac{\hat{t}}{\hat{u}}+\frac{\hat{u}}{\hat{t}}+\frac{2Q^2\hat{s}}{\hat{t}\hat{u}}\right) \tag{8.14}$$

$$\frac{d^2\sigma^{gq}}{dQ^2\,d\hat{t}} = \frac{\alpha^2\alpha_s}{9Q^2}\frac{1}{\hat{s}^2}\left(-\frac{\hat{s}}{\hat{u}}-\frac{\hat{u}}{\hat{s}}-\frac{2Q^2\hat{t}}{\hat{s}\hat{u}}\right) \tag{8.15}$$

where $\hat{s}$, $\hat{t}$ and $\hat{u}$ are the usual kinematical invariants for the corresponding subprocess, and it is a simple kinematic exercise to show that $p_T^2=\hat{t}\hat{u}/\hat{s}$. The strongest infrared singularity has the $q\bar{q}$ annihilation process in (8.14) which diverges as $1/p_T^2$ for $p_T\to 0$ (parallel emission); the divergence of the gq process in (8.15) is somewhat softer which goes like $1/p_T$ as $p_T\to 0$. This makes clear that eqs. (8.14) and (8.15) are only applicable for the hard p_T spectrum, typically $p_T\gtrsim 1$ GeV, but not for smaller values of p_T where non-perturbative ("smearing") effects become important. Therefore, p_T *moments* [205, 206, 118] defined by

$$\langle p_T^n\rangle \sim \int p_T^n \frac{d^2\sigma}{dQ^2\,d\hat{t}}\,d\hat{t} \tag{8.16}$$

are always *finite* for $n\geq 1$. A simple calculation gives for example [118]

$$\begin{aligned}\langle p_T\rangle\frac{d\sigma}{dQ^2} = {} & \frac{\alpha^2\alpha_s\pi}{18Q^3}\int_\tau^1\frac{dx_1}{x_1}\int_{\tau/x_1}^1\frac{dx_2}{x_2}\sqrt{\tau_{12}}(1-\tau_{12})\\ & \times\Big\{x_1x_2\sum_{\text{flavors}}e_q^2q_1(x_1,Q^2)\,\bar{q}_2(x_2,Q^2)\Big[4(1-\tau_{12})+\frac{32}{3}\frac{\tau_{12}}{1-\tau_{12}}\Big]+x_1x_2\sum_{\text{flavors}}e_q^2G_1(x_1,Q^2)\\ & \times[q_2(x_2,Q^2)+\bar{q}_2(x_2,Q^2)]\Big[1+\frac{1}{8}(1-\tau_{12})^2-\frac{3}{2}\tau_{12}(1-\tau_{12})\Big]+(1\leftrightarrow 2)\Big\}\end{aligned} \tag{8.17}$$

with $\tau_{12}=\tau/x_1x_2$ and where $d\sigma/dQ^2$ is the total p_T integrated cross section in eq. (8.4). Similar

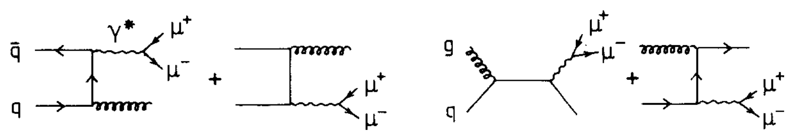

Fig. 8.2. Lowest order contributions to (large) transverse dimuon momenta.

expressions can be obtained for [206] $\langle p_T^2 \rangle$ and also for [118] $\langle p_T^n \rangle$ at c.m. rapidity $y = 0$ where most of the present measurements are done. (The numerical calculations of expressions such as (8.17) are greatly facilitated by using the simple parametrizations as given in ref. [114] for the exact x and Q^2 dependence of parton distributions as predicted by QCD.) Equation (8.17) implies that

$$\langle p_T \rangle = \alpha_s(Q^2) \sqrt{s}\, f(\tau, \alpha_s(Q^2)) \tag{8.18}$$

up to an unknown constant due to non-perturbative intrinsic k_T effects of partons. Experimentally [209]

$$\langle p_T \rangle = (0.6 + 0.022\sqrt{s})\ \mathrm{GeV} \tag{8.19}$$

which agrees with the slope calculated from eq. (8.17). Note that at present it is not possible to make very precise comparisons of theoretically predicted slopes with measurements of pp scattering, say, because of the importance of the badly known (so far mainly guessed) gluon distribution $G(x, Q_0^2)$. For a critical and comprehensive discussion of various moments and their comparison with experiment I refer the interested reader to ref. [118] and to the review articles of Glück [210], Hwa [211], Halzen [212] and Berger [213].

Although only p_T-moments are well behaved (finite) and therefore the prescription for calculating them is unambiguous, the integration down to small p_T is delicate; α_s becomes substantially different and so may the scale breaking effects in the parton distributions. We therefore will now turn to the explicit p_T spectrum of dileptons and concentrate on the large p_T tail (>1 GeV) where eqs. (8.14) and (8.15) are strictly applicable and have to be able to reproduce the measured p_T spectrum if QCD is at work. A straightforward kinematical analysis [207, 214, 215] yields the following expression for the p_T spectrum of massive dileptons

$$\begin{aligned}\frac{d\sigma}{dQ^2\, dy\, dp_T^2} = \int_{x_1^{\min}}^{1} dx_1 \frac{s}{x_1 s - \sqrt{s} m_T e^y} \Big\{ & x_1 x_2 \Big[\sum_q e_q^2\, q_1(x_1, Q^2)\, \bar{q}_2(x_2, Q^2) + (1 \leftrightarrow 2)\Big] \frac{d^2\sigma^{q\bar{q}}}{dQ^2\, d\hat{t}} \\ & + x_1 x_2 \sum_q e_q^2\, G_1(x_1, Q^2)\, [q_2(x_2, Q^2) + \bar{q}_2(x_2, Q^2)]\, \frac{d^2\sigma^{gq}}{dQ^2\, d\hat{t}}(\hat{u}, \hat{t}) \\ & + x_1 x_2 \sum_q e_q^2\, G_2(x_2, Q^2)\, [q_1(x_1, Q^2) + \bar{q}_1(x_1, Q^2)]\, \frac{d^2\sigma^{gq}}{dQ^2\, d\hat{t}}(\hat{t}, \hat{u}) \Big\}\end{aligned} \tag{8.20}$$

where we have denoted the gq cross section in eq. (8.15) by $d^2\sigma^{gq}(\hat{u}, \hat{t})$, and the kinematics are

$$\begin{aligned} x_1^{\min} &= \frac{\sqrt{s} m_T e^y - Q^2}{s - \sqrt{s} m_T e^{-y}}, & m_T &= \sqrt{Q^2 + p_T^2} \\ x_2 &= \frac{x_1 \sqrt{s} m_T e^{-y} - Q^2}{x_1 s - \sqrt{s} m_T e^y}, & \hat{s} &= x_1 x_2 s \\ \hat{t} &= Q^2 - x_1 \sqrt{s} m_T e^{-y}, & \hat{u} &= Q^2 - x_2 \sqrt{s} m_T e^y. \end{aligned} \tag{8.21}$$

In fig. 8.3 we compare the predictions of this hard scattering formula with pN data at $y = 0$ for dilepton

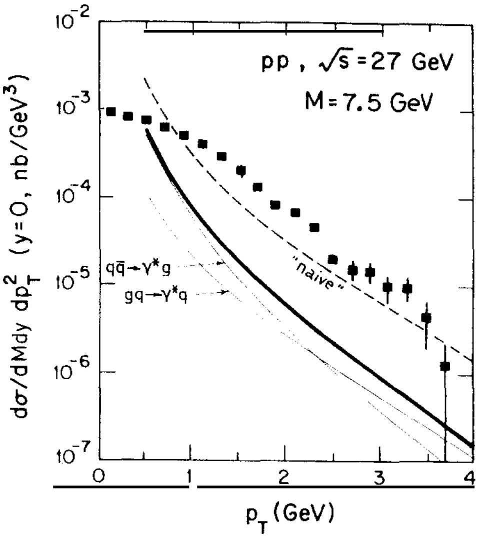

Fig. 8.3. Comparing dilepton p_T data [209] with the predictions (solid curves) of eq. (8.20) using the dilepton mass scale $Q^2 \equiv M^2$, and where the individual contributions of fig. 8.2 are separately shown. The parton distributions of ref. [114] have been used for the actual calculations. The dashed curve is the prediction of the naive parton model, i.e., with Q^2 independent parton distributions.

masses of $M \equiv Q = 7.5\,\mathrm{GeV}$. As can be seen, the absolute magnitude of the total QCD prediction (solid curve) disagrees with the data. However, we have made the most pessimistic choice for the mass scale, namely the dilepton mass Q^2 itself, i.e. $\alpha_s = \alpha_s(Q^2)$, $q = q(x, Q^2)$ etc. Taking instead the mass scale to be p_T^2, i.e. $\alpha_s(p_T^2)$ etc. greatly improves [215] the situation. In order to get a "perfect" agreement with the large-p_T data ($\gtrsim 1\,\mathrm{GeV}$) it seems, however, that a larger sea and harder (flatter) gluon distribution, as for example in eq. (5.137), is required [197, 198, 216] than the standard counting rule like distributions [114] used in all our calculations: $x\xi(x, Q_0^2) = 0.15(1-x)^7$ and $xG(x, Q_0^2) = 2.4(1-x)^5$ for $Q_0^2 \simeq 2\,\mathrm{GeV}^2$. For comparison we also show in fig. 8.3 the prediction of the naive parton model using these latter Q^2 independent parton distributions. Unfortunately present deep inelastic lepton–nucleon scattering experiments are not accurate enough to decisively pin down the exact shape and magnitude of $G(x, Q_0^2)$ which is crucial for the dominant contribution of the $gq \to \gamma^* q$ subprocess.

In the region $p_T^2 \ll Q^2$ the cross section in fig. 8.3 diverges and the "hard scattering" perturbation theory in eqs. (8.14) and (8.15) breaks down. One way to handle these non-perturbative effects for $p_T \lesssim 1\,\mathrm{GeV}$ is to invent some sort of "smearing" procedure [217], i.e., to guess some k_T dependence for parton distributions and to fit such expressions, appropriately added to the hard scattering prediction (8.20), to the experimentally measured p_T spectrum. The resulting k_T is then usually referred to as "intrinsic" transverse momentum of partons; in this way one obtains rather sizeable values of about $\langle k_T \rangle \simeq 0.5$–$0.8\,\mathrm{GeV}$. Alternatively, one might try to approach the small p_T region more theoretically. Since $p_T^2 \ll Q^2$, new large logarithms $\ln(Q^2/p_T^2)$ appear, besides the ones encountered so far ($\ln Q^2/\mu^2$), and the naive perturbation theory breaks down. One can try to resum these logs which result from soft gluon emissions, in addition to the hard (single) gluon processes in fig. 8.2, using again Bethe–Salpeter ladder techniques (as briefly discussed in section 6.2). This has been originally done by the Leningrad-group [169, 218] which yields the much-publicized "DDT formula"

$$\frac{d\sigma}{dQ^2\, dy\, dp_T^2} = \frac{4\pi\alpha^2}{9Q^2 s} \frac{1}{p_T^2} \frac{\partial}{\partial \ln p_T^2} [T_{\mathrm{DDT}}^2(Q^2, p_T^2)\, q_1(x_1, p_T^2)\, \bar{q}_2(x_2, p_T^2) + (1 \leftrightarrow 2)] \tag{8.22}$$

with the DDT form factor given by [169, 219, 220]

$$T_{\mathrm{DDT}}(Q^2, p_T^2) = \exp\left[-\frac{\alpha_s(p_T^2)}{3\pi} \ln^2 \frac{Q^2}{p_T^2}\right]. \tag{8.23}$$

Two important conclusions [215, 218, 221] emerge from these resummed soft gluon emission form factor analyses. They provide the type of concavity of $d\sigma/dp_T^2$ which is seen in the data, i.e., as $p_T \to 0$ the distribution begins to flatten (fig. 8.3); a second improvement is in the absolute magnitude which is increased with respect to the simple $O(\alpha_s)$ result (8.20).

9. Hadronic production of heavy quark flavors

The hadronic production of heavy quark flavors $Q = c, b, \ldots$ can be viewed as a direct generalization of the standard Drell–Yan mechanism: Instead of producing $\mu^+\mu^-$ pairs via a virtual photon γ^* (fig. 7.1(a)), heavy quark pairs $Q\bar{Q}$ are now supposed to be produced via a virtual gluon g. Let us begin with $J/\psi = (c\bar{c})$ production

$$h_1 h_2 \to J/\psi + X \tag{9.1}$$

for various beam particles $h_1 = p, \bar{p}, \pi, K$ and with the target being a nucleon, $h_2 = N$. Since we are considering a $c\bar{c}$ bound state, one naively might expect the fusion of heavy charmed quarks [222] to be responsible for producing the J/ψ system as shown in fig. 9.1(a). Here, however, the very small charmed sea [96, 97] enters the cross section *quadratically* ($\sim c_1(x_1, Q^2)\, \bar{c}_2(x_2, Q^2)$, by generalizing eq. (8.4)) so that this mechanism yields only a negligible contribution to the total measured cross section. Most of all the absence of extra muons [223] produced in association with J/ψ suggests that such a charmed sea fusion cannot be dominant [224]; in other words the associated $D\bar{D}$ production (fig. 9.1(b)) is observed to be small [223], i.e.,

$$\frac{\sigma(J/\psi\, D\bar{D})}{\sigma(J/\psi)} < 0.01 \tag{9.2}$$

whereas this ratio is expected to be 1 in the charm fusion model of fig. 9.1 (unless one invents some fancy ad hoc confinement mechanism for the remaining c and $\bar{c}$ quarks in fig. 9.1(b)).

Within QCD the only realistic description of hadronically produced heavy quark systems appears to be given by the subprocesses [225] $q\bar{q} \to c\bar{c}$ and [226, 227] $gg \to c\bar{c}$. In the first case, suggested by Fritzsch

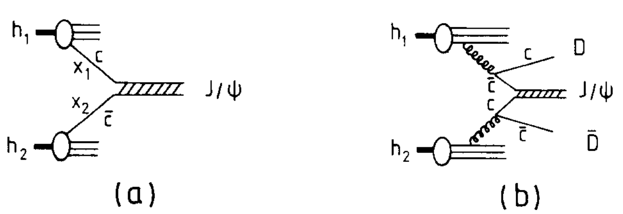

Fig. 9.1. Charmed quark fusion diagrams responsible for (a) J/ψ production and (b) associated $D\bar{D}$ production which gives rise for extra muons.

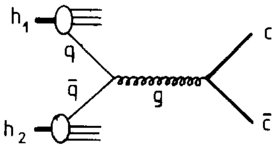

Fig. 9.2. Production of J/ψ states through fusion of ordinary light u, d, s quarks into a *single* colored gluon which decays into a c$\bar{c}$ pair. The emission of "soft" gluons from the final charmed quarks is implicitly implied in order to form colorless $C = \pm 1$ states.

[225], ordinary light SU(3) quarks q = u, d, s fuse in order to produce a highly virtual gluon which then decays into a c$\bar{c}$ pair as shown in fig. 9.2. The production of a particular state, e.g. J/ψ, depends on the dynamical details of the strong interaction mechanism by which the color-octet c$\bar{c}$ configuration rearranges itself, by "soft" gluon emission, into a definite outgoing color-neutral c$\bar{c}$ state. Adopting the semi-local duality approach of ref. [225] to somehow account for this unknown formation of the observed bound states, the cross section for producing any c$\bar{c}$ state below open charm threshold through q$\bar{q}$ fusion reads

$$\frac{d\sigma^{h_1h_2}_{q\bar{q}}}{dx_F} = \sum_{q=u,d,s} \int_{4m_c^2}^{4m'^2} \frac{dQ^2}{Q^2} \frac{x_1x_2}{x_1+x_2} [q_1(x_1, Q^2)\, \bar{q}_2(x_2, Q^2) + (1 \leftrightarrow 2)]\sigma^{q\bar{q}\to c\bar{c}}(Q^2) \tag{9.3}$$

with $x_{1,2}$ being the same as in eq. (8.6) and

$$\sigma^{q\bar{q}\to c\bar{c}} = \frac{2}{9} \frac{4\pi\alpha_s^2(Q^2)}{3Q^2} (1 + \tfrac{1}{2}\gamma)\sqrt{1-\gamma} \tag{9.4}$$

where $\gamma = 4m_c^2/Q^2$ and $m' \simeq m_D \simeq 1.85\,\text{GeV}$. In order to obtain the presently measured total cross section we just have to integrate eq. (9.3) over $0 \leq x_F \leq 1 - Q^2/s$ with the lower limit being dictated by experimental cuts. Note that now the sea ($\bar{q}$) enters the cross section only *linearly*. The second contribution comes from the [226, 227] gg→c$\bar{c}$ subprocess shown in fig. 9.3. The last two diagrams of fig. 9.3 resemble the original Einhorn–Ellis [228] graphs which have been studied [228, 229] in connection with the production of $C = +1$ states (η_c or p-wave χ states) which can also decay into a J/ψ by emitting a soft photon. That part of the total hadronic J/ψ production might indeed proceed via χ-states is suggested by the observed rate [230] of associated photons with the J/ψ: $\sigma(\psi\gamma)/\sigma(\psi) \simeq 0.5 \pm 0.2$; but this ratio can in principle also be accommodated by the process in fig. 9.2 since it is of the order α/α_s ("soft"). The total contribution of the gg→c$\bar{c}$ subprocess in fig. 9.3 is now given by [227]

$$\frac{d\sigma^{h_1h_2}_{gg}}{dx_F} = \int_{4m_c^2}^{4m'^2} \frac{dQ^2}{Q^2} \frac{x_1x_2}{x_1+x_2} G_1(x_1, Q^2)\, G_2(x_2, Q^2)\, \sigma^{gg\to c\bar{c}}(Q^2) \tag{9.5}$$

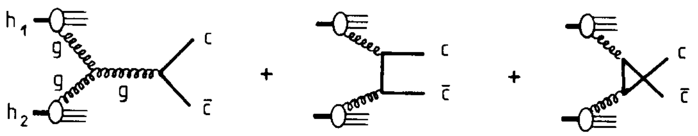

Fig. 9.3. Production of J/ψ states through gluon fusion. Again, "soft" gluon emission is implicitly implied to form physical colorless states.

with

$$\sigma^{gg\to c\bar{c}} = \frac{\pi\alpha_s^2(Q^2)}{3Q^2}\left[\left(1+\gamma+\frac{1}{16}\gamma^2\right)\ln\frac{1+\sqrt{1-\gamma}}{1-\sqrt{1-\gamma}} - \left(\frac{7}{4}+\frac{31}{16}\gamma\right)\sqrt{1-\gamma}\right] \tag{9.6}$$

and again $\gamma = 4m_c^2/Q^2$. The total cross section for producing a $c\bar{c}$ state is then the *sum* of eqs. (9.3) and (9.5):

$$d\sigma^{h_1h_2} = d\sigma_{q\bar{q}}^{h_1h_2} + d\sigma_{gg}^{h_1h_2}. \tag{9.7}$$

It should be emphasized that the two contributing subprocesses $q\bar{q}\to c\bar{c}$ and $gg\to c\bar{c}$ make very different and definite predictions for J/ψ production ratios by different beams. Specifically, the $q\bar{q}$ fusion predicts for $\bar{p}/p = \sigma^{\bar{p}N\to J/\psi+X}/\sigma^{pN\to J/\psi+X}$ very *large* values [225], typically $\bar{p}/p = 30$–50, whereas experimentally [231] $\bar{p}/p = 6.7\pm 3.0$ at $p_{lab} = 39.5$ GeV/c. Since gluons are flavor blind, the gg fusion process trivially gives $\bar{p}/p = 1$. Thus the experimental observation that the $\bar{p}/p$ ratio is *not* very large but close to one provides us with direct evidence that nucleons consist of additional flavorless constituents (gluons!); furthermore it tells us that the observed J/ψ cross section has to be a *combination* of the $q\bar{q}$ and the gg fusion process as stated in eq. (9.7).

Without going into too many details we just would like to mention that a comparison of the measured x_F distributions of J/ψ's produced by π-beams [231] with the predictions of eq. (9.7) allows us already to pin down [227] the pionic valence-quark distribution at large values of x: The resulting $xv^\pi \sim (1-x)$ as $x\to 1$ (see eq. (8.11)) agrees with the recently found xv^π extracted from Drell–Yan $\mu^+\mu^-$ continuum production [204], which is also in agreement with the naive dimensional counting rules [59–61] in eq. (5.102). Similar successful predictions for x_F distributions are obtained [227] for measurements at higher energies for π as well as p beams. A sample of very significant beam ratio predictions for J/ψ production are shown in fig. 9.4. The calculations have been made for two very

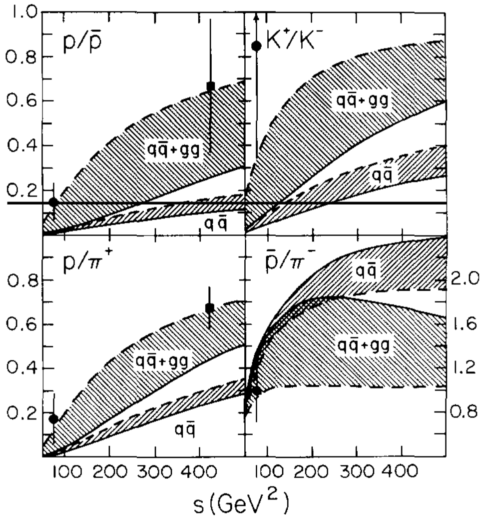

Fig. 9.4. Predictions [227] for beam ratios of total J/ψ production cross sections using incident p, p̄, $\pi^\pm$ and $K^\pm$ beams. The solid curves correspond to the dynamical QCD distributions [112] (see section 5.7) and the dashed curves refer to counting rule like parton densities [233], which appear to be more adequate, are very similar to those used in most of our calculations (eqs. (5.135) and (5.136)). The data ($x_F > 0$) are taken from refs. [231] and [232].

different sets of parton distributions in order to show the sensitivity of these predictions, but the dashed curves, corresponding to the counting rule like distributions, should be taken more seriously since they are in better agreement with all hard scattering data known so far. From fig. 9.4 it is clear that the $q\bar{q}$ fusion model alone (eq. (9.3)) is not capable of accounting for the data. The additional contribution from the gluon–gluon (gg) fusion in eq. (9.5) is not only required by the low-energy CERN–SPS data [231] but also by the high-energy Fermilab measurements [232] of $p/\bar{p}$ and p/π^+ ratios. The latter clearly demonstrate the essential role of the gg fusion mechanism and are striking evidence for the *existence of gluons* in hadrons! That gluons are responsible for the strong increase of beam ratios, say $p/\bar{p}$, with energy s is clear because increasing s means decreasing $x_1 \simeq \sqrt{\tau} \equiv \sqrt{Q^2/s}$ (see the discussion following eq. (8.4)) and therefore gluons will dominate (eq. (9.5)) since they are concentrated mainly in the small x-region.

Within our semilocal duality approach we expect total "open charm" ($D\bar{D}$, etc.) production to be described [226, 234–240, 212] by the same formulae as above with integration limits in eqs. (9.3) and (9.5) changed to $m_c \to m'$ and $2m' \to \sqrt{s}$. In fig. 9.5 we show a few predictions [235] for "open charm" production, and although the experimental situation [241, 242] is rather confused [243], the QCD predictions lie at best an order of magnitude (!) below present experimental limits. One possibility to account for this discrepancy would be either to increase the "standard" gluon distribution in eq. (5.136) drastically (perhaps taking also into account collective nuclear effects [235] for measurements involving nuclear targets), or to give up the purely perturbative fusion models of figs. 9.2 and 9.3 and to invent instead some non-perturbative vector–meson-dominance like model for $D\bar{D}$ production as suggested by Fritzsch and Streng [244].

Taking the semi-local duality ideas to an extreme [235], it is also possible to predict even the *absolute* normalizations [235] for the heavy quark production cross sections (9.3) and (9.5), in good agreement with experiment; this applies also to quarkonia production in γp collisions [235] as well as for deep inelastic electroproduction of quarkonia [96]. Furthermore, the gg fusion mechanism also offers us the

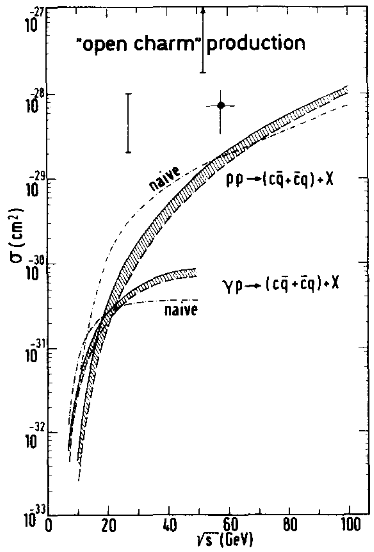

Fig. 9.5. Predictions [235] for "open charm" production in proton–proton collisions (and in γp collisions) using the parton distributions of ref. [114]. The data are taken from refs. [241] and [242].

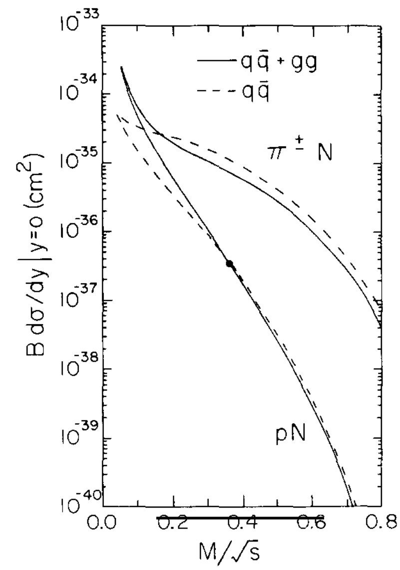

Fig. 9.6. Predictions [114] for Υ production using pion and proton beams. The pN predictions have been normalized to the 400 GeV/c data point [245] shown. More recent measurements can be found in ref. [246].

exciting possibility to explain and understand [236] the rising total pp cross section (at least for $\sqrt{s} \gtrsim 80$ GeV).

The above analyses for charm production can be straightforwardly extended [114] to the production of heavier quark flavors, such as $\Upsilon = (b\bar{b})$, by performing the obvious substitutions of masses in eqs. (9.3) and (9.5). In fig. 9.6 we show typical predictions [114] for producing Υ's with p and π beams: At large values of $\sqrt{\tau} = M/\sqrt{s}$, where gg fusion plays a negligible role, the production of Υ in πN collisions can be more than 2 orders of magnitude larger than in pN reactions since "valence–valence" scattering dominates in eq. (9.3) for πN (see also eq. (8.10)). These predictions [114] are in good agreement with recent measurements [246]. Along similar lines, many other interesting predictions have been calculated [114, 234–240, 244] for heavy quark production.

It is also very interesting, although much more involved, to calculate the (hard) transverse momentum spectra of heavy quarkonia $Q\bar{Q}$ (J/ψ, Υ) produced in pp and $\bar{p}$p collisions [247]. This is a direct

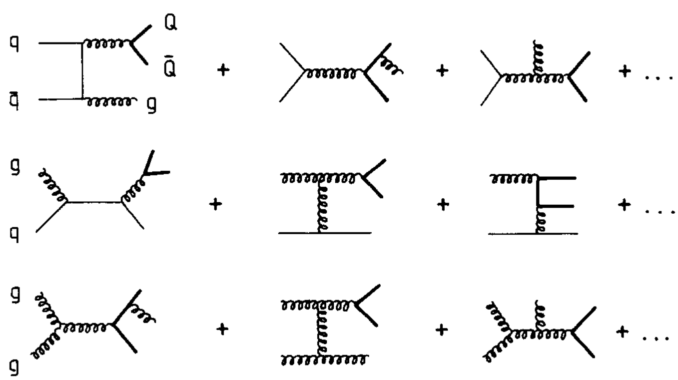

Fig. 9.7. Lowest-order contributions to the transverse momenta of heavy quarkonia $Q\bar{Q}$. There are 5 diagrams for each $q\bar{q}$ and gq initiated process, whereas there are 16 $ggQ\bar{Q}$ Feynman diagrams and 5 corresponding ghost graphs.

generalization of the mechanism responsible for giving transverse momenta to Drell–Yan dimuons in $q\bar{q} \to \mu^+\mu^-$: Here we needed the $q\bar{q} \to \mu^+\mu^- g$ and $gq \to \mu^+\mu^- q$ subprocesses of fig. 8.2 to produce large p_T's of the observed dimuons. Similarly, in order to obtain transverse momenta of $Q\bar{Q}$ pairs produced in the $q\bar{q} \to Q\bar{Q}$ and $gg \to Q\bar{Q}$ fusion processes of figs. 9.2 and 9.3, we have to attach a hard gluon radiation to the appropriate quark and gluon lines: Thus the transverse momentum of a given quarkonium state comes from the purely hadronic $2 \to 3$ processes $q\bar{q} \to Q\bar{Q}g$, $gq \to Q\bar{Q}q$ and $gg \to Q\bar{Q}g$ shown in fig. 9.7. For details of the calculation as well as for a comparison of these predictions with present data we refer the interested reader to ref. [247]. Typically at ISR energies $\sqrt{s} \simeq 60$ GeV, the predicted p_T dependence of $d\sigma/dp_T^2$ for J/ψ production is steeper than the corresponding $\mu^+\mu^-$ spectrum [247] in agreement with present measurements.

10. Semi-inclusive processes: Fragmentation functions

We now consider processes where at least one of the final hadrons h is observed such as $eN \to e + h + X$, $\nu N \to \mu + h + X$, $e^+e^- \to h + X$, etc. as shown in fig. 10.1. As for the totally inclusive processes where one introduces probabilities $q(x)$ of finding quarks with fractional momentum x of the original parent hadron, one now defines [248–250] (perturbatively not calculable) fragmentation functions $D_q^h(z)$ which describe the probability that a quark q decays into a hadron h carrying fractional momentum z of the parent quark q (see fig. 10.1). Suppressing, for the time being, all Q^2 dependences in parton and fragmentation functions, the predictions for semi-inclusive cross sections can be directly read off fig. 10.1 and we expect [248–250]

$$\frac{1}{\sigma}\frac{d\sigma^{e^+e^-\to hX}}{dz} = \frac{1}{\sum_q e_q^2}\sum_q e_q^2 (D_q^h + D_{\bar{q}}^h) \tag{10.1}$$

$$\frac{1}{d\sigma/dx}\frac{d^2\sigma^{eN\to ehX}}{dx\,dz} = \frac{\sum_q e_q^2\, q(x)\, D_q^h(z)}{\sum_q e_q^2\, q(x)} \tag{10.2}$$

$$\frac{1}{d\sigma/dx}\frac{d^2\sigma^{\nu p\to\mu^- hX}}{dx\,dz} = \frac{d(x)\,D_u^h(z) + \frac{1}{3}\bar{u}(x)\,D_{\bar{d}}^h(z)}{d(x) + \frac{1}{3}\bar{u}(x)} \simeq D_u^h(z) \tag{10.3}$$

$$\frac{1}{d\sigma/dx}\frac{d^2\sigma^{\bar{\nu} p\to\mu^+ hX}}{dx\,dz} = \frac{\bar{d}(x)\,D_{\bar{u}}^h(z) + \frac{1}{3}u(x)\,D_d^h(z)}{\bar{d}(x) + \frac{1}{3}u(x)} \simeq D_{\bar{d}}^h(z) \tag{10.4}$$

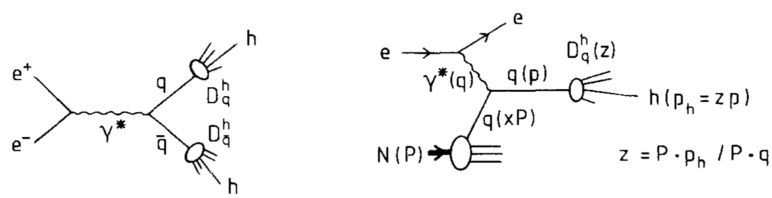

Fig. 10.1. Semi-inclusive processes where at least one hadron $h(=\pi, K, p, \ldots)$ is observed in the final state with fractional momentum $z = E_h/E_{beam}$.

where for the neutrino induced reactions we have put $\theta_c = 0$ and neglected charm; furthermore, neglecting the small antiquark (sea) distributions we expect eqs. (10.3) and (10.4) to be independent of x. Of course, the fragmentation functions themselves have to satisfy constraints, similar to those for parton distributions, such as sum rules coming from energy-momentum conservation

$$\sum_h \int_0^1 dz\, z\, D_q^h(z) = 1 \tag{10.5}$$

and one stemming from isospin conservation (compare eq. (5.15))

$$\sum_h \int_0^1 dz\, I_3^h\, D_q^h(z) = I_{3q}. \tag{10.6}$$

As an intuitive example let us first discuss a model of how to construct fragmentation functions for pions and kaons, but neglecting baryons [251]. Isospin and charge-conjugation invariance reduces the number of independent D_q^π fragmentation (or quark decay) functions to three [249]; these can be further reduced to two by assuming [250] that $D_s^{\pi^+}$ is approximately equal to $D_d^{\pi^+}$, both of which are unfavored ("sea") with respect to $D_u^{\pi^+}$ (the favored "valence" decay function) since the parent quark u can directly form a π^+ by combining with a $\bar{d}$ (produced from a bremsstrahlung gluon which converts into a $d\bar{d}$), whereas to make a π^+ from either d or s requires the creation (via gluon bremsstrahlung) of at least two new flavor pairs $u\bar{u}$ and $d\bar{d}$. Thus we have (remember that $\pi^+ = (u\bar{d})$ and $\pi^- = (\bar{u}d)$)

$$D_u^{\pi^+} = D_d^{\pi^-} = D_{\bar{u}}^{\pi^-} = D_{\bar{d}}^{\pi^+},$$
$$D_u^{\pi^-} = D_d^{\pi^+} = D_{\bar{d}}^{\pi^-} = D_{\bar{u}}^{\pi^+} \simeq D_s^{\pi^+} = D_s^{\pi^-} = D_{\bar{s}}^{\pi^+} = D_{\bar{s}}^{\pi^-}, \tag{10.7}$$

and

$$D_q^{\pi^0} = \tfrac{1}{2}(D_q^{\pi^+} + D_q^{\pi^-})$$

for each flavored quark. Following the same reasoning [249, 250] the number of independent fragmentation functions for producing K mesons can be reduced to three (recall that $K^+ = (u\bar{s})$, $K^- = (\bar{u}s)$, $K^0 = (d\bar{s})$ and $\bar{K}^0 = (\bar{d}s)$)

$$\begin{aligned}
D_u^{K^+} &= D_d^{K^0} = D_{\bar{u}}^{K^-} = D_{\bar{d}}^{\bar{K}^0},\\
D_s^{K^-} &= D_s^{\bar{K}^0} = D_{\bar{s}}^{K^+} = D_{\bar{s}}^{K^0},\\
D_u^{K^-} &= D_d^{\bar{K}^0} = D_{\bar{u}}^{K^+} = D_{\bar{d}}^{K^0}\\
&\simeq D_d^{K^-} = D_u^{\bar{K}^0} = D_{\bar{d}}^{K^+} = D_{\bar{u}}^{K^0}\\
&\simeq D_d^{K^+} = D_u^{K^0} = D_{\bar{d}}^{K^-} = D_{\bar{u}}^{\bar{K}^0}\\
&\simeq D_s^{K^+} = D_s^{K^0} = D_{\bar{s}}^{K^-} = D_{\bar{s}}^{\bar{K}^0}.
\end{aligned} \tag{10.8}$$

Furthermore, we expect [250] the following physical constraints to hold:

(i) As $z \to 1$ it is, for an outgoing quark in fig. 10.1, just as easy for an $\bar{s}$-quark to pick up a u-quark and become a K^+ as it is for a $\bar{d}$-quark to pick up a u-quark and become a π^+

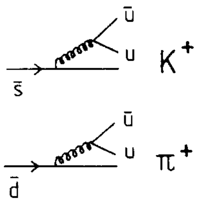

$$: \quad \frac{D_{\bar{s}}^{K^+}}{D_{\bar{d}}^{\pi^+}} = \frac{D_{s}^{K^-}}{D_{u}^{\pi^+}} \xrightarrow[z\to 1]{} 1 \tag{10.9}$$

where for illustration we have also used eqs. (10.7) and (10.8);

(ii) As $z \to 0$ the K^+ meson no longer "remembers" that it originated from a u or $\bar{s}$ quark (since most of the available energy has been used to produce an arbitrary amount of soft $s\bar{s}$ and $u\bar{u}$ "sea" quarks)

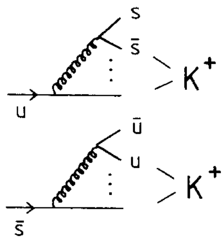

$$: \quad \frac{D_{u}^{K^+}}{D_{\bar{s}}^{K^+}} = \frac{D_{u}^{K^+}}{D_{s}^{K^-}} \xrightarrow[z\to 0]{} 1 \tag{10.10}$$

where for illustration we have again used eq. (10.8);

(iii) Since s-quarks are heavier than u- and d-quarks, it will be harder to make new $s\bar{s}$ pairs than $u\bar{u}$ and $d\bar{d}$ pairs with large z; thus we expect in general for the unfavored "sea" decay functions $D_u^{K^-} < D_u^{\pi^-}$ for large z (SU(3) symmetry breaking). We only can guess the amount of SU(3) breaking and choose for definiteness [250]

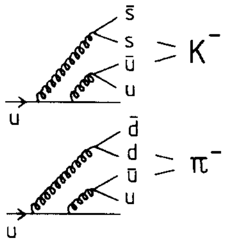

$$: \quad \frac{D_{u}^{K^-}}{D_{u}^{\pi^-}} \xrightarrow[z\to 1]{} \frac{1}{2} \tag{10.11}$$

although our results are rather insensitive to this choice.

Further constraints come from experiment [252]. Semi-inclusive neutrino reactions (eqs. (10.3) and (10.4)) tell us that the favored "valence" distributions such as $D_u^{\pi^+}$, behave as $D_u^{\pi^+} \sim (c - z)$ for $z \to 1$ with $c \gtrsim 1$ (but close to 1). Similarly, data [252] on the $\nu(\bar{\nu})$ induced production ratio π^+/π^- (π^-/π^+) dictate the z-dependence of the ratio of favored ("valence") to unfavored ("sea") fragmentation functions [253] to be $D_u^{\pi^+}/D_u^{\pi^-} \sim (c - z)^{-1}$ with $c \gtrsim 1$ (but close to 1); for simplicity we assume this latter ratio to hold also for kaons. This implies for the unfavored sea decay functions in (10.11) to behave as

$(c-z)^2$ with $c \simeq 1$. All these constraints are satisfied by the following simple ansatz

$$\begin{aligned} zD_u^{\pi^+} &= a\sqrt{z}\,(c-z)+\xi_\pi(1-z)^2, \qquad & zD_u^{\pi^-} &= \xi_\pi(1-z)^2 \\ zD_u^{K^+} &= b\sqrt{z}\,(c-z)+\tfrac{1}{2}\xi_\pi(1-z)^2, \qquad & zD_u^{K^-} &= \tfrac{1}{2}\xi_\pi(1-z)^2 \\ zD_s^{K^-} &= a\sqrt{z}\,(c-z)+\tfrac{1}{2}\xi_\pi(1-z)^2 & & \end{aligned} \tag{10.12}$$

where, analogously to parton distributions, we have decomposed the favored fragmentation functions into "valence" ($\sim\sqrt{z}$) and "sea" components. This ansatz is intuitively plausible as can be seen from the following argument. As $z\to 0$ more and more $q\bar{q}$ pairs are produced via gluon bremsstrahlung off the original outgoing quark. Thus most of the observed mesons will come from a combination of a q and $\bar{q}$ from this gluon produced sea. Alternatively, for $z\to 1$ much fewer $q\bar{q}$ pairs can be produced and therefore the original outgoing quark will dominantly participate in forming the observed meson, as illustrated for the valence functions in eq. (10.9). The remaining three parameters in (10.12), a, b and ξ_π, are fixed by the two independent constraints resulting from the momentum-conservation sum rules (10.5) and by the isospin sum rule (10.6) which gives one independent equation (taking $q = u$, for example):

$$a = 2b = \frac{1}{5c-\frac{5}{3}}, \qquad \xi_\pi = \frac{3}{5}\left(1-\frac{\frac{4}{3}c-\frac{4}{5}}{5c-\frac{5}{3}}\right). \tag{10.13}$$

Note that the solution for our ansatz (10.12) implies always automatically $b/a = 1/2$, i.e. $D_u^{K^+}/D_u^{\pi^+}\to 0.5$

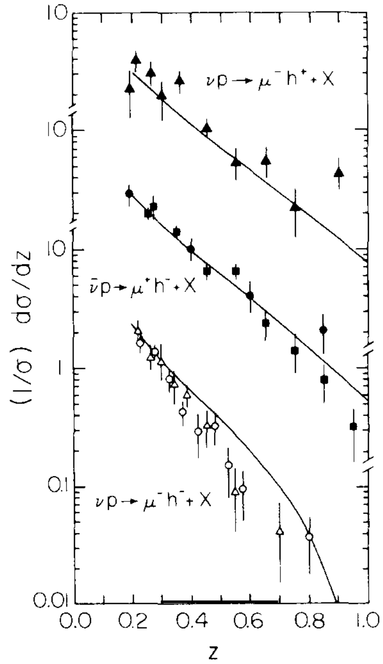

Fig. 10.2. Comparison [251] of the predictions of the fragmentation functions in (10.12), with $c = 11/9$ in (10.13), with charged hadron multiplicity distributions measured in deep-inelastic neutrino scattering. The top curve corresponds to the valence functions $D_u^{\pi^+}+D_u^{K^+}$, the curve in the middle to $D_{\bar{d}}^{\pi^-}+D_{\bar{d}}^{K^-}$, and the bottom curve to the pure unfavored sea functions $D_u^{\pi^-}+D_u^{K^-}$.

as $z \to 1$ as naively expected [250] from flavor SU(3) breaking and as required by the experimental result that the high-p_T production ratio $\sigma(pp \to K^+X)/\sigma(pp \to \pi^+X)$ is about 0.5 at large $x_T \equiv 2p_T/\sqrt{s}$ (see, for example refs. [250] and [251]). In fig. 10.2 we compare the predictions of our fragmentation functions with some neutrino data choosing $c = 11/9$ in eq. (10.13). However, in view of the rather poor data for large z, it should be emphasized that most experiments can be equally well described [254] using $c = 1$. An outstanding and still unsolved problem is to calculate quark fragmentation functions into *baryons*, D_q^h with $h = p, \bar{p}$, etc. Although it is possible to construct [254, 255] such decay functions which are in good agreement with all lepton induced semi-inclusive processes (ep, νp, e^+e^-, etc.), they do not work for purely hadronic reactions such as their predictions [255] for the p_T-dependence of high-p_T production ratios $\sigma(pp \to pX)/\sigma(pp \to \pi^+X)$ and $\sigma(pp \to \bar{p}X)/\sigma(pp \to \pi^-X)$.

Along similar lines we can also attempt to construct gluon decay functions. In any field-theoretic model where $q\bar{q}$ pairs are produced via gluons emitted by the initial quarks, the gluon fragmentation function $D_g^h(z)$ must obviously be steeper than the favored "valence" component ($\sim(1-z)^1$) of D_q^h in eq. (10.9), and flatter than the unfavored "sea" ($\sim(1-z)^2$) distributions. This is so, simply because a gluon has to produce at least *four* final quark lines which can combine to a physical hadron:

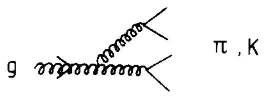

Thus, guided by eq. (10.12), we take [251]

$$zD_g^\pi = c_\pi(1-z)^{1.5}, \qquad zD_g^K = \tfrac{1}{2}c_\pi(1-z)^{1.5} \tag{10.14}$$

where we assumed the same SU(3) breaking as in eq. (10.11). Total momentum conservation

$$\int_0^1 dz\, z(3D_g^\pi + 4D_g^K) = 1 \tag{10.15}$$

then yields $c_\pi = \frac{1}{2}$. Qualitatively similar gluon decay functions can be constructed using the "parent–child" relation [256, 257] or the "dynamical" renormalization group ideas [258] as discussed in section 5.7 for calculating gluon and sea distributions.

So far we have suppressed any explicit Q^2 dependence of the fragmentation functions. Strictly speaking, all $D_q^h(z)$ and $D_g^h(z)$ have to be interpreted as $D_q^h(z) \equiv D_q^h(z, Q_0^2)$, i.e. as distributions fitted to experiment at a given momentum scale Q_0^2, and where all infrared sensitive pieces are absorbed (factorized) into $D_q^h(z, Q_0^2)$ in the sense discussed in section 7 for parton distributions. Again one can prove [169, 171, 179, 180] that this infrared factorization holds to all logarithmic orders in α_s and that the Q^2 is governed by the same anomalous dimensions (or Altarelli–Parisi decay functions P_{ij}) found for parton distributions. As an example, let us consider the semi-inclusive deep inelastic process in fig. 10.1. Instead of summing hard collinear gluon emissions off the initial quark (fig. 6.6), we now have to consider hard gluon emissions off the outgoing quark in fig. 10.1 (see also fig. 5.26). Squaring these diagrams we arrive at the so called generalized "rainbows" (fig. 10.3) which yield [171] the leading logarithmic Q^2 dependence of $D_q^h(z, Q^2)$. This then allows us to write down similar evolution equations

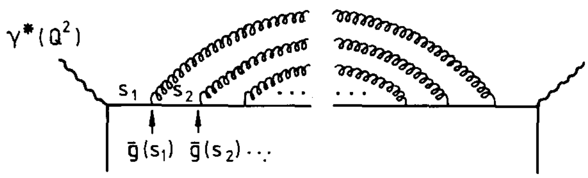

Fig. 10.3. Rainbow diagrams ($s_i > s_{i+1}$) giving rise to the Q^2 dependence of $D_q^h(z, Q^2)$.

for fragmentation functions [259] as Altarelli and Parisi obtained for parton distributions in (6.16):

$$Q^2 \frac{dD_q^h(z,Q^2)}{dQ^2} = \frac{\alpha_s(Q^2)}{2\pi} \int_z^1 \frac{dy}{y} \left[P_{qq}\left(\frac{z}{y}\right) D_q^h(y,Q^2) + P_{gq}\left(\frac{z}{y}\right) D_g^h(y,Q^2) \right]$$
$$Q^2 \frac{dD_g^h(z,Q^2)}{dQ^2} = \frac{\alpha_s(Q^2)}{2\pi} \int_z^1 \frac{dy}{y} \left[P_{qg}\left(\frac{z}{y}\right) \sum_i^{2N_f} D_{q_i}^h(y,Q^2) + P_{gg}\left(\frac{z}{y}\right) D_g^h(y,Q^2) \right] \tag{10.16}$$

with P_{ij} given by eqs. (6.17)–(6.20). Note that the splitting functions P_{qg} and P_{gq} are interchanged in going from eq. (6.16) to eq. (10.16). That this has to be the case is clear because now, for example, a specific quark q has first to decay into a gluon (P_{gq}) which in turn decays into the observed hadron h; in eq. (6.16), in contrast, we encounter this specific quark q via the initial gluon which then decays into q (P_{qg}). For large values of $z (\gtrsim 0.5)$ we can use instead of (10.16) the simpler Gross formula (5.133) for the Q^2 dependence of the dominant "valence" function $D_q^h(z, Q^2)$.

It is of utmost importance to observe the predicted Q^2 dependence of fragmentation functions experimentally, not only in neutrino induced reactions [260], but also in deep inelastic e(μ)p processes and most of all in e^+e^- annihilation processes. Going beyond the leading log order predictions we expect, in addition, a breakdown of the simple factorization in eqs. (10.1)–(10.4) due to "finite" α_s corrections [261], i.e., $d\sigma(x, z, Q^2) \sim q(x, Q^2)\, D_q^h(z, Q^2) + \alpha_s(Q^2) f(x, z)$ where the "finite" corrections $f(x, z)$ do not factorize in x and z, and again result from diagrams shown for example after eq. (5.170) or in figs. 6.2 and 6.3. These "finite" order α_s corrections are of course process dependent, in contrast to the universal validity of the leading logarithmic Q^2 dependencies of $q(x, Q^2)$ and $D_q^h(z, Q^2)$, and give very significant predictions for various kinematical regions [261] which will be hopefully testable in the near future.

11. High-p_T reactions

We now turn to the purely hadronic single-particle inclusive high-p_T processes where a hadron $h = \pi, K, \ldots$ is produced with large transverse momentum relative to the beam axis of the colliding incoming hadrons, as for example in proton–proton scattering $pp \to h + X$ shown in fig. 7.3(a). Due to (collinear) gluonic corrections (fig. 7.3(b)) the naive parton model predictions [185] for high-p_T processes in eq. (7.16) will be modified, as has been discussed in section 7, to the extent that we have to use Q^2 dependent parton distributions and fragmentation functions which, to leading logarithmic order, are expected to be the same as in deep inelastic lepton–nucleon scattering processes. Thus, the invariant inclusive cross section for the reaction $A+B\to C+X$ for producing a hadron C at large p_T in the c.m. system of A and B is given by (neglecting intrinsic transverse momenta)

$$E_C\frac{d\sigma}{d^3p_C}=\frac{1}{\pi}\sum_{\substack{a,b\\c,d}}\int_{x_a^{\min}}^{1}dx_a\int_{x_b^{\min}}^{1}dx_b\,P_A^a(x_a,Q^2)\,P_B^b(x_b,Q^2)\frac{d\sigma^{ab\to cd}}{-d\hat{t}}\frac{1}{z_C}D_c^C(z_C,Q^2) \tag{11.1}$$

where the sum over partons (a, b, c, d) includes gluons as well as quarks, and the longitudinal fractions $x_a=p_a/p_A$, $x_b=p_b/p_B$ and $z\equiv z_C=p_C/p_c$ (see fig. 7.3(a)) determine the $ab\to cd$ subreaction kinematics through $\hat{s}=x_ax_bs$, $\hat{t}=x_at/z$, $\hat{u}=x_bu/z$ with $s=(p_A+p_B)^2$, $t=(p_A-p_C)^2$, $u=(p_B-p_C)^2$. The conditions $\hat{s}+\hat{t}+\hat{u}=0$ and $z=x_1/x_a+x_2/x_b\le 1$ fix the lower limits of integration at

$$x_a^{\min}=\frac{x_1}{1-x_2}\,,\qquad x_b^{\min}=\frac{x_ax_2}{x_a-x_1}$$

with $x_1=-u/s$ and $x_2=-t/s$. Furthermore, in writing the invariant cross section in eq. (11.1), we have made use of the relation

$$d\hat{t}\,dz=\frac{d^3p_C}{E_C}\frac{1}{\pi z}.$$

The parton distributions are denoted by $P_A^a(x_a,Q^2)$ representing the probability for the constituent a of the hadron A to have fractional longitudinal momentum x_a, i.e. $P_p^u(x_a,Q^2)\equiv u(x_a,Q^2)$, $P_p^g(x_a,Q^2)\equiv G(x_a,Q^2)$, etc. The dependence of these distributions as well as of the fragmentation functions D_c^C on Q^2 refers to their appropriate scaling violations discussed so far. Since the parton distributions and fragmentation functions are rather well known from deep inelastic inclusive and semi-inclusive lepton–nucleon scattering processes, respectively, the purely hadronic high-p_T cross sections in eq. (11.1) can be uniquely predicted, to leading order in perturbation theory, without any free parameter once the fundamental parton scattering cross sections $d\sigma^{ab\to cd}$ are given.

In the most naive scale-invariant version of the hard-collision model [185] with Q^2 independent parton distributions in eq. (11.1), where a *single hard* collision between the quarks of the incident hadrons (fig. 7.3(a)) is responsible for the observed high-p_T secondaries, one expects the invariant inclusive single-particle cross section to decrease as p_T^{-4} at fixed c.m. scattering angle θ and fixed $x_T=2p_T/\sqrt{s}$. This is so, because for vector exchanges in fig. 7.3(a) we always have $d\sigma^{qq\to qq}/d\hat{t}\sim\hat{s}^{-2}\sim p_T^{-4}$. However, at currently attainable energies the experimental data seem to scale roughly as p_T^{-8} for $p_T\lesssim 6\,\mathrm{GeV}/c$. Taking into account Q^2 dependent quark distributions and fragmentation functions together with the correct QCD coupling $\alpha_s(Q^2)$, it has already been shown a long time ago [262] that the lowest order QCD quark–quark scattering (fig. 7.3) cannot account for the high-p_T data, giving contributions which are about two orders of magnitude below the experiments and yielding p_T distributions which are still too flat.

If perturbative QCD is considered to be the theoretical basis for large-p_T hadron production, which should be the case for p_T not too small, then it is certainly not sufficient to consider only elastic quark–quark scattering ($qq\to qq$) as the dominant subprocess, which constitutes at most a lower bound for the total production cross section. In addition to quarks, hadrons contain also colored vector gluons which can scatter off quarks and other gluons in an approximately scale-invariant manner. Since the

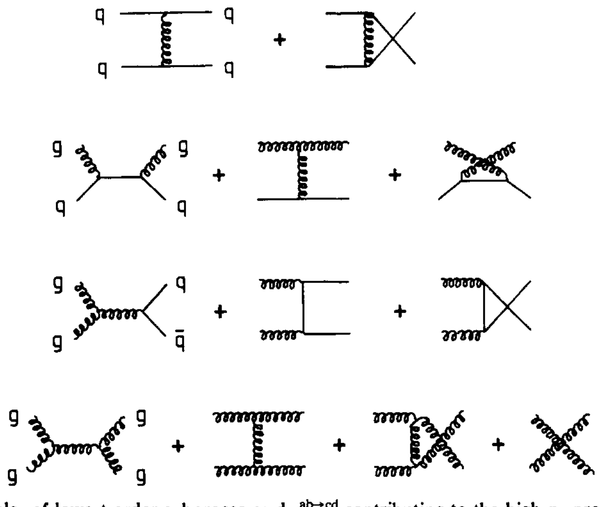

Fig. 11.1. Examples of lowest-order subprocesses $d\sigma^{ab\to cd}$ contributing to the high-p_T process in eq. (11.1).

gluon distribution in the nucleon is sizeable in the region relevant for present high-p_T experiments (typically $x \simeq 0.2$), gluon induced subprocesses will give non-negligible contributions to the total cross section in eq. (11.1). Typically, QCD predicts the following fundamental subprocesses ab → cd in eq. (11.1) to be relevant for high-p_T reactions [251, 263, 264]: In addition to the purely fermionic processes qq → qq and q$\bar{q}$ → q$\bar{q}$, we have gluonic processes such as gq → gq, gg → q$\bar{q}$, q$\bar{q}$ → gg and gg → gg, examples of which are shown in fig. 11.1. The explicit expressions for $d\sigma^{ab\to cd}/d\hat{t}$ can be found in refs. [251, 263 and 264]. The importance of the gg → q$\bar{q}$ subprocess (see, for example, fig. 9.3) for hadronic heavy Q$\bar{Q}$ production (J/ψ, Υ, etc.) has already been discussed [227] and demonstrated in section 9.

In order to demonstrate the relevance of gluonic subprocesses we show in fig. 11.2 the predictions for the inclusive single-π production reaction pp → π + X together with all contributing individual subprocesses in eq. (11.1). Although each subprocess scales as p_T^{-4}, the predicted total invariant cross section in fig. 11.2 falls off faster with p_T for $p_T \lesssim 8$ GeV/c. This is due to the fact that the Q^2 dependent parton distributions and fragmentation functions do not scale and similarly $\alpha_s(Q^2)$. Furthermore, the absolute magnitude of the total cross section for $p_T \lesssim 8$ GeV/c is greatly improved by taking into account the gluonic subprocesses as compared to the simple minded approach [262] of keeping only the qq → qq process. The reason for this is obvious by keeping in mind that the contribution of these subprocesses are weighted by the appropriate quark and gluon distributions of the initial states in eq. (11.1) which are known to have a radically different $x \sim 2p_T/\sqrt{s}$ dependence when x becomes small or large. For $p_T \simeq 2$–3 GeV/c the dominant subprocess is gluon–quark with gluon–gluon and quark–quark scattering also providing substantial contributions. The three subprocesses q$\bar{q}$ → q$\bar{q}$, gg → q$\bar{q}$ and q$\bar{q}$ → gg are negligible for all values of p_T shown here. As p_T increases the gluon–gluon term decreases more rapidly than either the gluon–quark or quark–quark terms, since the gluon distribution in the nucleon strongly decreases for increasing $x_T = 2p_T/\sqrt{s}$. At higher p_T the relative importance of the gluon–quark term also decreases, eventually leaving only the quark–quark scattering contribution which is dominated by the broad (hard) valence–valence quark distributions. This latter term alone scales as p_T^{-4} up to logarithmic terms coming from the Q^2 dependence of the scaling violations and from $\alpha_s(Q^2)$. It is thus clear that the large gluon–gluon and gluon–quark terms are responsible not only for obtaining the correct normalization but also, in part, for obtaining the observed rapid falloff in the intermediate-p_T region.

From fig. 11.2 and comparing several other high-p_T observables with QCD predictions [251] an

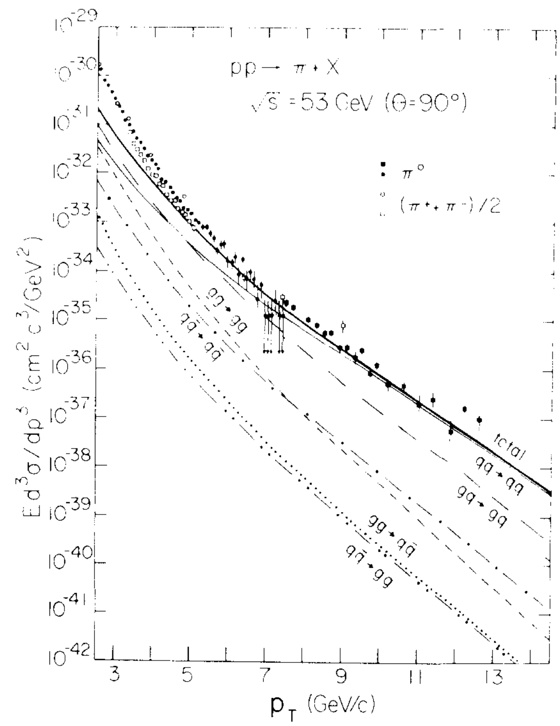

Fig. 11.2. QCD predictions [251] for the production of high-p_T π's at CERN-ISR energies. The individual contributions of the various subprocesses ab → cd in eq. (11.1) are explicitly shown. The data are taken from ref. [265].

excellent prescription of the data is obtained for $p_T \gtrsim 4.5$ GeV/c, whereas for smaller p_T values the predictions lie below the data. There are several reasons which might be responsible for this remaining discrepancy:

(i) For the calculations shown we have chosen $Q^2 = -\hat{t}$. This is a rather pessimistic choice in as far as it yields on the average the largest values for Q^2 possible and therefore induces large scaling violations in the parton distributions in (11.1) which diminish, together with $\alpha_s^2(Q^2)$, the final cross sections significantly. This is in contrast to the more "optimistic" choice [98, 266] $Q^2 = 2\hat{s}\hat{t}\hat{u}/(\hat{s}^2 + \hat{t}^2 + \hat{u}^2)$ which results in a lower average Q^2 and therefore increases the predicted cross sections (see also the discussion in section 7).

(ii) So far we have not considered the intrinsic transverse momenta of partons. These (ill understood) non-perturbative effects due to the k_T of partons within hadrons, and of hadrons within the outgoing jet, called "k_T smearing" effects appear to be particularly important for large p_T calculations [267–269, 98, 266]. Here one usually makes an ad hoc ansatz for the k_T dependence of parton distributions and fragmentation functions with $\langle k_T \rangle$ being a free parameter to be fitted to experiment. The average transverse momenta $\langle k_T \rangle$ obtained in this rather naive way lie typically between 800 and 1000 MeV/c! The effect of this (huge) k_T smearing is illustrated in fig. 11.3 where the behavior of p_T^8 times $E_C\,d\sigma/d^3p_C$ for pp → π + X is shown for various fixed values of $x_T = 2p_T/\sqrt{s}$. The intrinsic k_T effects are obviously most significant in the small p_T region ($\lesssim 4$ GeV/c) where they account for most of the steep decrease of $E\,d\sigma/d^3p$ with p_T as compared to the unsmeared ($k_T = 0$) prediction shown by the dotted curve in fig. 11.3; note that this latter curve corresponds roughly to the "total" solid line of fig. 11.2. At large values of p_T the comparatively small intrinsic k_T's become unimportant and the predictions approach the same

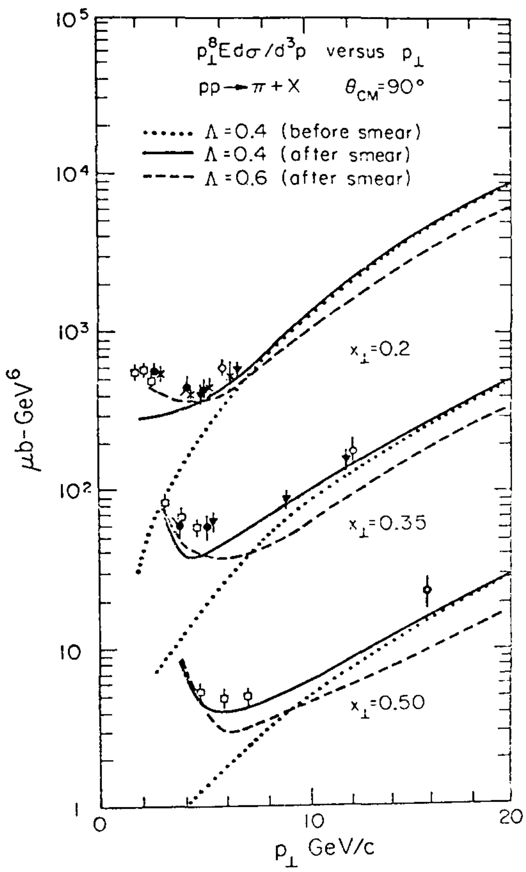

Fig. 11.3. The influence of intrinsic k_T effects on the p_T dependence of high-p_T cross sections [266, 197, 216]. The dotted curves refer to the QCD predictions before smearing ($k_T = 0$), whereas the solid and dashed curves include the intrinsic k_T effects. The dependence of the predictions on different choices for Λ is also shown. The data are taken from refs. [265, 270 and 271]; the recent ISR data [271] at large values of p_T do indeed show a deviation from a straight line (p_T^{-8}) behavior as expected from QCD (as also shown and discussed in fig. 11.2).

p_T dependence as shown in fig. 11.2 which goes roughly as p_T^{-6}, i.e. the naive scaling behavior p_T^{-4} of the $qq \to qq$ subprocess is corrected by logarithmic scaling violations in quark distributions and in $\alpha_s^2(Q^2)$. Intrinsic k_T effects are also important for explaining more subtle effects such as 'away-side' correlations and hadron multiplicities, and p_{out} distributions [98, 266] in two-hadron inclusive high-p_T reactions (we shall come back to this point at the end of this section).

(iii) In addition to the lowest order diagrams in fig. 11.1, subdominant hard $2 \to 3$ parton processes of $O(\alpha_s^3)$ such as $qq \to qqg$, $gq \to ggq$, $gg \to ggg$, etc., could be a significant source for increasing the transverse momenta of the observed hadrons. These three-jet hard scattering Born cross sections (*hard* gluon radiation) have been recently calculated [272–274] and seem to play a non-negligible role for correlation-predictions, acoplanarity and p_{out} distributions [272, 273]. However, since the virtual gluon- and quark-loop contributions to the $O(\alpha_s^2)$ diagrams in fig. 11.1 have not been calculated yet, we do not know the entire amount of α_s corrections to leading order-α_s^2 quantities such as the total single-particle inclusive cross section in eq. (11.1). Once these calculations are completed it will be very instructive to see to what extent these $O(\alpha_s^3)$ corrections can fill the gap between the $O(\alpha_s^2)$ predictions for $p_T \lesssim 4$ GeV/c and the data in fig. 11.2, and also to redo the intrinsic-k_T smearing with $O(\alpha_s^3)$

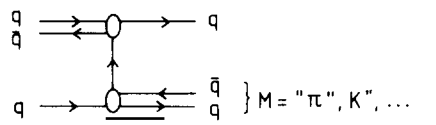

Fig. 11.4. A typical CIM subprocess [275] qM → qM which contributes a p_T^{-8} component to the total single inclusive high-p_T cross section.

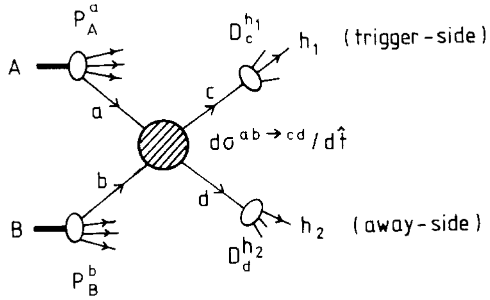

Fig. 11.5. Illustration of the underlying structure of the high-p_T two-particle inclusive process $AB \to h_1h_2 + X$.

corrections added which should result in *smaller* values for $\langle k_T \rangle$ than the ones naively obtained as discussed in (ii).

(iv) Another possible source for explaining the discrepancy between the QCD predictions and the data for $p_T \lesssim 4.5\,\mathrm{GeV}/c$ in fig. 11.2 could come from nonelementary subprocesses such as elastic quark–meson scattering as in the constituent-interchange model (CIM) [275, 276]. Here one envisages that partons don't scatter point-like but rather interact with virtual $q\bar{q}$ bound states ("mesons") inside the nucleon by exchanging flavor (quark) quantum numbers as shown for example in fig. 11.4. Therefore, such contributions are supposed to represent in some way non-perturbative bound state effects which might become important in the soft (small) p_T region [275, 276].

As for the single-particle inclusive high-p_T reaction $AB \to h_1 + X$, the effects of scaling violations [277, 266, 98] and intrinsic k_T smearing are equally important for two-particle inclusive processes $AB \to h_1h_2 + X$ where now a second hadron h_2 is also measured in the away-side trigger (fig. 11.5). The cross section for producing two hadrons h_1 and h_2 derives [185, 277, 278] from a straightforward generalization of eq. (11.1). The most popular observables studied are, besides correlation properties between h_1 and h_2, p_{out} and multiplicity $n(x_e)$ distributions [277, 278, 98, 197, 216] of the away-side hadron h_2, with the kinematics illustrated in fig. 11.6. Significant QCD effects, combined with intrinsic-k_T smearing, are for example a considerable increase of p_{out} in the large x_e region, and a drop of (the transverse momentum sharing distribution) $n(x_e)$ with increasing trigger momentum p_{T1}. We refer the interested reader to the literature [277, 278, 98, 197, 216] where these effects have been extensively discussed. It should be emphasized that the subdominant $2 \to 3$ parton processes of $O(\alpha_s^3)$, producing three hard jet events, play again a significant role in explaining large-p_T characteristics, such as azimuthal correlations, acoplanarity and p_{out} distributions [272, 273].

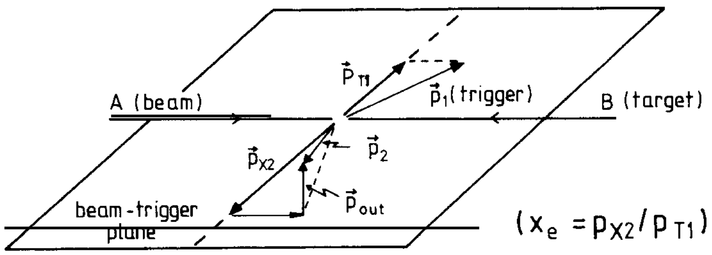

Fig. 11.6. Kinematics of large-p_T events.

Similar studies can be performed for hadronic high-p_T jet production [185, 98, 197, 216, 272, 273, 279, 280], where all produced hadrons at the trigger-side, say, are supposed to be collimated into a narrow cone along the outgoing quark. The single-jet cross section, for example, can then easily be obtained from the single-particle cross section in eq. (11.1) by simply replacing the parton fragmentation functions by δ-functions, i.e., $D_c^C(z, Q^2) \to \delta(1-z)$.

12. The total hadronic e^+e^- cross section: $R_{e^+e^-}$

Before discussing the basic properties of quark and gluon jets in e^+e^- annihilation, let us first briefly recapitulate the QCD corrections to the total hadronic cross section $\sigma(e^+e^- \to \gamma^* \to \text{hadrons})$. At large enough values of q^2 (where again we are dealing with short distance phenomena [5], $z^2 \sim 1/q^2$, as was the case for example in eqs. (5.2) and (5.32)) the total cross section should be given, to leading order in perturbation theory, by the square of the $e^+e^- \to q\bar{q}$ diagram (fig. 1.1) or equivalently, using the optical theorem, by

$\sigma(e^+e^- \to \text{hadrons}) \sim \text{Im}$ 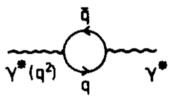 (12.1)

where we have suppressed the trivial lepton lines. This yields eq. (1.9). The $O(\alpha_s)$ corrections come then simply from the gluon radiative corrections to the q and $\bar{q}$ lines in (12.1) as illustrated in fig. 12.1(b). These diagrams are the same as in QED up to the non-abelian quark–gluon coupling (2.6) giving rise to the color factor $C_2(R) = \frac{4}{3}$ given by eq. (4.3). Therefore the α_s correction to eq. (1.9) becomes [281]

$$R_{e^+e^-} = 3 \sum_q e_q^2 \left[1 + C_2(R) \frac{3}{4} \frac{\alpha_s(q^2)}{\pi}\right] = 3 \sum_q e_q^2 \left[1 + \frac{\alpha_s(q^2)}{\pi}\right] \tag{12.2}$$

i.e., asymptotically the scaling limit is approached from *above*. Typically, the α_s correction in (12.2) amounts to about 10%. Recently even the next-to-leading QCD α_s^2-corrections have been computed [282] which, although depending on the renormalization prescription chosen, are roughly an order of magnitude smaller than the α_s term in (12.2), and are therefore much smaller than present experimental uncertainties. A more quantitative discussion of these various correction terms can be found for example in ref. [283].

In fig. 12.2 we show a compilation [284, 285] of recent measurements of $R_{e^+e^-}$ together with the naive expectations according to eq. (12.2), where $R_{e^+e^-}$ is predicted to be a step function with a rise above each new quark threshold. In general, however, eq. (12.2) is strictly valid only for space-like $q^2 < 0$: The appearance of the running coupling $\alpha_s(q^2)$ is due to the use of the renormalization group [281] which strictly applies only there. In order to obtain the experimentally measured quantity in eq. (12.2) one has to extrapolate from $q^2 < 0$ to $q^2 > 0$. This is certainly a non-trivial task for values of q^2 not too far away

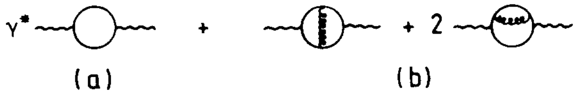

Fig. 12.1 Gluonic QCD corrections (b) to the zeroth order e^+e^- annihilation cross section (a).

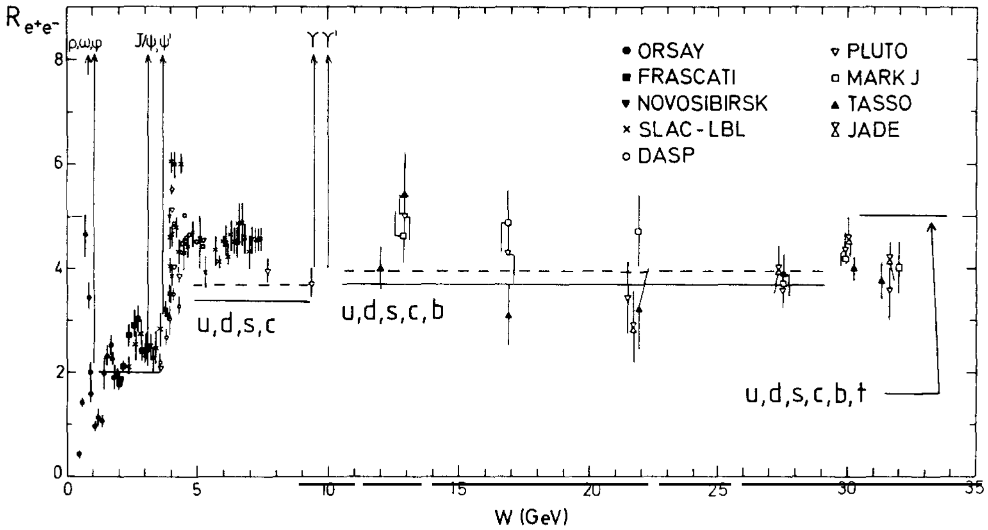

Fig. 12.2. A compilation [284, 285] of measurements of $R_{e^+e^-}$ as a function of the total c.m. energy $W \equiv \sqrt{q^2}$. The solid lines show the predictions (1.9) from the naive quark model, and the dashed lines include the α_s correction due to gluon emission according to eq. (12.2).

from new quark thresholds. These complications can be somehow taken care of by using dispersion relations [286] for the analytic continuation in q^2. This method allows us to analytically extend the data ($q^2 > 0$) to the negative q^2 axis (where the perturbation expansion is not sensitive to non-perturbative bound state effects), and is usually referred to as "smearing method". Without going into any details, let us just mention the basic idea of this procedure. According to Cauchy's theorem one can write [286] a "finite energy sum rule" for $R_{e^+e^-}(s)$

$$\int_{C_1} R_{e^+e^-}(s)\,ds = -\int_{C_2} R_{e^+e^-}(s)\,ds \tag{12.3}$$

where the integration contours C_i in the complex $s \equiv q^2$ plane are as follows:

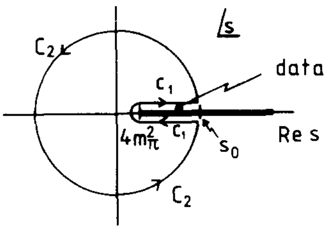

Since the integral over C_1 can be performed by using $R_{e^+e^-}$ from experiment whereas the integrand along the path C_2 is fixed by QCD, eq. (12.3) becomes

$$\int_{4m_\pi^2}^{s_0} R_{e^+e^-}^{\text{exp}}(s)\,ds = \int_{0}^{s_0} R_{e^+e^-}^{\text{QCD}}(s)\,ds \tag{12.4}$$

where s_0 is the total c.m. energy squared up to which data are available, and $R^{\rm QCD}_{e^+e^-}$ is given by eq. (12.2) appropriately generalized to include heavy quark mass effects [287], due to the massive quark propagators in fig. 12.1,

$$R^{\rm QCD}_{e^+e^-}(s) = 3\Big\{\underbrace{\sum_{q=u,d,s} e_q^2\Big[1+\frac{\alpha_s(s)}{\pi}\Big]}_{\text{(light)}} + \underbrace{\sum_{Q=c,b,\dots} e_Q^2\theta(s-4m_Q^2)\, v_Q\frac{3-v_Q^2}{2}\big[1+\tfrac{4}{3}\alpha_s f(v_Q)\big]}_{\text{(heavy)}}\Big\} \qquad (12.5)$$

where $v_Q = \sqrt{1-4m_Q^2/s}$ and with Schwinger's function given by

$$f(v) = \frac{\pi}{2v} - \frac{3+v}{4}\left(\frac{\pi}{2} - \frac{3}{4\pi}\right).$$

In eq. (12.5) we have written only the purely hadronic contribution to $R_{e^+e^-}$ since the leptonic contribution is usually subtracted experimentally. In general of course eq. (12.5) receives a further term due to heavy leptons in fig. 12.1a which reads $+\frac{1}{2}\Sigma_l\, v_l(3-v_l^2)$. Quantitative analyses along these lines yielded the result [286], long before the experimental discovery of the b-quark, that $R^{\rm QCD}_{e^+e^-}$ with only four flavors (u, d, s, c) and one heavy lepton does not suffice to describe the data; only an additional quark flavor with $|e_q| = 1/3$ or an additional heavy lepton gave satisfactory fits [286] to the data.

13. Jets in e^+e^- annihilation

As we have learned so far, the predominant QCD corrections to any hard scattering process are those due to collinear gluon radiation and pair-creation. To leading order, these give rise to dominant *two* jet configurations in e^+e^- annihilation due to the $e^+e^- \to q\bar{q}$ subprocess in fig. 1.1 which, together with the hadronization of quarks into physical objects, is illustrated in fig. 13.1 in the e^+e^- c.m. system. This two jet structure has indeed been discovered 1975 at SLAC (SPEAR) [288] and subsequently confirmed by many different groups at DESY at much higher c.m. energies [284, 289, 290]. This two-jet interpretation is especially convincing since the distribution of the jet axis in the angle θ (see fig. 13.1) relative to the e^+e^- axis is found [288, 290, 291] to be consistent with a form $\sim(1+\cos^2\theta)$ which is expected for the production of a pair of spin 1/2 point-like quarks:

$$\frac{d\sigma^{e^+e^-\to q\bar{q}}}{d\Omega} = \frac{\alpha^2}{4s}\, 3\sum_q e_q^2(1+\cos^2\theta) \qquad (13.1)$$

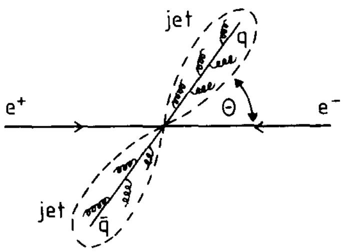

Fig. 13.1. Dominant 2-jet configuration in $e^+e^- \to q\bar{q} \to$ hadrons.

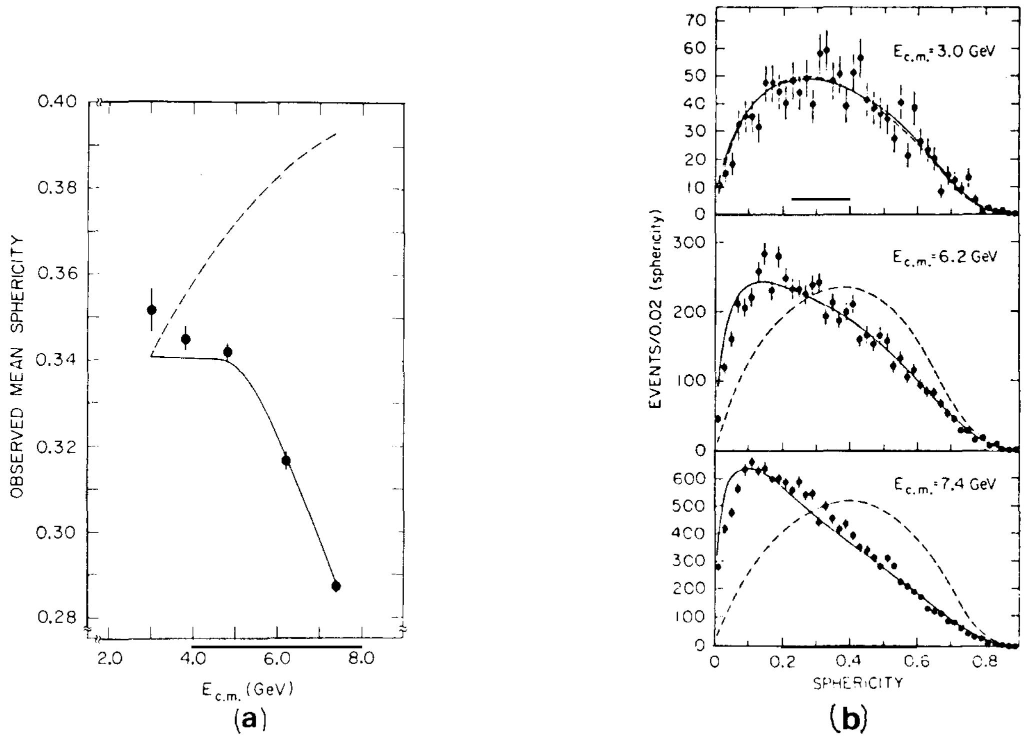

Fig. 13.2. (a) Observed mean sphericity $\langle\hat{S}\rangle$ versus the c.m. energy $\sqrt{s} \equiv E_{\mathrm{cm}}$. (b) Sphericity distributions for increasing c.m. energies. The data [288] are compared with a Monte Carlo 2-jet model using an intrinsic transverse momentum $\langle k_{\mathrm{T}}\rangle \simeq 0.3$ GeV (solid curves) and with a Monte Carlo phase-space model (dashed curves).

with the c.m. energy squared $s \equiv q^2$ held fixed. A representative sample of the historical evidence [288] for the (q, q̄)-jet structure is shown in fig. 13.2.

Experimentalists measured the sphericity [292] of an event,

$$\hat{S} = \tfrac{3}{2} \min\left\{ \sum_i |\boldsymbol{p}_{\mathrm{T}}^{(i)}|^2 \Big/ \sum_i |\boldsymbol{p}^{(i)}|^2 \right\} \tag{13.2}$$

where the sum runs over all observed particles (tracks) and the p_{T}'s are transverse to the "jet" axis which is chosen to minimize $\hat{S}$. Indeed, the observed sphericity *decreases* with energy which means that the hadron jets in fig. 13.1 become more and more collimated the higher $\sqrt{s} \equiv E_{\mathrm{cm}}$. In brief, the hadronic events are more "jetty" the larger the energy. This is completely the opposite of what one would expect from a pure (isotropic) phase space behavior of hadronic events as indicated by the dashed curves in fig. 13.2. The same "jettiness" of events has been also confirmed at higher energies [290, 293] as shown in fig. 13.3.

In general, however, it is not possible to compute $\mathrm{d}\sigma/\mathrm{d}\hat{S}$ reliably in perturbation theory, because the sphericity $\hat{S}$ acquires infrared singularities due to its being proportional to the sum over momenta *squared* in eq. (13.2). The infrared problem has been solved in QED [294] where it is known that the infrared singularities in individual diagrams (such as those shown in fig. 13.4) are cancelled if one considers cross sections with suitable energy and angle cut-offs which may be related to practical

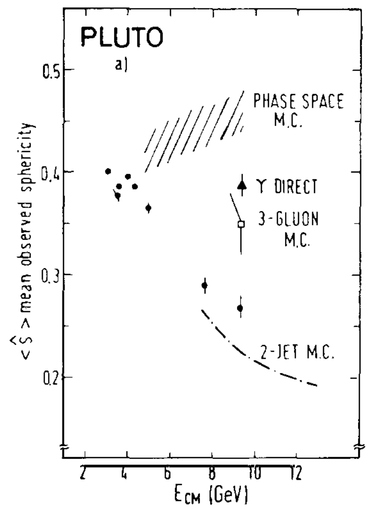

Fig. 13.3. Observed [293] mean sphericity as a function of the total c.m. energy for the 2-jet ($q\bar{q}$) events (●). Shown is also the measurement for the 3-gluon-jet events on resonance, i.e. the decay of the Υ resonance (▲).

experimental resolutions. In other words, only if we add the appropriate amplitudes and then taking the square of these expressions we will obtain infrared-finite observables. Therefore, only variables where the *momenta* are summed *linearly* (instead of quadratically as in eq. (13.2)) are insensitive to soft or collinear gluon emission. Various authors [295–297] have proposed variables for measuring the "jettiness" of e^+e^- events which are arguably infrared insensitive. They include a linearly summed version of eq. (13.2) called the "spherocity" [295]

$$S = \left(\frac{4}{\pi}\right)^2 \min\left(\sum_i |\boldsymbol{p}_T^{(i)}| \Big/ \sum_i |\boldsymbol{p}^{(i)}|\right)^2, \tag{13.3}$$

or the maximum directed momentum called "thrust" [296]

$$T = 2 \max\left\{\sum_i{}' p_\parallel^{(i)} \Big/ \sum_i |\boldsymbol{p}^{(i)}|\right\} \tag{13.4}$$

where the Σ' in the numerator runs over all observed particles in only one hemisphere, and $p_\parallel^{(i)}$ are the hadron's momenta parallel to the "jet" axis which is normal to the plane defining the hemispheres and chosen to maximize T. It is a simple matter to convince oneself that, in going from an isotropic to a

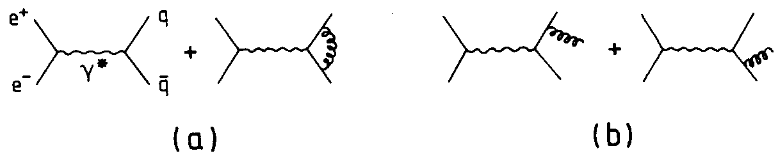

Fig. 13.4. Lowest order radiative corrections to $e^+e^- \to q\bar{q}$.

jet-like structure, $\hat{S}$, S and T run through the following ranges of values:

isotropic				perfect jet
1	$\geq$	$\hat{S}$	$\geq$	0
1	$\geq$	S	$\geq$	0
$\frac{1}{2}$	$\leq$	T	$\leq$	$1.$

Experimentally there seems to be very little difference between the axis defined by S and T.

While in leptoproduction, Drell–Yan processes or semi-inclusive hadron production in e^+e^- annihilation (involving fragmentation functions) the (soft) infrared complicacies can be absorbed in the definition of parton densities, as has been discussed in detail in section 7 (see, for example, eqs. (7.4)–(7.6)), in the present jet case all predictable quantities (*not* involving fragmentation functions) must be free of infrared problems. Before proceeding with QCD, let us first briefly discuss the equivalent situation in QED in order to elucidate the origin of the two different types of singularities encountered in the amplitudes of fig. 13.4(b) when the emitted gluon (photon) is either infrared soft or collinear with one of the quarks [298]. Let us consider the scattering of an electron off a charged source (Mott scattering), and which emits a photon with momentum k (fig. 13.5). The amplitude corresponding to a photon of momentum k emitted by the outgoing electron is given up to irrelevant factors by

$$
\begin{aligned}
M &= \frac{2\varepsilon \cdot p_2}{(k+p_2)^2 - m_e^2} \\
&\simeq \frac{\boldsymbol{\varepsilon} \cdot \boldsymbol{p}_2}{k|\boldsymbol{p}_2|(1-\cos\theta + m_e^2/2|\boldsymbol{p}_2|^2)} \qquad \text{for } m_e^2 \ll \boldsymbol{p}_2^2
\end{aligned}
\tag{13.5}
$$

where we have taken into account the mass-shell conditions $k^2 = 0$ and $p_2^2 = m_e^2$, and where θ is the angle between the outgoing electron and the photon. In eq. (13.5) we have only exhibited the electron propagator and the emission vertex $\varepsilon \cdot p_2$ which are the only relevant factors for understanding the (collinear) mass singularity when $m_e^2 \to 0$. From eq. (13.5) we can see that the collinear singularity for $\theta = 0$, which becomes dangerous for massless gluons in QCD, is in fact regulated by the finite electron mass. The factor $1/k$ is of course responsible for the usual soft infrared divergencies, due to the emission of soft photons. In order to reproduce the situation of QCD as closely as possible, let us neglect the electron mass in (13.5) in which case the denominator will behave like θ^2 for small values of θ. Furthermore, since the polarization vector $\boldsymbol{\varepsilon}$ of a real photon is perpendicular to $\boldsymbol{k}$, we have

$$\boldsymbol{\varepsilon} \cdot \boldsymbol{p}_2 = |\boldsymbol{p}_2| \sin\theta \simeq |\boldsymbol{p}_2|\theta$$

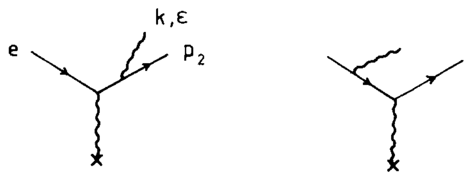

Fig. 13.5. Lowest-order diagrams for photon radiation by an electron in the presence of an external field.

and thus the amplitude in (13.5) behaves both in the infrared ($k \simeq 0$) and collinear ($\theta \simeq 0$) region as

$$M \simeq 1/k\theta. \tag{13.6}$$

The cross section for photon bremsstrahlung is then obtained to be proportional to

$$\int \frac{d^3k}{2k_0} |M|^2 \simeq \int \frac{k^2\, dk}{k}\, d(\cos\theta) \frac{1}{k^2\theta^2} \simeq \int \frac{dk}{k} \frac{d\theta}{\theta} \tag{13.7}$$

which exhibits the infrared and collinear singularities of the form $\ln(|\boldsymbol{p}_2|/\mu_\gamma)\ln(|\boldsymbol{p}_2|/m_e)$, with μ_γ being some fictitious virtual photon mass.

We can get rid of this *infrared* singularity by calculating cross sections for final states with finite *energy* resolution ΔE, i.e. a photon of energy $k < \Delta E$ is emitted in fig. 13.5; then, when the elastic amplitudes with virtual photon corrections (fig. 13.4(a)) are added ($\sim -\ln(|\boldsymbol{p}|/\mu_\gamma)\ln(|\boldsymbol{p}|/m_e)$), infrared divergences cancel and in the final result the limit $\mu_\gamma \to 0$ can be safely taken. One obtains a correction factor which is proportional to the above logarithms except that the mass μ_γ is replaced by the energy resolution ΔE. This is summarized in the famous Kinoshita–Lee–Nauenberg theorem [294]. In the same way one can regulate the *collinear* singularities by introducing an *angular* resolution δ and by computing transition rates to nearly degenerate states which include the electron plus an arbitrary number of collinear (not necessarily soft) photons. (This latter configuration can be regarded as an electron jet characterized by its quantum numbers such as the electric charge and energy.) Only now the limit $m_e \to 0$ can be safely taken and the total cross section is free of collinear mass singularities.

Exactly the same principles can be applied to QCD which has been first done by Sterman and Weinberg [299] in order to obtain a well defined two-jet cross section in e^+e^- annihilation, i.e., a cross section which is *finite* in the zero-mass limit. Let us consider the quantity $\sigma(\sqrt{s}, \theta, \varepsilon, \delta)$ which is defined as the cross section for all annihilation events where a fraction $(1-\varepsilon)$ of the total available energy $\sqrt{s}$ is emitted within a pair of oppositely directed cones of opening angle 2δ with both $\varepsilon, \delta \ll 1$ (fig. 13.6). Performing the calculations with a vanishing quark mass and with some fictitious gluon mass $\mu_g \ll \varepsilon\sqrt{s}$, we obtain, to order $\alpha_s(s)$, the following three contributions to the total jet cross section: The *vertex* correction stemming from the diagrams in fig. 13.4(a) (i.e., virtual gluon correction)

$$\left(\frac{d\sigma}{d\Omega}\right)_{\text{vertex}} = \left(\frac{d\sigma}{d\Omega}\right)_0 \left[1 + \frac{4\alpha_s}{3\pi}\left(-\frac{1}{2}\ln^2\frac{s}{\mu_g^2} + \frac{3}{2}\ln\frac{s}{\mu_g^2} + \frac{\pi^2}{6} - \frac{7}{4}\right)\right] \tag{13.8}$$

where the zeroth-order ($\alpha_s = 0$, $\varepsilon = 1$, $\delta \to 0$; free quark case) Born cross section $(d\sigma/d\Omega)_0$ for $e^+e^- \to q\bar{q}$

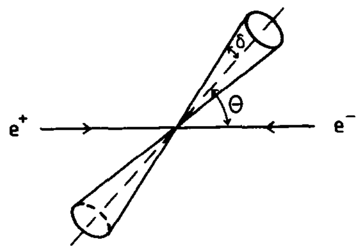

Fig. 13.6. The two opposite cones of half-angle δ at a c.m. angle θ used in the derivation of the Sterman–Weinberg [299] two-jet cross section.

is given by eq. (13.1). The contribution due to *soft* gluon emission in the diagrams of fig. 13.4(b) where the gluon energy $E_g < \varepsilon\sqrt{s}$ (corresponding to the soft infrared singularity $k \to 0$) is given by

$$\left(\frac{d\sigma}{d\Omega}\right)_{soft} = \left(\frac{d\sigma}{d\Omega}\right)_0 \frac{4\alpha_s}{3\pi}\left[\frac{1}{2}\ln^2\frac{4\varepsilon^2 s}{\mu_g^2} - \frac{\pi^2}{6}\right]. \tag{13.9}$$

Finally, the third contribution comes from *hard* collinear gluon emissions in the diagrams of fig. 13.4(b), where $E_g > \varepsilon\sqrt{s}$ but $p_2 \cdot k \to 0$ in the notation of fig. 13.5, i.e. $\theta_g < \delta$ (corresponding to the collinear mass singularities):

$$\left(\frac{d\sigma}{d\Omega}\right)_{hard} = \left(\frac{d\sigma}{d\Omega}\right)_0 \frac{4\alpha_s}{3\pi}\left[-\frac{3}{2}\ln\frac{\delta^2 s}{\mu_g^2} - \frac{1}{2}\ln^2(4\varepsilon^2) - \ln\frac{\delta^2 s}{\mu_g^2}\ln(4\varepsilon^2) + \frac{17}{4} - \frac{\pi^2}{3}\right]. \tag{13.10}$$

Note that each of these three contributions separately are singular for $\mu_g \to 0$. However, the "miracle" happens if we add them: In the *sum* $d\sigma = d\sigma_{vertex} + d\sigma_{soft} + d\sigma_{hard}$ the μ_g dependence cancels and we obtain a cross section which is *finite* in the zeroth-mass limit:

$$\frac{d\sigma}{d\Omega} = \left(\frac{d\sigma}{d\Omega}\right)_0 \left[1 - \frac{4\alpha_s}{3\pi}\left(3\ln\delta + 4\ln\delta\ln 2\varepsilon + \frac{\pi^2}{3} - \frac{5}{2}\right)\right], \tag{13.11}$$

which is the famous Sterman–Weinberg result [299]. Recall that the introduction of a small but finite value of ε renders the final result infrared finite, whereas δ assures the absence of the (hard) collinear mass singularities. Comparing this result with the total e^+e^- cross section in eq. (12.2),

$$\sigma = \frac{4\pi\alpha^2}{3s}3\sum_q e_q^2\left[1 + C_2(R)\frac{3\alpha_s}{4\pi}\right] \tag{13.12}$$

one can now calculate the fraction $f(\varepsilon, \delta)$ of all two-jet events which are such that the energy $(1-\varepsilon)\sqrt{s}$ is emitted in a pair of opposite cones of half-angle δ around the outgoing quarks:

$$\begin{aligned} f(\varepsilon,\delta) &= \frac{1 - C_2(R)(\alpha_s/\pi)[3\ln\delta + 4\ln\delta\ln 2\varepsilon + \pi^2/3 - \frac{5}{2} + r]}{1 + C_2(R)(3\alpha_s/4\pi)} \\ &= 1 - C_2(R)\frac{\alpha_s}{\pi}\left[\ln\delta\,(4\ln 2\varepsilon + 3) + \frac{\pi^2}{3} - \frac{7}{4} + r\right] + O(\alpha_s^2) \end{aligned} \tag{13.13}$$

with $C_2(R) = 4/3$ and the remainder $r(\varepsilon, \delta)$ are additional subleading correction terms [300] to the Sterman–Weinberg formula (13.11) which are finite in the limit $\varepsilon, \delta \to 0$. Note that the regime of applicability of eq. (13.11) and hence of eq. (13.13), neglecting r, requires ε and δ sufficiently small, presumably so that the logarithmic terms are larger than the constant terms. On the other hand, in order to apply perturbation theory, α_s must be sufficiently small so that the corrections to the cross section in (13.11) or to f in eq. (13.13) are small. Even at highest PEP or PETRA energies of $\sqrt{s} = 30$–40 GeV, these conditions are not easy to fulfil [300, 301].

We can now use eq. (13.13) to study specific characteristics of quark-jets more quantitatively, such as the energy dependence of the jet opening angle $\delta_q \equiv \delta(\sqrt{s})$. Solving eq. (13.13) for δ, by using $\alpha_s(s)$ in eq. (4.9), gives

$$\delta_q(\sqrt{s}) = (\sqrt{s}/\Lambda)^{-d_q(f,\varepsilon)} \tag{13.14}$$

with

$$d_q(f,\varepsilon) = \frac{1}{8}\left(\frac{33-2N_f}{-4\ln 2\varepsilon - 3}\right)(1-f+r_q), \qquad r_q = -\frac{\alpha_s}{\pi}\frac{4}{3}\left(\frac{\pi^2}{3} - \frac{7}{4} + O(\varepsilon,\delta)\right). \tag{13.15}$$

Numerically, for example, using $N_f = 3$,

$$d_q(f, 0.1) = 0.98(1-f+r_q). \tag{13.16}$$

Or, if we require 70% of all events ($f = 0.7$) such that at least 80% of $\sqrt{s}$ ($\varepsilon = 0.2$) is emitted in the two opposite cones, their half-angle is predicted to be δ_q (30 GeV) $\simeq 1^\circ$. Further quantitative results can be found, for example, in refs. [300] and [302].

Instead of considering an outgoing quark which radiates a gluon (fig. 13.4), one can imagine an outgoing gluon-jet which radiates gluons as well as $q\bar{q}$ pairs as illustrated in fig. 13.7. This mechanism will give rise to an opening angle of a gluon-jet which in general will be different from that of a quark-jet, δ_q. A similar calculation as above yields [301, 303] to leading order in $\alpha_s(s)$

$$f(\varepsilon,\delta) = 1 - \frac{\alpha_s}{\pi}\left[C_2(G)\left(4\ln\delta\ln 2\varepsilon + \frac{11}{3}\ln\delta\right) - \frac{2}{3}N_f\ln\delta\right] + r_g \tag{13.17}$$

where the remainder

$$r_g(\varepsilon,\delta) = -\frac{\alpha_s}{\pi}\left[C_2(G)\left(\frac{\pi^2}{3} - \frac{49}{36}\right) + \frac{1}{9}N_f + O(\varepsilon,\delta)\right]$$

is finite in the limit $\varepsilon, \delta \to 0$. Note that now the dominant contribution is proportional to the color charge $C_2(G) = 3$ of a gluon, due to the gluon–gluon interaction in diagrams like in fig. 13.7(a), in contrast to the quark-jet in eq. (13.13) where the leading term is proportional to the smaller color charge $C_2(R) = 4/3$ of quarks which derives from the quark–gluon interactions in fig. 13.4. Solving eq. (13.17) for $\delta_g \equiv \delta(\sqrt{s})$, using $\alpha_s(s)$ in eq. (4.9), yields the energy dependence of the opening angle of a gluon jet

$$\delta_g(\sqrt{s}) = (\sqrt{s}/\Lambda)^{-d_g(f,\varepsilon)} \tag{13.18}$$

Fig. 13.7. Gluon-jet production from a source (e.g., a quark) which contribute to the opening angle δ_g of a gluon-jet.

with

$$d_g(f,\varepsilon)=\frac{1}{18}\left(\frac{33-2N_f}{-4\ln 2\varepsilon-(33-2N_f)/9}\right)(1-f+r_g). \tag{13.19}$$

Numerically, for example, using $N_f=3$,

$$d_g(f,0.1)=0.44(1-f+r_g). \tag{13.20}$$

This is smaller than d_q in (13.16) which suggest that the collimation of gluon jets will shrink much more *slowly* than for quark jets. Since $C_2(G)>C_2(R)$, this is of course a general result, i.e. we always have $d_g(f,\varepsilon)<d_q(f,\varepsilon)$. If we compare just the dominant $\ln 2\varepsilon$ terms in (13.15) and (13.19), then eqs. (13.14) and (13.18) predict

$$\delta_g(\sqrt{s})\simeq\delta_q(\sqrt{s})^{C_2(R)/C_2(G)}=\delta_q(\sqrt{s})^{4/9} \tag{13.21}$$

i.e. a gluon jet should be much *broader* than a quark jet! In other words gluon jets are more effective in radiating particles with large p_T due to their color charge $C_2(G)=3$ being much *larger* than the color charge $C_2(R)=4/3$ of quarks [304]. Hence, gluon jets are less jet-like, i.e. are more difficult to be observed experimentally. All these purely perturbative effects discussed thus far, are of course contaminated by non-perturbative contributions due to the intrinsic transverse momentum k_T of the hadrons inside the jet (fig. 13.1): For a parton of momentum P the non-perturbative opening angle is expected to be $\delta_{n.p.}\simeq\langle k_T\rangle/P$ where $\langle k_T\rangle\simeq 0.3$–$0.5$ GeV is anticipated to be independent of the large momentum of the original quark or gluon. For example, for $P=15$ GeV we expect $\delta_{n.p.}\simeq 1$–$2°$. At finite energies, this gives a lower limit on the range of applicability of the above perturbative QCD predictions.

Besides the two-jet ($q\bar{q}$) structure discussed thus far, we also expect (less frequently) a *three*-jet ($q\bar{q}g$) structure in e^+e^- annihilation if one of the quarks in fig. 13.4(b) emits a hard gluon with a large angle relative to the outgoing quark direction [305–308]. Since the production of each jet costs an extra factor of $\alpha_s(s)$ we expect, for example, in e^+e^- annihilation

$$\sigma(\text{2-jet}):\sigma(\text{3-jet}):\sigma(\text{4-jet})=1:\alpha_s:\alpha_s^2,$$

so that $\sigma(q\bar{q}g)/\sigma(q\bar{q})\simeq 10\%$. For such 3-jet ($q\bar{q}g$) events we generally expect [309] that $\langle p_T\rangle$ will grow to some extent as $\sqrt{s}$ increases, where p_T is measured for example with respect to the thrust or sphericity axis. More specifically the average transverse momentum of the emitted gluon, say, is predicted to increase like $\langle p_T\rangle\sim\alpha_s(s)\sqrt{s}\sim\sqrt{s}/\ln s$. This is in contrast to the non-perturbative $\langle k_T\rangle\simeq 0.3$ GeV which is inherent to each jet and is expected to be independent of the energy and therefore should be asymptotically negligible with respect to the relative p_T of the jets. In other words, the large-p_T cross section $d\sigma^{q\bar{q}g}/dp_T^2$ in e^+e^- annihilation should grow for increasing energies, i.e. the p_T distribution should become substantially flatter [305] the larger $\sqrt{s}$. For example, at $\sqrt{s}=15$ GeV the p_T distribution $d\sigma^{q\bar{q}g}/dp_T^2$ should become substantially flatter for $p_T\gtrsim 1$ GeV than the one for simple two-jet events $d\sigma^{q\bar{q}}/dp_T^2$, the latter being due to non-perturbative intrinsic-k_T effects. Indeed, big and increasing large-p_T cross sections have been recently observed at PETRA [310–312]. Figure 13.8 shows the TASSO data [310] together with the original 1976 prediction [305] which is based on the three-jet cross section

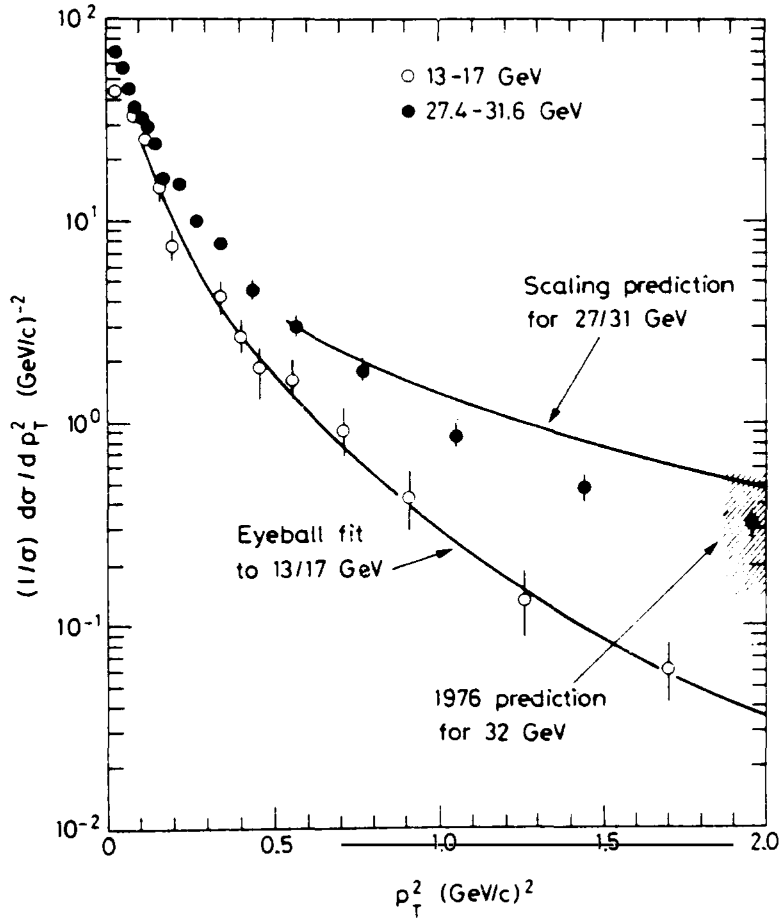

Fig. 13.8. The p_T distributions found by the TASSO collaboration [310] at different c.m. energies. The 1976 prediction [305] is based on the $e^+e^- \to q\bar{q}g$ cross section in eq. (13.22). The figure is taken from ref. [283].

(fig. 13.4(b))

$$\frac{1}{\sigma_0^{q\bar{q}}} \frac{d^2\sigma^{q\bar{q}g}}{dx_q\, dx_{\bar{q}}} = \frac{2\alpha_s}{3\pi} \frac{x_q^2 + x_{\bar{q}}^2}{(1-x_q)(1-x_{\bar{q}})} \tag{13.22}$$

with $x_{q,\bar{q}} = 2E_{jet}/\sqrt{s}$, and which is normalized to the zeroth-order two-jet cross section $\sigma_0^{q\bar{q}}$ (fig. 13.4(a)). Also shown in fig. 13.8 is the scaling prediction for large energies according to the naive dimensional scaling law

$$\frac{1}{\sigma_0^{q\bar{q}}} \frac{d\sigma}{dp_T^2} = \frac{1}{s} f(x_T) \times [O(\alpha_s) \text{ corrections}] \tag{13.23}$$

where $x_T = 2p_T/\sqrt{s}$; at $p_T \gtrsim 1$ GeV naive scaling, which of course is expected to hold only asymptotically, is broken by 50 to 100%, but this may be partly due to the logarithmic corrections in eq. (13.23).

Alternatively, we can express these increasing p_T-distributions by thrust or spherocity distributions

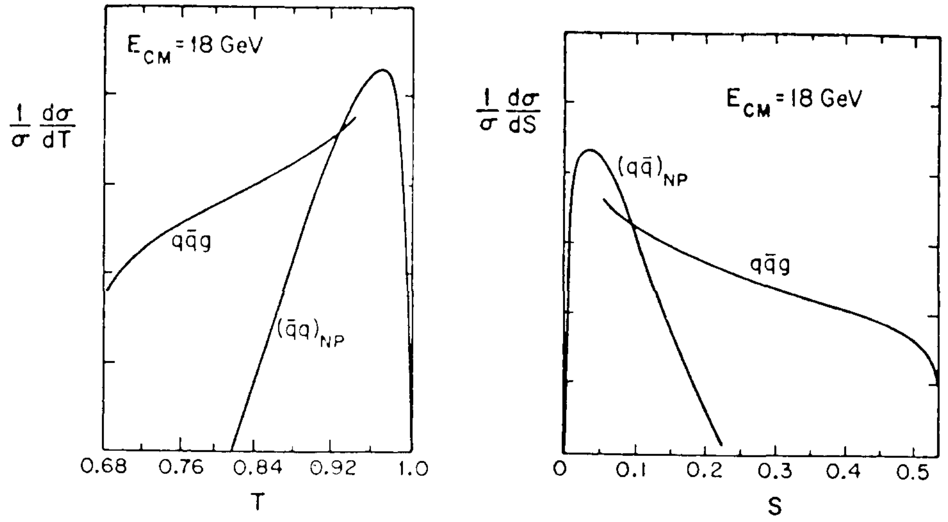

Fig. 13.9. Thrust and spherocity distributions [306] for 3-jet ($q\bar{q}g$) and non-perturbative 2-jet ($q\bar{q}$) events in e^+e^- annihilation.

[306, 307] as shown, for example in fig. 13.9. According to the definitions (13.3) and (13.4) the 3-jet ($q\bar{q}g$) events due to the hard wide-angle gluon radiation off an (anti)quark are expected at small (large) values of $T(S)$, i.e. at large values of p_T. The curves labelled by $(q\bar{q})_{NP}$ represent an estimate [306] of the thrust and spherocity distributions arising from non-perturbative hadronization effects for a 2-jet event, assuming an intrinsic transverse momentum of $\langle k_T\rangle \simeq 0.3$ GeV. Again, these predictions seem to be in agreement with experimental observations [311, 312]. One usually makes a cut in thrust or sperocity in order to (hopefully) suppress the huge non-perturbative background $(q\bar{q})_{NP}$ in fig. 13.9, a procedure which should be increasingly effective at higher energies. Nevertheless, still another caveat is the possibility that contributions to low (high) thrust (spherocity) for heavy quark production [313] may drown the hard gluon bremsstrahlung $q\bar{q}g$ signal: As we increase the total energy $\sqrt{s}$ we hit the thresholds for heavy quark–antiquark ($Q\bar{Q}$) pair production which in turn decay weakly ($e^+e^- \to Q\bar{Q} \to 6$ jets with $Q = c, b, \ldots$) giving rise to large p_T's of jets.

We can go even further and try to display more explicitly the three-jet character of the three quanta final states [306]. To this end one selects an event sample in $e^+e^- \to$ hadrons with $1 - T \gg (\Delta T)_{NP}$, where typically $(\Delta T)_{NP} \gtrsim 0.9$, for which one measures the energy flow in the plane of the three quanta q, $\bar{q}$ and g. In practice one then defines [306] a "pointing vector"

$$P(\sqrt{s}, T, \theta) = p(\theta) \frac{d^2\sigma}{dT\, d\cos\theta} \tag{13.24}$$

where $p(\theta)$ is the total momentum in the element $d\theta$ around θ, with θ being the angle in the event plane relative to the most energetic jet, i.e. to the axis corresponding to maximum thrust. This axis is aligned in the $\theta = 0$ direction with the angular direction being defined so that the second most energetic jet has $\theta < 180°$. The variation in length and in angle of the remaining two momentum vectors, corresponding to the two less energetic jets, will then depend on the dynamics, i.e., in our case on the matrix element for $e^+e^- \to \gamma^* \to q\bar{q}g$. (This is like measuring the power emitted by an antenna as a function of angle.) This variation of the "pointing vector" is shown in fig. 13.10. The dominant 2-jet "background" in fig.

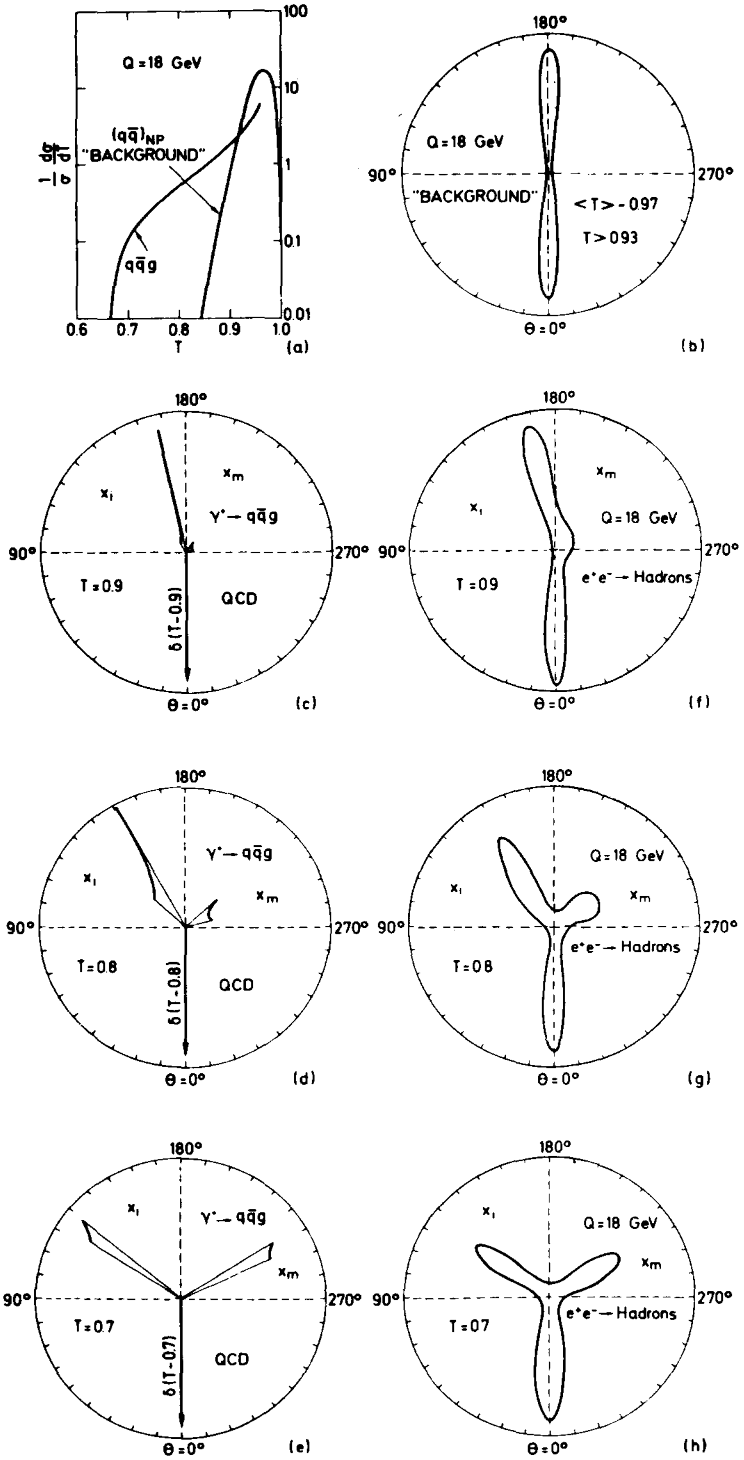

Fig. 13.10. "Pointing vector" distributions [306] for $q\bar{q}g$ jets without (c–e) and with (f–h) hadronization effects (using $\langle k_T \rangle^{\text{intrinsic}} \simeq 300$ MeV), and for the $q\bar{q}$ background (b) at a c.m. energy $Q \equiv \sqrt{s} = 18$ GeV.

13.10(b) is due to the (non-perturbative) thrust distribution in fig. 13.10(a) peaked at $T \simeq 1$ and which has been calculated by using an intrinsic transverse momentum smearing of $\langle k_T \rangle \simeq 0.3$ GeV. The same "smearing" has been used to obtain the pointing vectors for the "smeared" 3-jet events for decreasing T (figs. 13.10(f)–(h)) from the idealized ones ($k_T = 0$) in figs. 13.10(c)–(e). Various recent experiments [310–312, 284, 289] seem indeed to be consistent with these striking predictions of QCD jets.

So far we have been solely concerned with the 3-jet $q\bar{q}g$ events which result from a hard wide-angle gluon radiation off the outgoing quarks and antiquarks. A similar 3-jet structure is expected [314–316] also "on-resonance" when a produced heavy quark ($Q\bar{Q}$) bound state decays via gluon emission [287]. The hadronic decay of very heavy $J^{PC} = 1^{--}$ $Q\bar{Q}$ states ("quarkonium") must proceed via an intermediate state consisting of at least 3 color-octet gluons [317] giving rise to a 3-gluon jet structure provided the energy (mass) is large enough so that purely perturbative α_s effects take over:

$$e^+e^- \to \gamma^* \to Q\bar{Q} \to 3\,\text{gluons} \to 3\,\text{gluon jets}$$

with Q = c, b, ... This reaction is illustrated in fig. 13.11 which is a straightforward generalization (by adding just color factors and possible gluon fragmentation functions) of the well-known Ore–Powell formula [318] for the 3γ decay of orthopositronium in QED. The decay of the $\Upsilon(9.4)$ ($= b\bar{b}$ bound state) might already be dominated by 3g-jet events [314–316], although the average energy of one gluon jet is still rather small: $\langle E_g \rangle = \frac{1}{3} M_\Upsilon \simeq 3$ GeV. The expected three-gluon jet events in the decay $\Upsilon \to 3g$ look very similar [306] to those shown in fig. 13.10 for $q\bar{q}g$-jets. Especially at large thrust, for example, we expect similar "Mercedes star" events as shown in fig. 13.10(h). Although present data [289, 290, 293, 319] are in very good agreement with the 3-gluon decay model, they are not fully conclusive. Presumably the hadronic decay of even heavier $Q\bar{Q}$ bound states (for example $t\bar{t}$ quarkonium, if it exists) should provide us with additional unambiguous tests of QCD [320]. Note that in the e^+e^- annihilation continuum one expects the zeroth-order $q\bar{q}$ final states (fig. 13.4(a)) to dominate over the $O(\alpha_s)$ three-jet process in fig. 13.4(b), and hence

$$\langle 1-T \rangle, \langle S \rangle, \cdots \sim d\sigma^{q\bar{q}g}/d\sigma^{q\bar{q}} = O(\alpha_s), \tag{13.25}$$

whereas the three-gluon decays of quarkonia (J/ψ, ψ', Υ, ...) should give

$$\langle 1-T \rangle, \langle S \rangle, \cdots = O(1) \tag{13.26}$$

since the $Q\bar{Q} \to 3g$ process in fig. 13.11 is itself the leading contribution "on-resonance". Therefore 3-jet events "on-resonance" should always be *less* "jetty" (i.e. broader) than those off-resonance, in agreement with experiment (see fig. 13.3).

A closely related and very interesting decay channel is $Q\bar{Q} \to \gamma + \text{hadrons}$ (i.e., "direct photons" in $Q\bar{Q}$ decays, rather than photons produced via π^0 or η decays). This process [314–316] is simply obtained by substituting a gluon in $Q\bar{Q} \to 3g$ (fig. 13.11) by a photon as shown in fig. 13.12. Therefore the

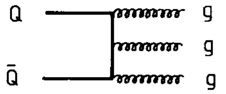

Fig. 13.11. The decay of a heavy $Q\bar{Q}$ vector meson into three gluons, giving rise to a 3g-jet structure of the hadronic final state.

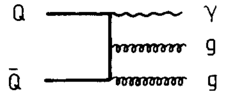

Fig. 13.12. Production of "direct photons" in $Q\bar{Q} \to \gamma + 2g$.

radiative decay $Q\bar{Q}\to\gamma gg$ will take place with a branching ratio [314–316]

$$B_\gamma^{Q\bar{Q}} \equiv \frac{\Gamma(Q\bar{Q}\to\gamma gg)}{\Gamma(Q\bar{Q}\to 3g)} = \frac{\alpha}{\alpha_s}\frac{36}{5}e_Q^2 \qquad (13.27)$$

which is just the ratio of the two diagrams squared of figs. 13.12 and 13.11, and where 36/5 is a simple color SU(3) factor. The predicted inclusive radiative rate is surprisingly large: For example, for the charmonium family we expect $B_\gamma^{J/\psi} \simeq 6\%$. A measurement of this rate might offer us the best chance [321] for finding "gluonium" or "gluon balls" (i.e. colorless gg bound states [23]). The known decays $\psi\to\gamma\eta$, $\gamma\eta'$, γf give a total width of $\lesssim 1\%$, whereas SPEAR has recently reported [321] a single-γ continuum contribution (with mass recoiling against the γ of $\lesssim 1.7$–1.8 GeV) consistent with a total radiative branching ratio of about 5%. This may indeed be indicative for the existence of gluonium – a topic certainly exciting enough to be persued much further.

Finally we would like to stress the importance of two-photon processes [322, 323] as a possible source of hadronic jets, i.e. $e^+e^-\to e^+e^-\gamma\gamma\to e^+e^-q\bar{q}\to e^+e^- + \text{jets}$. The outstanding virtue and theoretical beauty of this process is based on the fact that it allows us to test QCD in the "cleanest" way possible since here even the basic subprocess $\gamma\gamma\to q\bar{q}$ can be calculated from first principles. This allows us to make even *absolute* predictions for complicated systems such as multi-jet processes or distributions of quarks and gluons in photons and electrons [140, 141, 323], as was the case for "direct photon" production in deep inelastic reactions discussed in section 5.9. These two-photon processes will become experimentally accessible at energies in the $\sqrt{s} = 100$ GeV range where future e^+e^- super-colliders like LEP should provide us with the most reliable tests of QCD.

Acknowledgments

Most of all I would like to thank M. Glück with whom many of the topics discussed here have been elaborated on in numerous discussions during the past years, and some of the work described here has been done in collaboration with him. I am also grateful to A.J. Buras for a few helpful remarks. Furthermore, it is a pleasure to thank H. Bienlein for providing and creating the excellent atmosphere at the Maria Laach School, and for his everlasting encouragement to write a full-fledged review. Finally, I also would like to thank Mrs. H. Laudien for her heroic and efficient typing.

References

[1] H.D. Politzer, Phys. Reports 14C (1974) 129.
[2] G. Altarelli, Rivista Nuovo Cimento 4 (1974) 335.
[3] D.J. Gross, in: Methods in Field Theory, Les Houches 1975, eds. R. Balian and J. Zinn-Justin (North-Holland, Amsterdam, 1976) p. 141.
[4] G. Parisi, Proc. XIth Rencontre de Moriond on Weak Interactions and Neutrino Physics, Flaine 1976, ed. J. Tran Thanh Van, p. 83.
[5] J. Ellis, in: Weak and Electromagnetic Interactions at High Energies, Les Houches 1976, eds. R. Balian and C.H. Llewellyn Smith (North-Holland, Amsterdam, 1977) p. 1.
[6] M.K. Gaillard, Asymptotic Freedom and Deep Inelastic Scattering, lectures presented at the XIIth Rencontre de Moriond, Flaine 1977; and Ref. TH. 2318-CERN.
[7] C.H. Llewellyn Smith, Deep Inelastic Phenomena, lectures presented at the 1977 Cargèse Summer Institute; and Oxford preprint Ref. 2/78.
[8] G. Altarelli, Partons in Quantum Chromodynamics, lectures given at the 9th Ecole d'Eté de Physique de Particules, Gif-sur-Yvette 1977, Rome preprint n.701; and Proc. XIIIth Rencontre de Moriond on Gauge Theories and Leptons, Les Arcs 1978, ed. J. Tran Thanh Van, p. 395.

[9] H. Fritzsch, Schladming lectures 1978, Acta Physica Austriaca, Suppl. XIX (1978) 249.
[10] A. Peterman, Phys. Reports 53 (1979) 157.
[11] A.J. Buras, Rev. Mod. Phys. 52 (1980) 199.
[12] M. Böhm and H. Joos, lectures held at the Herbstschule für Hochenergiephysik, Maria Laach 1977; and DESY 78/27 (in German).
[13] B. Geyer, D. Robaschik and E. Wieczorek, Theorie der tiefinelastischen Lepton-Hadron Streuung I, II, Akademie der Wissenschaften Berlin-Zeuthen preprint PHE 77-5 (1977), and Fortschritte d. Physik 27 (1979) 75.
[14] W. Marciano and H. Pagels, Phys. Reports 36C (1978) 137.
[15] M. Gell-Mann, Schladming lectures 1972, Acta Physica Austriaca, Suppl. IX (1972) 733;
W.A. Bardeen, H. Fritzsch and M. Gell-Mann, Scale and Conformal Symmetries in Hadron Physics, ed. R. Gatto (Wiley, New York, 1973);
H. Fritzsch and M. Gell-Mann, Proc. XVI Intern. Conf. on High Energy Physics, Chicago 1972, eds. J.D. Jackson and A. Roberts (Batavia) vol. 2, p. 135.
[16] H. Fritzsch, M. Gell-Mann and H. Leutwyler, Phys. Lett. 47B (1973) 365.
[17] S.L. Adler, Lectures on Elementary Particles and Quantum Field Theory, Brandeis 1970, eds. S. Deser, M. Grisaru and H. Pendleton (MIT Press, Cambridge, 1971) p. 1.
[18] DASP coll., R. Brandelik et al., Phys. Lett. 76B (1978) 361.
[19] S.L. Adler, Phys. Rev. 177 (1969) 2426;
J.S. Bell and R. Jackiw, Nuovo Cim. 60 (1969) 47.
[20] For reviews, see B. Zumino, Proc. XVI Intern. Conf. on High Energy Physics, Chicago 1972, eds. J.D. Jackson and A. Roberts (Batavia) vol. 2, p. 285;
H. Fritzsch and P. Minkowski, Flavordynamics of Quarks and Leptons, Physics Reports, to be published.
[21] H. Georgi and S.L. Glashow, Phys. Rev. D6 (1972) 429;
D.J. Gross and R. Jackiw, Phys. Rev. D6 (1972) 477.
[22] M.K. Gaillard and B.W. Lee, Phys. Rev. Lett. 33 (1974) 108;
G. Altarelli and L. Maiani, Phys. Lett. 52B (1974) 351;
M.K. Gaillard, 1978 SLAC Summer Institute and Fermilab-Conf-78/64-THY (1978).
[23] H. Fritzsch and P. Minkowski, Nuovo Cim. 30A (1975) 393;
D. Robson, Phys. Lett. 66B (1977) 267, and Nucl. Phys. B130 (1977) 328;
P. Roy and T.F. Walsh, Phys. Lett. 78B (1978) 62.
[24] D.J. Gross and F. Wilczek, Phys. Rev. Lett. 30 (1973) 1343, Phys. Rev. D8 (1973) 3633;
H.D. Politzer, Phys. Rev. Lett. 30 (1973) 1346.
[25] S. Coleman and D.J. Gross, Phys. Rev. Lett. 31 (1973) 851.
[26] E. Stueckelberg and A. Peterman, Helv. Phys. Acta 26 (1953) 499;
M. Gell-Mann and F. Low, Phys. Rev. 95 (1954) 1300;
L.V. Ovsiannikov, Dokl. Akad. Nauk SSSR 109 (1956) 1112.
[27] C.G. Callan, Phys. Rev. D2 (1970) 1541;
K. Symanzik, Comm. Math. Phys. 18 (1970) 227.
[28] S. Coleman, Proc. 1971 Intern. Summer School of Physics, "Ettore Majorana", Erice, ed. A. Zichichi (Editrice Compositori, Bologna, 1973) p. 358.
[29] S. Weinberg, Phys. Rev. 118 (1960) 838.
[30] N.N. Bogoliubov and O.S. Parasiuk, Acta Math. 97 (1957) 227;
K. Hepp, Comm. Math. Phys. 2 (1966) 301;
for an introductory discussion see also S. Coleman, Proc. 1971 Intern. Summer School of Physics "Ettore Majorana", Erice, ed. A. Zichichi (Editrice Compositori, Bologna, 1973) p. 604.
[31] A. de Rújula, H. Georgi and H.D. Politzer, Ann. of Phys. 103 (1977) 315.
[32] V.F. Weisskopf, Intuitive Approaches to Field Theories, in: Lepton and Hadron Structure, Erice 1974, ed. A. Zichichi (Academic Press, New York, 1975) p. 306; and Ref. TH. 1938-CERN (1974).
[33] K.G. Wilson, Phys. Rev. D3 (1971) 1818.
[34] N. Christ, B. Hasslacher and A.H. Mueller, Phys. Rev. D6 (1972) 3543.
[35] C.G. Callan and D.J. Gross, Phys. Rev. D8 (1973) 4383;
J. Kogut and L. Susskind, Phys. Rev. D9 (1974) 3391.
[36] A. Zee, Phys. Rev. D7 (1973) 3630.
[37] N.N. Khuri, Phys. Lett. 82B (1979) 83, and references therein.
[38] For a detailed treatise of the naive parton model and all the relevant kinematics see, for example, F.E. Close, Partons and Quarks, Daresbury Lecture Note Series DNPL/R31 (1973); and An Introduction to Quarks and Partons (Academic Press, 1979).
[39] J.D. Bjorken, Phys. Rev. 179 (1969) 1547.
[40] J.D. Bjorken and E.A. Paschos, Phys. Rev. 185 (1969) 1975;
R.P. Feynman, Phys. Rev. Lett. 23 (1969) 1415; Photon Hadron Interactions (Benjamin, New York, 1972).
[41] More detailed relations between structure functions and parton distributions can be found, for example, in refs. [2] and [11].
[42] C.G. Callan and D.J. Gross, Phys. Rev. Lett. 22 (1969) 156.
[43] BEBC coll., P.C. Bosetti et al., Nucl. Phys. B142 (1978) 1.

[44] CDHS coll., J.G.H. de Groot et al., Phys. Lett. 82B (1979) 456.
[45] CDHS coll., J.G.H. de Groot et al., Z. Physik C, Particles and Fields 1 (1979) 143.
[46] S.L. Adler, Phys. Rev. 143 (1966) 1144.
[47] D.J. Gross and C.H. Llewellyn Smith, Nucl. Phys. B14 (1969) 337.
[48] A. Bodek et al., Phys. Rev. Lett. 30 (1973) 1087;
J.S. Poucher et al., Phys. Rev. Lett. 32 (1974) 118;
A. Bodek et al., Phys. Rev. D20 (1979) 1471.
[49] J.W. Moffat, Schladming lectures 1972, Acta Physica Austriaca, Suppl. IX (1972) 605.
[50] K.G. Wilson, Phys. Rev. 179 (1969) 1499.
[51] R.A. Brandt and G. Preparata, Nucl. Phys. B27 (1971) 541;
Y. Frishman, Phys. Rev. Lett. 25 (1970) 966; Ann. of Phys. 66 (1971) 373;
R. Jackiw, R. van Royen and G.B. West, Phys. Rev. D2 (1970) 2473.
[52] D.J. Gross and S.B. Treiman, Phys. Rev. D4 (1971) 1059.
[53] H. Georgi and H.D. Politzer, Phys. Rev. D9 (1974) 416.
[54] D.J. Gross and F. Wilczek, Phys. Rev. D9 (1974) 980.
[55] Further details of the calculation of anomalous dimensions using the Feynman rules implied by Wilson operators can be found in the Appendix of ref. [54] and in the short review by F. Legovini, Oxford report Ref. 88/78 (1978).
[56] M. Glück and E. Reya, Phys. Rev. D14 (1976) 3034.
[57] G. Altarelli, R. Petronzio and G. Parisi, Phys. Lett. 63B (1976) 183.
[58] A. de Rújula, H. Georgi and H.D. Politzer, Phys. Rev. D15 (1977) 2495.
[59] S.J. Brodsky and G.R. Farrar, Phys. Rev. Lett. 31 (1973) 1153;
V.A. Matveev, R.M. Muradyan and A.N. Tavkhelidze, Nuovo Cim. Lett. 7 (1973) 719.
[60] J.F. Gunion, Phys. Rev. D10 (1974) 242.
[61] G.R. Farrar, Nucl. Phys. B77 (1974) 429.
[62] CDHS coll., J.G.H. de Groot et al., Phys. Lett. 82B (1979) 292.
[63] O. Nachtmann, Nucl. Phys. B63 (1973) 237;
S. Wandzura, Nucl. Phys. B122 (1977) 412.
[64] V. Baluni and E. Eichten, Phys. Rev. D14 (1976) 3045.
[65] H. Georgi and H.D. Politzer, Phys. Rev. D14 (1976) 1829.
[66] R. Barbieri, J. Ellis, M.K. Gaillard and G.G. Ross, Nucl. Phys. B117 (1976) 50.
[67] P.H. Frampton, UCLA/76/TEP/6 (1976).
[68] E.D. Bloom and F.J. Gilman, Phys. Rev. Lett. 25 (1970) 1140.
[69] E. Reya, Phys. Lett. 84B (1979) 445.
[70] For an alternative view, which is based on taking into account measurements also at Q^2 values as small as $0.8\,\mathrm{GeV}^2$, we refer to J. Ellis, Current Trends in the Theory of Fields, AIP Conf. Proc. No. 48 (1978) p. 81; SLAC-PUB-2177 (1978); and Proc. Intern. Conf. "Neutrino 79" (Bergen, 1979), Ref. TH. 2701-CERN.
[71] For further measured slopes we refer to refs. [62] and [43] but these are not to be construed as giving several independent tests of QCD, since the moments are highly correlated with one another and not much new information is provided once the result for one pair of moments is given.
[72] M. Glück and E. Reya, Nucl. Phys. B156 (1979) 456.
[73] B.A. Gordon et al., Phys. Rev. Lett. 41 (1978) 615;
H.L. Anderson et al., Phys. Rev. Lett. 40 (1978) 1061.
[74] H.L. Anderson et al., FERMILAB-Pub-79/30-EXP (1979), Phys. Rev. D20 (1979) 2645.
[75] M. Glück and E. Reya, Phys. Lett. 69B (1977) 77.
[76] M. Glück and E. Reya, Phys. Rev. D16 (1977) 3242.
[77] D.K. Choudhury and L.G.F. Vanryckeghem, Phys. Rev. D17 (1978) 1766.
[78] Combined field theoretic models of QCD and fixed point theories, the latter being treated as a small perturbation, can of course, at the present state of art, not be excluded by presently available experiments. See, for example, K. Watanabe, Prog. Theor. Phys. 61 (1979) 1150.
[79] F. Oberhettinger, Tables of Mellin Transforms (Springer, New York, 1974).
[80] D. Gross, in: Proc. XVII Intern. Conf. on High Energy Physics, London, 1974, ed. J.R. Smith (Rutherford Lab., Chilton, Didcot, 1974) p. III-65.
[81] G. Parisi, Phys. Lett. 43B (1973) 207; 50B (1974) 367.
[82] A. de Rújula, H. Georgi and H.D. Politzer, Phys. Rev. D10 (1974) 2141.
[83] M. Glück and E. Reya, Phys. Lett. 64B (1976) 169.
[84] R.E. Taylor, in: Intern. Symp. on Lepton and Photon Interactions (Stanford, 1975) p. 679; and SLAC-PUB-1729.
[85] D.J. Gross, Phys. Rev. Lett. 32 (1974) 1071.
[86] G. Eilam, M. Glück and E. Reya, Comparing Asymptotically Free Theories with Experiment, University of Mainz report MZ-TH 75/6 (1975), unpublished.
[87] A. de Rújula, S.L. Glashow, H.D. Politzer, S.B. Treiman, F. Wilczek and A. Zee, Phys. Rev. D10 (1974) 1649.

[88] G. Parisi and R. Petronzio, A Dynamical Approach to Deep Inelastic Scattering, University of Rome report n. 617 (1975); Phys. Lett. 62B (1976) 331.
[89] I. Hinchliffe and C.H. Llewellyn Smith, Nucl. Phys. B128 (1977) 93.
[90] A.J. Buras and K.J.F. Gaemers, Nucl. Phys. B132 (1978) 249.
[91] P.W. Johnson and W.K. Tung, Phys. Rev. D16 (1977) 2769.
[92] G.C. Fox, Nucl. Phys. B131 (1977) 107.
[93] P. Savaria, E.M. Haacke and R.H. Graham, Phys. Rev. D19 (1979) 112.
[94] E.M. Riordan et al., SLAC-PUB-1634 (1975);
A. Bodek et al., Phys. Rev. D20 (1979) 1471.
[95] E. Witten, Nucl. Phys. B104 (1976) 445;
M.A. Shifman, A.I. Vainshtein and V.I. Zakharov, Nucl. Phys. B136 (1978) 157.
[96] M. Glück and E. Reya, Phys. Lett. 83B (1979) 98.
[97] J.P. Leveille and T. Weiler, Nucl. Phys. B147 (1979) 147;
V. Barger, W.Y. Keung and R.J.N. Phillips, Phys. Rev. D20 (1979) 630.
[98] R.P. Feynman, R.D. Field and G.C. Fox, Phys. Rev. D18 (1978) 3320.
[99] A.R. Clark et al., Phys. Rev. Lett. 43 (1979) 187.
[100] R.M. Barnett, H. Georgi and H.D. Politzer, Phys. Rev. Lett. 37 (1976) 1313.
[101] A.J. Buras, Nucl. Phys. B125 (1977) 125.
[102] I. Hinchliffe and C.H. Llewellyn Smith, Phys. Lett. 70B (1977) 247.
[103] A.J. Buras and K.J.F. Gaemers, Phys. Lett. 71B (1977) 106.
[104] G.C. Fox, Nucl. Phys. B134 (1978) 269.
[105] See, for example, M. Greco, in: Lepton and Hadron Structure, Erice 1974, p. 262, and references therein;
R. Kögerler and D. Schildknecht, Phys. Lett. 66B (1977) 461.
[106] P. Castorina, G. Nardulli and G. Preparata, Nucl. Phys. B163 (1980) 333.
[107] G.J. Gounaris and S.B. Sarantakos, Phys. Rev. D18 (1978) 670.
[108] I. Karliner and J.D. Sullivan, Phys. Rev. D18 (1978) 3202.
[109] H. Georgi, How to Observe Quarks and Gluons, Harvard report HUTP-78/A049 (1978).
[110] H. Georgi, in: Orbis Scientiae 1978 on New Frontiers in High-Energy Physics (Coral Gables, Florida) p. 475; and HUTP-78/A003.
[111] V.A. Novikov, M.A. Shifman, A.I. Vainshtein and V.I. Zakharov, JETP Lett. 24 (1976) 341; Ann. of Phys. 105 (1977) 276.
[112] M. Glück and E. Reya, Nucl. Phys. B130 (1977) 76.
[113] T. Eichten et al., Phys. Lett. 46B (1973) 274;
H. Deden et al., Nucl. Phys. B85 (1975) 269.
[114] J.F. Owens and E. Reya, Phys. Rev. D17 (1978) 3003.
[115] A. Zee, F. Wilczek and S.B. Treiman, Phys. Rev. D10 (1974) 2881.
[116] D.V. Nanopoulos and G.G. Ross, Phys. Lett. 58B (1975) 105.
[117] P.V. Landshoff, J.C. Polkinghorne and R.D. Scott, Nucl. Phys. B28 (1970) 225;
P.V. Landshoff and J.C. Polkinghorne, Phys. Rep. 5C (1972) 1.
[118] M. Glück and E. Reya, Nucl. Phys. B145 (1978) 24.
[119] P.V. Landshoff, Phys. Lett. 66B (1977) 452;
J.F. Gunion, Phys. Rev. D15 (1977) 3317;
S. Wada, Prog. Theor. Phys. 62 (1979) 475;
U. Ellwanger, Nucl. Phys. B154 (1979) 358.
[120] See also references quoted in ref. [118].
[121] A.J. Buras, E.G. Floratos, D.A. Ross and C.T. Sachrajda, Nucl. Phys. B131 (1977) 308.
[122] R.E. Taylor, XIX Intern. Conf. on High Energy Physics, Tokyo 1978, p. 285.
[123] E. Reya, Phys. Rev. Lett. 43 (1979) 8.
[124] E.G. Floratos, Nuovo Cimento 43A (1978) 241.
[125] K.H. Craig and C.H. Llewellyn Smith, Phys. Lett. 72B (1978) 349.
[126] G. Altarelli and G. Martinelli, Phys. Lett. 76B (1978) 89.
[127] A. Mendez, Nucl. Phys. B145 (1978) 199;
A. Mendez, A. Raychaudhuri and V.J. Stenger, Nucl. Phys. B148 (1979) 499.
[128] A. Mendez and T. Weiler, Phys. Lett. 83B (1979) 221.
[129] H. Georgi and J. Sheiman, Phys. Rev. D20 (1979) 111.
[130] P. Mazzanti, R. Odorico and V. Roberto, Phys. Lett. 81B (1979) 219.
[131] P. Binétruy and G. Girardi, Nucl. Phys. B155 (1979) 150.
[132] P.M. Stevenson, Imperial College report ICTP/78-79/1 (1979).
[133] P.V. Landshoff, in: Probing Hadrons with Leptons, Erice, March 1979, eds. G. Preparata and J.J. Aubert (Plenum Press, 1980) p. 275.
[134] P.C. Bosetti et al., ABCLOS coll., Oxford Univ. report 58/78 (1978).
[135] H. Georgi and H.D. Politzer, Phys. Rev. Lett. 40 (1978) 3.

[136] J. Cleymans, Phys. Rev. D18 (1978) 954.
[137] G. Köpp, R. Maciejko and P.M. Zerwas, Nucl. Phys. B144 (1978) 123.
[138] R.N. Cahn, Phys. Lett. 78B (1978) 269.
[139] P. Mazzanti, R. Odorico and V. Roberto, Phys. Lett. 80B (1978) 111.
[140] C.H. Llewellyn Smith, Phys. Lett. 79B (1978) 83.
[141] E. Witten, Nucl. Phys. B120 (1977) 189.
[142] H. Fritzsch and P. Minkowski, Phys. Lett. 69B (1977) 316.
[143] W.E. Caswell, Phys. Rev. Lett. 33 (1974) 244;
D.R.T. Jones, Nucl. Phys. B75 (1974) 531.
[144] E.G. Floratos, D.A. Ross and C.T. Sachrajda, Nucl. Phys. B129 (1977) 66; Erratum B139 (1978) 545.
[145] E.G. Floratos, D.A. Ross and C.T. Sachrajda, Phys. Lett. 80B (1979) 269; Erratum 87B (1979) 403; Nucl. Phys. B152 (1979) 493.
[146] W.A. Bardeen, A.J. Buras, D.W. Duke and T. Muta, Phys. Rev. D18 (1978) 3998.
[147] M. Calvo, Phys. Rev. D15 (1977) 730.
[148] J. Abad and B. Humpert, Phys. Lett. 78B (1978) 627; Univ. of Wisconsin reports COO-881-43 and 44 (1978).
[149] G. Altarelli, R.K. Ellis and G. Martinelli, Nucl. Phys. B143 (1978) 521; Erratum B146 (1978) 544.
[150] D.A. Ross, Caltech report CALT-68-699 (1979).
[151] A. Para and C.T. Sachrajda, Phys. Lett. 86B (1979) 331.
[152] T.W. Quirk et al., Phys. Lett. 91B (1980) 285.
[153] L.F. Abbott and R.M. Barnett, Ann. Phys. (N.Y.) 125 (1980) 276;
L.F. Abbott, in: Orbis Scientiae, Coral Gables 1979, and SLAC-PUB-2296.
[154] E. Reya, in: Probing Hadrons with Leptons, Erice 1979, eds. G. Preparata and J.J. Aubert (Plenum Press, 1980) p. 441.
[155] J. Abad and B. Humpert, Phys. Lett. 80B (1979) 286.
[156] A.P. Contogouris and J. Kripfganz, Phys. Rev. D19 (1979) 2207; Phys. Lett. 84B (1979) 473; Phys. Rev. D20 (1979) 2295.
the Drell–Yan Formula, McGill Univ. report, 1979.
[157] J. Kubar-André and F.E. Paige, Phys. Rev. D19 (1979) 221.
[158] K. Harada, T. Kaneko and N. Sakai, Nucl. Phys. B155 (1979) 169.
[159] G. Altarelli, R.K. Ellis and G. Martinelli, Nucl. Phys. B157 (1979) 461.
[160] C.F. Weizsäcker, Z. Physik 88 (1934) 612;
E.J. Williams, Phys. Rev. 45 (1934) 729.
[161] V.N. Baier, V.S. Fadin and V.A. Khoze, Nucl. Phys. B65 (1973) 381.
[162] J. Kogut and L. Susskind, Phys. Rev. D9 (1974) 697.
[163] G. Altarelli and G. Parisi, Nucl. Phys. B126 (1977) 298;
[164] From eq. (6.2) it appears that two diagrams contribute to $\sigma_2^{\gamma^* q\to gq}$, i.e. to P_{qq}. The second diagram in eq. (6.2), the one with the gluon being emitted by the final quark, seems superficially to contradict our philosophy for the P functions, while the first one is directly of the parton type in that the emitted gluon could be considered as part of the proton blob. But looking more closely one discovers that, in a general gauge, this second diagram is only necessary to cancel the contribution of the unphysical longitudinal and scalar gluons. In other words, if we only sum over transverse gluons the contribution of the first parton diagram in eq. (6.2), where the gluon is emitted by the initial gluon, is the only relevant one for the terms which contain the leading ln Q^2 terms.
[165] J.D. Bjorken and S.D. Drell, Relativistic Quantum Fields (McGraw-Hill, 1965).
[166] Apart from straightforward color factors, most of the amplitudes relevant for QCD, except those involving gluon self-couplings, can be found for example in: Landau–Lifshitz, vol. 4.1, Relativistic Quantum Theory (Pergamon Press, 1971).
[167] S.J. Chang and P.M. Fishbane, Phys. Rev. D2 (1970) 1084.
[168] V.N. Gribov and L.N. Lipatov, Soviet J. Nucl. Phys. 15 (1972) 438 and 675.
[169] Yu.L. Dokshitzer, D.I. D'yakonov and S.I. Troyan, Phys. Reports 58 (1980) 269; Proc. 13th Leningrad Winter School (1978) vol. 1, p. 3 (English Translation SLAC-TRANS-183 (1978)); Phys. Lett. 78B (1978) 290.
[170] K.H. Craig and C.H. Llewellyn Smith, Phys. Lett. 72B (1978) 349.
[171] C.H. Llewellyn Smith, Schladming Lectures 1978, Acta Physica Austriaca XIX (1978) 331.
[172] W.R. Frazer and J.F. Gunion, Phys. Rev. D19 (1979) 2447.
[173] L.N. Lipatov, Soviet J. Nucl. Phys. 20 (1975) 94.
[174] H.D. Politzer, Nucl. Phys. B129 (1977) 301.
[175] A.V. Radyushkin, Phys. Lett. 69B (1977) 245.
[176] C.T. Sachrajda, Phys. Lett. 73B (1978) 185;
J. Kripfganz, Phys. Lett. 82B (1979) 79.
[177] S.D. Drell and T.M. Yan, Phys. Rev. Lett. 25 (1970) 316; Ann. of Phys. 66 (1971) 578.
[178] It is clear that one cannot use an operator product expansion to analyze the Drell–Yan process in the limit $Q^2 \equiv +q^2 \to +\infty$. The reason is that now, in contrast to electroproduction, matrix elements of the local operators O_i are *not* taken between *fixed* states, i.e. $C_i(Q^2)\langle P_1, P_2|O_i|P_1, P_2\rangle$ with P_i being the momenta of the external hadrons. Hence $\langle P_1, P_2|O_i|P_1, P_2\rangle$ depends on $s = (P_1 + P_2)^2$ and therefore we cannot expect the subleading singularities of $C_i(Q^2)$ to vanish as $Q^2 \to \infty$ since $s > Q^2$ in the physical region and also $s \to \infty$ in this limit.

[179] D. Amati, R. Petronzio and G. Veneziano, Nucl. Phys. B140 (1978) 54; B146 (1978) 29.
[180] R.K. Ellis, H. Georgi, M. Machacek, H.D. Politzer and G.G. Ross, Nucl. Phys. B152 (1979) 285.
[181] S.B. Libby and G. Sterman, Phys. Lett. 78B (1978) 618; Phys. Rev. D18 (1978) 3252, 4737.
[182] A.H. Mueller, Phys. Rev. D18 (1978) 3705.
[183] W.J. Stirling, Nucl. Phys. B145 (1978) 477.
[184] J. Frenkel, M.J. Shailer and J.C. Taylor, Nucl. Phys. B148 (1979) 228.
[185] S.M. Berman, J.D. Bjorken and J.B. Kogut, Phys. Rev. D4 (1971) 3388;
S.D. Ellis and M.B. Kislinger, Phys. Rev. D9 (1974) 2027;
D. Sivers, S.J. Brodsky and R. Blankenbecler, Physics Reports 23C (1976) 1.
[186] C.T. Sachrajda, Phys. Lett. 76B (1978) 100.
[187] G. Chu and J.F. Gunion, Phys. Rev. D10 (1974) 3672; D11 (1975) 73.
[188] I. Hinchliffe and C.H. Llewellyn Smith, Phys. Lett. 66B (1977) 281.
[189] J. Kogut and J. Shigemitsu, Nucl. Phys. B129 (1977) 461.
[190] R.F. Peierls, T.L. Trueman and L.L. Wang, Phys. Rev. D16 (1977) 1397;
L.B. Okun and M.B. Voloshin, Nucl. Phys. B120 (1977) 459;
C. Quigg, Rev. Mod. Phys. 49 (1977) 297.
[191] F. Halzen and D.M. Scott, Phys. Lett. 78B (1978) 318.
[192] M. Chaichian, O. Dumbrajs and M. Hayashi, Phys. Rev. D20 (1979) 2873.
[193] J. Ellis, second reference in ref. [70].
[194] J.H. Cobb et al., Phys. Lett. 72B (1977) 273.
[195] D. Antreasyan et al., Phys. Rev. Lett. 39 (1977) 906.
[196] D.M. Kaplan et al., Phys. Rev. Lett. 40 (1978) 435.
[197] R.D. Field, Proc. 19th Intern. Conf. on High Energy Physics, Tokyo 1978, p. 743.
[198] R.P. Feynman, R.D. Field and G.C. Fox, Phys. Rev. D18 (1978) 3320.
[199] T. Eichten et al., Phys. Lett. 46B (1973) 274;
H. Deden et al., Nucl. Phys. B85 (1975) 269.
[200] An updated compilation of these data can be found in J. Alspector et al., Phys. Lett. 81B (1979) 397.
[201] J.G. Branson et al., Phys. Rev. Lett. 38 (1977) 1334.
[202] K.J. Anderson et al., Phys. Rev. Lett. 42 (1979) 944;
G.E. Hogan et al., Phys. Rev. Lett. 42 (1979) 948;
C. Reece et al., Phys. Lett. 85B (1979) 427.
[203] M.J. Corden et al., Phys. Lett. 76B (1978) 226;
J. Badier et al., CERN/EP 79-68 (1979).
[204] C.B. Newman et al., Phys. Rev. Lett. 42 (1979) 951;
D. McCal et al., Phys. Lett. 85B (1979) 432;
R. Moore, J. Phys. G5 (1979) 1509.
[205] H. Fritzsch and P. Minkowski, Phys. Lett. 73B (1978) 80.
[206] G. Altarelli, G. Parisi and R. Petronzio, Phys. Lett. 76B (1978) 351.
[207] K. Kajantie and R. Raitio, Nucl. Phys. B139 (1978) 72.
[208] V.N. Baier and V.A. Khoze, JETP (Sov. Phys.) 21 (1965) 629.
[209] For a review and compilation of recent measurements see, for example, L.M. Lederman, Proc. 19th Intern. Conf. on High Energy Physics, Tokyo 1978, p. 706.
[210] M. Glück, Proc. Workshop on Lepton-Pair production in Hadron–Hadron Collisions, Bielefeld 1978, p. 96.
[211] R.C. Hwa, Proc. XIIIth Rencontre de Moriond on Phenomenology of QCD, Les Arcs 1978, p. 197; and Rutherford Lab. report RL-78-044.
[212] F. Halzen, Proc. 19th Intern. Conf. on High Energy Physics, Tokyo 1978, p. 214.
[213] E.L. Berger, in: Orbis Scientiae 1979 (Coral Gables, Florida); and SLAC-PUB-2314.
[214] F. Halzen and D.M. Scott, Phys. Rev. D18 (1978) 3378.
[215] F. Halzen and D.M. Scott, Phys. Rev. D21 (1980) 131.
[216] R.D. Field, Lectures given at the La Jolla Institute Summer Workshop 1978, CALT-68-696.
[217] See, for example, G. Altarelli, G. Parisi and R. Petronzio, Phys. Lett. 76B (1978) 356.
[218] Yu.L. Dokshitzer, D.I. D'yakonov and S.I. Troyan, Phys. Lett. 79B (1978) 269;
Yu.L. Dokshitzer and D.I. D'yakonov, Phys. Lett. 84B (1979) 234.
[219] G. Parisi and R. Petronzio, Nucl. Phys. B154 (1979) 427.
[220] C.Y. Lo and J.D. Sullivan, Phys. Lett. 86B (1979) 327;
S.D. Ellis and W.J. Stirling, Univ. of Washington, Seattle, report RLO-1388-821 (1980).
[221] K. Kajantie and J. Lindfors, Nucl. Phys. B146 (1978) 465.
[222] D. Sivers, Nucl. Phys. B106 (1976) 95;
A. Donnachie and P.V. Landshoff, Nucl. Phys. B112 (1976) 233;
R. Moore and A. Donnachie, J. Phys. G4 (1978) 1835;

for a detailed theoretical criticism of the charm fusion mechanism see, for example, M.J. Teper, Proc. XIIth Recontre de Moriond, Flaine 1977, p. 425; and Orsay report LPTPE 77/15.
[223] J.G. Branson et al., Phys. Rev. Lett. 38 (1977) 580; 38 (1977) 791(E).
[224] See, for example, C. Michael, Proc. XIVth Recontre de Moriond, Les Arcs 1979; and Univ. of Liverpool report LTH 52.
[225] H. Fritzsch, Phys. Lett. 67B (1977) 217.
[226] L.M. Jones and H.W. Wyld, Phys. Rev. D17 (1978) 1782.
[227] M. Glück, J.F. Owens and E. Reya, Phys. Rev. D17 (1978) 2324.
[228] M.B. Einhorn and S.D. Ellis, Phys. Rev. D12 (1975) 2007.
[229] S.D. Ellis, M.B. Einhorn and C. Quigg, Phys. Rev. Lett. 36 (1976) 1263;
C.E. Carlson and R. Suaya, Phys. Rev. D18 (1978) 760; Phys. Lett. 81B (1979) 329;
S. Nandi and H.R. Schneider, Bonn-HE-78-1 (1978);
J.H. Kühn, Second Intern. Symp. on Hadron Structure and Multiparticle Production, Kasimierz 1979; and MPI Munich report MPI-PAE/PTh 29/79.
[230] J.H. Cobb et al., Phys. Lett. 72B (1978) 497;
T.B.W. Kirk et al., Phys. Rev. Lett. 42 (1979) 619;
C. Kourkoumelis et al., Phys. Lett. 81B (1979) 405.
[231] M.J. Corden et al., Phys. Lett. 68B (1977) 96.
[232] J.G. Branson et al., Phys. Rev. Lett. 38 (1977) 1331;
K.J. Anderson et al., Phys. Rev. Lett. 42 (1979) 944.
[233] V. Barger and R.J.N. Phillips, Nucl. Phys. B73 (1974) 269.
[234] L.M. Jones and H.W. Wyld, Phys. Rev. D17 (1978) 2332.
[235] M. Glück and E. Reya, Phys. Lett. 79B (1978) 453.
[236] H.M. Georgi, S.L. Glashow, M.E. Machacek and D.V. Nanopoulos, Ann. of Phys. 114 (1978) 273.
[237] J. Babcock, D. Sivers and S. Wolfram, Phys. Rev. D18 (1978) 162;
K. Hagiwara and T. Yoshino, Phys. Lett. 80B (1979) 282.
[238] R.J. DeWitt, D.E. Willen and H.W. Wyld, Univ. of Illinois at Urbana-Champaign report ILL-(TH)-78-45 (1978).
[239] F. Halzen, Hadronic Production of Charmed and Other Favorite Particles, Univ. of Wisconsin report, 1978.
[240] B.L. Combridge, Nucl. Phys. B151 (1979) 429.
[241] P. Alibran et al., Phys. Lett. 74B (1978) 134;
T. Hansl et al., Phys. Lett. 74B (1978) 139;
P.C. Bosetti et al., Phys. Lett. 74B (1978) 143.
[242] A.G. Clark et al., Phys. Lett. 77B (1978) 339;
D. Drijard et al., Phys. Lett. 81B (1979) 250.
[243] A detailed discussion of the difficulties and assumptions involved in present experimental analyses for charm searches can be found in: W.M. Geist, Proc. EPS Intern. Conf. on High Energy Physics, Geneva 1979, vol. 2; and CERN/EP 79-78 (1979).
[244] H. Fritzsch and K.H. Streng, Phys. Lett. 78B (1978) 447.
[245] S.W. Herb et al., Phys. Rev. Lett. 39 (1977) 252.
[246] J. Badier et al., Phys. Lett. 86B (1979) 98; this paper gives also a complete compilation of previous pN measurements of Υ production.
[247] Z. Kunszt, E. Pietarinen and E. Reya, Phys. Rev. D21 (1980) 733.
[248] Second reference of ref. [40].
[249] M. Gronau, F. Ravndal and Y. Zarmi, Nucl. Phys. B51 (1973) 611.
[250] R.D. Field and R.P. Feynman, Phys. Rev. D15 (1977) 2590.
[251] J.F. Owens, E. Reya and M. Glück, Phys. Rev. D18 (1978) 1501.
[252] For excellent reviews we refer to:
L.N. Hand, Proc. 1977 Intern. Symp. on Lepton and Photon Interactions at High Energies (Hamburg, DESY, 1977) p. 417;
L.M. Sehgal, ibid., p. 837.
[253] L.M. Sehgal, Nucl. Phys. B90 (1975) 471.
[254] See, for example, K. Bruns, M. Glück and E. Reya, 1978 (unpublished);
K. Bruns, Diplomarbeit, University of Mainz, 1979.
[255] J.F. Owens, Phys. Rev. D19 (1979) 3279.
[256] K. Koller and T.F. Walsh, Phys. Lett. 72B (1977) 227; Erratum 73B (1978) 504; Nucl. Phys. B140 (1978) 449.
[257] S.J. Brodsky, T.A. deGrand, R.R. Horgan and D.G. Coyne, Phys. Lett. 73B (1978) 203.
[258] J. Dias de Deus and N. Sakai, Phys. Lett. 86B (1979) 321.
[259] T. Uematsu, Kyoto University preprint RIFP-292, June 1977, and submitted to the 1977 Intern. Symposium on Lepton and Photon Interactions, Hamburg (DESY, 1977); Phys. Lett. 79B (1978) 97;
see also J.F. Owens, Phys. Lett. 76B (1978) 85.
[260] D.H. Perkins, Oxford Univ. Nuclear Physics Lab. report 2/79 (1979);
J. Blietschau et al., Phys. Lett. 87B (1979) 281.
[261] N. Sakai, Phys. Lett. 85B (1979) 67;

R. Baier and K. Fey, Z. Physik C, Particles and Fields 2 (1979) 339;
G. Altarelli, R.K. Ellis, G. Martinelli and S.Y. Pi, Nucl. Phys. B160 (1979) 301.
[262] R.F. Cahalan, K.A. Geer, J. Kogut and L. Susskind, Phys. Rev. D11 (1975) 1199.
[263] B.L. Combridge, J. Kripfganz and J. Ranft, Phys. Lett. 70B (1977) 234.
[264] R. Cutler and D. Sivers, Phys. Rev. D17 (1978) 196.
[265] B. Alper et al., Nucl. Phys. B100 (1975) 237;
F.W. Büsser et al., Nucl. Phys. B106 (1976) 1;
B.G. Pope, in: Particles and Fields – 1977, Proc. Meeting of the APS Division of Particles and Fields (AIP, New York, 1978) p. 239.
[266] R.D. Field, Phys. Rev. Lett. 40 (1978) 997.
[267] M. Fontannaz and D. Schiff, Nucl. Phys. B132 (1978) 457;
J. Ranft and G. Ranft, Ref. TH. 2363-CERN (1977), and Leipzig report KMU-HEP-78-06 (1978).
[268] A.P. Contogouris, R. Gaskell and S. Papadopoulos, Phys. Rev. D17 (1978) 2314.
[269] J.F. Owens and J.D. Kimel, Phys. Rev. D18 (1978) 3313.
[270] J.W. Cronin et al., Phys. Rev. D11 (1975) 2105;
D. Antreasyan et al., Phys. Rev. Lett. 38 (1977) 112 and 115.
[271] A.G. Clark et al., Phys. Lett. 74B (1978) 267;
CERN-Columbia-Oxford-Rockefeller Coll., reported by L. DiLella at the Workshop on Future ISR Physics, Sept. 1977, ed. M. Jacob; and at the Symp. on Jets in High Energy Collisions, NORDITA, Copenhagen 1978.
[272] Z. Kunszt and E. Pietarinen, Z. Physik C, Particles and Fields 2 (1979) 355; Nucl. Phys. B164 (1980) 45.
[273] A. Schiller, J. Phys. G5 (1979) 1329.
[274] T. Gottschalk and D. Sivers, Phys. Rev. D21 (1980) 102.
[275] R. Blankenbecler and S.J. Brodsky, Phys. Rev. D10 (1974) 2973;
R. Blankenbecler, S.J. Brodsky and J.F. Gunion, Phys. Rev. D12 (1975) 3469;
S.J. Brodsky, Invited talk presented at the VIII Intern. Symp. on Multiparticle Dynamics, Kayserberg, France, 1977, and SLAC-PUB-2009 (1977).
[276] For a detailed comparative study of hard scattering models and the CIM see, for example:
G.C. Fox, Invited talk at the Brookhaven APS meeting, Oct. 1976, and CALT-68-573;
M.K. Chase and W.J. Stirling, Nucl. Phys. B133 (1978) 157;
J.F. Gunion, The Interrelationship of the Constituent Interchange Model and QCD, Univ. of California, Davis report, and presented at the Discussion Meeting on Large Transverse Momentum Phenomena, SLAC, 1978.
[277] A.P. Contogouris, R. Gaskell and A. Nicolaidis, Phys. Rev. D17 (1978) 2992.
[278] For a detailed discussion of two-particle inclusive high-p_T reactions within the *naive* parton model, see for example:
R. Baier, J. Cleymans, K. Kinoshita and B. Petersson, Nucl. Phys. B118 (1977) 139;
R.P. Feynman, R.D. Field and G.C. Fox, Nucl. Phys. B128 (1977) 1.
[279] J.F. Owens, Phys. Rev. D20 (1979) 221; Coral Gables Conf. "Orbis Scientiae", January 1979.
[280] R. Baier, J. Engels and B. Petersson, Z. Physik C, Particles and Fields 2 (1979) 265.
[281] T. Appelquist and H. Georgi, Phys. Rev. D8 (1973) 4000;
A. Zee, Phys. Rev. D8 (1973) 4038.
[282] M. Dine and J. Sapirstein, Phys. Rev. Lett. 43 (1979) 668;
K.G. Chetyrkin, A.L. Kataev and F.V. Tkachov, Phys. Lett. 85B (1979) 277.
[283] J. Ellis, in: Proc. 1979 Intern. Symp. on Lepton and Photon Interactions, Fermilab, Batavia, p. 412; and Ref. TH. 2744-CERN (1979).
[284] G. Wolf, Rapporteur talk given at the 1979 EPS Intern. Conf. on High Energy Physics, Geneva, vol. 1, p. 220;
Mark J Collaboration, Phys. Reports 63 (1980) 337.
[285] W. Bartel et al. (JADE coll.), Phys. Lett. 88B (1979) 171.
[286] S.L. Adler, Phys. Rev. D10 (1974) 3714;
A. de Rújula and H. Georgi, Phys. Rev. D13 (1976) 1296;
E.C. Poggio, H.R. Quinn and S. Weinberg, Phys. Rev. D13 (1976) 1958;
R. Shankar, Phys. Rev. D15 (1977) 755;
K.G. Chetyrkin, N.V. Krasnikov and A.N. Tavkhelidze, Phys. Lett. 76B (1978) 83.
[287] T. Appelquist and H.D. Politzer, Phys. Rev. Lett. 34 (1975) 43; Phys. Rev. D12 (1975) 1404.
[288] G. Hanson et al., Phys. Rev. Lett. 35 (1975) 1609;
G. Hanson, Talks given at the VIIth Intern. Colloquium on Multiparticle Reactions, Tutzing, Munich 1976, and the XVIIIth Intern. Conf. on High Energy Physics, Tbilisi, U.S.S.R. 1976; and SLAC-PUB-1814.
[289] P. Söding, Rapporteur talk given at the 1979 EPS Intern. Conf. on High Energy Physics, Geneva, vol. 1, p. 271;
R.J. Cashmore (TASSO coll.), ibid., p. 330.
[290] Ch. Berger et al. (PLUTO coll.), Phys. Lett. 78B (1978) 176; Phys. Lett. 81B (1979) 410.
[291] R.F. Schwitters et al., Phys. Rev. Lett. 35 (1975) 1320.
[292] J.D. Bjorken and S.J. Brodsky, Phys. Rev. D1 (1970) 1416.
[293] Ch. Berger et al. (PLUTO coll.), Phys. Lett. 82B (1979) 449.

[294] T. Kinoshita, J. Math. Phys. (N.Y.) 3 (1962) 650;
T.D. Lee and M. Nauenberg, Phys. Rev. 133 (1964) B1549.
[295] H. Georgi and M. Machacek, Phys. Rev. Lett. 39 (1977) 1237.
[296] E. Farhi, Phys. Rev. Lett. 39 (1977) 1587.
[297] S. Brandt and H.D. Dahmen, Z. Physik C, Particles and Fields 1 (1979) 61.
[298] A brief and clear discussion of infrared and (collinear) mass singularities can be found, for example, in: V. Alessandrini, Hard Processes in QCD Perturbation Theory, XIVth Recontre de Moriond, Les Arcs, 1979.
[299] G. Sterman and S. Weinberg, Phys. Rev. Lett. 39 (1977) 1436.
[300] P.M. Stevenson, Phys. Lett. 78B (1978) 451;
B.G. Weeks, Phys. Lett. 81B (1979) 377.
[301] M.B. Einhorn and B.G. Weeks, Nucl. Phys. B146 (1978) 445.
[302] M.K. Gaillard, Rapporteur talk given at the 1979 EPS Intern. Conf. on High Energy Physics, Geneva, vol. 1, p. 390; and in: Probing Hadrons with Leptons, Erice, March 1979, eds. G. Preparata and J.J. Aubert (Plenum Press, 1980) p. 47.
[303] K. Shizuya and S.-H.H. Tye, Phys. Rev. Lett. 41 (1978) 787 and 1195(E); Phys. Rev. D20 (1979) 1101.
[304] For similar reasons we expect the gluonic hadron multiplicity to be larger than the one resulting from a decaying quark; this effect should become more pronounced at larger energies $\sqrt{s}$ when hard gluon jets become more effective; S.J. Brodsky and J.F. Gunion, Phys. Rev. Lett. 37 (1976) 402.
[305] J. Ellis, M.K. Gaillard and G.G. Ross, Nucl. Phys. B111 (1976) 253.
[306] A. de Rújula, J. Ellis, E.G. Floratos and M.K. Gaillard, Nucl. Phys. B138 (1978) 387.
[307] P. Hoyer, P. Osland, G.H. Sander, T.F. Walsh and P.M. Zerwas, Nucl. Phys. B161 (1979) 349.
[308] For an interesting algorithm on calculating QCD jets, see: K. Konishi, A. Ukawa and G. Veneziano, Phys. Lett. 78B (1978) 243; 80B (1979) 259.
[309] J. Kogut and L. Susskind, ref. [35].
[310] R. Brandelik et al. (TASSO coll.), Phys. Lett. 86B (1979) 243.
[311] Ch. Berger et al. (PLUTO coll.), Phys. Lett. 86B (1979) 418.
[312] D.P. Barber et al. (MARK-J coll.), Phys. Rev. Lett. 43 (1979) 830.
[313] A. Ali, J.G. Körner, G. Kramer and J. Willrodt, Z. Physik C, Particles and Fields 1 (1979) 203; and DESY 79/63.
[314] D. Koller and T.F. Walsh, Phys. Lett. 72B (1977) 227; Erratum 73B (1978) 504; Nucl. Phys. B140 (1978) 449;
K. Koller, H. Krasemann and T.F. Walsh, Z. Physik C, Particles and Fields 1 (1979) 71.
[315] S.J. Brodsky, T.A. DeGrand, R.R. Horgan and D.G. Coyne, Phys. Lett. 73B (1978) 203.
[316] H. Fritzsch and K.H. Streng, Phys. Lett. 74B (1978) 90.
[317] One-gluon intermediate states are forbidden by color, since physical states have to be colorless, i.e. color-singlets, whereas two gluons are forbidden by charge-conjugation invariance.
[318] A. Ore and J.L. Powell, Phys. Rev. 75 (1949) 1696;
see also ref. [166] p. 312.
[319] H. Meyer (PLUTO coll.), in: Probing Hadrons with Leptons, Erice, March 1979;
S. Brandt (PLUTO coll.), Intern. Conf. on High Energy Physics, Geneva, 1979, vol. 1, p. 338.
[320] A discussion of further tests involving also other quarkonium spin-states decaying into gluons and giving rise to specific angular distributions can be found, for example, in:
M. Krammer and H. Krasemann, Schladming lectures 1979; and DESY 79/20;
V.A. Novikov, L.B. Okun, M.A. Shifman, A.I. Vainshtein, M.B. Voloshin and V.I. Zakharov, Phys. Reports 41 (1978) 1.
[321] A recent discussion on gluonium can be found in:
J.D. Bjorken, Intern. Conf. on High Energy Physics, Geneva 1979, p. 245; and SLAC-PUB-2366; SLAC Summer School 1979, SLAC-PUB-2372.
[322] S.J. Brodsky, T.A. DeGrand, J.F. Gunion and J.H. Weis, Phys. Rev. Lett. 41 (1978) 672;
K. Kajantie and R. Raitio, Nucl. Phys. B159 (1979) 528.
[323] Recent reviews have been given, for example, by:
S.J. Brodsky, talk presented at the J.M. Weis Memorial Symposium on Strong Interactions, Seattle, 1978; and SLAC-PUB-2240;
K. Kajantie, Schladming lectures 1979; and Univ. of Helsinki report HU-TFT-79-5 (1979).